New measurements techniques

Optical methods for characterizing sound fields

Torras Rosell, Antoni

Publication date:
2014

Document Version
Publisher's PDF, also known as Version of record

Technical University of Denmark

Antoni Torras Rosell

New measurements techniques: Optical methods for characterizing sound fields

PhD thesis, January 2014

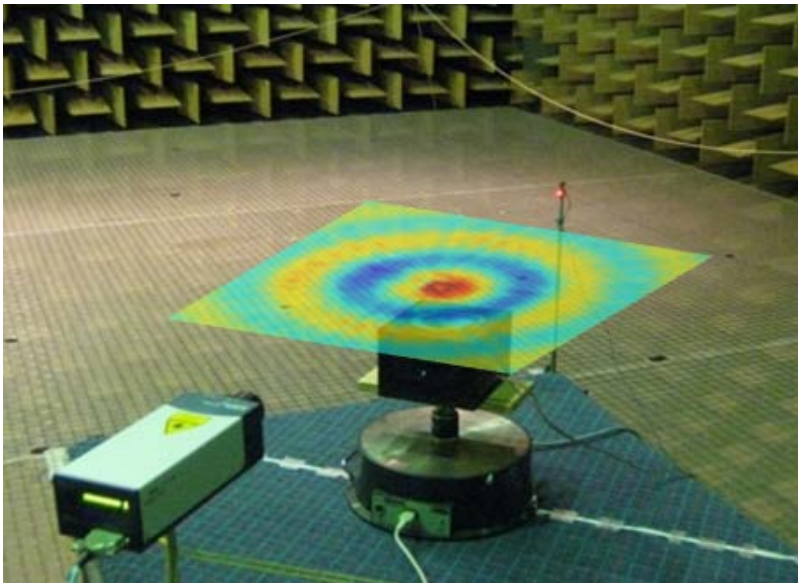

DTU Electrical Engineering
Department of Electrical Engineering

New measurement techniques: Optical methods for characterizing sound fields

PhD thesis by

Antoni Torras Rosell

Technical University of Denmark

2014

This thesis was submitted to the Technical University of Denmark (DTU) as partial fulfillment of the requirements for the degree of Doctor of Philosophy (Ph.D.) in Electronics and Communication. The work presented in this thesis was completed between April 1, 2010 and July 31, 2013 at Acoustic Technology, Department of Electrical Engineering, DTU, under the supervision of Associate Professors Finn Jacobsen and Finn T. Agerkvist, and Dr. Salvador Barrera Figueroa. The project was funded by DFM (Danish National Metrology Institute) under the Industrial PhD programme supported by the Ministry of Science, Innovation and Higher Education.

Cover illustration:
Acousto-optic reconstruction of the sound waves radiated
by a loudspeaker

Department of Electrical Engineering
Technical University of Denmark
ISBN 978-87-92465-46-7 DK-2800 KONGENS LYNGBY, Denmark

Printed in Denmark by Rosendahls - Schultz Grafisk a/s

To Finn Jacobsen
(April 1949 – June 2013)

"No significant learning can occur without a significant relationship."
James P. Comer

Abstract

Acoustic measurements are traditionally based on transducers, and in particular, the most advanced measurement techniques are nowadays based on transducer arrays. This poses a fundamental problem, namely the influence of the transducer itself on the actual properties of sound when the transducer is immersed into the sound field. Typically, this influence is assumed to be negligible when the size of the transducer is small compared to the wavelength of the sound wave, or is rendered negligible by using a transducer-based correction that depends on the frequency. Either solution introduces additional uncertainties to the measurement process. Optical techniques may help overcoming this problem because the sensing element is not a bulky instrument, but a beam of light that does not change the properties of sound. Optical methods are thus non-invasive and can thereby enhance the current state of the art in the measurement of sound.

The present PhD study primarily examines the use of the acousto-optic effect, that is, the interaction between sound and light, as a means to characterize acoustic fields. The acousto-optic measuring principle does not provide a direct measure of the pressure, but the integral of the pressure encountered by the 'sensing' light when traveling through the acoustic field. Far from being a limitation, this integral principle is exploited for sound field visualization using tomography. The most innovative contribution of this PhD project is the applicability of the acousto-optic measuring principle to acoustic holography and beamforming. On the one hand, a new method called near-field acousto-optic holography (NAOH) has been proposed and makes it possible to predict properties of sound at planes different from the measuring one. In comparison with conventional near-field acoustic holography (NAH), the suggested holographic method features novel spectral properties in the wavenumber domain. On the other hand, an acousto-optic beamformer has been designed and validated experimentally for the localization of sound sources located in the far field. In this case, a laser beam is interpreted as a line array of microphones with infinite resolution, which makes the proposed acousto-optic beamformer immune to spatial aliasing.

In addition, the present PhD study investigates the applicability of photon correlation spectroscopy as a primary method for microphone calibration under free-field

conditions. Various signal processing refinements are proposed to improve the accuracy of this measurement technique.

Keywords: Optical methods, acousto-optic effect, laser Doppler vibrometry, tomography, sound visualization, near-field acoustic holography, beamforming, photon correlation spectroscopy.

Resumé

Akustiske målinger er baseret på transducere og de mest avancerede teknikker er baseret på transducer arrays. Dette medfører et grundlæggende problem, nemlig at lydfeltet ændrer sig, når transduceren placeres i lydfeltet. Denne indvirkning er frekvensafhængig og kun ubetydelig, når størrelsen af transduceren er lille i forhold til bølgelængden. Hvis lydfeltet er kendt, er det muligt at korrigere for indvirkningen, men under alle omstændigheder bidrager transduceren fysiske form til usikkerhed på målingen. Optiske metoder kan bidrage til at løse dette problem, fordi føleren er en lysstråle, som ikke påvirker lydens fysiske egenskaber. Optiske metoder er således ikke-invasive.

I dette Ph.D. projekt undersøges primært anvendelsen af den akusto-optiske effekt, dvs. vekselvirkningen mellem lyd og lys, som et middel til at karakterisere lydfelter. Det akusto-optiske måleprincip giver ikke et direkte mål af lydtrykket i et punkt, men integrerer lydtrykket langs den optiske vej. Dette integrationsprincip kan udnyttes til visualisering af lydfeltet ved hjælp af tomografi. I projektet undersøges også anvendeligheden af det akusto-optiske måleprincip til akustisk holografi og beamforming. På den ene side foreslås en ny metode kaldet akusto-optisk nærfeltsholografi (NAOH), som gør det muligt at forudsige lydfeltet i et andet plan end det der måles i. NAOH har særlige gunstige spektrale egenskaber i bølgetalsdomænet i forhold til konventionel akustisk nærfeltsholografi (NAH). På den anden side er en akusto-optisk beamformer udviklet til lokalisering af lydkilder i fjernfeltet. I dette tilfælde tolkes en laserstråle som et 'line array' af mikrofoner med uendelig opløsning, hvilket gør at den foreslåede akusto-optiske beamformer ikke begrænses af rumlig aliasering ved høje frekvenser. Desuden er fotonkorrelationsspektroskopis anvendelighed som en primær metode til mikrofon kalibrering i frit felt undersøgt. Der foreslås forskellige forbedringer af signalbehandlingen for at opnå den nøjagtighed, der kræves af de metrologiske standarder.

Nøgleord: Optiske metoder, akusto-optisk effekt, laser Doppler vibrometer, tomografi, lydfelt visualisering, akustisk nærfeltsholografi, beamforming, fotonkorrelationsspektroskopi.

Acknowledgment

Foremost, I would like to express my deepest gratitude to Finn Jacobsen and Salvador Barrera Figueroa, main supervisors of this PhD study, for the permanent availability, patience, encouragement, guidance and priceless insights. Certainly, the outcome of the project would not have been the same without your approach to science and research. It has been undoubtedly a privilege to take this journey with you both. That I take with me for the rest of my life.

I feel grateful to Finn T. Agerkvist for accepting the supervision of this project at its latest stage, in spite of the amount of work and responsibilities he was suddenly compelled to undertake during the last months.

I feel very thankful to DFM, the industrial partner of this PhD project, for supporting the project since the beginning, as well as for considering me as another employee of the company rather than a transitory PhD student. I deeply appreciate Michael Kjær and Hans D. Jensen's effort in moving this project forward.

As industrial PhD student, I must also acknowledge the framework provided in the Industrial PhD Programme supported by the Ministry of Science, Innovation and Higher Education of Denmark. The advances in research promoted by initiatives like this PhD programme are invaluable for a country.

Many thanks to everybody in the 'House of Acoustics', both in Acoustic Technology and in Hearing Systems, for the nice and friendly atmosphere as well as the passion devoted to acoustics. I especially thank my fellows and friends at Acoustic Technology for support, feedback and enthusiasm along the project. Even though I was sitting at the department part time, I have always felt at home. Special thanks to Joe Jensen, I cannot imagine a better office mate. I owe a great deal of the experimental work to Tom A. Petersen and in particular to Jørgen Rasmussen for all their prompt, efficient and custom technical support.

Important parts of this work would not have been possible without the contributions of Ester Creixell Mediante, Oliver Lylloff and Efren Fernandez Grande. Thanks Ester for your assistance and ability to prepare the experimental setups when I was away in London. Thanks Oliver for your motivation and great assistance in the always intriguing

world of inverse methods. And thanks Efren for the stimulating discussions, guidance and insights in the matter of acoustic holography.

My sincere gratitude to Richard Barham for making the two months research stay at NPL possible. I am also thankful to everyone in the Acoustics Group of NPL for their kind hospitality and for letting me contribute to the ongoing research projects as another peer. I would expressly like to thank Ian Butterworth, Ben Piper and Triantafillos Koukoulas for all the work we did together. In particular, I am truly and deeply indebted to Triantafillos for all his dedication and teaching in optics, all the inspiring and thrilling discussions, and his precious feedback on early versions of this manuscript.

My family and friends have been very much supportive. Thanks for being understanding, patient and cheering along the whole PhD project. I would sincerely like to thank my parents for their timely support, particularly during the last month of the PhD project. I undoubtedly owe a lot of joy to my little son Quim, born during the course of the PhD project and whose permanent curiosity for discovering things reminds me how lucky I am when doing research.

Finally, I am deeply grateful to Elisabet Tiana Roig. This has also been a long journey for you, where you have contributed countless times reviewing papers, giving inspiring lectures, transmitting enthusiasm in the findings and warm support in the hard moments. Thanks for being there and for taking care of our little family.

Contents

Structure of the thesis

The present PhD dissertation follows a paper-based model. It thereby comprises a synopsis of the subject under investigation, a clear statement of contributions in the matter as well as a collection of papers produced during the course of the PhD study. The research undertaken in this PhD project involves two main disciplines, namely acoustics and optics. Since the thesis is submitted as a partial fulfillment of the requirements for a PhD degree in Acoustics, the PhD candidate has taken a special effort to strengthen the connection between these two disciplines, presuming that some of the readers may not be that familiar with the topic.

Chapter 1 (Introduction) states the scope of the thesis and provides a historical view on the science of light as well as a state of the art on the measurement of sound. Chapter 2 (Light and sound) is devoted to describe the various forms of interaction between sound and light and discusses some fundamental aspects of this interaction. Chapter 3 (Optical methods in acoustics) begins with a review of the different optical techniques that are related to or used in acoustics. It then focuses on the measurement of sound based on the acousto-optic measuring principle, and analyzes the limitations encountered with this technique given the available technology. It continues examining a completely different optical technique, namely photon correlation spectroscopy, and analyzing possible means of improving the current performance of this technique. A brief remark on the calibration of optical methods is given at the end of this chapter. Chapter 4 (Contributions) elaborates on the originality and novelty of the work, with special emphasis on the papers appended at the end of the thesis. Chapter 5 (Conclusions) provides an overview of the work, restates the novelty and significance of the research, and draws up some remarks and perspectives on the use of optical methods in acoustics.

The dissertation is completed with a selection of nine papers written during the course of the PhD project. Two of them are published in a peer reviewed journal, the Journal of the Acoustical Society of America, and the rest are published or accepted for publication in proceedings of different acoustic conferences.

List of publications

The following publications appended at the end of the thesis constitute the core of the research done in the present PhD study:

Paper A "An investigation of sound fields based on the acousto-optic effect", in Proceedings of ICSV18, Rio de Janeiro, Brazil, 2011.

Paper B "Sound field reconstruction using acousto-optic tomography", J. Acoust. Soc. Am., vol. **131**(5), pp. 3786–3793, 2012.

Paper C "Reconstruction methods for sound visualization based on acousto-optic tomography", in Proceedings of Inter-Noise 2013, Innsbruck, Austria, 2013.

Paper D "Investigating the use of the acousto-optic effect for acoustic holography", in Proceedings of Inter-Noise 2012, New York, USA, 2012.

Paper E "Holographic reconstruction of sound fields based on the acousto-optic effect", in Proceedings of Inter-Noise 2013, Innsbruck, Austria, 2013.*

Paper F "An acousto-optic beamformer", J. Acoust. Soc. Am., vol. **132**(1), pp. 144–149, 2012.

Paper G "A beamforming system based on the acousto-optic effect", in Proceedings of Euro-Noise 2012, Prague, Czech Republic, 2012.

Paper H "The versatility of the acousto-optic measuring principle in characterizing sound fields", in Proceedings of the Institute of Acoustics, vol. **35**(1), pp. 242–250, 2013.

Paper I "Advances in the free-field measurement of acoustic particle velocity using gated photon correlation spectroscopy", in Proceedings of the Institute of Acoustics, vol. **35**(1), pp. 207–214, 2013.*

*The author of this dissertation is not the first author of the paper.

List of abbreviations

AOT	Acousto-optic tomography
BIPM	International Bureau of Weights and Measures
CCD	Charge-coupled device
CT	Computerized tomography
DSPI	Digital speckle pattern interferometry
ESPI	Electronic speckle pattern interferometry
FFT	Fast Fourier transform
LASER	Light amplification by stimulated emission radiation
LDA	Laser Doppler anemometry
LDV	Laser Doppler vibrometer
MASER	Microwave amplification by stimulated emission radiation
MEMS	MicroElectroMechanical System
MSL	Maximum side lobe
NAH	Near-field acoustic holography
NAOH	Near-field acousto-optic holography
NPL	National Physical Laboratory
PIV	Particle image velocimetry
PCS	Photon correlation spectroscopy
RADAR	Radio detection and ranging
RMS	Root mean square
SI	Structural similarity
SNR	Signal-to-noise ratio
SONAR	Sound navigation and ranging
TV	Television
1D	One-dimensional
2D	Two-dimensional

Glossary of symbols

A	Amplitude of the acoustic wave
c	Speed of sound in the medium of propagation
c'	Speed of light in the medium of propagation
c_0	Speed of light in vacuum
D	Frequency to velocity converter
$f(t)$	Instantaneous frequency
f_s	Frequency shift introduced by an acousto-optic modulator
γ	Ratio of specific heats
J_0	Bessel function of the first kind of order zero
k_0	Optical wavenumber in vacuum
k	Acoustic wavenumber
$L(t)$	Length of the probe beam
L_0	Length of the probe beam under static conditions
$l(t)$	Displacement of a vibrating point
λ	Acoustic wavelength
λ'	Optical wavelength
n	Refractive index of a medium
n_0	Refractive index of a medium under static conditions
ω	Acoustic angular frequency
p	Sound pressure
$\hat{p}$	Sound pressure in complex notation
p_0	Static pressure
p_{rms}	Root mean square value of p
$R(\tau)$	Autocorrelation function of scattered photons
R_p	Theoretical Radon transform of an acoustic field

$\tilde{R}_p$	Measured Radon transform of an acoustic field
$v_{\text{LDV}}(t)$	Velocity measured with an LDV
$v_{\text{ao}}(t)$	Apparent velocity caused by the acousto-optic effect
$v_{\text{ao,rms}}$	Root mean square value of $v_{\text{ao}}(t)$
$v_{\text{mec}}(t)$	Velocity of a vibrating surface
$\phi(t)$	Phase of the laser beam at a certain point
θ	Angle of projection of the tomographic data
θ_i	Angle of incidence of plane waves approaching a laser beam
θ'	Half-angle of the intersecting beams
$\hat{\mathbf{u}}$	Particle velocity vector in complex notation
$\hat{u}_x$	Particle velocity of a propagating plane wave in complex notation
$\hat{u}_r$	Particle velocity of a spherical wave in complex notation
u_m	Amplitude of the particle velocity
u_f	Mean flow velocity
$(\partial n/\partial p)_S$	Piezo-optic coefficient

Chapter 1

Introduction

Two out of the five human senses rely on sound and light. This is a clear sign of the tremendous value that these two physical quantities have in nature. Many have pursued the comprehension of these phenomena, and not in vain, science has devoted two of its numerous disciplines to study them, namely acoustics and optics. While acoustics has matured from a solid foundation of knowledge for several centuries, optics has struggled unraveling the properties of light. Whether the nature of light is more difficult than that of sound or not, quite a few of the greatest technological advances nowadays, e.g., the deployment of optical communications for the Internet, are the result of the vertiginous progress in the science of light during the last decades. This thesis is an attempt to enlighten the necessity and benefits of incorporating optical technology into the measurement of sound.

1.1 Optics odyssey

The first evidences of optical utensils, and thus, the notion of optics, date back to the ancient cultures. The first optical lenses have been credited to the ancient Egyptians and Mesopotamians, whereas the first theories of light were to come later on, when the Greek and Indian philosophers tried to understand the essence of nature. There was already at that time a controversy among the Greek philosophers about how human beings perceive light [1]. On the one hand, Plato, Euclid and others claimed that vision was possible because of rays emitted by the eyes, the so-called emission theory. On the other hand, Aristotle and other philosophers defended the intro-mission model, which stated that vision was simply 'something' casted off the objects (at that time, they could

not explain exactly what it was) that was entering through the eyes. Despite the resemblance of the intro-mission theory with the current understanding of visual perception, neither of the two theories could prove valid due to the lack of experimental basis. Nevertheless, Euclid was the first to relate vision with geometry [2], a discipline that he mastered and that brought him to deduce the principles of what is nowadays referred to as Euclidean geometry. This represented the origin of geometrical optics, that is, the study of light as propagating rays.

In the middle ages, optics evolved with the wisdom of the Islamic world, especially refining the fundamentals of geometrical optics [3, 4]. The first eyeglasses were invented by the end of the 13th century in Italy [5], giving rise to the first optical industry that expanded to other regions of Europe along the 14th century. Since then, the process of manufacturing lenses was progressively mastered, and this combined with considerable doses of experimentalism led to a very important milestone in optical instrumentation by the beginning of the 17th century: the invention of the optical microscope [6] and the telescope [7]. By combining lenses in an appropriate manner, it was suddenly possible to examine tiny creatures and to explore the Universe. In particular, the discovery of the telescope was indeed crucial for Galileo and Kepler's astronomical observations that championed the heliocentric model of the Universe originally suggested by Copernicus in the previous century [8]. The fundamentals of geometrical optics were also firmly grounded in the 17th century, when Willebrord Snellius, Descartes, and other scientists derived the so-called Snell's law that describes the refraction of light [9].

However, the use of rays for describing the propagation of light was just an approximation of how light propagates in reality. Although geometrical optics could provide excellent results when the wavelength was significantly smaller than the objects with whom light interacted, it could not explain phenomena such as the diffraction and interference of light. It was thus time for new theories, and Newton became the most fervent advocate of the so-called corpuscular theory of light [10], which considered light as streams of discrete and very small particles, referred to as 'corpuscles', traveling in straight lines. In his experiment on the diffraction of light in a prism, Newton asserted that white light got fanned out of the prism in different colors because 'corpuscles' of light with different color traveled through the prism with different velocities. Newton also observed that the red light emerging from the prism would not change color after going through a second prism. Newton then concluded that light emitted by objects

could not be produced by themselves, and therefore, the observed colors had to be already contained in the incident light. This was a breaking discovery because until that time it was believed that white light was colorless. Opposed to Newton's conviction on the nature of light, Huygens championed a theory that regarded light as a wave emerging from a light source in all directions and propagating through aether, a substance that was postulated to fill the medium in order to explain several unresolved phenomena [11]. Huygens's wave theory was however eclipsed by Newton's corpuscular theory for several decades, probably due to the recognition and popularity granted to Newton in other fields of physics, for instance, after deriving the laws of motion and universal gravitation.

The wave theory gained again supporters early in the 19th century, after Thomas Young performed his famous double-slit interference experiment [12]. This experiment showed that monochromatic light passing through a parallel double slit yielded an interference pattern that could only be explained by describing the propagation of light as a wave. Later on the 20th century, modifications on this experiment would illustrate with clarity the wave-particle duality of light. In the meantime, Fresnel incorporated the polarization of light into the wave theory and derived the corresponding laws of reflection and transmission commonly referred to as the Fresnel equations [13]. Still in the 19th century, Maxwell formulated the theory of electromagnetic waves based on four equations capable of describing phenomena in electricity, magnetism and optics that were considered unrelated until that moment [14]. Maxwell also estimated that the speed of propagation of an electromagnetic wave was approximately the same as the speed of light, and could not refrain himself from concluding that light could be described as an electromagnetic wave. After Maxwell's interpretation, light was seen from then on as electromagnetic radiation from the visible electromagnetic spectrum. From that time, there was no doubt among the scientific community that light was a wave-like phenomenon.

The hegemony of the wave theory was yet to be challenged again with the entrance to the 20th century. The wave theory seemed to present some flaws in experiments where light interacted with matter. Max Planck revolutionized the classical theory of physics by assuming, in his study of blackbody radiation, that atoms emitted light in discrete energy amounts rather than in a continuous manner [15, 16]. This suggested the existence of a quantum of light, which represented the birth of quantum physics and the return to the wave-particle controversy. In the following years, Albert Einstein

could explain the photoelectric effect, that is, the emission of electrons from a metal surface irradiated with light, using the theory of discrete energy levels of light quanta announced by Planck [17]. Shortly after, Niels Bohr also included the quantum of light into his model about the emission and absorption processes of the hydrogen atom [18], and Arthur Compton could also explain the scattering of X-rays induced by electrons as collisions between light quanta and electrons [19]. At that point, it was incontestable that light also featured particle-like properties. It was not until 1924, when Louis de Broglie hypothesized that all particles with mass had wave properties, the so-called wave-particle duality [20], that the paradox about the nature of light could be understood.

Since then, the main advances in modern optics have been driven by the principles of quantum physics. Probably, one of the most significant breakthroughs was the inventions of the MASER and in particular the LASER in the 1950s [21], whose acronyms stand for Microwave and Light Amplification by Stimulated Emission Radiation, respectively. These devices were capable of producing coherent electromagnetic waves, namely microwaves and light, based on a quantum phenomenon called stimulated emission, which was already discovered by Albert Einstein in 1917. In particular, it is difficult to imagine how technology would be nowadays without the invention of the laser. One can find lasers in simple devices such as laser pointers and read/write audio and video devices, but lasers have also simplified many surgical procedures, increased the accuracy of many industrial measurements, provided unique methods for inferring properties of atoms and molecules in physics and chemistry, and they have also been deployed for restoration and cleaning of artwork as well as for many other purposes in biology, astronomy, metrology, telecommunications, engineering, etc.

1.2 Acoustic measurements on the 21st century

The measurement of sound has been realized with microphone transducers for several decades. Inspired by the invention of the telephone, the first microphone as such, the carbon microphone, was invented in the late 1870s [22]. Many other types were to come along the 20th century, e.g., the condenser and the ribbon microphones. Naturally, microphones have improved in quality, efficiency and accuracy by incorporating new technological advances, changing materials, mastering manufacturing processes, and upgrading electronics. New acoustic transducers such as the sound intensity probe

have also appeared to complete and provide a full insight into the measurement of sound beyond the realization of the acoustic pressure. In any case, acoustic transducers perform in general single point measurements, as for instance the microphone of a sound level meter, and this somehow limits the information that can be extracted from the acoustical space under analysis. Traditionally, and probably for practical reasons, this inconvenience has often been resolved by repeating the measurement over an ensemble of positions, and thus, by assuming the spatial average of the ensemble as a good approximation of the physical quantity to be determined. Alternatively, the appearance of the first transducer array techniques, in the 1970s for far-field measurements [23] and in 1980s for near-field measurements [24], made it possible to measure acoustic fields at different positions at the same time. The instantaneity of such measurements posed strict requirements on the measuring equipment, e.g., in terms of stability and 'perfect' match among transducers. The resulting multichannel array systems were quite complex and required cumbersome calibration procedures. It has not been until the last two decades that the increasing capabilities of computer systems have made it possible to deploy transducer array technology for *in situ* measurements. Near-field acoustic holography [25] (NAH) and acoustic beamforming [26] are probably two of the most powerful array techniques used nowadays for instance in the automotive and aeronautic industries. The applicability of these techniques goes beyond the visualization of acoustic maps, and it rather eases complicated tasks such as sound source identification and localization, environmental noise diagnosis, and vibro-acoustic analysis. In addition to the increasing capabilities of the existing array systems, the appearance of innovative array designs is favoring the renaissance of classical expansion methods that exploit the decomposition of an acoustic field into a set of orthogonal functions, e.g., spherical or cylindrical harmonics. Array-based acoustic measurements are today developed to a high degree of sophistication, and this turns array systems into very powerful measurement tools, though not always affordable.

1.3 Scope of the thesis

Transducer-based measurements have been used extensively in acoustics. From a technological point of view, there is always the possibility that a new discovery leads to the next generation of transducers. However, such technological advances cannot avoid the inherent problems derived from using a transducer: the interaction required between

the transducer and the acoustic field can itself bias the original sound properties under investigation. While this effect is indeed negligible for a vast majority of applications where the dimensions of the measuring device are sufficiently small compared to the wavelength of the sound waves, this effect can become significant at high frequencies, typically causing undesired scattering effects. This fundamental problem is well-known and there are ways to circumvent it in practice by limiting the frequency range of analysis or by applying a transducer-based correction in form of a frequency response. The latter can though only account for the scattering effects caused by sound waves coming from a certain direction, typically normal incidence.

Array-based measurements are potentially more vulnerable to this problem. In this case, not one but rather an ensemble of transducers together with their corresponding frame and wiring are immersed into the sound field. The difficulty of applying individualized frequency response corrections to each of the transducers is apparent. Besides, the accuracy of array methods is in principle improved with increasing the number of transducers, and moreover, the density of transducers needs to be further increased at high frequencies in accordance with the Nyquist theorem. The scattering effects resulting from using a high density of transducers can unfortunately cause amplitude and phase mismatches among the array sensors. This can be a serious source of error, and thereby, it can limit the highest frequency of analysis to a value below the Nyquist frequency.

Ideally, the invasiveness of transducer-based measurements could be avoided if no sensor was to be immersed into the sound field. On the search for such an ideal measurement principle, optical methods manifest unique features capable of sensing sound without changing its properties. Depending on the optical setup, different properties of light can be used to realize acoustic quantities, but in any case, the use of light as a sensing element is indeed non-invasive since the light traveling through the acoustic field does not change the nature of sound (at least not in a macroscopic scale). Besides, the progress made in laser optics in the last century and the fact that laser and optic technology is becoming more stable, accurate and less expensive indicate that optical methods have a great potential for advanced acoustic measurements.

All in all, the present PhD thesis explores the interaction between sound and light as a means to sense sound without changing its properties and to devise new acoustic measurement techniques that may eventually in the future supplement, improve or even provide novel features to the methods existing today.

Chapter 2

Light and sound

Sound is an oscillating phenomenon that propagates as a mechanical wave, that is, a pressure fluctuation of the medium. The nature of light is not that straightforward, but the wave-particle duality principle seems to give satisfactory answers to all light phenomena known up to date. In short, light can be regarded as an electromagnetic wave when the propagation of light is under study, whereas light is better described as an ensemble of traveling particles, namely photons, when it interacts with matter. As waves, both sound and light have quite a few features in common, e.g., they can be reflected, diffracted and interfere, but they also differ in some other aspects that stem from their respective mechanical and electromagnetic nature. Unlike sound, light can propagate in vacuum, and a clear example of that is the sunlight, which supports almost any form of life on earth after traveling on average (along the calendar seasons) 149.6×10^6 km in vacuum. Another significant difference between acoustic and light waves is the duration of their oscillations. The visible spectrum of light oscillates at frequencies between 400 and 790 THz, whereas audible sound is confined between 20 Hz and 20 kHz, and ultrasonic waves oscillate from 20 kHz up to several gigahertz. The speed of propagation is also tremendously different as evidences the always delayed thunder that comes after the lighting. While light travels at about 3×10^8 m/s in air, sound propagates approximately at 343 m/s in air and almost at 1500 m/s in water. Hence, in terms of wavelength, visible light ranges from 380 to 740 nm, whereas ultrasound involves wavelengths from a few micrometers to centimeters, and audible sound extends this range up to several meters.

Both sound and light can be exploited for measurement purposes in combination with the Doppler effect. In classical physics, this effect describes the frequency shift in-

duced in waves when the receiver and the wave source move with respect to each other. Roughly speaking, when the source and the receiver are getting closer, the Doppler shift is positive, meaning that the measured frequency is higher than the frequency originally emitted by the source. Instead, when the source and the receiver are moving apart, the measured frequency is lower. This phenomenon was originally proposed by Christian Doppler for astronomical purposes, though the first experimental results were conducted with sound waves [27]. Nowadays, the Doppler effect is exploited in a broad variety of applications. In astronomy, it is for example used to analyze how stars and galaxies move with respect to us. In fact, it has been observed that light coming from distant galaxies is in general shifted towards the red light (the so-called redshift), that is, a shift towards lower frequencies, and this is a clear evidence that the Universe is expanding, or at least it was by the time that the light was emitted. More down to earth, measurement techniques such as the RADAR (RAdio Detection And Ranging) are commonly used to track the position, direction and speed of objects such as speeding vehicles. The technique SONAR (SOund Navigation And Ranging) is analogous to RADAR, but in this case, the Doppler effect is retrieved from acoustic waves instead of radio waves. Even our hearing system uses the Doppler effect to detect moving sources, e.g., when perceiving the pitch changes of an ambulance's siren. More to the point of this thesis, the Doppler effect can also be used to characterize the acousto-optic effect, that is, the interaction between sound and light. The rest of this chapter illustrates this and discusses other fundamental aspects of this interaction.

2.1 The interaction between sound and light

2.1.1 A brief history of the acousto-optic effect

The French physicist León Brillouin was the first to predict sound-light interaction while investigating the problem of light scattering in 1922 [28]. The first experimental evidences of this interaction were to come one decade after, when Debye and Sears in America and independently Lucas and Biquard in France measured light diffraction patterns driven by high frequency sound waves [29, 30]. A general model for describing the diffraction of light by ultrasonic waves was progressively proposed by Raman and Nath in a series of articles published between 1935 and 1936 [31–36]. Raman and Nath's theory was capable of determining the angle and the intensity of each order of diffrac-

tion, when the incident light was normal or oblique to the acoustic waves [31, 32]. It also predicted that each order of diffraction underwent a Doppler shift, which could be quantified for two cases, namely for progressive and standing ultrasonic waves [33, 34]. Raman and Nath's theory was originally derived for cases where light would interact with sound along a relatively short optical path. It was however soon noticed that other diffraction patterns different from the ones predicted by Raman and Nath could occur under oblique incidence when using wider ultrasonic cells (longer optical paths of interaction), higher ultrasonic frequencies and/or higher acoustic intensities [37, 38]. Such patterns could be explained by means of the so-called Bragg's law (which was originally formulated for X-ray diffraction in 1913 [39]) and were easily identified because Bragg diffraction was much sharper, would typically include only the first order of diffraction, and could only be observed for certain angles of incidence.

After the invention of the first lasers in the 1950s, several studies reviewed the acousto-optic effect along the 1960s and, yet in the high ultrasonic frequency range, investigated its potential for laser-based applications [40–43]. It is worth noting that until that time the acousto-optic effect was only researched for characterizing the diffraction of light, or in other words, sound was used to characterize light, rather than the opposite. Besides, all theories were developed based on ultrasonic waves oscillating from a few megahertz up to several hundreds of megahertz, and the experiments were mostly conducted in liquid or solid media. Probably, the most notable application resulting from these studies on light diffraction has been the invention of the so-called acousto-optic modulator, often referred to as Bragg cell. This optical device is commonly used nowadays in optical telecommunications and interferometry, and depending on the exact design, it exploits the acousto-optic effect for deflecting, or inducing a frequency shift, or changing the intensity, phase or polarization of an incoming beam of light. In addition, with the arrival of laser technology, new optical techniques were developed for flow, vibration, stress and strain measurements. In fact, quite a few of these techniques could be used for both vibration and flow analysis, and they could also be adapted to acoustic measurements by measuring the acousto-optic effect in transparent media. This represented indeed the beginning of the acousto-optic effect as acoustic measuring principle.

The way in which the acousto-optic effect has been exploited for acoustic measurements since the 1960s has changed with the performance and availability of laser systems. In the last two decades, the acousto-optic measuring principle has been used

mainly to measure and characterize ultrasonic fields, above all in water rather than in air. A more thorough overview of optical methods in acoustics is given in Chapter 3.

2.1.2 Light as a sensing element

If light is used as a sensing element, it is important to understand what indeed influences the propagation of light, so that it makes it eligible as a measuring principle. One way to approach this is to look at the refractive index n of the medium to be investigated. Since, from an optical point of view, the refractive index describes how light propagates through the medium, the problem thus reduces to determine what parameters are susceptible to change the refractive index. For instance, in air, it has been found that the most important parameters are the static pressure, the temperature and the humidity [44–49]. However, these parameters are rather stationary, at least under standard measurement conditions, and thus, they cannot explain how light and sound interact.

In vacuum, the refractive index equals unity, in air, it is slightly above this value (about 1.0003), and in water, the refractive index is about 1.33. These three examples immediately indicate that dense media have higher refractive indices, and since the speed of light c' is inversely proportional to n, that is, $c' = c_0/n$ where c_0 is the speed of light in vacuum, light propagates more slowly in dense media. By recalling that sound propagates as pressure waves that inherently involve density fluctuations, it seems plausible that sound can potentially influence the refractive index and consequently the propagation of light. On the search for a formulation where refractive index and sound pressure meet explicitly, it is generally accepted that by regarding the propagation of sound as an adiabatic process, the relation between the refractive index and the acoustic pressure p can be described by the following first order Taylor expansion,

$$n = n_0 + \left(\frac{\partial n}{\partial p}\right)_S p, \tag{2.1}$$

where n_0 is the refractive index under static conditions, and the term $(\partial n/\partial p)_S$ is often referred to as the piezo-optic coefficient*. This linear relationship eases the use of the acousto-optic effect as a measuring principle. In the absence of sound, the refractive index equals n_0 and this value is progressively modified as the acoustic waves propa-

*The subscript S indicates a partial derivative under constant entropy, and so it denotes the propagation of sound as a reversible adiabatic process.

gate into the medium. The piezo-optic coefficient thus quantifies the coupling between sound and light. For ease of reference, in water at a temperature of $25°\mathrm{C}$ and for the wavelength of a helium-neon laser ($\lambda' = 633$ nm), the piezo-optic coefficient equals 1.444×10^{-10} Pa^{-1} [50], whereas in air at the same temperature and for the same optical wavelength, it equals 1.879×10^{-9} Pa^{-1} (see Paper B for a thorough derivation of equation (2.1), where an expression for the piezo-optic coefficient in air can be identified). Despite the fact that the piezo-optic coefficient is one order of magnitude larger in air, the acousto-optic effect is not in practice more prominent in air than in water. The measurable refractive index variations caused by the acousto-optic effect correspond to the product of the piezo-optic coefficient times the acoustic pressure, and this product is much larger in water than in air. Typical ultrasonic pressures in underwater measurements range from a few kilopascals up to a few megapascals, whereas in air they are normally below a few hundreds of pascal. It should be noted in any case that equation (2.1) is just a first order approximation, and therefore, this expression must be reconsidered when measuring beyond the weak acousto-optic interaction.

Coming back to the idea on how sound influences the speed of light, it is easy to see now that when the sound pressure increases/decreases, the density of the medium varies accordingly, and then, the light travels slower/faster. As already mentioned in the previous section, for very high ultrasonic frequencies light diffraction may occur. Indeed, at those frequencies the acoustic wavelength is very small, in general smaller than the cross-sectional area of a laser beam, and thus, the light wavefronts may not travel at the same speed. The frequency and the intensity of the acoustic field play an important role on whether the diffraction of light occurs in the Raman-Nath or the Bragg regime, but in the lower ultrasonic frequency range (larger acoustic wavelengths), light diffraction is seldom, and definitely inexistent within the audible frequency range. In fact, for audible frequencies, the acousto-optic effect can simply be modeled as a phase modulation effect, because the acoustic wavelength is much larger than the diameter of the laser beam, and thus, the light wavefronts do not get corrugated along the optical path and simply travel a bit faster or slower depending on the local sound pressure levels. This phenomenon can also be somehow understood as a Doppler effect. For instance, if the pressure along the optical path defined from the laser source up to an arbitrary position of the laser beam is increased, the light will suddenly travel slower within this portion of the optical path. This would be equivalent to saying that a receiver located at the end of this path is moving away from the laser source or vice versa. As a

result, the frequency of the modulated light is temporarily decreased. A pressure drop would instead be equivalent to the opposite situation where the source and the receiver get closer, and thus, the Doppler effect would in this case correspond to an increase in frequency of the modulated light.

Another way of using light as a sensing element is to analyze the light scattered by medium particles. An example of that is the blue color of the sky, which is a consequence of the so-called Rayleigh scattering. According to Lord Rayleigh, when the medium particles are much smaller than the wavelength λ' of light, the intensity of the scattered light is inversely proportional to λ'^4 [51]. This explains why the atmosphere scatters a greater proportion of blue light than that of red light, since the latter has a larger wavelength than the former. This is also clearly exemplified in sunsets, when the grating incidence of sunlight, forces the light to travel longer paths through the atmosphere, magnifying in this way the scattering of blue light, and thus, resulting in the characteristic reddened horizon. Despite the difficulty of measuring this kind of scattering induced by very small particles, a recent study has reported sound pressure measurements based on Rayleigh scattering [52]. However, the experimental results, which were obtained in a standing wave tube excited with a pure tone oscillating at 570.3 Hz, revealed that the laser beam used to probe the sound had to be exposed to acoustic amplitudes higher than 75 Pa in order to measure sound pressures with a precision of ± 14 Pa. This indicates that the applicability of this technique is restricted to measurement of very high sound pressure levels.

A better sensitivity can be achieved if the medium of propagation is seeded with particles that are carefully selected to ease the scattering of light. Generally, seeding particles are not smaller than the wavelength of light, they are usually at least of the order of micrometers, and this means that the resulting scattering effects cannot be described as Rayleigh scattering but rather using the so-called Lorenz-Mie scattering model where the tracer particles are treated as spheres [53]. The light scattered by seeding particles depends, among other parameters, on the particle size and composition. These will mainly define how faithfully the seeding can follow the fluctuations of the acoustic field, and thereby, how well the scattered light can represent the acoustic properties of the medium under investigation.

The acoustic information carried by the scattered light can once again be interpreted as a Doppler effect. To envision this, let us consider that the photodetector used to detect the scattered light sits next to the laser source. Then, roughly speaking, pho-

tons scattered off the tracer particles moving towards the photodetector will reach the sensor earlier than expected, and thus, the Doppler shift will increase the frequency of the photons. Instead, when the scattering particles travel away from the laser source and the photodetector, the frequency of the photons will reduce. Several optical techniques rely on the Doppler effect of light scattered in seeded media. A review as well as a discussion on the advantages and disadvantages of these methods are given in Chapter 3.

2.1.3 Twisting the nature of sound-light interaction

The previous sections have so far described how sound can scatter light, change its frequency and modulate its phase, but sound can also generate light under very extreme conditions. This phenomenon is called sonoluminescence and it occurs when a gas bubble trapped in a liquid is excited with acoustic waves that induce a cavitation process. The bubble ends up collapsing and emitting flashes of light that last for a few picoseconds [54]. The acoustic waves used to drive the sonoluminescence have usually large amplitudes of the order of tens or hundreds of kilopascals, and oscillate at a frequency slightly above 20 kHz [55, 56]. It has also been shown that the spectrum of the emitted light is dominated by ultraviolet light [54, 56].

On the other hand, beyond its sensing capabilities, light can also act as an 'acoustic' source. The lightning preceding a thunder is a manifest example of that, although it could be arguable whether there are other electric processes taking part of this natural phenomenon. Briefly, the high temperatures induced by the lightning (in the range of 24.000 K) cause a sudden expansion of air around and inside the lightning-discharge channel that yields shock waves similar to the ones encountered in explosions [57]. The generation of sound by light, commonly referred to as the photoacoustic effect, was not discovered until the early 1880s. The eminent inventor of the telephone Alexander Graham Bell, during his investigations on the transmission of speech on a beam of light which eventually led him to the invention of the 'photophone' [58], was the first to realize that sound waves could emerge from a solid sample when exposed to an intermittent beam of sunlight [59, 60]. In short, what happens is that by absorbing the intermittent light, the molecules of the material, liquid or gas under investigation are excited, leading to an increase of temperature, that eventually causes the formation of thermal and acoustic waves by local heating. This phenomenon is nowadays mostly

exploited in photoacoustic spectroscopy, which is commonly used for gas concentration analysis and monitoring [61].

2.2 Non-invasiveness of light

The most outstanding feature that makes light so unique in many areas of research is its non-invasiveness as a measuring principle. A priori, this may somehow be hard to accept since we, human beings, sense a macroscopic world ruled by Newton's laws of motion, and in particular, quoting Newton's third law "to every action there is always and equal and opposite reaction" [62]. Light can certainly interact with matter and change its properties, though the physics of that is always explained in a microscopic scale. Examples of that are the photoelectric effect, crucial for the development of quantum mechanics, and the photosynthesis, which brings every day many organisms on earth to life. As appointed in the previous section, light can even generate sound, but such a phenomenon can only occur under very extreme conditions.

In a first attempt to examine light's intrusiveness on sound measurements, it should be noted that the piezo-optic coefficient, which characterizes the coupling between optical and acoustic properties of a medium, is extremely small, e.g., of the order of 10^{-9} in air and under normal atmospheric conditions. Inspired by Newton's third law, one could tentatively estimate light's influence on sound to be of the same order of magnitude in air. While such an order of magnitude of the refractive index variations are surprisingly measurable with optical instrumentation, it is questionable that equivalent variations on the sound pressure are detectable with any acoustic transducer, especially when taking into account that the unit of pascal is nowadays realized with an uncertainty of the order of 10^{-3} in primary laboratories certified by the International Bureau of Weights and Measures (BIPM) [63].

If light causes yet any change on the properties of sound, the wave-particle duality of light gives us two different approaches for exploring such a possibility. As a wave, the electromagnetic properties of light do not offer any plausible coupling with the mechanical nature of sound, at least not under standard measurement conditions [64]. By considering the light as an ensemble of photons that travel through the acoustic field, one could in principle question the intrusiveness of photons in a similar fashion as it is done in measurements with bulky transducers or windy conditions. On the one hand, the simple presence of photons into the sound field can rapidly be discarded as a possible

source of bias since the dimensions of the photons are ridiculously smaller than any acoustic wavelength. On the other hand, one may wonder whether the momentum of the photons can actually induce changes in the medium particles that in turn can influence its acoustic properties. We may naively envision this as a drag effect on the medium particles 'similar' to the one caused by a wind stream. This approach recognizes that the momentum of the photons can exert a force on matter, a force that was actually predicted by Maxwell in 1873 [14] and confirmed experimentally by Peter Lebedew in 1901 [65]. This force is often called light pressure, and for laser sources is defined as the laser power divided by the speed of light, when the light of the laser is totally absorbed by the target. This definition immediately indicates that this force is extremely weak, e.g., it equals 3.3 pN for a common laser pointer of 1 mW. According to Ref. [66], one could actually lift a penny with light pressure, but it would take 30 billion laser pointers to do it. In conventional acoustic measurements, light is neither totally absorbed by the medium nor radiated at powers above a few milliwatts. Therefore, the influence of the momentum of the photons on the measurement of sound can also be disregarded.

As mentioned in section 2.1.2, there exist a number of optical methods that measure sound based on the light scattered off seeding particles. In this case, it is the seeding that can potentially change the properties of sound, rather than the light itself (see section 3.1.4 for further details).

All in all, it can be asserted with a high degree of confidence that the invasiveness of light on the measurement of sound is certainly negligible.

Chapter 3

Optical methods in acoustics

Besides the unique properties of light as a sensing element, optical methods also stand out for their high versatility, sensitivity and spatial resolution. This chapter emphasizes these technological-related aspects by briefly reviewing several optical methods (section 3.1), and afterwards elaborates on the two measurement principles that have been examined thoroughly during the course of the current PhD study, namely the acousto-optic measuring principle (section 3.2) and the technique photon correlation spectroscopy (section 3.3). Sections 3.2 and 3.3 serve thus as a supplement to the work presented in the articles appended at the end of the thesis. The chapter ends with a comment on the calibration of optical methods (section 3.4).

3.1 A survey of methods

3.1.1 The classics of flow visualization

Many of the optical methods used along the history of acoustics were originally developed as flow visualization techniques. The simplest of these methods is the shadowgraph [67, 68], a technique that basically requires a light source and a recording plane* where the shadow effect is captured. This effect, first reported by Robert Hooke in 1665 [69], is simply the inflection of a ray of light due to the refractive index variations of the fluid. The inflected rays cause brighter areas onto the recording plane, whereas the positions where the rays should have impinged remain darker. The intensity contrast of the resulting image provides a qualitative insight of the flow field, though this

*A photographic film in early systems; a CCD camera or an array of photodetectors in modern systems.

is not suitable enough for many applications due to the dramatic changes of refractive index required for quantitative analysis. Its lack of sophistication makes it suitable for measurements in both laboratory and open environments. In spite of its simplicity, this technique gives particularly good results for shock wave visualization.

The so-called schlieren[†] system [67, 68] is more sensitive to refractive index variations than the shadowgraph. This is achieved by intercepting some of the light deflected by the flow with a knife-edge. As can be seen in figure 3.1a, the collimated light passes through the fluid and is afterwards focused with a lens in order to form an image that is partly blocked at the focal point of the lens with a knife-edge. In case of illuminating a fluid with uniform density, the knife-edge simply reduces the brightness of the image (less light is being projected onto the recording plane), while in flows with density fluctuations, the deflected light focuses imperfectly at the focal point, meaning that some areas of the illuminated fluid are blocked by the knife-edge. This yields an image with intensity contrasts that characterizes the density gradient of the fluid in the direction perpendicular to the knife-edge.

Several studies have been endeavored to enhance the sensitivity of the schlieren method. An interesting one in acoustics was based on resonant refractivity [70]. By mixing air with an unusual gas such as sodium vapor, the refractivity of the gas could be magnified by more than one order of magnitude, thus, amplifying by the same scale factor the refractive index variations caused by acoustic waves. The study showed that conventional schlieren would require sound pressure levels of at least 143 dB re 20μPa in order to image a 1 kHz pure tone. Instead, by introducing a certain concentration of sodium vapor in air, the requirements could be lowered to 82 dB for the same pure tone, and a reduction of 20 dB per decade could be obtained with increasing frequency. Unfortunately, the inconvenience of introducing rare gases with resonant refractivity in air, often reactive and irritating, prevented the method from becoming a practical tool for sound and flow visualization.

Another alternative for improving the sensitivity of the schlieren method is to replace the knife-edge located at the focal point of the lens by a shearing element, typically a Wollaston prism [67, 68, 71]. A sketch of the optical setup is depicted in figure 3.1b. Unlike the knife-edge, the shearing element does not block any ray of

[†]Plural of the German word *schliere*, which means streak. The technique was given this name because of the visible streaks observed in transparent media due to the variations of the refractive index caused by density fluctuations.

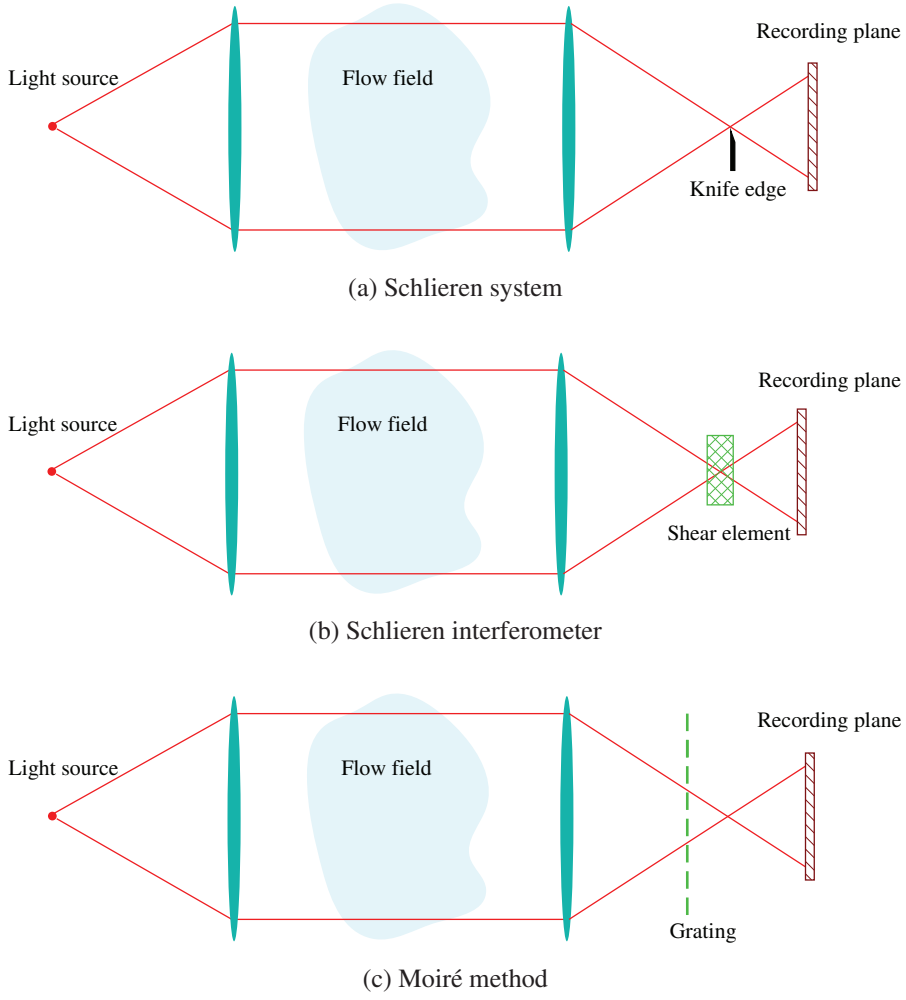

Figure 3.1: Classical optical methods for flow visualization. Note that these sketches simply pinpoint the most relevant features of each method. Real optical setups normally require the use of secondary optical components that have been omitted from the sketches for simplicity's sake. There are also several optical configurations that can be used depending on the exact application, and these are not represented here either.

light, but generates an interference pattern on the recording plane when the light is not exposed to any disturbance. This pattern serves as a reference, and the variations of this pattern observed when the light is exposed to a disturbing field provide a means to characterize density changes of the medium. Such a modified schlieren system is often referred to as schlieren interferometer. Apart from flow visualization, schlieren interferometers have also been used to characterize ultrasonic waves [72, 73].

Yet another alternative to the schlieren system is a set of techniques usually referred to as the Moiré[‡] methods [74]. There are plenty of different optical configurations, but

[‡]This term originates from the French word *moiré*, which was first used for a type of textile made of silk

the main difference with a conventional schlieren interferometer is that the reference fringe pattern is normally synthesized by placing a diffracting element such as a grating between the lens and its focal point as sketched in figure 3.1c. The grid yields an interference pattern that corresponds indeed to a Moiré pattern when a disturbance is introduced across the optical path. Moiré methods have not only been applied to study fluid dynamic, but have also been widely used to analyze vibrating structures [75, 76].

3.1.2 Interferometric techniques

Pursuing higher sensitivities, a great variety of techniques are based on optical interferometry, that is, the superposition of light exposed to a disturbance with light traveling along an homogeneous optical path that acts as a reference.[§] A classical example of this is the method called holographic (or hologram) interferometry [77, 78], a technique that represented a breakthrough in the mid 1960s, when extending Gabor's holography method [79] to the measurement of vibrating objects. The great advantage of the holographic method is that light rays impinging on the hologram at different instants of time yield interference patterns. This means that a hologram, which carries amplitude and phase information of the object under test, can be recorded while the object is vibrating. The resulting hologram is thus a fringe pattern that characterizes the vibrations captured during a certain exposure time. It should be noted that all this information is encoded into the hologram but cannot be retrieved unless the hologram is illuminated once again with the reference beam used during the recording process. A sketch of the recording and reconstruction processes are illustrated in figure 3.2. Depending on the exact methodology used to record the hologram, one can distinguish three different holographic techniques [74, 80, 81]: time-average, double exposure (or double-pulsed), and real-time holographic interferometry. The latter is often used for preliminary measurements where, for practical reasons, a quick and visual inspection is required to assess the problem. The long exposure time used in time-average holographic interferometry yields normally better interferograms suitable for quantitative analysis. Double-pulsed

with a rippled texture. Thus, the name of these techniques stems from the resemblance between interference and moiré patterns. However, strictly speaking, a moiré pattern is the superimposition of (two) patterns, not the superposition of (two) patterns that yields an interference as the ones typically encountered with physical waves.

[§]Despite the fact that some of the methods presented in the previous section 3.1.1 are also based on interferometric patterns, such patterns were, for instance, created by a shear element or a grating in the case of the schlieren interferometer or the Moiré technique, not by an independent beam of light.

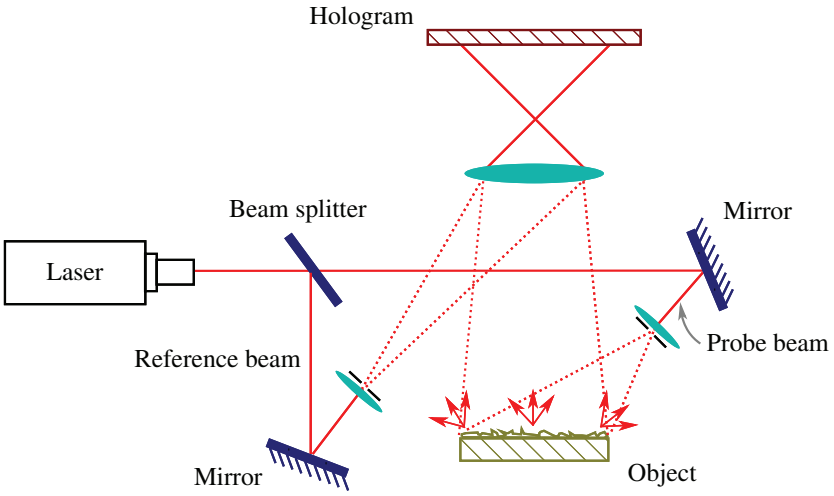

(a) Hologram synthesis

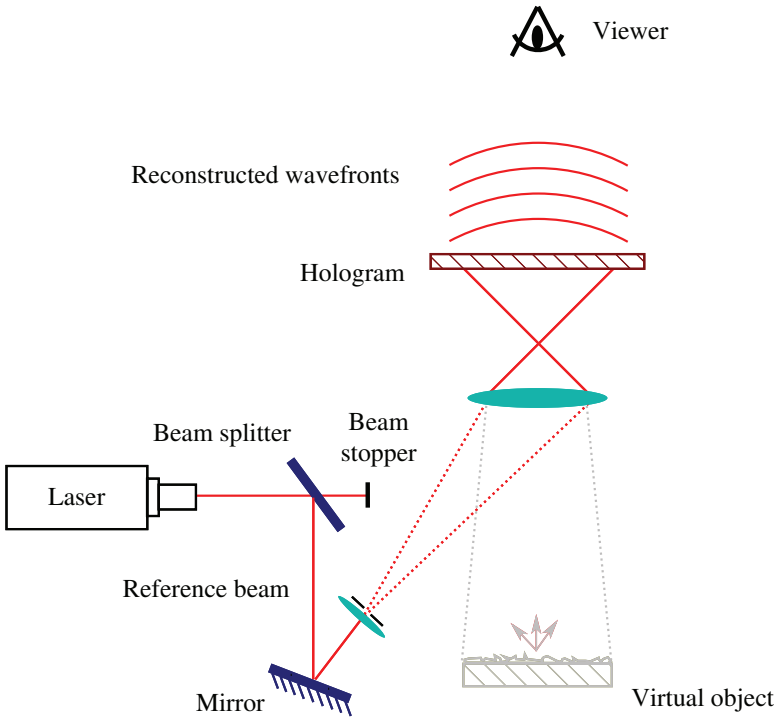

(b) Reconstruction of the hologram

Figure 3.2: Sketches of the optical setups used in holographic interferometry when recording and reconstructing the hologram. Although the hologram contains both the amplitude and phase information of the phenomenon under investigation, it cannot be interpreted directly. The hologram needs to be illuminated with the same reference beam used during the recording process in order to visualize the interferogram. Although the depicted sketches represent the optical setups used in vibration measurements, holographic interferometry can also be used to measure refractive index variations. In such a case, it is important that the probe beam is not reflected off any vibrating surface.

holographic interferometry is most adequate for deformation, stress and strain analysis as well as for capturing transient phenomena. Besides, depending on the exact configuration of the optical setup, in particular the angle between the reference and probe beams, holographic interferometry can measure either in-plane or out-plane motion.

Holographic interferometry has been used widely for vibration analysis and nondestructive testing, but from an acoustical perspective, this technique has provided a precious insight in the field of musical acoustics unraveling the vibration modes of many instruments [82]. Holographic interferometry can also sense refractive index variations in a similar fashion as the shadowgraph and schlieren methods [74, 83], and it has also been researched for sound pressure measurements [84–86].

An interferometric device that is commonly used nowadays for non-contact vibration measurements is the laser Doppler vibrometer (LDV). A sketch of its optical setup is depicted in figure 3.3. A laser beam is first split into two, but only one of the beams is sent towards the vibrating surface. The other beam serves as a reference and is normally shifted in frequency using a Bragg cell. After this frequency shift, the reference and probe beams are conveniently recombined so that they interfere. The intensity of the resulting interference is captured with a photodetector, and frequency demodulated in order to extract the Doppler shift taking place at the reflecting surface while this is vibrating. It can be shown that the instantaneous frequency $f(t)$ of the demodulated signal equals [87]

$$f(t) = f_s + \frac{2v(t)}{\lambda'}, \tag{3.1}$$

where f_s is the stationary frequency shift introduced by the Bragg cell and $v(t)$ is the velocity of the vibrating surface. Note that without the Bragg cell ($f_s = 0$), it would not be possible to retrieve the sign of $v(t)$, since the negative frequency components would automatically be mirrored to the positive part of the spectrum. Instead, with the Bragg cell, the sign is simply determined by evaluating whether the instantaneous frequency is above or below f_s. It should also be noted that an LDV measures the velocity component of the vibrating surface along the optical axis defined by the laser beam. Hence, if the laser beam is not normal to the test surface, but approaches it from a certain angle, then a correction needs to be applied.

LDV measurements present a clear advantage over classical vibration measurements based on accelerometer transducers: the contact-free principle of the LDV avoids any possible loading effect on the vibrating structure, which is in turn a common prob-

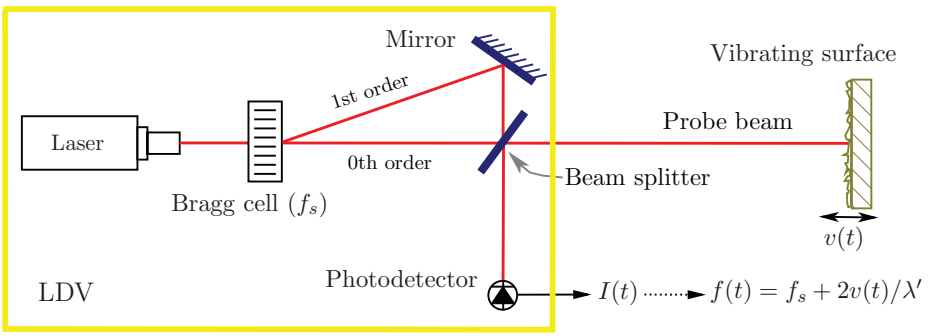

Figure 3.3: Sketch of the optical setup of an LDV. The Bragg cell introduces a frequency shift between the reference and the probe beams so that not only the amplitude of the vibrations can be inferred but also the sign. An LDV can also be used to measure refractive index variations along the probe beam. In such a case, it is important to minimize the motion of the reflecting surface.

lem for accelerometer-based measurements. As a result of this loading effect, the estimate of the resonance frequencies of the structure are biased with a frequency drift towards the low frequencies. The rising popularity of LDV systems is probably due to their versatility, broadband and dynamic ranges of analysis, as well as their compactness (at least the laser head). LDV measurements are extremely easy to set up in comparison to holographic interferometry (all the alignment between the probe and reference beams is already done inside the laser head). Although an LDV uses a single point measurement principle, there are several manufacturers providing LDV systems with scanning capabilities, the so-called scanning laser Doppler vibrometer (scanning LDV). This is basically done by incorporating a scanning mirror at the opening of the laser head that is controlled electronically by software and that makes it possible to steer the probe beam over a user-defined grid of points.

During the last decade, LDV systems have also been exploited for sound field measurements based on the acousto-optic effect. Section 3.2.2 is devoted to discuss this particular application.

3.1.3 Speckle methods

Another optical phenomenon that has been exploited broadly for acoustic and vibration measurements is the speckle pattern created when a coherent beam of light is scattered off a diffusely reflecting surface. The size of the speckles is inversely proportional to the dimensions of the optical aperture under investigation. This effect is usually not transcendent for holographic interferometry, because the measured aperture is typically

fairly large [81]. However, speckles were regarded as optical noise until the appearance of speckle-based techniques. The turning point for disregarding them as optical aberrations was to realize that speckles act as a fingerprint of the surface where the light is reflected off [88]. Hence, both macroscopic and microscopic properties of an object could be examined by analyzing the changes on the speckle pattern. There are many different procedures, e.g., based on correlation or phase modulation principles, to extract the information carried in a speckle pattern, but the technique speckle photography [74, 80] is probably the simplest of these speckle-based methods (see a sketch of the measurement principle in figure 3.4a). In this case, results are simply interpreted from an interferogram resulting from the superposition of two speckle patterns describing two different states of the object. Since the technique does not use a reference beam, the requirements for mechanical stability are far less strict than those for holographic interferometry. This made speckle photography very attractive for the industry, though the trade-off for such a simple optical setup was a moderate sensitivity compared to holographic interferometry.

Speckle interferometry [74, 80] enhances the sensitivity to levels comparable to that of holographic interferometry by creating an interference between the speckle pattern and a reference beam/wavefront at the recording plane, see figure 3.4b. The increased sensitivity of speckle interferometry with respect to speckle photography can be understood considering the case where the object is moving in the horizontal axial direction. In such a case, the speckle distribution remains the same as it is not translated over the recording plate. It is in fact the phase of the light reflected off the object that carries information about the object's motion, not its intensity, and this can only be detected if a reference beam, whose optical path is not perturbed, is present. This example also points out that speckle photography is adequate for in-plane motion measurements rather than out-of-plane. On the other hand, similarly to holographic interferometry, speckle pattern interferometry methods, can adapt their sensitivity to both in-plane and out-of-plane motion by changing the configuration of the object's illumination. In fact, speckle interferometry is sometimes considered as an offshoot of holographic interferometry due to their resemblance.

In the 1970s, a series of techniques were developed based on speckle interferometry and television (TV) systems, e.g., electronic speckle pattern interferometry (ESPI) [91–94], sometimes also referred to as TV holography. The great advantage of these methods was that no photographic material was involved in the recording process, and thus,

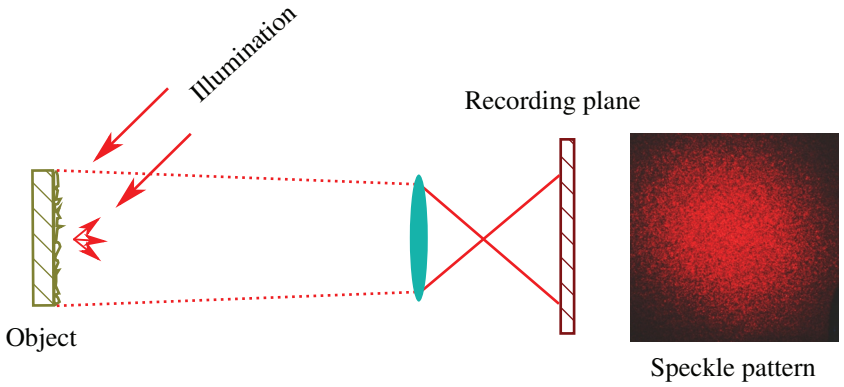

(a) Speckle photography

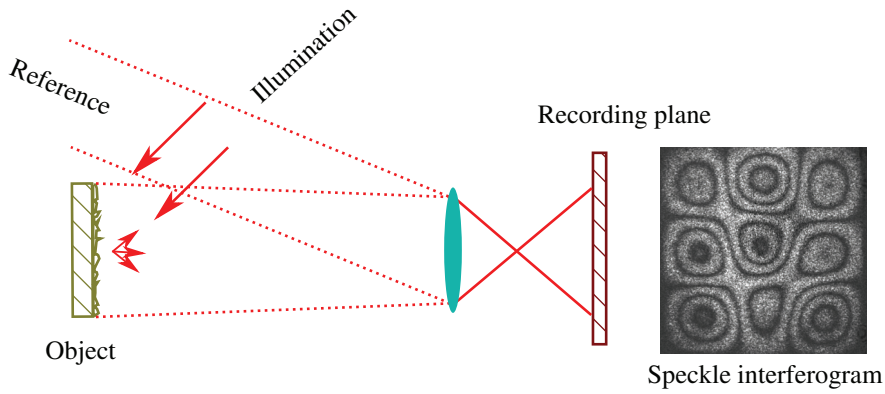

(b) Speckle interferometry

Figure 3.4: Sketches of the optical setups used in speckle photography and speckle interferometry. The roughness of the reflecting surface causes mutual interference of a set of wavefronts reflected off different parts of the reflecting object. The speckle patterns are taken from [89, 90].

all the tedious and time-consuming tasks related to that, e.g., development of the films, could be avoided. Instead, with these techniques, the light was recorded with a video camera that transferred the data to a video recording system, where the data were stored as television images. Then, an interferogram could be synthesized by subtracting two images at a time, and a full-wave rectification of the signal was performed to accommodate the interferogram to a TV system. The resulting dark fringes identified areas of the object where the measured physical quantity was unchanged, whereas the bright and speckled fringes corresponded to parts of the object that had been altered. Note that the interferograms were updated at usual TV rates (25-30 images per second), which was a tremendous advance in comparison with the time required to process the data with

the classical photographic films. Later, with the arrival of the digital era in the 1980s, some of these techniques were progressively upgraded with digital technology [95–98], in some cases giving raise to a new generation of methods, e.g., ESPI was renamed to digital speckle pattern interferometry (DSPI). The research on speckle pattern interferometry, including the one based on TV systems, has been focused mainly on static and dynamic measurement of structures. However, some studies have also been devoted to vibration analysis of musical instruments [99, 100] and to sound pressure measurements based on the acousto-optic effect [101–106].

3.1.4 Tracer methods

The methods described until now infer properties of an object or medium by analyzing either the light reflected off a surface or the changes of refractive index of the medium. There is though a set of optical techniques broadly used nowadays in flow measurements that extract information from the medium based on light scattered off tracer particles conveniently inserted into the medium. Several features of the seeding particles can enhance the strength of the scattered light, e.g., their size, shape and refractive index as well as their concentration and distribution over the measuring volume/area. Selecting the optimal seeding is thus critical: the seeding particles must be large enough to scatter sufficient light but small enough to follow the motion of the medium faithfully without changing its properties [107]. While this can normally be achieved in liquid fluids by matching the density of the seeding particles with that of the fluid, the situation is quite different in gaseous fluids such as the air. Out of these tracer methods, laser Doppler anemometry (LDA) and particle image velocimetry (PIV) are probably two of the most researched methods in fluid dynamics. On the one hand, the LDA method, which is also referred to as laser Doppler velocimetry[¶], is a single point measurement technique that measures the velocity at the intersection of two laser beams [108]. The velocity is measured in the direction perpendicular to the bisector of the beams. The interference of the beams yields a fringe pattern in a very small measuring volume, which has the shape of an ellipsoid. Particles crossing the volume with a certain velocity scatter photons that can be measured with a photodetector. As the particle translates through the dark and bright areas of the fringe pattern the photodetector generates an

[¶]Also abbreviated as LDV, but not to be confused in this context with laser Doppler vibrometer. In the present manuscript, the abbreviation LDV is only used for laser Doppler vibrometer.

electric current that fluctuates accordingly, see figure 3.5. As discussed in section 2.1.2,

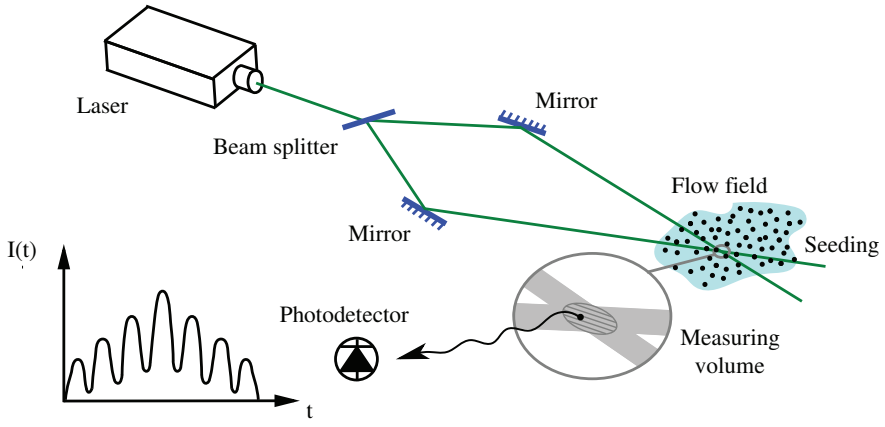

Figure 3.5: Conventional LDA systems measure a certain velocity component by crossing two laser beams at the position of the medium under investigation. The plot shown next to the photodetector illustrates a typical intensity profile of the scattered photons when a seeding particle travels through the measuring volume. If no frequency shift is introduced between the two beam, it is only possible to retrieved the amplitude of the velocity, but not its direction.

when light is scattered off seeding particles, a Doppler effect takes place. The velocity component that is normal to the bisector of the interfering beams can then be realized by demodulating the Doppler shift of the scattered photons. Similarly to a vibrometer, when the interfering beams have the same frequency, it is only possible to resolve the absolute value of the velocity. Again, the sign ambiguity can be overcome by means of an acousto-optic modulator, e.g., a Bragg cell, that introduces a frequency shift between the two beams.

In flow measurements, the estimated velocity will vary from sample to sample, and thus, the measured data need to be treated statistically in order to extract flow properties such as the mean flow velocity. In acoustic measurements, the tracer particles move in consonance with the acoustic field, which means that they oscillate more or less back and forth, in and out, and through the measuring volume. Depending on the amplitude and the frequency of the oscillations, it can even be that the particle remains inside the probe volume without crossing any fringes until a reminiscent mean flow or the gravity drags the particle out of the volume. This often limits the frequency range of analysis and, in order to ensure that the tracer particles cross a sufficient number of fringes, measurements must be conducted at relatively high sound pressure levels. In any case, the resulting electric current of the photodetector is not easy to interpret, and

as a result, acoustic measurements require more sophisticated processing techniques that those used in conventional LDA measurements [109, 110].

Although LDA was originally conceived for flow measurements in 1964 [111], acoustic measurements started to proliferate in the late 1970s and beginning of the 1980s [112, 113]. The potential of this technique in acoustics was quite substantial, since the lack of proper velocity transducers at that time made particle velocity measurements far more complicated than pressure measurements. However, technical challenges such as the need for seeding as well as the development of new velocity transducers for industrial applications have refrained LDA from becoming a useful acoustic measurement technique beyond laboratory environments. Recent studies have though shown that measurements can be conducted under very low concentration of seeding when the scattered photons are analyzed by means of their autocorrelation function [114–116]. While such a reduced concentration of seeding does not yet qualify the technique for industrial applications, it certainly relaxes the constraints arising from the use of seeding in acoustic metrology. This modified version of the LDA technique is referred to as photon correlation spectroscopy (PCS) and is further examined in section 3.3.

Unlike LDA, PIV is suited to velocity measurements over a large area. In this case, the tracer particles are illuminated with a laser sheet and the scattered photons are captured with a CCD camera, see figure 3.6. With this technique, the amount of seeding is such that individual particles can be identified in each frame captured with the CCD camera. Hence, by knowing accurately enough the frame rate, the in-plane velocity can be determined by cross-correlating two consecutive frames. Out-of-plane velocity measurements are also possible with stereoscopic PIV [117], that is, by imaging the seeding particles with two cameras located at different positions. This makes it possible to reconstruct the 3D velocity components from 2D velocity measurements taken from two different perspectives.

As for LDA measurements, PIV was originally developed for flow measurements, and it also requires more sophisticated signal processing for extracting the small particle velocities usually encountered in acoustic measurements [118, 119]. Choosing the optimal seeding is also crucial [120]. Furthermore, since the measurement is performed over an area instead of a single point, significant amounts of seeding are required, which can potentially change the properties of the medium (in particular air), and the seeding needs to be more or less uniformly distributed. The laser sheet thickness plays an im-

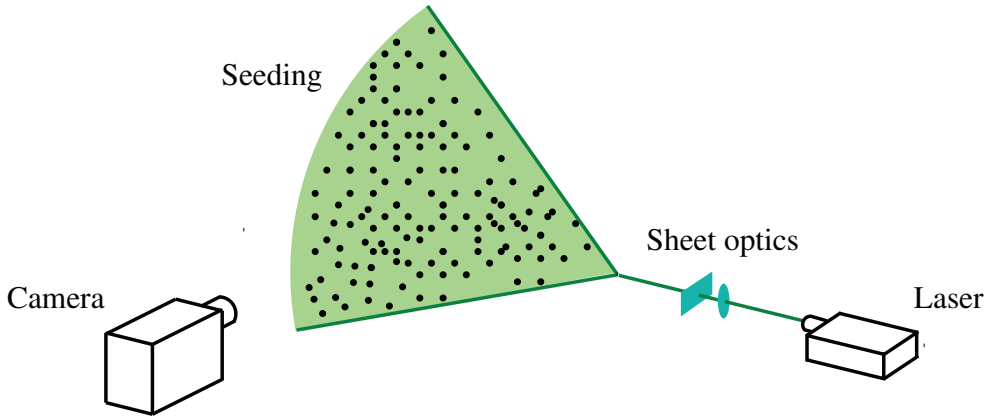

Figure 3.6: Conventional PIV systems image the in-plane velocity components by capturing with a CCD camera the light scattered off seeding particles that cross a laser sheet.

portant role as well. If it is not thin enough, the resulting velocities are averaged over the depth of the illumination sheet. The size of the tracer particles as well as the number of pixels and the field of view of the camera determine the spatial resolution of the PIV measurement. For many years, many applications were constrained by the fact that the existing cameras were not fast enough to sample the acoustic field. Nowadays, high speed cameras capable of capturing massive amounts of information have emerged so that the bottleneck is normally the transfer of data from the camera to the corresponding analyzer.

In air, both LDA and PIV are nowadays restricted to acoustic measurements within the lower audible frequency range, say below 5 or 10 kHz, and to rather high sound pressure levels, typically clearly above 100 dB re 20μPa. In addition, research is currently focused on measurements where the acoustic particle velocity needs to be decoupled from a mean flow velocity [121].

3.1.5 Optical microphones

Optics has also come into the development of new microphone transducers. The majority though keep the moving element that senses the sound, e.g., a membrane, and simply replace the electronics that transform the vibrations of the membrane into an electrical signal, e.g., a condenser, with a fiber optic sensor. The working principle of fiber optic microphones is based on optical modulation mechanisms, that is, the acoustic pressure is realized by analyzing the modulation induced in a beam of light when the membrane

vibrates. The type of modulation effect depends on the used fiber optic technology. For instance, intensity modulated fiber optic microphones [122] are the simplest, but also have the lowest sensitivity. In this case, a fiber simply guides the light from the laser source to the probe where the light is directed towards the rear side of the membrane with a certain angle. When sound waves impinge on the membrane, the light reflected off is modulated in intensity, and coupled to another fiber that transmits the light to a photodetector for further signal processing.

Alternatively, phase modulated fiber optic microphones exhibit higher sensitivities by guiding the light through fibers arranged according to an interferometric scheme, e.g., the Michelson or the Fabry-Perot interferometer [123, 124]. In this type of configuration, the acoustically excited membrane modulates the phase of the light used to probe the membrane, and this can be used to realize the acoustic pressure.

Another interesting possibility is to attach the membrane of the microphone to a fiber Bragg grating[‖]. Fiber Bragg grating microphones realize sound pressure by measuring the optical wavelength shift caused by the Bragg grating when the fiber is stretch or compressed due to the motion of the membrane [125].

In any case, fiber optic microphones carry on the same fundamental inconveniences given for conventional microphones. The fact that the sensor consists of a mechanical element implies that the response of the microphone drops at high frequencies due to resonances on the membrane that lead to non-uniform displacements. The area of the membrane can be reduced in order to shift the resonances towards higher frequencies, but this normally stiffens the membrane and consequently reduces the sensitivity of the microphone. Changing the material of the membrane for a softer one can enhance the sensitivity, but at the same time, it can also lower the resonance frequencies of the membrane. In order to circumvent these problems, membrane-free optical microphones have also been researched. An example of this is a newly developed optical transducer that is based on a Fabry-Perot etalon [126]. In short, by embedding a Fabry-Perot interferometer in a small, open cavity, a laser beam can be used directly as a sensing element, capturing indeed the acousto-optic effect. The multiple beam interference created by the Fabry-Perot interferometer provides a highly sensitive acoustic sensor. However, the cavity where the light is exposed to the sound field may cause acoustic resonances

[‖]Not to confuse with a Bragg cell. A fiber Bragg grating is introduced in a short segment of an optical fiber in order to reflect specific optical wavelengths inside the fiber. This effect is created by introducing periodic variations of the refractive index in the fiber core.

at high frequencies, that is, when the wavelength of the sound waves is comparable to or smaller than the dimensions of the cavity. Since the pressure is assumed to be constant inside the cavity, these acoustic resonances can bias the estimate of the pressure in a similar manner as the scattering caused by the membrane of conventional microphones. Therefore, accurate measurements still require a frequency response correction that accounts for this effect.

Another interesting optical transducer without membrane that has been recently reported exploits the optical principle of total internal reflection [127, 128]. In this design, the sound waves impinge on a sensor made of glass with a cylindrical surface. At the same time, a laser beam gets internally reflected at the boundary between the glass and the air. The pressure fluctuations induced by the acoustic waves on the surface of the sensor change the refractive index of the glass, and this affects the amount of light that is totally reflected at the cylindrical surface of the sensor. This intensity variation can be used to realize the acoustic pressure. Although this line of research seems to be in a preliminary stage, the studies reveal that the sensitivity of such a microphone is low, which limits its use to high sound pressure measurements. As for any other microphone, scattering effects caused by the immersion of this transducer into the sound field is also an issue at high frequencies.

Optical microphones are being progressively deployed in many acoustic applications. The absence of electrical components in their design makes them immune to electromagnetic interference, and thus suitable for measurements in electrically hazardous environments. It should be noted that unlike conventional microphones, optical microphones are not reciprocal, that is, they can only act as receivers, but they cannot radiate sound. This poses some restrictions when calibrating this type of microphones using reciprocity techniques [129, 130].

3.2 Acousto-optic measuring principle

3.2.1 Refractive index measurement

The previous section has reviewed various means of using light for flow, vibration and acoustic measurements. Several techniques exploit the light scattered off moving surfaces to assess mechanical vibrations in a non-contact manner. Some of them do that by measuring the intensity variations of the scattered light, but the majority employ inter-

ferometric principles to measure the phase of the scattered light, increasing in this way the sensitivity of the measurement.

If properties about a medium, not an object, have to be determined, techniques such as LDA and PIV use seeding particles as 'reflecting objects' that scatter light and provide, in this way, information about the motion of the medium. The difficulties arising from the use of seeding have already been mentioned in section 3.1.4. Alternatively, other optical techniques, including most of the interferometric methods, are capable of determining properties of the medium by measuring refractive index variations. Such refractive index fluctuations can change either the direction of propagation or the speed of light, or a combination of both. Thus, roughly speaking, light accumulates information about the medium while traveling through it. The exact properties of the medium that can be extracted will depend on the measurement technique. Table 3.1 illustrates this for a simple case where light originally propagates parallel to the horizontal direction denoted as x. The integral symbols stated on the third column connote the idea

Table 3.1: The refractive index variation captured when light travels through a transparent medium depend on the measurement technique.

Technique	Key feature	Relation with refractive index
Shadowgraph	Intensity contrast	$\int \frac{\partial^2 n}{\partial y^2} \mathrm{d}x$
Schlieren	Intensity contrast	$\int \frac{\partial n}{\partial y} \mathrm{d}x$
Moiré	Fringe pattern	
Speckle photography	Speckle pattern	
Schlieren interferometry	Fringe pattern	
Holographic interferometry	Fringe pattern	$\int n \mathrm{d}x$
TV Holography	Fringe pattern	
LDV	Phase shift	

that light accumulates information along its propagation. Although the shadowgraph and the schlieren techniques sense the second and first derivative of the refractive index respectively, they simply capture streaks of light caused by medium fluctuations, and these streaks only cause intensity contrasts on the recording plane.

Moiré and schlieren interferometry measure the first derivative of the refractive index, and it is important to bear in mind that their optical setups promote the interference of light by means of gratings or shear elements (recall figure 3.1), even in the absence of disturbing fields. Hence, the recording plane always captures a fringe pattern, the vari-

ations of which provide information about the medium. Speckle photography analyzes instead the changes of a speckle pattern, which is in fact an intensity pattern. Thus, the variations of this pattern observed when light is deflected by a disturbing field, provide information about the first derivative of the refractive index.

Finally, the last three methods are purely interferometric, that is, they all base their observations relative to a reference beam. The main difference among them is that an LDV measures at a single point, whereas holographic interferometry and TV holography measure over an aperture. As a result, the output of an LDV is a frequency modulated signal whose Doppler effect characterizes the line integral of the refractive index, whereas the other two methods measure the phase shifts of the same integral over an aperture, and these phase shifts are detected in form of fringe patterns.

In principle, any of these optical methods could measure the acousto-optic effect. It would only require to insert equation (2.1), which states the relation between the refractive index and the acoustic pressure, into the integral expressions defined in table 3.1. In practice, it is the sensitivity of the methods, which eventually rely on the optical setups, that determines whether this is feasible or not. As mentioned previously, the interferometric methods that use a reference beam/wavefront tend to render higher sensitivities, and thus, they are normally better qualified to measure the acousto-optic effect. We can thereby define the acousto-optic measuring principle as the spatial integral of the refractive index performed by light waves traveling through an acoustic field.

The following two sections elaborate on various aspects of the acousto-optic measuring principle when implemented with an LDV. The technique of measuring the acousto-optic effect with an LDV is sometimes generically referred to as refracto-vibrometry [131–133]. An LDV-based technique is preferred over other interferometric techniques due to the simplicity, robustness and versatility of the existing LDV systems.

3.2.2 Sound pressure measurement using laser Doppler vibrometry

Fundamental ideas

It can be shown that the phase of a laser beam that travels from the sensor head of an LDV to a target where the light is reflected off equals to the integral of the refractive index along the optical path **L** followed by the light (see Paper B for further details),

$$\phi(t) = k_0 \int_{\mathbf{L}} n \, \mathrm{d}l, \tag{3.2}$$

where k_0 is the wavenumber of the light in vacuum. By inserting the relation between the refractive index and the sound pressure p stated in equation (2.1),

$$\phi(t) = k_0 \int_{\mathbf{L}} \left(n_0 + \left(\frac{\partial n}{\partial p} \right)_S p \right) \, \mathrm{d}l = k_0 n_0 \left(\int_{\mathbf{L}} \mathrm{d}l + \frac{1}{n_0} \left(\frac{\partial n}{\partial p} \right)_S \int_{\mathbf{L}} p \, \mathrm{d}l \right), \quad (3.3)$$

where n_0 and the piezo-optic coefficient $(\partial n/\partial p)_S$ are regarded to be constant during the integration process. The first integral of the previous equation corresponds simply to the physical distance $L(t)$ traveled by the beam, where the time dependence accounts for the possible vibrations of the target, that is,

$$L(t) = L_0 + l(t), \quad (3.4)$$

where L_0 is the distance existing between the LDV and the target in the absence of any kind of disturbance, and $l(t)$ is the displacement of the target. The second integral in equation (3.3) contains the information about the acousto-optic effect. The velocity measured by the LDV can then be calculated as follows,

$$\begin{aligned} v_{\mathrm{LDV}}(t) &= \frac{1}{k_0 n_0} \frac{\mathrm{d}\phi(t)}{\mathrm{d}t} \\ &= \frac{\mathrm{d}L(t)}{\mathrm{d}t} + \frac{1}{n_0} \left(\frac{\partial n}{\partial p} \right)_S \frac{\mathrm{d}}{\mathrm{d}t} \left(\int_{\mathbf{L}} p \, \mathrm{d}l \right) \\ &= \frac{\mathrm{d}l(t)}{\mathrm{d}t} + \frac{1}{n_0} \left(\frac{\partial n}{\partial p} \right)_S \frac{\mathrm{d}}{\mathrm{d}t} \left(\int_{\mathbf{L}} p \, \mathrm{d}l \right) \\ &= v_{\mathrm{mec}}(t) + v_{\mathrm{ao}}(t), \end{aligned} \quad (3.5)$$

where $v_{\mathrm{mec}}(t)$ is the mechanical velocity of the target point where the light is reflected off, and $v_{\mathrm{ao}}(t)$ is the apparent velocity caused by the acousto-optic effect. Note that in the absence of sound ($p = 0$), the velocity of the LDV reduces to $v_{\mathrm{mec}}(t)$, which is indeed the original purpose of an LDV, that is, to measure mechanical vibrations. Instead, when the reflecting target is motionless ($l(t) = 0$), the output of the vibrometer is capable of capturing the acousto-optic effect along the laser beam,

$$v_{\mathrm{LDV}}(t) = v_{\mathrm{ao}}(t) = \frac{1}{n_0} \left(\frac{\partial n}{\partial p} \right)_S \frac{\mathrm{d}}{\mathrm{d}t} \left(\int_{\mathbf{L}} p \, \mathrm{d}l \right). \quad (3.6)$$

Measuring in practice

Equation (3.5) reflects one of the main challenges in measuring the acousto-optic effect with an LDV: the mechanical vibration of the reflecting point. Such vibrations can either stem from structural vibrations caused by activities unrelated to the experiment or be induced by the actual sound field under investigation. In any case, it is desirable to design the measurement setup so that these vibrations are avoided or reduced to negligible levels with respect to $v_{\text{ao}}(t)$. This is of course not necessarily an easy task, particularly at low frequencies. In the worse case scenario where the mechanical vibrations cannot be mitigated, one can alternatively isolate the contribution of the acousto-optic effect by monitoring the mechanical vibrations of the reflecting point with, for instance, an accelerometer,

$$v_{\text{ao}}(t) \cong v_{\text{LDV}}(t) - v_{\text{mec}}(t), \tag{3.7}$$

where $v_{\text{mec}}(t)$ represents here the mechanical vibrations of the target point sensed with an accelerometer. Despite the simplicity of this compensation method, it should be noted that the accelerometer, as a transducer, has a frequency response that needs to be accounted for before estimating the apparent velocity of the acousto-optic effect. This typically requires a careful calibration of the transducer.

Alternatively, time-selective techniques can also help in some cases to decouple the acousto-optic effect from mechanical vibrations. In a measurement setup expressly design to measure the acousto-optic effect, the sound waves will generally influence the propagation of the laser beam first and reach the surface where the light is reflected off afterwards. This is particularly simple to exploit in ultrasonic measurements, where the short ultrasonic pulses typically used in these type measurements can be easily resolved in time.

Acousto-optic bias

The acousto-optic effect can in principle bias the mechanical velocity measured with an LDV. This can potentially happen when the laser beam is exposed to a sufficiently intense sound field during its excursion from the laser head to the target surface under investigation. This effect is however not likely to be significant in airborne sound measurements within the audible frequency range. To illustrate it, let us consider a very simple case where a set of plane waves travel perpendicularly to the laser beam. In such

a situation where the wavefronts of the sound waves are parallel to the laser beam, the acoustic pressure along the beam can be written as

$$p = A\sin(\omega t + \varphi_0), \tag{3.8}$$

where A and ω are the amplitude and the angular frequency of the plane waves, and φ_0 is the initial phase at $t = 0$. For ease of simplicity, let us also assume that the target where the laser beam is reflected off is completely motionless. The apparent velocity of the LDV is then

$$\begin{aligned} v_{\text{ao}}(t) &= \frac{1}{n_0}\left(\frac{\partial n}{\partial p}\right)_S \frac{\mathrm{d}}{\mathrm{d}t}\left(\int_0^{L_0} A\sin(\omega t + \varphi_0)\,\mathrm{d}l\right) \\ &= -\frac{L_0}{n_0}\left(\frac{\partial n}{\partial p}\right)_S A\omega\cos(\omega t + \varphi_0), \end{aligned} \tag{3.9}$$

and the corresponding root mean square (rms) value is

$$v_{\text{ao,rms}} = \frac{\omega L_0}{n_0}\left(\frac{\partial n}{\partial p}\right)_S \frac{A}{\sqrt{2}} = \frac{\omega L_0}{n_0}\left(\frac{\partial n}{\partial p}\right)_S p_{\text{rms}}, \tag{3.10}$$

where p_{rms} is the rms pressure of the plane waves. From this expression, it is possible to have a rough estimate of the sound pressure level required in order to have an apparent velocity of a certain order of magnitude. For example, in air, under standard atmospheric conditions, and for a beam of light of 1 m of length, a sound pressure level of about 130 dB re 20μPa at 1 kHz would lead to an apparent velocity of the order of 10^{-3} m/s. For the same order of magnitude, a more general overview of sound pressure levels required within the audible frequency range and for different beam lengths can be seen in figure 3.7a. In addition, the levels required for a 1 m long beam in order to obtain apparent velocities of different orders of magnitude is shown in figure 3.7b. Although these results correspond to a very simple and probably unrealistic case where the influence of the acousto-optic effect is boosted by the geometry of the problem (the wavefronts of the acoustic waves are parallel to the laser beam), it provides a first insight into the possible influence of the acousto-optic effect on vibration measurements. From these figures, one can conclude that under such an idealized situation, very loud sounds could potentially lead to an apparent velocity with an order of magnitude comparable to that of a conventional vibration measurement, that is, in the range of 10^{-2}

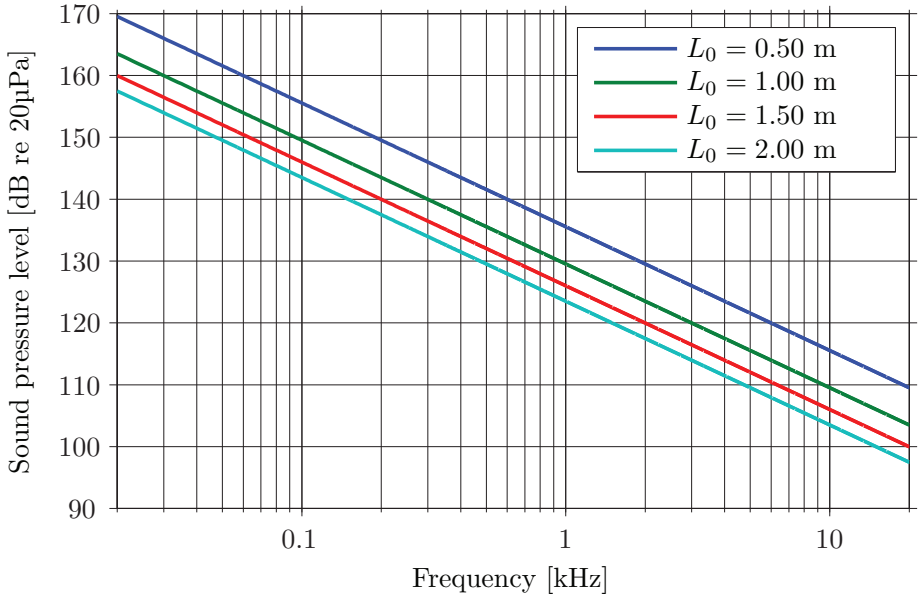

(a) Sound pressure levels causing an apparent velocity $v_{\text{ao,rms}} \propto 10^{-3}$ m/s for different laser beam lengths.

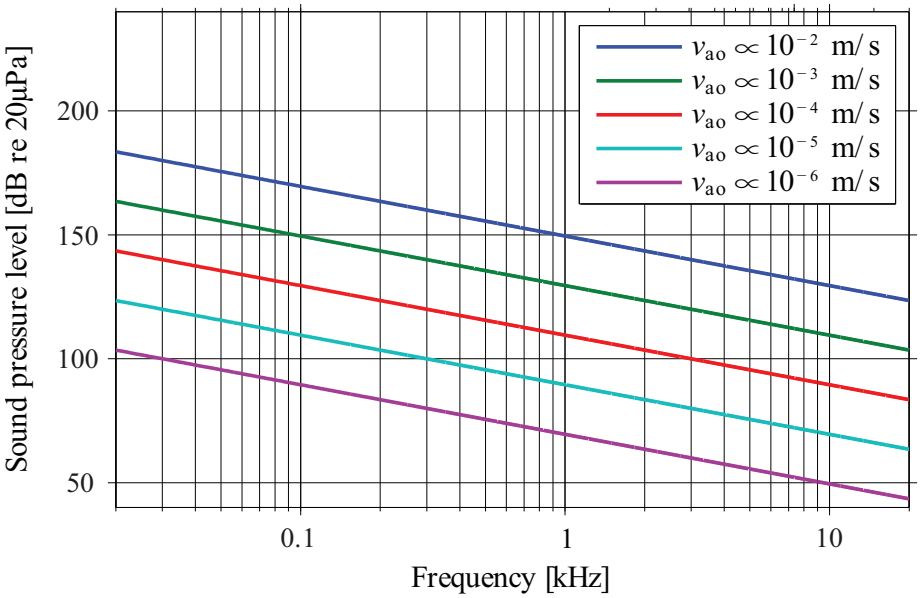

(b) Sound pressure levels required in order to induce different apparent velocities $v_{\text{ao,rms}}$ when measuring with a 1 m long laser beam ($L_0 = 1$ m).

Figure 3.7: Sound pressure levels causing an apparent velocity at the output of the LDV that is comparable to amplitudes commonly measured in vibration measurements. In this simulations, the wavefronts of the acoustic waves are parallel to the laser beam.

to 10^{-4} m/s approximately. It is also interesting to note that the acousto-optic effect requires lower sound pressure levels at higher frequencies in order to produce apparent velocities of the same order as the ones induced at lower frequencies. In a more realistic case though, the laser beam is probably exposed to sound waves emerging from the structure aimed by the LDV. Then, the pressure integrated by the laser beam is not constant along the optical path and tends to cancel out, at least partially, when integrating over several acoustic wavelengths. Hence, much higher sound pressure levels than the ones estimated in figure 3.7 are required in order to achieve the same apparent velocities in more realistic measurement scenarios.

The situation in underwater acoustics is substantially different. The acoustic pressures encountered in liquid media such as water, are normally much higher than those normally achieved in airborne sound pressure measurements. This means that the acousto-optic effect is normally more prominent in underwater measurements. In fact, there are several studies that investigate the bias introduced by the acousto-optic effect in optical measurements where light is used as a sensing element without exploiting the acousto-optic effect, namely for LDA measurements [134–136] and for vibration measurements based on LDV [137–143]. Briefly, the conclusions from the studies related to LDA measurements state that the bias introduced by the acousto-optic effect is not negligible when the sound waves approach the laser beams from the sides. The effect is also significant at high acoustic frequencies. This agrees very well with the conclusions extracted from the theoretical study discussed in the previous paragraph. For LDV measurements, the acousto-optic effect is also found to be notable when measuring vibration and directivity patterns of ultrasound transducers. In this case, the main source of acousto-optic bias stems from edge waves emerging from the radiating transducer.

Exploring the limits of the current technology

Assuming that the velocity output of an LDV is free of contributions from mechanical vibrations, it is worth investigating what would then be the minimum pressure that is measurable with an LDV. There is unfortunately no straight answer to this query, because an LDV does not measure the pressure at a single point, but it rather integrates the pressure along the optical path followed by the laser beam. We might however shed some light into the matter if we consider again the example of plane waves traveling perpendicularly to the laser beam.

In the absence of mechanical vibrations, the minimum measurable pressure is limited by the internal noise of the LDV. Figure 3.8 shows the background noise spectrum inherent in three different LDV systems, when they are set up at their corresponding highest sensitivities. The measurements were carried out within the audible frequency range, because the sound pressure levels in this range are substantially lower than those typically encountered in ultrasonic and underwater measurements. This means that the acousto-optic effect is more difficult to detect in these frequencies.

The three LDV systems examined for this comparison represent three different generations of LDV systems. The *PDV 100* is a standalone laser head LDV, the *OFV-505* system consist of a laser head and a separate controller unit where a range of velocity decoders are available (for this comparison, the velocity decoder *VD-02* was selected), and the PSV-400 system is a scanning LDV (the velocity decoder *VD-06* was chosen for this experiment). In order to make the comparison as fair as possible, all the demodulated signals from the LDVs were acquired with the same external sound card, avoiding in this way any possible difference in signal acquisition and processing applied by the available commercial hardware/software of the respective systems. The laser beams were approximately set to travel a 1 m distance in all the measurements.

As can be seen in figure 3.8, the three systems present different background noise levels, which denotes the different technologies embedded into each system. Surprisingly, although the *PDV 100* system is the oldest of the vibrometers under test, it presents the lowest overall levels, meaning that it is potentially more sensitive to the acousto-optic effect. The scanning LDV presents some unexpected resonances caused by internal noise, but it has the lowest levels of noise between 6 and 10 kHz and from 12 to 18 kHz. The LDV *OFV-505* lies somehow in between.

These curves represent the minimum apparent velocities that can be detected. The minimum measurable pressures can then be estimated using equation (3.10) from page 36, which corresponds to the plane wave case studied previously. The results obtained when inserting the background noise levels measured with the highest sensitivity of each of the vibrometers are depicted in figure 3.9. It should be noted at this point that the pressures estimated in figure 3.9 would induce an apparent velocity at the output of the LDV with approximately the same energy as the internal noise of the vibrometer, meaning that the apparent velocity caused by the acousto-optic effect would be measured with a signal-to-noise ratio (SNR) of about 0 dB. Despite the fact that the vibrometers are not designed to measure the acousto-optic effect, the pressures estimated

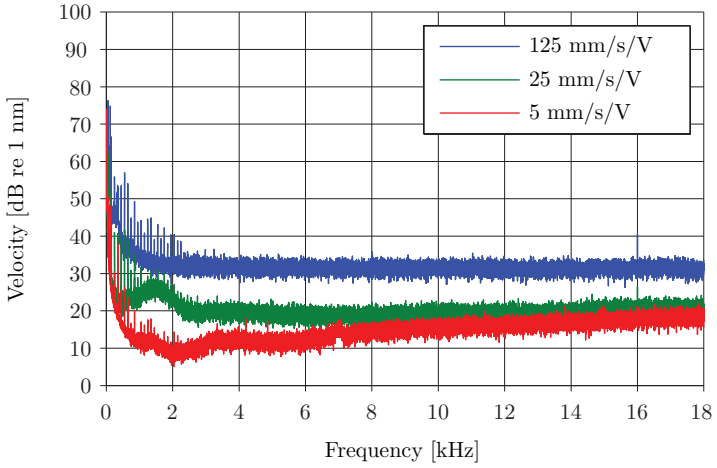

(a) PDV 100

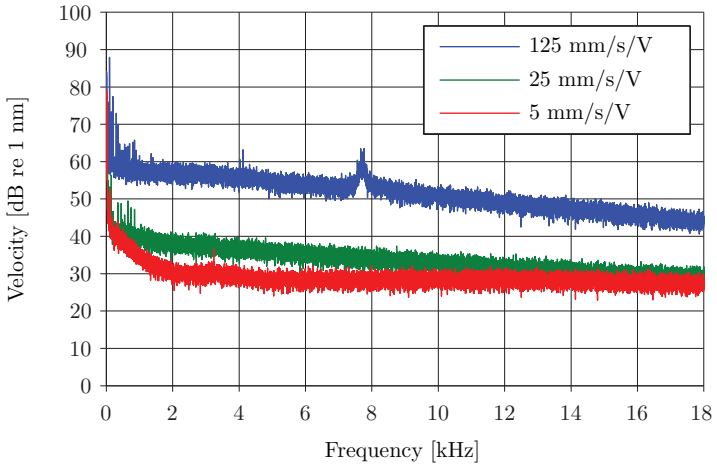

(b) OFV-505 VD02

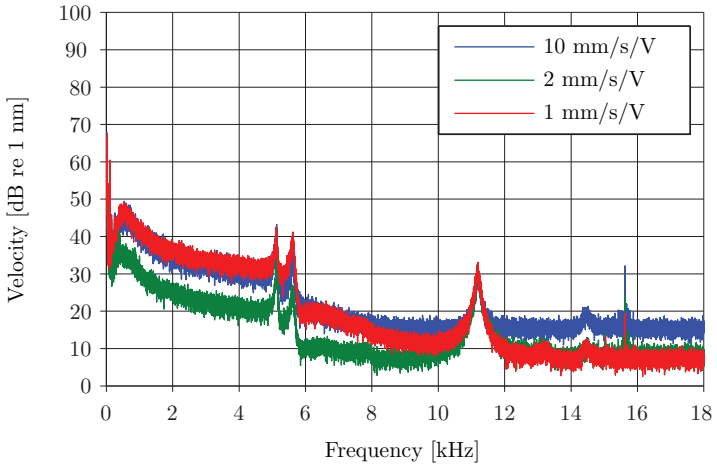

(c) PSV-400 VD-06

Figure 3.8: Background noise spectrum of three different LDV systems. In order to obtain a clearer representation of the background noise spectrum, each of the presented curves were averaged over 16 independent magnitude spectra. Each panel shows the results obtained with the three highest sensitivities of the LDV systems under test. The laser beam was approximately 1 m long.

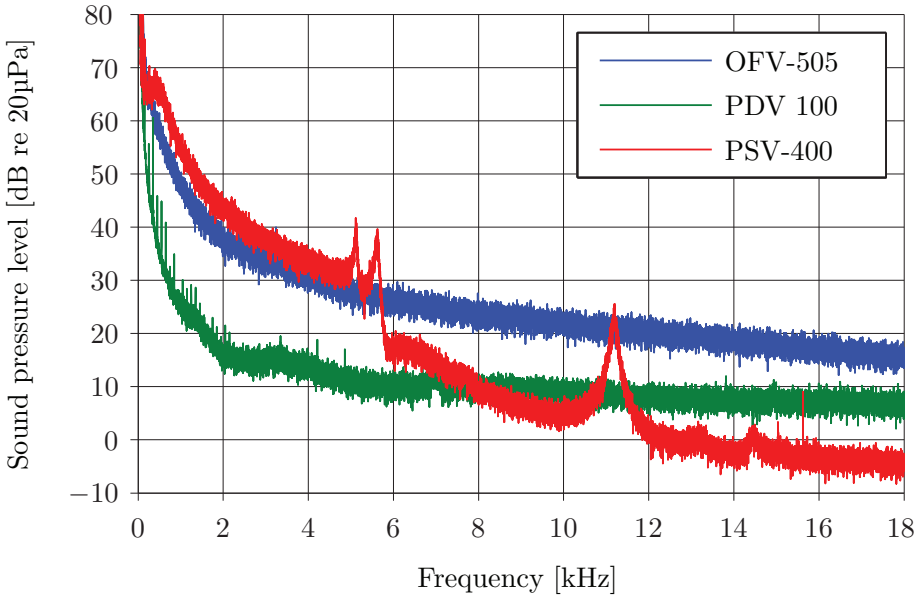

Figure 3.9: Minimum sound pressure levels that can be detected with the LDV systems under analysis, when plane waves are approaching the laser beam perpendicularly. For such sound pressure levels, the apparent velocity caused by the acousto-optic effect would be measured with a SNR of 0 dB.

in figure 3.9 are quite low. Again, the vibrometer *PDV 100* provides the best overall results, with a rather flat response. The scanning vibrometer does not seem to be adequate for measurements below 6 kHz, but it can detect lower sound pressure levels at high frequencies. The vibrometer *OFV-505* is the least sensitive to the acousto-optic effect at high frequencies. These curves provide just a very coarse idea of the sound pressure levels that would make the acousto-optic effect merely detectable under what probably are the most favorable measurement conditions. However, as soon as the plane waves approach the laser beam from another direction different from the normal direction, the integral of the pressure will in general drop substantially. In fact, the loss of sensitivity as a function of the angle of incidence is proportional to a *sinc* function,**

$$\left| \frac{1}{L_0} \int_{\mathbf{L}} p \, \mathrm{d}l \right|^2 = \left| A \mathrm{sinc}\big(k(L_0/2)\sin\theta_i\big) \right|^2, \tag{3.11}$$

where θ_i denotes the angle of oblique incidence and k is the acoustic wavenumber. Figure 3.10 illustrates how the integral of the plane waves depends on the angle of inci-

**This result is derived in Paper F and Paper G, although in these articles, the loss of sensitivity caused by oblique incidence of sound waves is exploited for localizing sound sources.

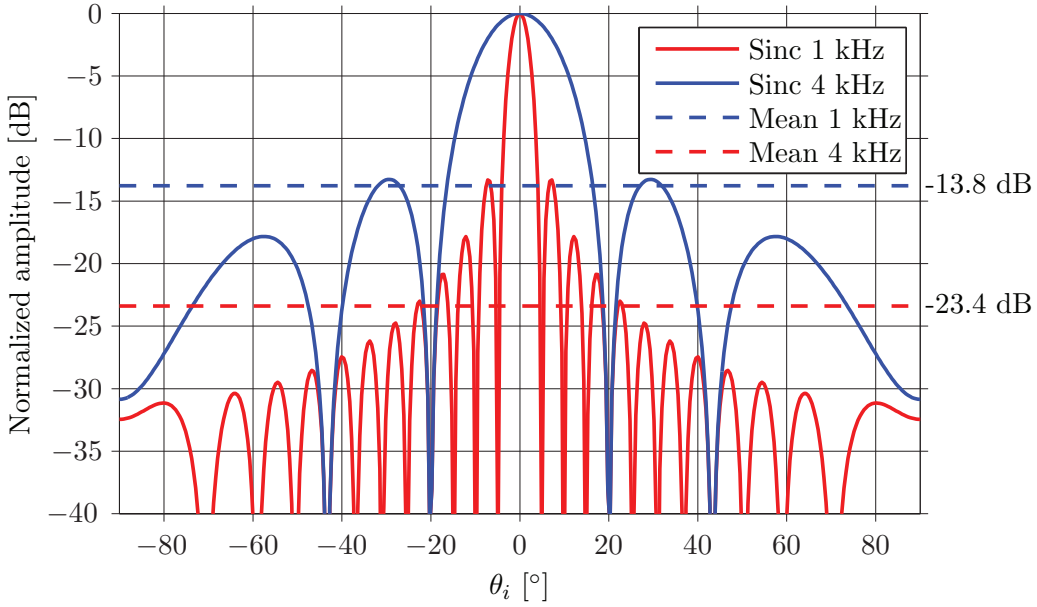

Figure 3.10: Loss of sensitivity of a 1 m long laser beam as a function of the angle of incidence of the plane waves. The sensitivity drops when the acoustic waves approach grazing incidence. This effect is more significant at high frequencies. The dashed curves correspond to the mean value of the respective *sinc* functions.

dence for two different acoustic frequencies and a 1 m long laser beam. As can be seen, the sensitivity of the laser beam drops as the acoustic waves approach grazing incidence as well as with increasing frequency. This effect is more pronounced for longer laser beams. The dashed curves plotted in figure 3.10 correspond to the mean value of the *sinc* functions when averaged over the different angles of incidence. As expected, the average loss of sensitivity is more prominent at high frequencies (-13.8 dB at 1 kHz versus -23.4 dB at 4 kHz). As a supplement, figure 3.11 shows this average loss of sensitivity over the entire audible frequency range.

Coming back to the question of determining the minimum sound pressure levels that are nowadays measurable in air with an LDV, it seems plausible to infer that the curves presented in figure 3.9 underestimate the sound pressure levels required to measure the acousto-optic effect in more realistic situations. Presumably, as hinted in figure 3.11, the minimum sound pressure levels might be in particular much higher towards the high frequencies. We may try to establish a more realistic set of curves by including the average loss of sensitivity presented in figure 3.11 into the minimum pressures estimated in figure 3.9. In addition, by introducing a positive offset of 30 dB to all the curves, the estimated pressures can be regarded to induce an apparent velocity at the

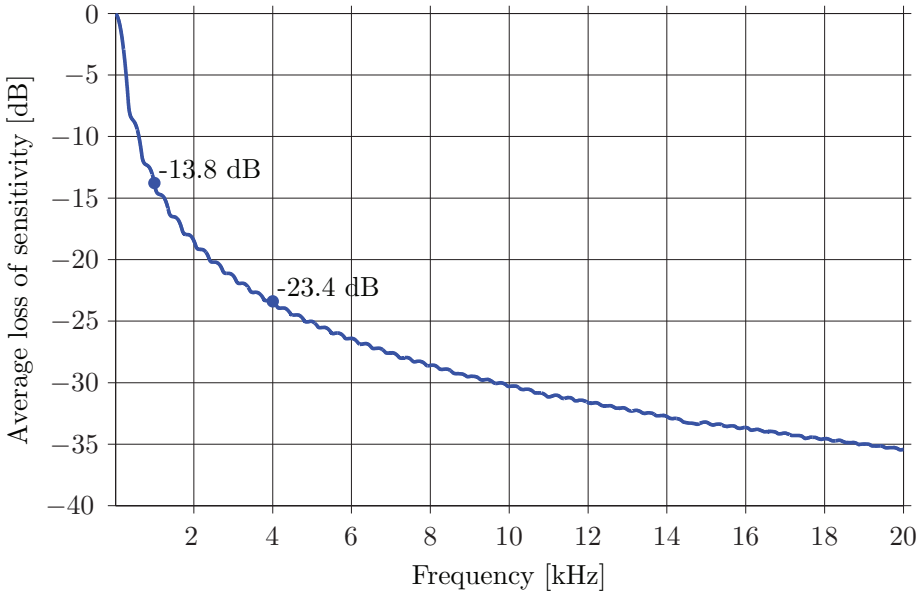

Figure 3.11: Average loss of sensitivity of a 1 m long laser beam exposed to plane waves. The average is performed over all the possible angles of incidence, that is, from 0° to 360°.

output of the examined LDV systems with a SNR of 30 dB. The resulting sound pressure levels are shown in figure 3.12. As can be seen, no sound pressure levels can be detected below 60 dB re 20μPa, at least not with a SNR lower than 30 dB. This makes it difficult to capture moderate sounds such as the ones encountered in a conversational speech. Furthermore, at frequencies below 6 kHz, the vibrometers *OFV-505* and *PSV-400* cannot accurately detect sound pressures that are below 80 dB re 20μPa. Hence, these curves clearly exemplify one of the main limitations currently faced when implementing the acousto-optic measuring principle with the existing technology, that is, the poor dynamic range of pressures that can be captured within the audible frequency range in comparison to that of the microphone technology.

Laser beam considerations

The acousto-optic measuring principle uses the totality of the laser beam exposed to the acoustic field as a sensing element. The length of the laser beam is normally determined by the characteristics of the acoustic field. At low frequencies, longer laser beams are usually required in order to cover the long wavelengths of the acoustic waves. Since the LDV relies on interferometric principles, the laser beam should not travel distances

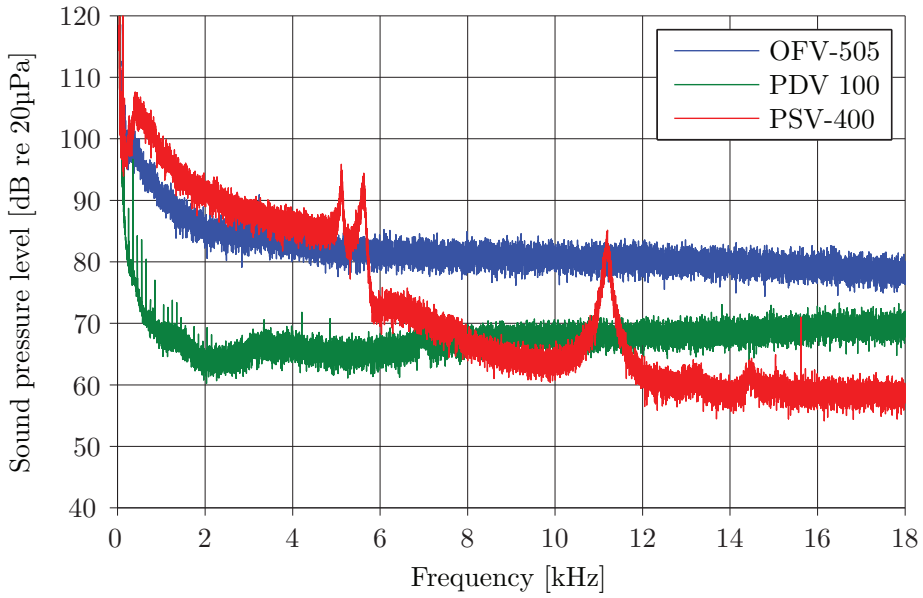

Figure 3.12: Minimum sound pressure levels that can be detected with the analyzed LDV systems in more realistic measurement scenarios. Such sound pressure levels would induced an apparent velocity at the output of the LDV with a SNR of 30 dB.

longer than the coherence length[††]. Otherwise, the laser beam exposed to the sound field will not interfere coherently with the reference beam, yielding incorrect results. This is fortunately not a problem in general for acoustic measurements based on the acousto-optic effect because the coherent length of the lasers used in conventional LDV systems are at least several meters long.

An LDV system can focus its laser beam into very small spot-sizes, rendering in this way a very high spatial resolution. This is done by adjusting the positions of the lenses from the laser head in accordance with the distance between the laser head and the target where the light is reflected off. For example, the spot-size of a mid range vibrometer OFV-505 is typically between 112 and 235 μm for laser beams between 1 and 2 m long [144]. However, the use of lenses for focusing the laser beam implies that the diameter of the laser beam is not constant along the optical path. It indeed reduces to its minimum value as the light approaches the focused target. While this is not an issue when measuring the acousto-optic effect in audible frequencies (the wavelength is still larger than 1 cm at 20 kHz), it can actually cause problems at higher frequencies when the acoustic wavelength is comparable to the diameter of the laser beam.

[††]The coherence length indicates the maximum distance that a wave can travel without degrading its coherence significantly.

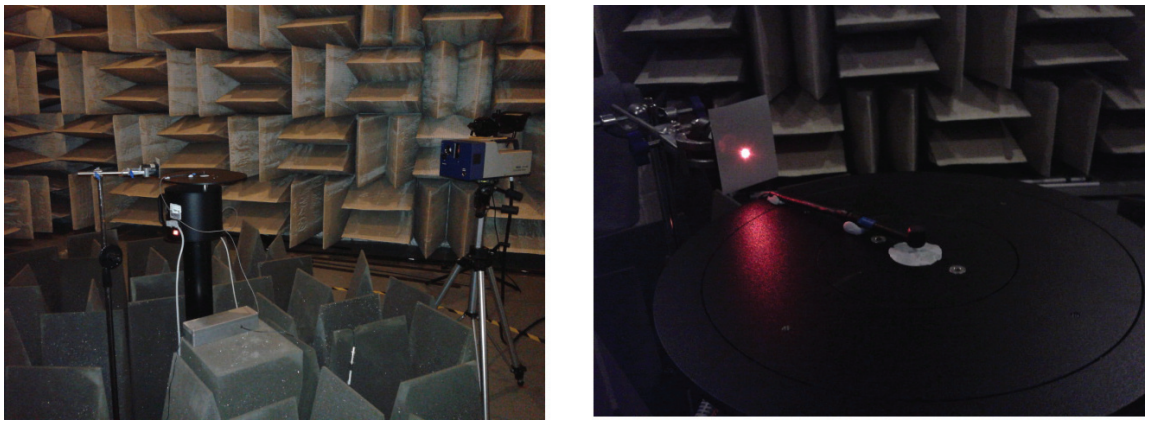

Figure 3.13: The acoustic field radiated by an ultrasonic transducer was probed with a scanning LDV. A retro-reflective tape was used to reflect the light off and back to the scanning LDV.

The following experiment, where the acousto-optic effect was induced with an ultrasonic transducer driven at 180 kHz (this corresponds to an acoustic wavelength λ of about 1.9 mm), may help to illustrate the importance of the diameter of the laser beam. Figure 3.13 shows a couple of pictures of the experimental setup. The ultrasound transducer was set to radiate sound waves in the vertical direction. The laser beam was about 1.5 m long. The acousto-optic effect was measured with a scanning LDV a few millimeters above the transducer. Considering $\lambda/10$ as the space where the wave properties can be regarded as constant, then the diameter of the beam should be smaller than 190 μm. While the spot size of the laser beam was probably smaller than this value at the retro-reflective tape, the diameter of the beam was likely to exceed it in the vicinity where the transducer was placed (about 16 cm from the reflecting tape). When the diameter of the laser beam is larger than $\lambda/10$, the acoustic information captured over the cross-section of the beam is somehow mixed and averaged out. In other words, the spatial resolution of the beam is not sufficient to represent the acoustic quantities in a point-wise manner. Since the ultrasonic transducer presents a very directive radiation pattern, it is important to have the narrowest part of the beam at the vertical plane where the transducer is located. In this way, the acousto-optic effect is probed with the highest spatial resolution. Therefore, it is advisable to focus the laser beam at the vertical plane where the acousto-optic effect is dominant, and let the beam diverge towards the retro-reflective tape during the measurements. Note that in such a case, the diameter of the laser beam will progressively increase after the focusing point, meaning that the spot-size at the reflecting surface will be larger.

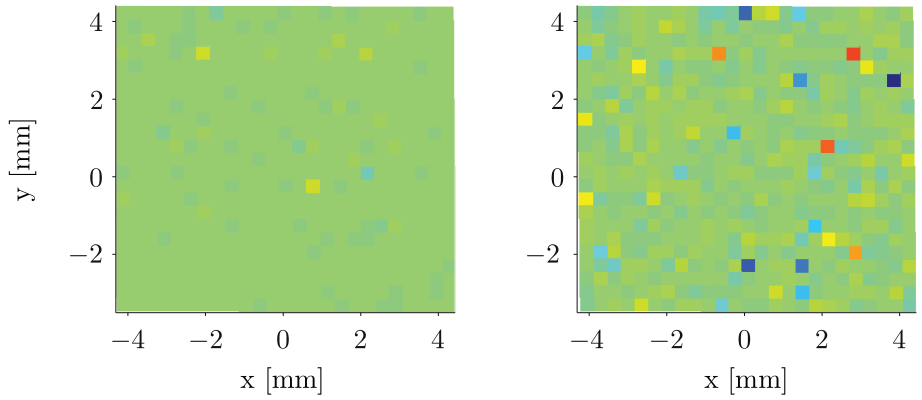

(a) $t = 0$ µs

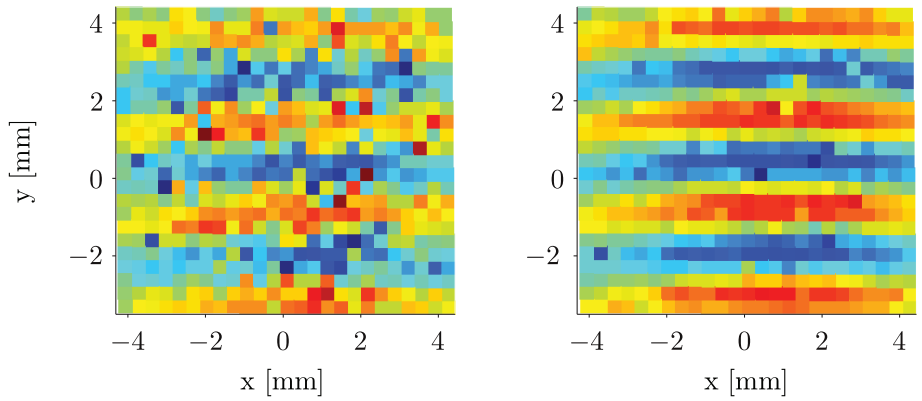

(b) $t = 136$ µs

Figure 3.14: Influence of the diameter of the laser beam on the apparent velocity measured with a scanning LDV when the laser beam is exposed to an ultrasonic sound field. The results shown on the left hand side were obtained when focusing the laser beam on the retro-reflective tape. The results on the right hand side correspond to the case where the laser beam was focused at the vertical plane where the transducer was located. The top panels illustrate the background noise in the absence of sound at $t = 0$µs. The bottom panels show and instantaneous representation of the acoustic waves traveling through the measuring volume at $t = 136$µs. Focusing on the vertical plane of the transducer yields a better picture of the acoustic field.

The benefits from this procedure are illustrated in figure 3.14. The panels on the left hand side correspond to the apparent velocities measured when the laser beam was focused on the retro-reflective tape. The results obtained when the laser beam was focused at the vertical plane where the ultrasound transducer was located are shown on the right hand side. The top panels show the results at $t = 0$ µs, that is, when the ultrasonic burst had not yet reached the field of view of the scanning LDV. The reason for having a noisier picture on the right panel can be explained by the fact that the laser beam was not focused on the retro-reflective tape. In that case, the spot-size on the reflecting surface was larger, and less light was reflected back to the scanning LDV,

yielding thus a poorer SNR. At $t = 136$ μs, the acoustic waves were already traveling across the field of view of the scanning system. Note that in this case, focusing on the vertical plane of the transducer yielded a clearer picture where the wavefronts can be better identified.

In underwater measurements, the speed of sound is more than four times the one in air, and thus, the frequency range where the diameter of the laser beam is comparable to the acoustic wavelength is shifted by the same scale factor towards the high frequencies.

3.2.3 Tomography

The acousto-optic measuring principle does not measure the pressure at a single point, but integrates it over space. It is thus not possible to realize the acoustic pressure directly, or at least not without assuming properties about the nature of the sound field. The previous section 3.2.2 has illustrated this for simple cases where the laser beam is exposed to progressive plane waves. In these cases, simple mathematical equations can be derived, and thus, a simple model can be used to reconstruct the integrated pressures. The accuracy of reconstructions based on theoretical models substantially relies on the validity of the model, which in practice may neither agree with the measurement conditions nor account for all the details of the sound field. This limits the use of theoretical models to acoustic measurements with simple and well-defined sound fields. An interesting example of a model-based reconstruction is given in Ref. [133], where the acousto-optic effect induced by plane waves is modeled in order to determine the sound absorption of materials placed in a standing wave tube.

A generic approach to tackle the sound pressure reconstruction without requiring any previous information or model of the sound field is to use tomography. This technique, whose name originates from the Greek word *tomos* that means 'slice' or 'section', images 'slices' of an object or medium by sensing it with any kind of radiation capable of penetrating or propagating through it. Tomography is mostly used in X-ray systems, a medical imaging procedure that reconstructs 'slices' of particular areas of our body. This application exemplifies very well the fundamental principle of tomography, that is, to visualize the interior of a specimen or region of a medium without perturbing it.[‡‡]

[‡‡]Even though in some medical applications there might be some secondary effects due to the exposure to ionizing radiation, e.g., X-rays.

The mathematical formulation describing the tomographic reconstruction from 'slices' of an object or medium were derived by the Austrian mathematician Johann Radon in 1917 [145]. He first defined an integral transform (nowadays referred to as the Radon transform) consisting of the integrals of a function over straight lines, and then established the fundamental principles of the tomographic reconstruction when deriving the corresponding inverse transform. As stated in equation (3.6) on page 34, the acousto-optic measuring principle is fundamentally the integral of the pressure along the laser beam used to sense the acoustic field. We can as well describe the acousto-optic measuring principle in terms of the Radon transform R_p of the acoustic field,

$$R_p = \int_{\mathbf{L}} p \, \mathrm{d}l, \tag{3.12}$$

and express the apparent velocity $v_{\text{ao}}(t)$ as a function of the Radon transform,

$$v_{\text{ao}}(t) = \frac{1}{n_0} \left(\frac{\partial n}{\partial p} \right)_S \frac{\mathrm{d}R_p}{\mathrm{d}t}. \tag{3.13}$$

This equation is very convenient because instead of expressing the output of the LDV as an indirect measure of the pressures along the laser beam, it reformulates the output of the LDV as a direct measure of the Radon transform. One could say that the Radon transform projects the two-dimensional (2D) pressure distribution into a one-dimensional (1D) function. It is easy to see now that the Radon transform of the acoustic field can in practice be retrieved from the apparent velocity of an LDV as follows,

$$\tilde{R}_p = n_0 \left(\frac{\partial n}{\partial p} \right)_S^{-1} \int v_{\text{ao}}(t) \, \mathrm{d}t. \tag{3.14}$$

The tilde denotes that the Radon transform $\tilde{R}_p$ is a measured quantity, potentially biased with measurement noise. Unfortunately, a single line scan does not contain enough information of the sound field, if this needs to be reconstruct over an aperture. A 2D reconstruction requires to scan the sound field all over the aperture of interest from different angles of view. In general, there are two types of tomographic schemes that can be used to scan the area of interest effectively, namely the parallel line and the fan-shape schemes. These are sketched in figure 3.15. The parallel line scheme starts scanning the aperture with a set of parallel lines for a certain angle of projection θ. This procedure is then repeated for several angles of projection from 0° to 180°. Note

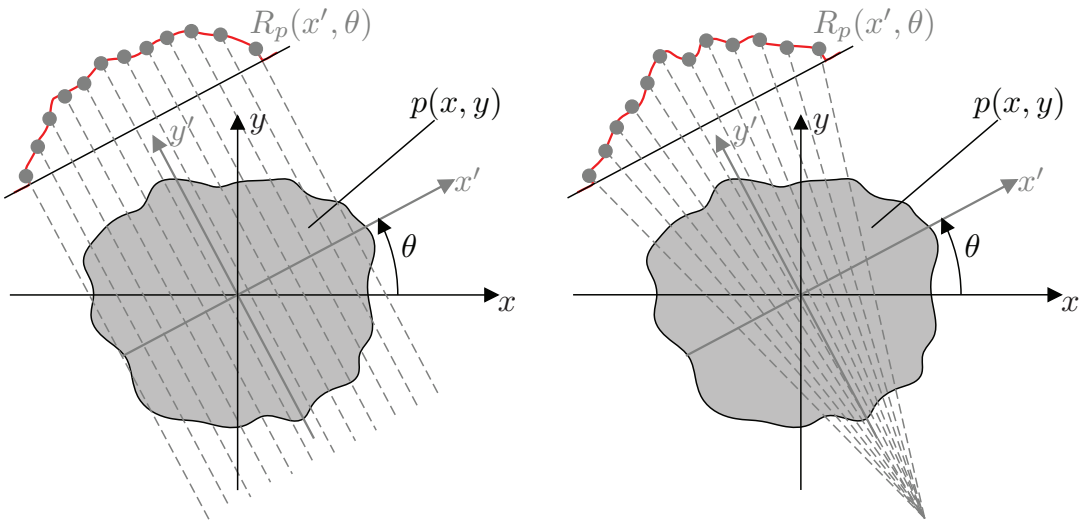

(a) Parallel line scanning

(b) Fan shape scanning

Figure 3.15: Classical tomographic schemes.

that there is no need to continue scanning for $\theta \geq 180°$, because the symmetry of the scan pattern does not include new information about the acoustic field in the projections taken when $\theta \geq 180°$.

In a fan-shape scheme, each angle of projection θ is scanned without translating the LDV, which is instead steered into a range of different angular directions. In this case, this procedure needs to be repeated from $0°$ to $360°$. The symmetry of this scan pattern does not make it possible to stop the procedure after projecting the sound field over the first $180°$.

Once the Radon transform is characterized with a set of line scans per angle of projection, from a pure mathematical point of view, the reconstruction of the acoustic field simply requires to apply the inverse Radon transform. In practice, such a straight reconstruction procedure may lead to completely unsatisfactory results due to the presence of noise in the measurement data. Hence, tomographic reconstruction algorithms need to implement both the inverse Radon transform and some sort of filtering capable of diminishing the influence of extraneous noise. The so-called filtered back projection method is the most famous reconstruction algorithm, and it has been reviewed extensively in the literature [146, 147], particularly for medical applications.

When the acoustic field is axissymmetric, the complexity of the tomographic reconstruction is simplified considerably due to the symmetry of the problem. Mathemat-

ically speaking, the Radon transform reduces to the so-called Abel transform [148]. In this case, for a given set of parallel line scans at a certain angle of projection, the inverse Abel transform assumes that the results obtained from the rest of angles projections are the same, and thus, unnecessary. This simplifies the measurements significantly, though the reconstructed sound fields are also notably simpler due to their symmetry. As for the inverse Radon transform, practical implementations of the inverse Abel transform need to account for the presence of measurement noise [149–151].

The theory presented in this section forms the basis for acousto-optic tomography, that is, the reconstruction of arbitrary sound fields under weak acousto-optic interaction. Further details about acousto-optic tomography in air and within the audible frequency range can be found in Papers B and C appended at the end of this thesis. This tomographic technique is sometimes also referred to as light refractive tomography in the ultrasound community [152–155].

As discussed in Chapter 2, the acousto-optic effect may also cause light diffraction at high ultrasonic frequencies. In such a case, the tomographic scheme needs to be slightly modified by expanding the diameter of the laser beam so that the different order of diffraction can be sensed, and the reconstruction algorithm must also account for the diffraction of light, e.g., based on Raman-Nath theory. The resulting tomographic method is often named light diffraction tomography [156–159].

3.3 Photon correlation spectroscopy

PCS was first proposed for acoustic measurements in the mid 1980s as an alternative to conventional LDA [160–162]. The sampling rates required for acoustic velocity measurements were much higher than those of flow measurements, and this posed serious constraints for LDA measurements. In general, at such sampling rates, the number of scattered photons per sampling time was not enough to unravel the Doppler shift, meaning that one had to increase the power of the laser source or the concentration of seeding considerably. Either solution would introduce additional problems in terms of laser safety or erratic seeding effects. Moreover, as mentioned previously, the tracer particles might not cross a sufficient number of fringes, which would complicate even more the detection of the Doppler shift. All these problems could be tackled using PCS.

This technique is often regarded as an offshoot of LDA. Indeed, its experimental setup is quite similar to the one used in LDA measurements (see figure 3.5 on page 27),

that is, the optical setup is designed to intersect two laser beams at a certain point where the velocity is measured, see figure 3.16. One of the main differences with respect to LDA arise from the signal processing technique used to analyze the scattered photons. In this case, instead of demodulating the instantaneous frequency of the measured intensity, the calculations are based on the autocorrelation function of the signal generated by the scattered photons.

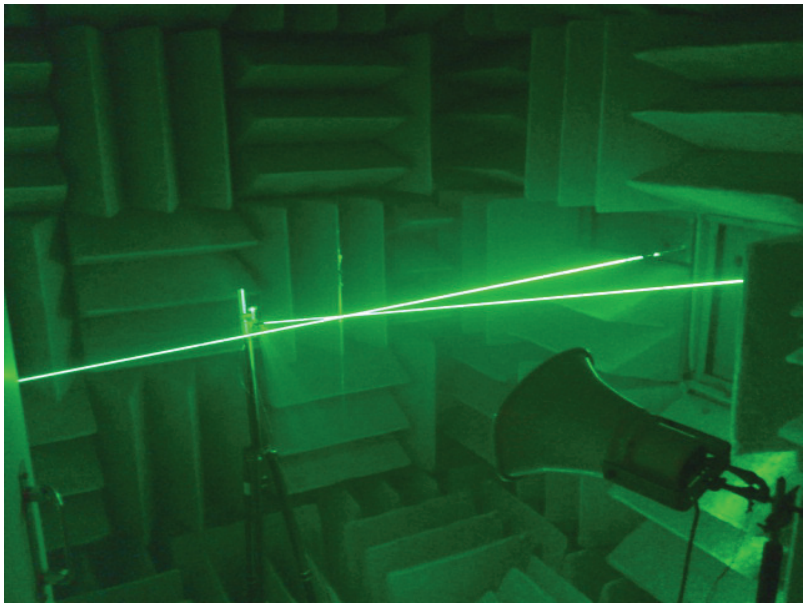

Figure 3.16: Two laser beams intersecting at the center of an anechoic chamber where the particle velocity generated by a horn loudspeaker is measured using PCS.

Since the mid 2000s, PCS has risen interest in the acoustic metrology community, because, as a non-intrusive technique, it offers the potential of realizing the acoustic pascal at a single point without the immersion of any transducer. Current microphone calibration techniques such as the reciprocity technique realize the sensitivity of a microphone indirectly, that is, the measurement procedure itself determines a set of electrical parameters of the microphone from which the sensitivity of the microphone can be derived afterwards. Although the precision achieved with the current calibration standards is high enough, the fact of using an indirect method is not suited from a metrological point of view.

3.3.1 Autocorrelation of scattered photons

Considering a general case, where the particles crossing the measuring volume are driven by a mean flow velocity u_f and a sound field consisting of a pure tone, then the autocorrelation function of the scattered photons equals [162]

$$R(\tau) = \frac{\kappa^2 C_1 g_0}{2}\sqrt{\frac{\pi}{2\beta^2}}\exp\left(-\frac{\beta^2(u_f^2\tau^2 + u_m^{'2}/2)}{2}\right) \times \left(M + \cos(Du_f\tau)J_0\left(u_m^{'}\sqrt{D^2 - \beta^4 u_f^2\tau^2}\right)\right) + C_D, \tag{3.15}$$

where κ is a constant related to the optical power and detector sensitivity, C_1 is related to the particles scattering cross section, g_0 is the average number of particles per unit length of the measuring volume, M is a constant that depends on the strength difference between the two beams (e.g., $M = 1$ when the two beams have the same strength), β is a parameter that characterizes the envelope of the probe volume due to the Gaussian cross section of the beams, C_D is a constant that corresponds to the square of the mean value of the Doppler signal, D is the so-called frequency to velocity converter,

$$D = \frac{4\pi\sin\theta'}{\lambda'}, \tag{3.16}$$

and

$$u_m^{'} = \frac{2u_m}{\omega}\sin\left(\frac{\omega\tau}{2}\right), \tag{3.17}$$

where θ' is the half-angle of the intersecting beams, u_m is the amplitude of the acoustic velocity and ω is the angular frequency of the acoustic field. In the absence of acoustic field ($u_m = 0$), the autocorrelation function reduces to,

$$R(\tau) = \frac{\kappa^2 C_1 g_0}{2}\sqrt{\frac{\pi}{2\beta^2}}\exp\left(-\frac{\beta^2 u_f^2\tau^2}{2}\right)(M + \cos(Du_f\tau)) + C_D, \tag{3.18}$$

whereas when the mean flow is negligible ($u_f \approx 0$), then the autocorrelation can be approximated as follows

$$R(\tau) = \frac{\kappa^2 C_1 g_0}{2}\sqrt{\frac{\pi}{2\beta^2}}\exp\left(-\frac{\beta^2 u_m^{'2}}{4}\right)\left(M + J_0\left(Du_m^{'}\right)\right) + C_D. \tag{3.19}$$

The latter case is the one exploited for microphone calibration, and it can actually be further simplified to the following proportionality

$$R(\tau) \propto J_0\left(Du_m^{'}\right). \tag{3.20}$$

The acoustic velocity can then be derived from the first minimum of the Bessel function J_0, knowing that the minimum takes place when the argument of the Bessel function equals 3.832:

$$R(\tau_{\text{min}}) \propto J_0\left(3.832\right) \Longleftrightarrow Du_m^{'} = 3.832. \tag{3.21}$$

This equation can be solved either analytically,

$$D\frac{2u_m}{\omega}\sin\left(\frac{\omega\tau_{\text{min}}}{2}\right) = 3.832 \Longleftrightarrow u_m = \frac{3.832\omega}{2D\sin\left(\omega\tau_{\text{min}}/2\right)}, \tag{3.22}$$

or using the small angle approximation:

$$\frac{\omega\tau_{\text{min}}}{2} \ll 1 \Longrightarrow D\frac{2u_m}{\omega}\frac{\omega\tau_{\text{min}}}{2} = 3.832 \Longleftrightarrow u_m = \frac{3.832}{D\tau_{\text{min}}}. \tag{3.23}$$

Despite the simplicity of the last expression, one has to be careful with this approximation, because it does not hold neither at high frequencies ($\omega \uparrow\uparrow$) nor for low velocities ($\tau_{\text{min}} \uparrow\uparrow$). Figure 3.17 shows the normalized error introduced by the use of the small angle approximation as a function of frequency and for different amplitudes of the theoretical particle velocity. This plot clearly shows the increase of relative error with increasing frequency and how it becomes more prominent for lower velocity amplitudes.

3.3.2 Velocity estimate

Once the autocorrelation function of the photons scattered from the measuring volume is calculated, the acoustic velocity is estimated using either equation (3.22) or (3.23). The most challenging part of this calculation is the determination of the time lag τ_{min} at which the first minimum of the Bessel function takes place. It is indeed critical because the only parameter from the equations (3.22) and (3.23) that is determined experimentally is τ_{min}. This means that the accuracy of the method strongly relies on its value, and thus, it is necessary to estimate it as accurately as possible. To do that, a

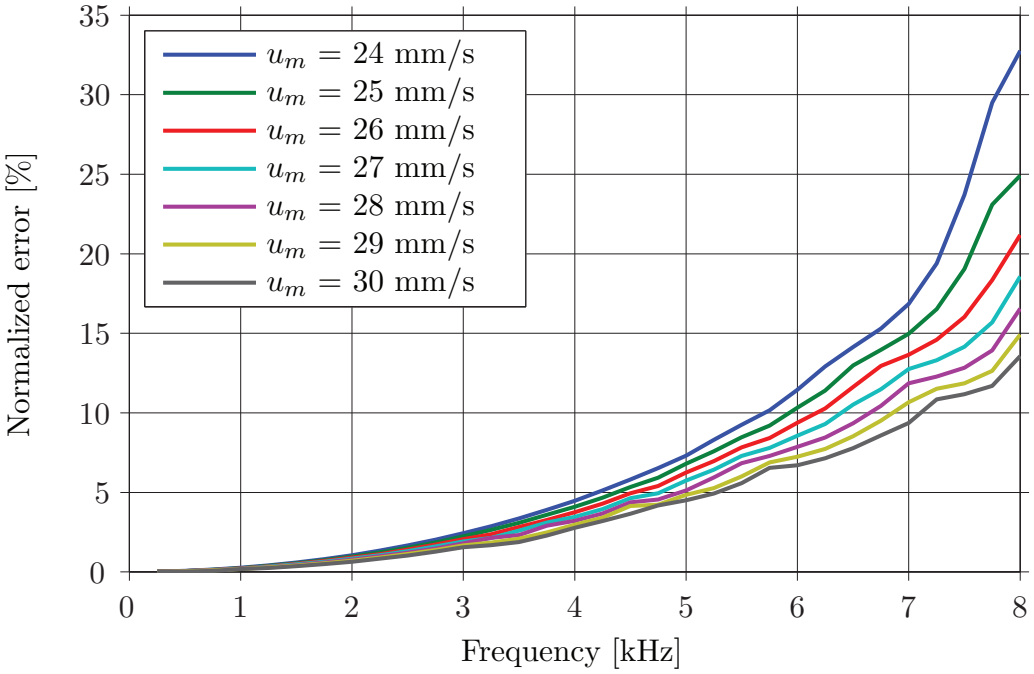

Figure 3.17: Normalized error caused by the small angle approximation as a function of frequency and for different amplitudes of the theoretical particle velocity.

Fourier series is first fitted to the measured autocorrelation function,

$$R(\tau) = \sum_{n=0}^{\infty} a_n \cos(\omega_n \tau) + b_n \sin(\omega_n \tau), \tag{3.24}$$

where a_n and b_n are the so-called Fourier coefficients, ω_n is the n'th harmonic of the fundamental frequency, that is, $\omega_n = n\omega_0$. To fit the measured data into a Fourier series makes it possible to interpolate between measured data points, and thus, increases the resolution/accuracy used to estimate τ_{min}. An example of a measured autocorrelation function is given in figure 3.18. The simplest way to determine τ_{min} from the Fourier series is to identify the time lag τ of the autocorrelation function that has an amplitude smaller than the one that follows immediately after. This indicates that the autocorrelation function has been through a relative minimum. Let us denote this search method as method A. Despite the simplicity of this method, its accuracy depends very much on the temporal resolution used to fit the Fourier series. Alternatively, another possibility (let us denote it as method B) is to exploit the fact that the autocorrelation function has

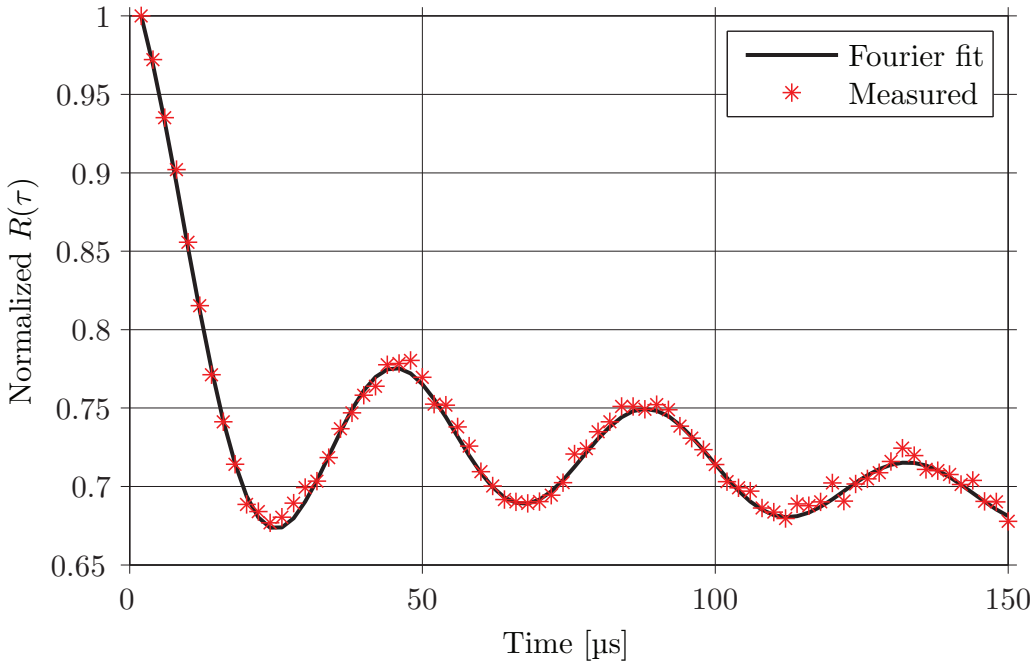

Figure 3.18: Example of autocorrelation function measured in the absence of mean flow.

a relative minimum when its first derivative equals zero:

$$\frac{\mathrm{d}R(\tau)}{\mathrm{d}\tau} = \sum_{n=0}^{\infty} \omega_n (b_n \cos(\omega_n \tau) - a_n \sin(\omega_n \tau)) \quad \Rightarrow \quad \frac{\mathrm{d}R(\tau_{\min})}{\mathrm{d}\tau} = 0. \tag{3.25}$$

Thus, finding the value of $\tau_{\min}$ is equivalent to determining the time lag at which the first derivative of the Fourier fit equals zero. This can easily be implemented using an iterative algorithm such as the bisection method [163]. Figure 3.19 illustrates the numerical error introduced by the methods A and B when introducing their corresponding values of $\tau_{\min}$ into equation (3.22) to determine the particle velocity in the measuring volume. The acoustic frequency of the simulated pure tone was set to 1 kHz. As can be seen, the performance of method A (on the left panel) strongly depends on the bin size of the Fourier fit and the velocity amplitude. As expected, a coarser time resolution of the Fourier series leads normally to larger errors. Furthermore, it is also apparent from the plot that larger velocities are more affected than lower ones. However, if the bin size is kept below or equal to 2 µs, then the error is most likely to be less than 5 %. Instead, the results achieved with the method B (on the right panel) show that this approach is independent of the bin size and the velocity amplitude. It leads to really small

numerical errors (less than 1 %) that are related to the nature of the iterative algorithm. This is very convenient because apart from introducing a very low bias into the velocity estimate, this bias is independent of the measurement. Similarly, figure 3.20 shows the results obtained with the small angle approximation, that is, using equation (3.23). The only difference with respect to the results plotted in figure 3.19 is that the small angle approximation is clearly not valid for low velocity amplitudes. Note that according to figure 3.17, this bias will be more prominent with increasing frequency.

3.3.3 Relationship between sound pressure and particle velocity

PCS provides a direct measurement of the particle velocity, instead of the acoustic pressure. In order to use this optical technique for microphone calibration, the relationship between sound pressure and particle velocity needs to be established. According to the Euler equation, the particle velocity and the acoustic pressure can be related as follows when expressed in complex notation [164]

$$\hat{\mathbf{u}} = \frac{1}{j\omega\rho}\nabla\hat{p}, \tag{3.26}$$

where $\hat{\mathbf{u}}$ is the particle velocity vector, ρ is the density of the medium and $\hat{p}$ is the acoustic pressure. For instance, in a standing wave tube (at low frequencies), the sound

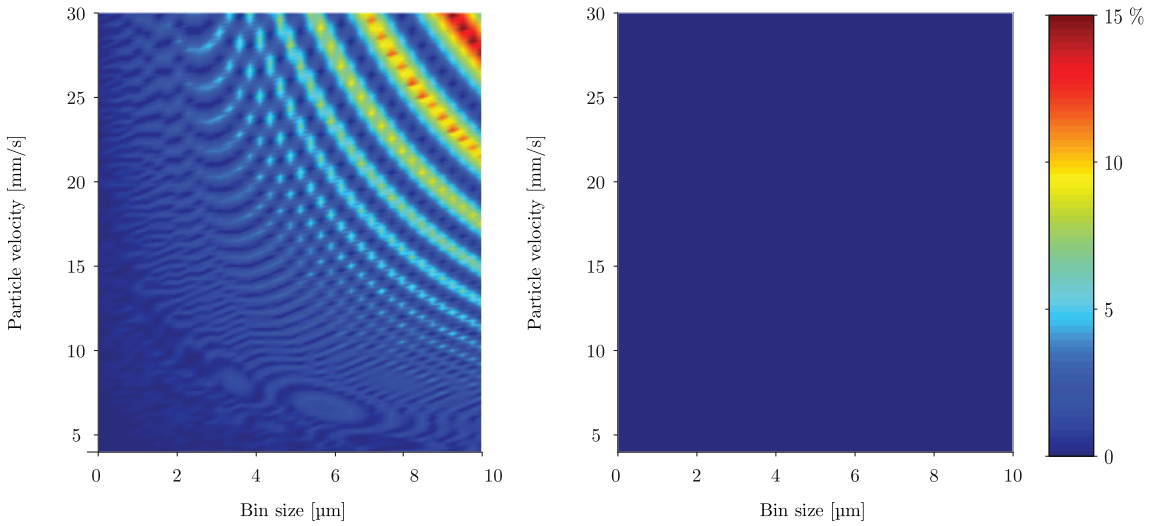

Figure 3.19: Numerical error of the velocity estimate introduced by the two methods used to compute τ_{min}. The normalized error obtained with method A is depicted on the left panel, and the one from method B is on the right panel. In this simulation, the acoustic frequency was set to 1 kHz.

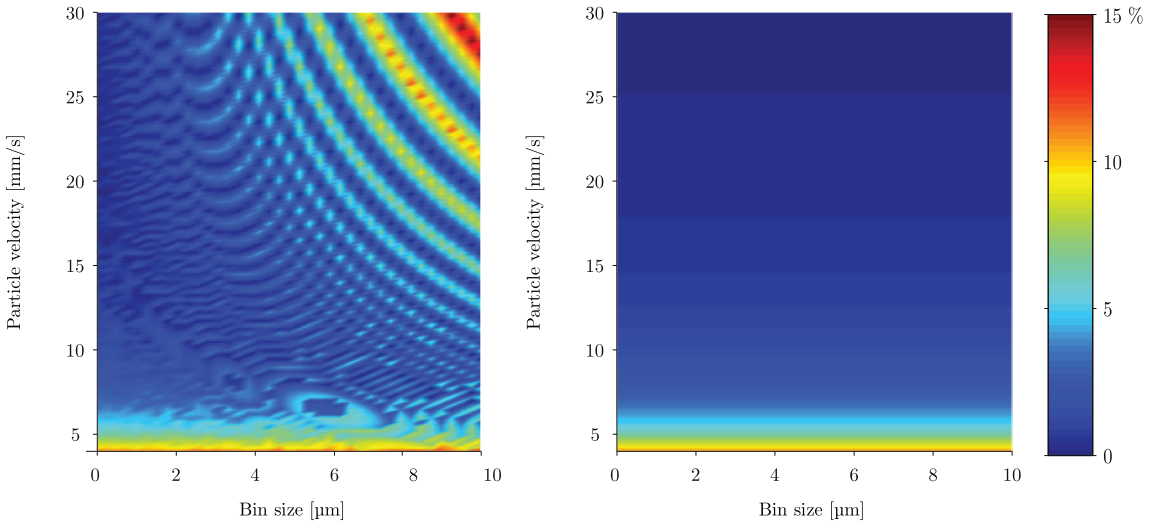

Figure 3.20: Numerical error of the velocity estimate when using the small angle approximation. The normalized error obtained with method A is depicted on the left panel, and the one from method B is on the right panel. In this simulation, the acoustic frequency was set to 1 kHz.

pressure inside the tube can be described by means of plane waves:

$$\hat{p} = Ae^{j(\omega t - kx)} \Longrightarrow \hat{u}_x = \frac{1}{j\omega\rho}\frac{\partial \hat{p}}{\partial x} = \frac{jk}{j\omega\rho}\hat{p} = \frac{\hat{p}}{\rho c}. \tag{3.27}$$

Instead, in free-field conditions, the sound pressure typically propagates as a spherical wave:

$$\hat{p} = \frac{A}{r}e^{j(\omega t - kr)} \Longrightarrow \hat{u}_r = \frac{1}{j\omega\rho}\frac{\partial \hat{p}}{\partial r} = \frac{\hat{p}}{\rho c}\left(1 + \frac{1}{jkr}\right). \tag{3.28}$$

Hence, the exact relationship between the acoustic velocity and the sound pressure depends on the nature of the sound field.

3.3.4 Considerations for acoustic metrology

A future primary method for free-field microphone calibration might be driven by PCS [165, 166]. Before that, all the possible aspects influencing the results obtained with this optical technique need to be identified and figured out. In what follows, a brief review of the main challenges derived from deploying the PCS technique for the calibration of microphones under free-field conditions is given.

Seeding and mean flow

Due to the relatively large dimensions of an anechoic chamber, it is very difficult to avoid convection effects arising from temperature gradients in the chamber, particularly when introducing the seeding. It is thus very important to minimize the influence of such a convection flow, otherwise the resulting mean flow velocity can totally ruin the estimate of the acoustic velocity. In practice, it is crucial to allow plenty of settling time after introducing the seeding. In this way, it is likely to obtain less convection effects and a more uniform density of tracers consisting indeed of smaller particles (the heavier ones are pulled down by gravity). As mentioned earlier in this chapter, selecting the optimal seeding is essential in tracer methods such as PCS. Given the long settling time required in free-field measurements, it is particularly important that the seeding particles are as light as possible, so they can remain airborne for long periods of time.

The use of a duty gate

PCS is so far developed for pure tone measurements. This means that in its basic form, the scattered photons are processed every acoustic cycle. It is however possible to select specific parts of the acoustic period by means of a duty gate, that is, by applying a square window conveniently shifted in time. This version of the PCS technique is known as gated PCS [166]. The effects of the duty gate's length have been reported for flow measurements [167]. This study shows that the autocorrelation of the duty gate yields a sawtooth function that distorts the original autocorrelation function of the mean flow and its power spectrum. A thorough analysis of the exact effects of the autocorrelation function of the duty gate on free-field calibration of microphones is still needed. However, a double duty gate scheme that samples the positive and negative peaks of the acoustic cycle has recently been proposed in order to compensate for the presence of mean flow during the measurements (see Paper I attached at the end of the thesis for further details).

Frequency range

While the calibration of microphones is usually carried out over a broad frequency range, the results reported in the literature for acoustic measurements based on PCS have been limited mainly to frequencies between 1 and 4 kHz [166]. The latest ad-

vances in the matter have though reported an extended frequency range from 500 Hz up to 8 kHz (see Paper I for further details). In practice, the lower frequencies are limited by the dimensions of the anechoic chamber, that is, below a certain frequency the free-field condition is not fulfilled anymore. The higher frequencies are limited by two different reasons. On the one hand, the higher the frequency, the shorter the measurement period used to analyze the data, meaning that less photon events are captured and included in the calculation of the autocorrelation function. On the other hand, for a given sound pressure level, the higher the frequency, the smaller the displacement of the tracer particles, and thus, they will cross less fringes of the interference pattern. Above a certain frequency, it could even happen that the tracers do not move beyond one fringe. More sophisticated processing techniques need to be developed in order to extend the frequency range to that of the standards required for microphone calibration.

Distortion

In order to ensure a good SNR, so that the seeding particles cross a sufficient number of fringes, and that the first minimum of the Bessel function of the autocorrelation function can be detected within the measurement period, the sound pressure level inside the anechoic chamber is usually fairly high, generally well above 100 dB re 20μPa. While microphones can surely be regarded as linear devices, loudspeakers are well-know for their nonlinear behavior. This means that the loudspeaker used to generate the sound pressure inside the chamber will inevitably create harmonic distortion when driven with a pure tone at high levels of amplification. PCS cannot distinguish different spectral components, and thus, the energy of all the harmonics integrates somehow on the energy of the fundamental component. The exact effect of these extraneous frequency components on the final estimate of the acoustic velocity remains still unknown.

Plane wave versus spherical wave

Under free field conditions, the waves emitted from the loudspeaker propagate as spherical waves rather than as plane waves. This means that the pressure inside the measuring volume should be estimated according to equation (3.28):

$$|p| = \frac{\rho c k r}{\sqrt{1 + (kr)^2}} u_m. \tag{3.29}$$

The use of this equation requires in practice to characterize very well the loudspeaker used to generate the sound pressure. In particular, if the loudspeaker is modeled as a monopole with a certain directivity pattern, it is then very important to determine the acoustic center of the loudspeaker as a function of frequency [168]. If a plane wave assumption is used instead, then figure 3.21 gives an idea of the bias introduced in the pressure calculation. As can be seen, as soon as we move away from the loudspeaker and increase the frequency of analysis, the bias is inferior to 0.3 dB.

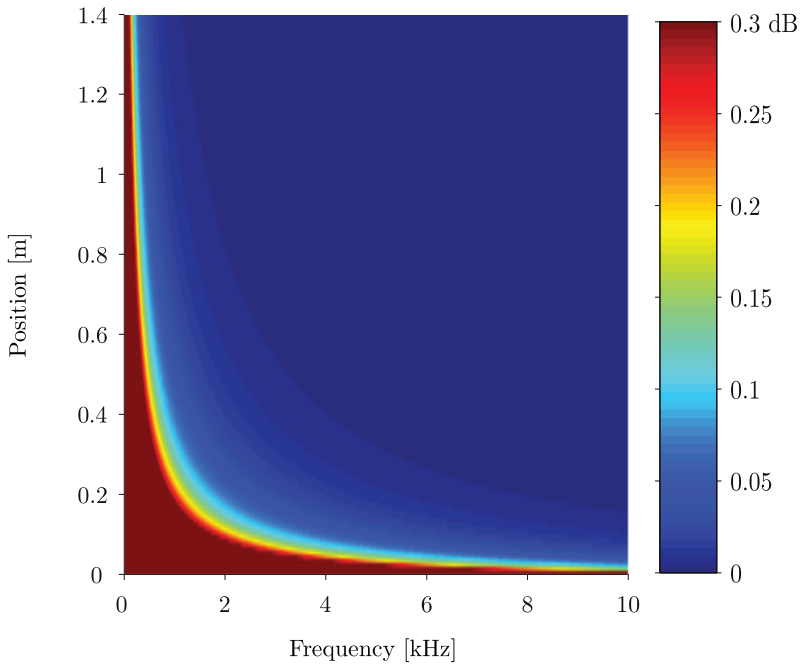

Figure 3.21: Level difference between the plane and the spherical wave models. The area of the plot that is colored in dark red should be understood as an area where the error is larger than 0.3 dB, with increasing value as the data points approach the edges of the plot.

Acousto-optic effect

Similarly to LDA measurements, PCS is also in principle vulnerable to the acousto-optic effect. As the sound pressure levels required in this type of measurements are rather high, the phases of the intersecting beams are susceptible to changes caused by the acousto-optic effect. Roughly speaking, one beam might propagate a bit faster or slower in certain regions of the chamber compared to the other beam. This could corrupt the stationarity of the fringe pattern, inducing perhaps fringe pattern fluctuations, and thus, bias the estimate of the velocity inside the measuring volume. Although this

phenomenon is believed to be very small and negligible in air (at least in the range of sound pressure levels encountered in conventional calibration procedures), a validation study should be conducted to determine whether the acousto-optic effect can prevent PCS from being used as a primary method for microphone calibration.

3.4 Comments on the calibration of optical methods

One of the arguments given sometimes in favor of optical methods is that they do not require calibration. Such an statement, perhaps influenced by the versatile and easy use of some commercial optical devices such as the LDV, is somehow misleading. As any other measuring technique, optical methods rely, in one way or another, on physical or instrumental parameters. This is very clear in the calibration of conventional transducers such as the microphone. In a transducer calibration, it is indispensable to determine the sensitivity of the sensing element, e.g., the membrane of a microphone. This sensitivity changes from transducer to transducer and depends on both the transducer's construction and the calibration conditions. The former relates to the technology embedded into the transducer (e.g., whether it is a condenser or a MEMS[§§] microphone), whereas the latter depends on the measurement procedure (e.g., free-field or pressure calibration) and the medium conditions (e.g., temperature, static pressure, etc.).

When light is used as a sensing element, there is no transducing device at the measurement point transforming a physical quantity into an electrical signal. The non-invasiveness of optical methods has already been remarked in the previous chapters, but the accuracy of optical methods relies on knowing fundamental properties of the light used as a probe , e.g., its wavelength, and other optical parameters of the experimental setup. For instance, calibration in acousto-optic measurements mainly relates to the determination of the piezo-optic coefficient, which describes the coupling between sound and light, or in other words, the sensitivity of the medium to the acousto-optic effect. By combining equation (2.1) and the derivation included in appendix A in Paper B, the adiabatic piezo-optic coefficient in air can be written as,

$$\left(\frac{\partial n}{\partial p}\right)_S = \frac{n_0 - 1}{\gamma p_0}, \tag{3.30}$$

[§§]MEMS originally stands for MicroElectroMechanical Systems. Such a technology is commonly incorporated into microphones of portable devices such as a mobile phone.

where γ is the ratio of specific heats, and n_0 and p_0 denote the dependence of the piezo-optic coefficient on the atmospheric conditions, not only on the static pressure p_0 that is explicitly stated in the last equation, but also on temperature and humidity which are known for influencing the refractive index n_0 [44–49].

Apart from the medium conditions, some optical techniques also require to know with substantial accuracy certain parameters of the optical setup. For example, in LDA measurements, it is crucial to determine the angle at which the two laser beams intersect as well as the frequency shift induced in one of the laser beams in order to unravel the sign ambiguity of the demodulated velocity.

Despite the very good accuracy at which optical parameters can be determined, and that they are normally very stable and do not require a constant monitoring procedure, optical methods are not detached from the need of calibration procedures.

Chapter 4

Contributions

The extensive bibliography provided in the previous chapter is a clear sign that the use of optical methods in acoustics is not a new area of research. This chapter thereby intends to pinpoint the originality of the research carried out during the present PhD study. The main area of contribution lies in the use of the acousto-optic effect for characterizing sound fields. Additionally, but to a lesser extent, some contributions have been made on the development of a future primary method for microphone calibration under free-field conditions based on PCS. The papers appended at the end of the thesis constitute the core of the findings. These are supplemented by the work presented in sections 3.2 and 3.3.

4.1 Acousto-optic effect

The acousto-optic interaction has been investigated mainly for ultrasound, and substantially less research has been devoted to audible frequencies. As a first contribution, the present PhD study has focused on the possibility of exploiting the acousto-optic effect for acoustic measurements within the audible frequency range. In particular, section 3.2 discusses the main advantages and disadvantages derived from measuring the acousto-optic effect with an LDV. This is important because LDVs are originally designed to measure mechanical vibrations, rather than the acousto-optic effect. The possible consequences of that are examined by providing a set of examples that illustrate the limitations of such off-the-shelf technology. An attempt to estimate the minimum acoustic pressures that can be measured with the current technology has been made. Practical

considerations on the length and width of the laser beam as well as recommendations on the use of LDV systems for acousto-optic and vibration measurements are also given.

More importantly, this study has contributed to the existing body of knowledge of sound visualization based on the acousto-optic effect, and has developed novel measurement techniques for acoustic holography and beamforming, where the acousto-optic effect exhibits unique properties.

4.1.1 Sound visualization

The laser beam projections of a sound field taken with an LDV contain already qualitative information of the acoustical space under investigation [131, 132, 169]. However, a complete sound pressure reconstruction requires tomography. The use of tomographic principles for sound visualization based on the acousto-optic effect is a well-known area of research within the ultrasound community, both in air (e.g., see Refs. [156, 170]) and water (e.g., see Refs. [152, 171, 172]). By contrast, a few studies have been conducted recently for airborne sound within the audible frequency range [173–176]. On the one hand, Refs. [174] and [176] are not based on laser Doppler vibrometry, but on a method founded on light diffraction. It should be noted that the higher orders of diffraction cannot be measured within the audible frequency range, and thus, the method only exploits the zero'th order of diffraction, which basically undergoes phase changes caused by the acousto-optic effect, as in laser Doppler vibrometry. However, the proposed method does not rely on interferometric principles, and thus, the phase variations are in this case detected as intensity modulations of the laser beam impinging on a photodetector. In Ref. [174], the tomographic reconstruction is based on the filtered back projection method, whereas no details about the reconstruction algorithm are given in Ref. [176]. Nevertheless, the latter extends the tomographic investigations to the visualization of sound in jet flows.

On the other hand, Refs. [173] and [175] apply the principles of computerized tomography (CT) to the reconstruction of sound fields based on laser beam projections. In particular, Ref. [173] exploits the directionality of the laser beam of a scanning LDV for conducting acousto-optic measurements following a fan-shape tomographic scheme. The reconstruction process is though performed assuming a parallel line scan pattern, which somehow restricts the accuracy of the reconstructed pressures. This work is extended to 3D reconstructions in Ref. [175]. In this case, the Radon transform of the

acoustic field is projected with a scanning LDV into a 2D projection plane rather than a 1D projection line. Besides, this paper also presents impulse response measurements based on the pressures reconstructed with CT. Both studies, Refs. [173] and [175], use the filtered back projection method to reconstruct sound pressures.

In short, the aforementioned studies conform the state of the art of acousto-optic tomography for audible sound. The present PhD study contributes to this with detailed theoretical, simulation and experimental studies where the physics of the acousto-optic effect are clearly linked to the Radon transform that characterizes the tomographic reconstruction (see, for instance, Paper B). Practical aspects such as the influence of the spatial and angular resolutions used in the tomographic reconstructions are also discussed. As expected, the higher the resolution the better the results, but it has also been shown that a compromise can be done in order to reduce the amount of data that needs to be measured.

Furthermore, the importance of controlling the mechanical vibrations of the measurement setup has also been remarked and examined experimentally (see, for instance, Paper A). All the measurements were carried out focusing the LDV on an accelerometer that monitored the mechanical vibrations captured with the LDV. This made it possible to clear up any suspicion of mechanical vibrations corrupting the acousto-optic measurements.

The results achieved during the PhD project confirm the potential of acousto-optic tomography as a visualization technique within the audible frequency range. This is in fact in line with previous results reported in the literature, but in this case, extra effort has been made to prove the validity of the technique as an absolute measure of the acoustic pressure. As a clear example of that, all the tomographic reconstructions have been compared to microphone array measurements, which served as a reliable reference given the maturity of the microphone array technology.

The relevance of the reconstruction algorithm has also been examined, in particular, by exploring the applicability of numerical methods in the computation of the inverse Radon transform (see Paper C). The results show that numerical methods can be a very good alternative to the well established filtered back projection method.

4.1.2 Near-field acoustic holography

Acousto-optic tomography has only been investigated for 2D sound field reconstructions in the present study. It is however natural to consider its expansion to 3D sound fields. Although this possibility has already been studied in Ref. [175], no research has been carried out in this PhD project in this direction, because 3D tomography requires a massive amount of data that makes its applicability to acousto-optic tomography difficult, especially when taking into account that there is no optimal technology readily available for exploiting the acousto-optic effect in sound measurements.

Alternatively, LDV measurements of the acousto-optic effect have been applied to NAH, which offers a number of substantial benefits. Firstly, 3D sound field reconstructions can be obtained from 1D measurements of the Radon transform taken from different angles of projection. The holographic algorithm extrapolates the measured data to parallel planes, reducing in this way dramatically the number of measurements required for 3D sound visualization. Furthermore, this approach makes it also possible to reconstruct the particle velocity of the acoustic field. This is a notable feature because the acousto-optic measuring principle has so far only been utilized for sound pressure measurements. As a result of these investigations, a new holographic technique, named near-field acousto-optic holography (NAOH), has been developed (see Papers D and E). The suggested method has been benchmarked against NAH by means of simulation and experimental results. Apart from the good agreement between the two techniques, NAOH stands out for its novel sampling pattern in the wavenumber domain.

4.1.3 Beamforming

As discussed in section 3.2, the sensitivity of a laser beam to progressive plane waves strongly depends on the incident direction of the sound wave approaching the laser beam. Instead of seeing this as a disadvantage, it has been devised a measurement technique that benefits from it and uses it for the localization of sound sources. Based on the principles of acoustic beamforming, the present PhD study has demonstrated that a laser beam can be regarded as a line array consisting of infinitely small microphones, infinitely close to each other. From this point of view, each infinitesimal point of the laser beam acts as a sensing element, and thus, a laser beam exhibits infinite spatial resolution. This has extraordinary implications: a laser beam can be seen as a beamforming system that is immune to spatial aliasing. This is a unique feature that cannot

be achieved with conventional beamforming systems based on transducers such as microphones. Advantages and disadvantages of this approach are discussed in Papers F and G.

4.2 Photon correlation spectroscopy

The investigations on PCS are the result of a research stay at the National Physical Laboratory (NPL) held during the course of the PhD project. The contributions on the ongoing research undertaken by NPL towards the development of a new primary standard for microphone calibration using PCS have been presented mainly in section 3.3. In order to extend the frequency range of analysis, it has been proven by means of simulations that the small angle approximation commonly used for the calculation of the particle velocity introduces significant errors at high frequencies. To overcome this, an analytical solution has been proposed. Besides this, the simulations also show that the small angle approximation is also inadequate for low velocity measurements.

The key parameter for estimating the particle velocity is the time lag (denoted as $\tau_{\min}$ in section 3.3) for which the Bessel function of the autocorrelation function reaches its first minimum. An iterative method based on the first derivative of the Bessel function has been suggested (method B defined on page 54 in section 3.3). The simulations show that this method is not only more accurate than the previously used method A, but also independent of the amplitude of the measured velocity and the temporal resolution used in the Fourier fit.

4.3 Overview of the included papers

The articles appended at the end of the thesis can be divided into six different subjects. Paper A investigates the fundamentals of the acousto-optic effect in simple sound fields. Papers B and C deal with acousto-optic tomography. The investigations on acoustic holography are presented in Papers D and E. The research in beamforming is included in Papers F and G. Paper H emphasizes the versatility of the acousto-optic measuring principle, and Paper I deals with some of the latest advances in PCS for microphone calibration.

4.3.1 Paper A: Acousto-optic effect

This paper presents the first investigations on the acousto-optic effect undertaken during the PhD study. It therefore aims to understand and validate the physics of the acousto-optic effect in simple acoustic fields, mainly consisting of either spherical or plane waves. This makes it possible to derive analytical expressions of the apparent velocity of the LDV from which the acoustic pressure can be estimated without using tomographic techniques. The studies were conducted with broadband signals, which illustrates the possibility of measuring the acousto-optic effect along a wide range of frequencies, even though an LDV is not expressly designed for that purpose. The importance of the measurement setup in order to minimize the effect of mechanical vibrations is also reflected.

The spherical-wave model developed for free-field measurements could characterize very well the sound pressure levels radiated by a loudspeaker. Additional measurements were carried out with a pressure microphone that served as reference for validating the model. Moreover, these measurements also illustrated the invasiveness of transducer-based methods at high frequencies, that is, when the dimensions of the transducer were comparable to the wavelength of the acoustic waves. The model also accounted for the influence of the loudspeaker's directivity, which was introducing a small loss of sensitivity in the acousto-optic model at the higher frequency range of analysis.

A plane-wave model was also implemented in a rectangular duct. Unlike the free-field case, the velocities measured with the LDV and the accelerometer were quite similar over the entire frequency range of analysis, meaning that the output of the LDV was dominated by mechanical vibrations. A rough attempt to estimate the contribution of the acousto-optic effect on the LDV output was made, and seemed to account for a great part of the differences between the velocity signals of the LDV and the accelerometer.

4.3.2 Papers B-C: Acousto-optic tomography

Paper B presents acousto-optic tomography as a non-invasive sound field visualization technique. The performance of the technique is examined for various spatial and angular resolutions, and it is shown that good sound field reconstructions can be achieved without requiring particularly high resolutions. Besides, results obtained with a planar array of 60 microphones confirm that the tomographic method can also provide an

absolute measure of the acoustic pressure. In fact, the good agreement between the microphone and the acousto-optic measurements indicates that acousto-optic tomography can potentially be used for the same applications as for microphone arrays, e.g., acoustic holography and beamforming.

The article is supplemented with two appendices. Appendix A derives the expression used to model the acousto-optic effect under weak acousto-optic interaction and clearly states its range of validity, that is, when the acoustic pressure is much smaller than the static pressure ($p/p_0 \ll 1$). Appendix B demonstrates how the acousto-optic effect can be modeled as a phase modulation effect by solving the electromagnetic wave equation when the refractive index is not constant and fluctuates at frequencies within the audible frequency range.

On the other hand, Paper C tackles the tomographic reconstruction as an inverse problem. In particular, five different numerical methods are explored as an alternative to the commonly used filtered back projection method. The performance of the methods is assessed by means of two different performance indicators, namely the mean square error and the so-called structural similarity (SI) index, which is based on image quality principles. The SI index is investigated as a complementary indicator to the classical mean square error, and seems particularly suitable in this work, because the ultimate purpose of the tomographic technique is to visualize sound.

The overall results show that three out of five numerical methods outperform the classical filtered back projection method, namely the singular value decomposition based on Tikhonov regularization, and the iterative Landweber and Kaczmarz methods. In addition, the simulation results also point out that, for low SNRs, acousto-optic tomography leads to better results than direct sound pressure measurements carried out with a microphone array, say for SNRs below 14 dB. This can be explained by the intrinsic regularization procedures of the tomographic algorithms, and confirms the potential of acousto-optic tomography not only as a visualization technique but more importantly as a quantitative method.

4.3.3 Papers D-E: Near-field acousto-optic holography

Paper D explores the use of the acousto-optic effect in acoustic holography. The obvious way to do it is to first use acousto-optic tomography to reconstruct the sound pressure over the measuring plane (like in sound visualization), and thereafter propagate the

reconstructed pressure with conventional NAH. This method is denoted as AOT-NAH in the article. However, this approach does not contribute much to the current state of the art in terms of acoustic holography, because the NAH algorithm is not upgraded with any original feature of the acousto-optic effect. It is actually exactly the same as the one used in microphone array measurements.

Alternatively, a method capable of propagating the Radon transform directly from the measuring to the reconstruction planes has also been investigated. Paper D shows that this is possible by means of the so-called Fourier slice theorem. The most interesting part of this approach is that the wavenumber spectrum of the acoustic field is not sampled with a regular grid of data points, but it is instead sampled with a circularly symmetric grid of points (see figure 4 in Paper D). In this way, the lower spatial frequencies, typically containing the information of interest of the acoustic field, are sampled with a higher density of data points than the higher spatial frequencies. This is very convenient because the higher spatial frequencies normally need to be filtered out due to the presence of measurement noise. In Paper D, this new holographic method is referred to as NAOH.

Paper E continues developing NAOH modeling in this case the diagonals of the wavenumber spectrum of the acoustic field with an elementary wave expansion. In this manner, several shortcomings arising from the use of the FFT algorithm when computing the wavenumber spectrum can be avoided. The results show that the resulting NAOH method is more accurate than the one originally presented in Paper D.

4.3.4 Papers F-G: Beamforming

Paper F introduces the concept of acousto-optic beamformer, that is, a beamforming system consisting of a laser beam capable of localizing sound source in the farfield. The article demonstrates that the laser beam can be regarded as a line array with an infinite number of microphones infinitely close to each other. This makes the proposed acousto-optic beamformer immune to spatial aliasing, meaning that a single laser beam can be used to map sound sources within the entire audible frequency range. The vulnerability of conventional beamforming systems to spatial aliasing is illustrated for a line array of 19 microphones.

Paper G presents fundamentally the same results as in Paper F, but it also analyzes the output of the acousto-optic beamformer in terms of two performance indicators

commonly used in beamforming, namely the angular resolution and the maximum side lobe (MSL) level . There is also a section by the end of the article that examines the possibility of using the proposed acousto-optic beamformer for near-field beamforming. Although the immunity to spatial aliasing persists, the performance of the acousto-optic beamformer is degraded by the loss of sensitivity of the laser beam when the acoustic waves approaching the beam have spherical wavefronts.

4.3.5 Paper H: The versatility of the acousto-optic effect

Paper H includes a synopsis of the findings achieved during the PhD study in terms of the acousto-optic effect. Despite the fact that the acousto-optic effect has been researched mainly as a visualization technique, its potential in acoustic holography and beamforming is equally notable and opens up completely new areas of research. The main goal of the article is thus to be informative and to emphasize the versatility of the acousto-optic measuring principle.

4.3.6 Paper I: Photon correlation spectroscopy

Paper I describes some of the latest advances in PCS for microphone calibration under free-field conditions. As explained in section 3.3, one of the current issues under investigation is the use of a duty gate to select specific parts of the acoustic cycle. This paper mainly discusses two approaches to gating the velocity peaks. One approach is adequate for estimating the mean flow though it assumes the flow to be fairly stationary for several minutes (which is not necessarily the case). The other approach cancels the mean flow out before computing the autocorrelation function of the photons. In this case, no estimate of the mean flow can be obtained.

It should be noted that none of these gating methods has been developed as part of the present PhD study. However, two main contributions (not reported explicitly in the article) have been made. On the one hand, the small angle approximation commonly used to determine the particle velocity has been dropped in favor of the analytical solution presented in equation (3.22). On the other hand, the method B defined on page 54 in section 3.3 has been adopted as standard method for determining τ_{min} at the first minimum of the autocorrelation function.

Chapter 5

Conclusions

5.1 General conclusions

The vertiginous progress in the field of optics since the invention of the laser has made it possible to deploy optical technology into many different areas of research. The present PhD thesis has explored the use of optical methods for characterizing sound fields as a means to improve the current state of the art in the measurement of sound.

The most advanced measurement techniques in acoustics try nowadays to exploit the increasing capabilities of computer systems. This has led to the development of array techniques such as acoustic holography and beamforming. These techniques normally improve their performance with increasing the number of transducers. Unfortunately, this approach presents some practical limitations such as the fact that increasing the number of transducers immediately raises the costs of the array system as well as the potential bias introduced into the measured quantities when immersing the array into the sound field. The intrusiveness of a transducer can be compensated for by means of frequency response corrections or minimized by embedding the transducer into a structure that either was present in the sound field before the measurement or has very well defined scattering properties that can be again compensated for.

Optical methods render properties that can potentially overcome the limitations arising when transducer arrays are deployed. The most outstanding feature is probably the non-invasiveness of light as a sensing element. Such an ideal feature is not attainable with conventional acoustic transducers, which worsens typically the performance of array techniques at high frequencies. It is also remarkable the spatial and temporal resolution with which optical methods can be used to measure various acoustic phe-

nomena. The means to achieve such a high spatial resolution depends upon the optical setup. In LDV measurements, the spatial resolution is defined by the diameter of the laser beam, which can easily be focused to diameters of the order of hundreds of micrometers. In techniques such as PIV, the number of pixels of the CCD camera plays an important role. For example, the spatial resolution obtained when imaging a 1 m^2 aperture with a common 1024×1024 pixels CCD camera is about 1 mm. In comparison, conventional microphones are far from these figures because the spatial resolution is linked to the dimensions of the microphone membrane. This means that in order to improve the spatial resolution, the membrane needs to be reduced, and that normally yields a loss in sensitivity.

In terms of temporal resolution, optical methods based on pulsed lasers can provide extremely short pulses of the order of tens of picoseconds. Again, microphones are far from these numbers, because as transducers, they always have an inherent response determined by the mechanical properties of the membrane and the electronics embedded into the microphone. Another notable advantage of optical methods is the fact that light travels approximately at 3×10^8 m/s, and thus, several positions of a medium can be investigated 'instantaneously'.

An overview of optical techniques for acoustic measurements has been given in Chapter 3, with special focus on tracer and interferometric methods that are based on PCS and laser Doppler vibrometry, respectively. On the one hand, the tracer methods provide an absolute measure of the particle velocity of the medium under investigation. They can do this either in a point-wise manner as in PCS or over a large aperture as in PIV. Tracer methods require however the use of seeding, which can in some cases compromise the precious non-invasiveness originally sought in these methods. On the other hand, the interferometric techniques stand out for their sensitivity, which in this study has been used to measure the acousto-optic effect. Although the high sensitivity of the interferometric methods imposes strict requirements on the measurement setup in terms of mechanical stability, it is particularly impressive how the acousto-optic measuring principle can be used to investigate acoustic phenomena over a tremendously broad frequency range that goes from the very low audible frequencies up to the very high ultrasonic frequencies of the order of megahertz. Perhaps surprisingly at first glance, the acousto-optic measuring principle measures neither the particle velocity nor the acoustic pressure directly. It captures instead the integral of the pressure along the optical path followed by the sensing light. Far from being a limitation that shortens the poten-

tial of the technique, the present PhD study has taken benefit from this integral principle and has exploited it for sound visualization as well as for sound source diagnosis and localization.

5.2 Main findings

The dissertation has particularly presented new insights into the measurement of sound by means of the acousto-optic effect. The main contributions lie in the development of measurement techniques founded on the acousto-optic effect, when measured in air and within the audible frequency range.

Firstly, the thesis has revised the state of the art in acousto-optic tomography and contributed to extend it by proposing the use of numerical methods in the tomographic reconstruction. To formulate the tomographic reconstruction as an inverse problem makes it possible to exploit the regularization techniques commonly used in inverse problems. The results show that this approach leads to solutions that can outperform the results obtained with the well established and normally preferred filtered back projection method. Improving the accuracy of acousto-optic tomography strengthens the idea that this optical technique can be used not only for visualization purposes but also for quantitative measurements. Yet far from that stage where acousto-optic tomography can readily compete with the state of the art in microphone array measurements, the fact that there is no technological solution expressly designed to benefit from this measurement principle suggests that acousto-optic tomography can still evolve significantly in the future.

Secondly, the acousto-optic effect has also been investigated in two completely new areas of research, namely holography and beamforming. Given the difficulty of realizing 3D reconstructions based on acousto-optic tomography, partly because of the massive amount of data required for that as well as the inadequate available technology, a new method named NAOH have been proposed. NAOH measures the Radon transform of the acoustic field under investigation in a plane and propagates this information directly to another parallel plane, where both acoustic pressure and particle velocity can be reconstructed. By doing this over several planes, a 3D reconstruction of a sound field is available based on a single 2D measurement. Furthermore, the characterization of the 3D sound field is complete, because not only the pressure is reconstructed, but also the particle velocity, just as in conventional NAH based on microphone arrays. In addition,

by exploiting the fact that the acousto-optic measuring principle is indeed a direct measure of the Radon transform of the acoustic field, NAOH introduces a novel sampling pattern in the wavenumber domain where the lower spatial frequencies are sampled with a higher density of data points than the higher spatial frequencies. It is believed that this unique sampling pattern softens the requirements for regularization when propagating the data from one plane to another, because the high spatial frequencies, that normally contain more noise than useful data, are 'downsampled' in comparison to conventional NAH.

From a completely different perspective, the sensitivity of a laser beam to plane waves approaching the beam from different directions has been exploited for the localization of sound sources located in the farfield. By interpreting the laser beam as a line array of microphones with infinite resolution, an acousto-optic beamforming system that features immunity to spatial aliasing has been proposed. This is a unique feature, since conventional beamforming systems are based on a finite number of transducers, which makes them inherently vulnerable to spatial aliasing above a certain frequency.

Finally, and to a lesser extent, the present PhD study has also contributed in the development of a future primary method based on PCS for microphone calibration under free-field conditions. The investigations in this matter have basically yielded some refinements in the signal processing used to compute the velocity estimate from the measured autocorrelation function of the scattered photons. The most important contribution is probably the analysis that demonstrates the bias introduced in the velocity estimate when using the commonly accepted small angle approximation. The results show that this approximation is not valid at high frequencies and for low velocity levels. Although the error introduced by the small angle approximation might not be significant for many acoustic applications, it is conversely relevant in acoustic metrology, in case the technique is eventually deployed as a primary calibration method.

5.3 Future research

New technology

The overall results of the present PhD study reflect that the acousto-optic effect can potentially be used for the same applications for which conventional microphones are currently deployed, e.g., sound pressure measurement and visualization, acoustic holog-

raphy and beamforming. Furthermore, it has been shown that the acousto-optic effect together with the proposed techniques feature unique properties that cannot be achieved with conventional acoustic techniques, namely the non-invasiveness of light when used as a measurement principle, the immunity to spatial aliasing in beamforming applications, and the novel spectral properties in acoustic holography. Although the results obtained with the acousto-optic measuring principle are comparable to those obtained with microphone-based systems, the current implementation of the experimental setup conceived for this technique does not make the technique readily available for industrial applications. Therefore, one of the main areas of research in the future must be focused on developing new technology capable of exploiting the acousto-optic effect in real measurement scenarios. In short, such a technology must be sensitive to the acousto-optic effect, but 'immune' to mechanical vibrations. The latter is probably the most challenging part, because to enhance the sensitivity to the acousto-optic effect implies in principle a similar increase in sensitivity to vibrations. Therefore, it is necessary that the future technology monitors such vibrations and eventually compensates for them if necessary.

Assuming the existence of the aforementioned new technology, optical arrays founded on the acousto-optic measuring principle could serve the purpose of many acoustic measurements. A sketch of a possible optical array is presented in figure 5.1. Such an array would exploit all the benefits already described of the acousto-optic ef-

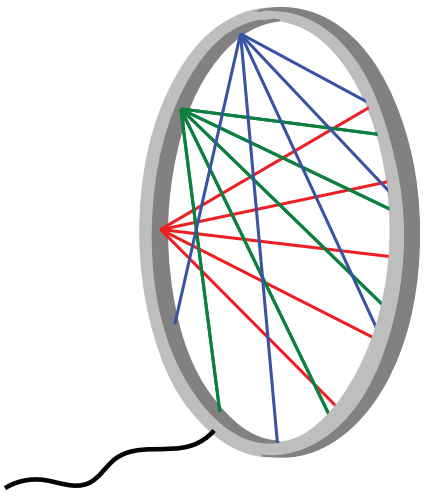

Figure 5.1: Sketch of an ideal optical array.

fect, and could also present a major technological advantage with respect to conventional array systems. The technology embedded into a transducer array scales up with the number of transducers, and that is precisely what makes it difficult to build up array systems consisting of many transducers. Instead, the envisioned optical array may increase the number of sensing beams by simply splitting the original beam emerging from the laser source into more sub-beams. This approach could reduce substantially the costs of array systems with high demands in terms of spatial resolution.

Beyond the acousto-optic measuring principle

Apart from the need for new technological advances, the acousto-optic measuring principle itself requires further investigations. This measurement principle is based on capturing the refractive index variations induced by acoustic pressure fluctuations. However, there are other phenomena that can also change the refractive index, e.g., flow and temperature gradients. There are two possible lines of research from this perspective. On the one hand, it would be relevant to determine how acoustic measurements based on the acousto-optic effect may degrade with the presence of flow and temperature gradients. On the other hand, many industrial applications require measurements under very extreme conditions, e.g., under high temperature and pressure gradients. Perhaps, the acousto-optic measuring principle could be further expanded in order to not only measure acoustic quantities, but also provide information about other atmospheric quantities.

Acousto-optic tomography

The results presented in Paper C suggest that numerical methods can yield better tomographic reconstructions than the filtered back projection method. However, this finding is fundamentally based on a simulation study where the best numerical solutions have been selected following a trial an error procedure, that is, the numerical method is tested for different values of its regularization parameters and the outputs are compared to a theoretical sound field that serves as a reference. Quite often, in practical situations, there is no previous information about the sound field under investigation, and thus, it is difficult to determine the optimal value of the regularization parameter. Future research in this direction should examine the use of parameter choice methods. This kind of methods are widely used in inverse problems because they can approximate the opti-

mal value of the regularization parameter based only on the measured data, or in other words, without previous knowledge of the system.

NAOH

Since NAOH is based on the Radon transform, and thus, is somehow related to acousto-optic tomography, it seems natural to transfer at some point all the knowledge gathered about numerical methods in acousto-optic tomography to NAOH. The future versions of NAOH should thereby include this knowledge and adapt it to the holographic problem. Besides, the unique spectral properties of NAOH in the wavenumber domain open up the possibility of designing new holographic algorithms with non-uniform sampling schemes. It would be interesting to explore whether it is possible to define a stable holographic method that concentrates the majority of data points over those spatial frequencies of interest, and reject in this way those frequency components that are mainly corrupted with noise. In addition, in a similar way as NAH, it would also be interesting to further develop the technique beyond the planar case, and ultimately to the case of non-conformal surfaces.

Acousto-optic beamforming

The proposed acousto-optic beamformer renders total immunity to spatial aliasing, but below the Nyquist frequency, it provides similar results to those featured by a line array of microphones. Conventional beamforming systems can be deployed into many different configurations and geometries. Although at the current state of the art it is difficult to imagine a different configuration for the proposed acousto-optic beamformer, it could be relevant in the future to explore the possibility of developing fibers capable of sensing sound along its optical path. This would make it possible to guide light into different directions, and thus, to implement new acousto-optic beamforming techniques based on the resulting geometries.

PCS as a primary calibration method

If PCS is ultimately deployed as a primary method for microphone calibration, the technique must be refined to accuracies up to the metrological standards. Some of the lines of research to follow to achieve that are the ones drawn in section 3.3.4. It

is particularly important to work out the ambiguities posed by some aspects of the technique such as the influence of the duty gate, the distortion of the loudspeaker and the possible bias introduced by the acousto-optic effect.

Bibliography

[1] G. ten Doesschate, "Oxford and the revival of optics in the thirteenth century," *Vision Research*, vol. 1, no. 5-6, pp. 313–342, 1962.

[2] H. E. Burton, "The optics of Euclid," *Journal of the Optical Society of America*, vol. 35, no. 5, pp. 357–372, 1945. Translation by H. E. Burton of the original essay written by Euclid.

[3] R. Rashed, "A pioneer in anaclastics: Ibn Sahl on burning mirrors and lenses," *The History of Science Society*, vol. 81, no. 3, pp. 464–491, 1990.

[4] G. Simon, "The gaze in Ibn al-Haytham," *The Medieval History Journal*, vol. 9, no. 1, pp. 89–98, 2006.

[5] V. Ilardi, *Renaissance Vision from Spectacles to Telescopes*. Philadelphia: American Philosophical Society, 2007. Chapter 1 – The invention of Spectacles Revisited, pp. 3–52.

[6] S. Bradbury, *The evolution of the microscope*. Pergamon Press, 1967.

[7] A. V. Helden, "The invention of the telescope," *Transactions of the American Philosophical Society*, vol. 67, no. 4, pp. 1–67, 1977.

[8] T. S. Kuhn, *The Copernican Revolution: Planetary Astronomy in the Development of Western Thought*. Harvard University Press, 1957.

[9] A. Kwan, J. Dudley, and E. Lantz, "Who really discovered Snell's law?," *Physics World*, vol. 15, no. 4, pp. 64–64, 2002.

[10] I. Newton, *Opticks: or, a Treatise of the Reflexions, Refractions, Inflexions and Colours of Light. Also two Treatises of the Species and Magnitude of Curvilinear Figures*. London: Printed for Sam Smith, and Benj. Walford, printers to the Royal Society, at the Prince's Arms in St. Paul's Church-yard, 1704.

[11] C. Huygens, *Traité de la Lumiere*. Leide: Pierre Vander Aa, 1690.

[12] T. Young, "The Bakerian Lecture: Experiments and calculations relative to physical optics," *Philosophical Transactions of the Royal Society of London*, vol. 94, pp. 1–16, 1804.

[13] F. L. Pedrotti, L. S. Pedrotti, and L. M. Pedrotti, *Introduction to Optics*. New Jersey: Pearson Prentice Hall, 3rd ed., 2007.

[14] J. C. Maxwell, *A Treatise on Electricity and Magnetism*. Clarendon Press, 1873.

[15] M. Planck, "Zur Theorie des Gesetzes der Energieverteilung im Normalspektrum," *Verhandlungen der Deutschen Physikalischen Gesellschaft*, vol. 2, no. 17, pp. 237–245, 1900.

[16] M. Planck, "Ueber das Gesetz der Energieverteilung im Normalspectrum," *Annalen der Physik*, vol. 4, no. 3, pp. 553–563, 1901.

[17] A. Einstein, "Über einen die Erzeugung und Verwandlung des Lichtes betreffenden heuristischen Gesichtspunkt," *Annalen der Physik*, vol. 17, no. 6, pp. 132–148, 1905.

[18] N. Bohr, "On the constitution of atoms and molecules," *Philosophical Magazine*, vol. 26, no. 153, pp. 476–502, 1913.

[19] A. H. Compton, "A quantum theory of the scattering of X-rays by light elements," *Physical Review*, vol. 21, no. 5, pp. 483–502, 1923.

[20] L. de Broglie, *Recherches sur la théorie des quanta*. PhD thesis, Université de Paris, Paris, 1924.

[21] B. A. Lengyel, "Evolution of Maser and Laser," *American Journal of Physics*, vol. 34, no. 10, pp. 903–913, 1966.

[22] J. Eargle, *The Microphone Book*. Focal Press, 2nd ed., 2005.

[23] J. B. R. Kinns, "The acoustic telescope," *Journal of Sound and Vibration*, vol. 48, no. 4, pp. 485–510, 1976.

[24] E. G. Williams, J. D. Maynard, and E. Skudrzyk, "Sound source reconstructions using a microphone array," *J. Acoust. Soc. Am.*, vol. 68, no. 1, pp. 340–344, 1980.

[25] E. G. Williams, *Fourier Acoustics: Sound Radiation and Nearfield Acoustical Holography*. Academic Press, 1999.

[26] D. H. Johnson and D. E. Dudgeon, *Array signal processing: Concepts and techniques*. Englewood Cliffs, New Jersey: PTR Prentice Hall, 1993.

[27] E. N. da C. Andrade, "Doppler and the Doppler effect," *Endeavour*, vol. 18, no. 69, pp. 14–19, 1959.

[28] L. Brillouin, “Diffusion of light and X-rays by a transparent homogeneous body,” *Annalen der Physik*, vol. 17, pp. 88–122, 1922.

[29] P. Debye and F. W. Sears, “On the scattering of light by supersonic waves,” in *Proceedings of the National Academy of Sciences of the United States of America*, vol. 18, pp. 409–414, 1932.

[30] R. Lucas and P. Biquard, “Optical properties of solid and liquid medias subjected to high-frequency elastic vibrations,” *Journal de Physique et le Radium*, vol. 3, pp. 464–477, 1932.

[31] C. V. Raman and N. S. N. Nath, “The diffraction of light by high frequency sound waves: Part I,” in *Proceedings of the Indian Academy of Sciences - Section A*, vol. 2, pp. 406–412, 1935.

[32] C. V. Raman and N. S. N. Nath, “The diffraction of light by high frequency sound waves: Part II,” in *Proceedings of the Indian Academy of Sciences - Section A*, vol. 2, pp. 413–420, 1935.

[33] C. V. Raman and N. S. N. Nath, “The diffraction of light by high frequency sound waves: Part III,” in *Proceedings of the Indian Academy of Sciences - Section A*, vol. 3, pp. 75–84, 1936.

[34] C. V. Raman and N. S. N. Nath, “The diffraction of light by high frequency sound waves: Part IV,” in *Proceedings of the Indian Academy of Sciences - Section A*, vol. 3, pp. 119–125, 1936.

[35] C. V. Raman and N. S. N. Nath, “The diffraction of light by high frequency sound waves: Part V,” in *Proceedings of the Indian Academy of Sciences - Section A*, vol. 3, pp. 459–465, 1936.

[36] N. S. N. Nath, “The diffraction of light by high frequency sound waves: Generalised theory,” in *Proceedings of the Indian Academy of Sciences - Section A*, vol. 4, pp. 222–242, 1936.

[37] G. W. Willard, “Criteria for normal and abnormal ultrasonic light diffraction effects,” *J. Acoust. Soc. Am.*, vol. 21, no. 2, pp. 101–108, 1949.

[38] W. G. Mayer, “Light diffraction by ultrasonic waves for oblique incidence,” *J. Acoust. Soc. Am.*, vol. 36, no. 4, pp. 779–781, 1964.

[39] W. L. Bragg, “Diffraction of short electromagnetic waves by a crystal,” in *Proceedings of the Cambrigde Philosophical Society*, vol. 17, pp. 43–57, 1913.

[40] C. F. Quate, C. D. Wilkinson, and D. K. Winslow, “Interaction of light and microwave sound,” in *Proceedings of the IEEE*, vol. 53, pp. 1604–1623, 1965.

[41] E. I. Gordon, "A review of acoustooptical deflection and modulation devices," in *Proceedings of the IEEE*, vol. 54, pp. 1391–1401, 1966.

[42] M. J. Brienza and A. J. DeMaria, "Continuously variable laser-acoustic delay line," *IEEE Journal of Quantum Electronics*, vol. 3, no. 6, pp. 261–262, 1967.

[43] R. Adler, "Interaction between sound and light," *IEEE Spectrum*, vol. 4, no. 5, pp. 42–54, 1967.

[44] J. C. Owens, "Optical refractive index of air: Dependence on pressure, temperature and composition," *Applied Optics*, vol. 6, no. 1, pp. 51–59, 1967.

[45] O. Cramer, "The variation of the specific heat ratio and the speed of sound in air with temperature, pressure, humidity, and CO2 concentration," *J. Acoust. Soc. Am.*, vol. 93, no. 5, pp. 2510–2516, 1993.

[46] K. P. Birch and M. J. Downs, "An updated Edlén equation for the refractive index of air," *Metrologia*, vol. 30, no. 3, pp. 155–162, 1993.

[47] K. P. Birch and M. J. Downs, "Correction to the updated Edlén equation for the refractive index of air," *Metrologia*, vol. 31, no. 4, pp. 315–316, 1994.

[48] P. E. Ciddor, "Refractive index of air: new equations for the visible and near infrared," *Applied Optics*, vol. 35, no. 9, pp. 1566–1573, 1996.

[49] G. Bönsch and E. Potulski, "Measurement of the refractive index of air and comparison with modified Edlén's formulae," *Metrologia*, vol. 35, no. 2, pp. 133–139, 1998.

[50] C. B. Scruby and L. E. Drain, *Laser ultrasonics: Techniques and applications*. New York: Taylor & Francis, 1990.

[51] J. W. Strutt, "On the transmission of light through an atmosphere containing small particles in suspension, and on the origin of the blue of the sky," *Philosophical Magazine*, vol. 47, no. 5, pp. 375–394, 1899.

[52] A. Rausch, A. Fischer, N. Kings, F. Bake, and I. Roehle, "Optical measurement of acoustic pressure amplitudes - at the sensitivity limits of rayleigh scattering," *Optics Letters*, vol. 37, no. 13, pp. 2685–2687, 2012.

[53] H.-E. Albrecht, M. Borys, N. Damaschke, and C. Tropea, *Laser Doppler and phase Doppler measurement techniques*. Experimental fluid Mechanics, Springer, 2003.

[54] S. J. Putterman, "Sonoluminescence. Sound into light," *Scientific American*, vol. 272, no. 2, pp. 46–51, 1995.

[55] D. F. Gaitan, L. A. . Crum, C. C. Churcha, and R. A. . Roy, "Sonoluminescence and bubble dynamics for a single, stable,cavitation bubble," *J. Acoust. Soc. Am.*, vol. 91, no. 6, pp. 3166–3183, 1992.

[56] M. P. Brenner, S. Hilgenfeldt, and D. Lohse, "Single-bubble sonoluminescence," *Reviews of Modern Physics*, vol. 74, no. 2, pp. 425–484, 2002.

[57] E. P. Krider and R. G. Roble, eds., *The Earth's Electrical Environment*. Washington, D. C.: National Academy Press, 1986. Chapter 4 – Acoustic radiations from lightning, pp. 46–60.

[58] A. G. Bell, "The photophone," *Science*, vol. 1, no. 11, pp. 130–134, 1880.

[59] A. G. Bell, "On the production and reproduction of sound by light," *American Journal of Sciences*, vol. 20, no. 118, pp. 305–324, 1880.

[60] A. G. Bell, "Upon the production of sound by radiant energy," *Philosophical Magazine*, vol. 11, no. 7, pp. 510–528, 1881.

[61] Z. Bozóki, A. Pogány, and G. Szabó, "Photoacoustic instruments for practical applications: Present, potentials, and future challenges," *Applied Spectroscopy Reviews*, vol. 46, no. 1, pp. 1–37, 2011.

[62] I. Newton, *Philosophiæ Naturalis Principia Mathematica*. J. Societatis Regiae ac Typis J. Streater, 1687.

[63] DFM (Danish National Metrology Institute) and BKSV-DPLA (Brüel & Kjær Sound & Vibration Measurement Ltd - Danish Primary Laboratory for Acoustics section), "Calibration and measurement capabilities." The BIPM key comparison database, January 2010.

[64] P. M. Morse and K. U. Ingard, *Theoretical Acoustics*. Princeton, New Jersey: Princeton University Press, 1st ed., 1986.

[65] P. Lebedew, "Untersuchungen über die Druckkräfte des Lichtes," *Annalen der Physik*, vol. 6, no. 11, pp. 433–458, 1901.

[66] H. X. Tang, "May the force of light be with you," *IEEE Spectrum*, vol. 46, no. 10, pp. 46–51, 2009.

[67] W. Merzkirch, *Flow visualization*. New York: Academic Press, 1974.

[68] W. Merzkirch, "Techniques of flow visualization," tech. rep., Advisory Group for Aerospace Research & Development, Loughton, Essex, 1987.

[69] R. Hooke, *Micrographia*. London: J. Martyn and J. Allestry., 1665. Observ. LVIII. – "Of a new Property of Air',. . . ".

[70] D. Bershader, "Improved flow visualization by use of resonant refractivity," tech. rep., Air Force Office of Scientific Research, Whashingon, D. C., 1979.

[71] R. D. Small, V. A. Sernas, and R. H. Page, "Single beam schlieren interferometer using a Wollaston prism," *Applied Optics*, vol. 11, no. 4, pp. 858–862, 1972.

[72] M. J. R. Schwar and F. J. Weinberg, "The measurement of velocity by applying schlieren-interferometry to Doppler-shifted laser light," in *Proceedings of the Royal Society of London*, vol. 311, pp. 469–476, 1969.

[73] D. Möller, N. Degen, and J. Dual, "Schlieren visualization of ultrasonic standing waves in mm-sized chambers for ultrasonic particle manipulation," *Journal of Nanobiotechnology*, vol. 11, no. 21, 2013. 5 pages.

[74] K. J. Gåsvik, *Optical Metrology*. West Sussex: John Wiley & Sons, 2002.

[75] K. G. Harding and J. S. Harris, "Projection moire interferometer for vibration analysis," *Applied Optics*, vol. 22, no. 6, pp. 856–861, 1983.

[76] C. Forno, "Deformation measurement using high resolution Moiré photography," *Optics and Lasers in Engineering*, vol. 8, no. 3–4, pp. 189–212, 1988.

[77] R. L. Powell and K. A. Stetson, "Interferometric vibration analysis by wavefront reconstruction," *Journal of the Optical Society of America*, vol. 55, no. 12, pp. 1593–1598, 1965.

[78] K. a. Stetson and R. L. Powell, "Hologram interferometry," *Journal of the Optical Society of America*, vol. 56, no. 9, pp. 1161–1166, 1966.

[79] D. Gabor, "A new microscopic principle," *Nature*, vol. 161, pp. 777–778, 1948.

[80] C. M. Vest, *Holographic interferometry*. New York: John Wiley & Sons, 1979.

[81] I. Weingärtner, "Holography - techniques and application," *Journal of Physics E: Scientific Instruments*, vol. 16, no. 1, pp. 16–23, 1983.

[82] N. H. Fletcher and T. D. Rossing, *The physics of musical intruments*. Springer, 2nd ed., 2010.

[83] M. H. Horman, "An application of wavefront reconstruction to interferometry," *Applied Optics*, vol. 4, no. 3, pp. 333–336, 1965.

[84] J. A. Clark, "Holographic visualization of acoustic fields," *Journal of Sound and Vibration*, vol. 56, no. 2, pp. 167–174, 1978.

[85] A. O. Wåhlin, P. Gren, and N.-E. Molin, "On structure-borne sound: experiments showing the initial transient acoustic wave field generated by an impacted plate," *J. Acoust. Soc. Am.*, vol. 96, no. 5, pp. 2791–2797, 1994.

[86] S. Schedin, A. O. Wåhlin, and P. O. Gren, "Transient acoustic near field in air generated by impacted plates," *J. Acoust. Soc. Am.*, vol. 99, no. 2, pp. 700–705, 1996.

[87] D. Havelock, S. Kuwano, and M. Vorländer, eds., *Handbook of Signal Processing in Acoustics*. Springer, 2008. See Chapter 71 - Laser Doppler velocimeter, by Nobutoshi Yoshida.

[88] L. Allen and D. G. C. Jones, "An analysis of the granularity of scattered optical maser light," *Physics Letters*, vol. 7, no. 5, pp. 321–323, 1963.

[89] "Speckle pattern." http://en.wikipedia.org/wiki/File:Objective_speckle.jpg. Licensing: public domain. From Wikimedia Commons.

[90] "ESPI interferogram." http://en.wikipedia.org/wiki/File:ESPIvibration.jpg. Licensing: public domain. From Wikimedia Commons.

[91] J. N. Butters, "Speckle pattern interferometry using video techniques," *SPIE J*, vol. 10, no. 1, pp. 5–9, 1971.

[92] K. Høgmoen and O. J. Løkberg, "Detection and measurement of small vibrations using electronic speckle pattern interferometry," *Applied Optics*, vol. 16, no. 7, pp. 1869–1875, 1977.

[93] G. A. Slettemoen, "Optimal signal processing in electronic speckle pattern interferometry," *Optics Communications*, vol. 23, no. 2, pp. 213–216, 1977.

[94] G. A. Slettemoen, "General analysis of fringe contrast in electronic speckle pattern interferometry," *Optica Acta*, vol. 26, no. 3, pp. 313–327, 1979.

[95] K. Creath and G. A. Slettemoen, "Vibration-observation techniques for digital speckle-pattern interferometry," *Journal of the Optical Society of America*, vol. 2, no. 10, pp. 1629–1636, 1985.

[96] K. Creath, "Digital speckle pattern interferometry (DSPI) using a 100×100 imaging array," in *SPIE - State-of-the-Art Imaging Arrays and Their Applications*, vol. 501, pp. 292–298, 1985.

[97] Ángel F. Doval, "A systematic approach to TV holography," *Measurement Science and Technology*, vol. 11, no. 1, pp. R1–R36, 2000.

[98] U. P. Kuma, Y. Kalyani, N. K. Mohan, and M. P. Kothiyal, "Time-average TV holography for vibration fringe analysis," *Applied Optics*, vol. 48, no. 16, pp. 3094–3101, 2009.

[99] S. Schedin, P. O. Gren, and T. D. Rossing, "Transient wave response of a cymbal using double-pulsed TV holography," *J. Acoust. Soc. Am.*, vol. 103, no. 2, pp. 1217–1220, 1998.

[100] T. D. Rossing and G. Eban, "Normal modes of a radially braced guitar determined by electronic TV holography," *J. Acoust. Soc. Am.*, vol. 106, no. 5, pp. 2991–2996, 1999.

[101] O. J. Løkberg, "Recording of sound emission and propagation in air using TV holography," *J. Acoust. Soc. Am.*, vol. 96, no. 4, pp. 2244–2250, 1994.

[102] O. J. Løkberg, "Sound in flight: measurement of sound fields by use of TV holography," *Applied Optics*, vol. 33, no. 13, pp. 2574–2584, 1994.

[103] M. Espeland, O. J. Løkberg, and R. Rustad, "Full field tomographic reconstruction of sound fields using TV holography," *J. Acoust. Soc. Am.*, vol. 98, no. 1, pp. 280–287, 1995.

[104] O. J. Løkberg, R. Rustad, and M. Espeland, "Tomographic reconstruction of sound fields in air using TV-holography," *Optics and Lasers in Engineering*, vol. 25, no. 4–5, pp. 361–372, 1996.

[105] P. Gren, S. Schedin, and X. Li, "Tomographic reconstruction of transient acoustic fields recorded by pulsed TV holography," *App*, vol. 37, no. 5, pp. 834–840, 1998.

[106] A. Runnemalm, "Standing waves in a rectangular sound box recorded by TV holography," *Journal of Sound and Vibration*, vol. 224, no. 4, pp. 689–707, 1999.

[107] A. Melling and J. H. Whitelaw, "Seeding of gas flows for laser anemometry," *DISA Information, Danske Industri Syndikat A/S*, no. 15, pp. 5–14, 1973.

[108] L. E. Drain, *The laser Doppler technique*. Norwich: John Wiley & Sons, 1980.

[109] J. C. Valière, P. Herzog, V. Valeau, and G. Tournois, "Acoustic velocity measurements in the air by means of laser Doppler velocimetry: Dynamic and frequency range limitations and signal processing improvements," *Journal of Sound and Vibration*, vol. 229, no. 3, pp. 607–626, 2000.

[110] B. Gazengel, S. Poggi, and J.-C. Valière, "Evaluation of the performance of two acquisition and signal processing systems for measuring acoustic particle velocities in air by means of laser Doppler velocimetry," *Measurement Science and Technology*, vol. 14, no. 12, pp. 2047–2064, 2003.

[111] Y. Yeh and H. Z. Cummins, "Localized fluid flow measurements with an He-Ne laser spectrometer," *Applied Physics Letters*, vol. 4, no. 10, pp. 176–178, 1964.

[112] K. J. Taylor, "Absolute measurement of acoustic particle velocity," *J. Acoust. Soc. Am.*, vol. 59, no. 3, pp. 691–694, 1976.

[113] K. J. Taylor, "Absolute calibration of microphones by a laser-Doppler technique," *J. Acoust. Soc. Am.*, vol. 70, no. 4, pp. 939–945, 1981.

[114] T. Koukoulas, P. Theobald, T. Schlicke, and R. Barham, "Airborne acoustic velocity measurement utilising laser Doppler anemometry combined with photon correlation in low seeded conditions," in *Proceedings of the Institute of Acoustics*, vol. 30, 2008.

[115] T. Koukoulas, P. Theobald, T. Schlicke, and R. Barham, "Towards a future primary method for microphone calibration: Optical measurement of acoustic velocity in low seeding conditions," *Optics and Lasers in Engineering*, vol. 46, no. 11, pp. 791–796, 2008.

[116] T. Koukoulas, P. Theobald, and R. Barham, "Airborne acoustic velocity measurements in enclosed and open air conditions using minimal articicial seeding and photon correlation spectroscopy: current issues an future challenges," in *16th International Congress on Sound and Vibration*, 2009.

[117] P. Arroyo and C. A. Greated, "Stereoscopic particle image velocimetry," *Measurement Science and Technology*, vol. 2, no. 12, pp. 1181–1186, 1991.

[118] D. B. Hann and C. A. Greated, "Particle image velocimetry for the measurement of mean and acoustic particle velocities," *Measurement Science and Technology*, vol. 8, no. 6, pp. 656–660, 1997.

[119] D. B. Hann and C. A. Greated, "The measurement of flow velocity and acoustic particle velocity using particle-image velocimetry," *Measurement Science and Technology*, vol. 8, no. 12, pp. 1517–1522, 1997.

[120] A. Melling, "Tracer particles and seeding for particle image velocimetry," *Measurement Science and Technology*, vol. 8, no. 12, pp. 1406–1416, 1997.

[121] M. Campbell, J. Cosgrove, C. A. Greated, S. Jack, and D. Rockliff, "Review of LDA and PIV applied to the measurement of sound and acoustic streaming," *Optics & Laser Technology*, vol. 32, no. 7–8, pp. 629–639, 2000.

[122] D. Garthe, "A fiber-optic microphone," *Sensors and Actuators A (Physical)*, vol. 26, no. 1–3, pp. 341–345, 1991.

[123] M. Yu and B. Balachandran, "Acoustic measurements using a fiber optic sensor system," *Journal of Intelligent Material Systems and Structures*, vol. 14, no. 7, pp. 409–414, 2003.

[124] P. Morris, A. Hurrell, A. Shaw, E. Zhang, and P. Beard, "A Fabry-Perot fiber-optic ultrasonic hydrophone for the simultaneous measurement of temperature and acoustic pressure," *J. Acoust. Soc. Am.*, vol. 125, no. 6, pp. 3611–3622, 2009.

[125] L. Mohanty, L. M. Koh, and S. C. Tjin, "Fiber Bragg grating microphone system," *Applied Physics Letters*, vol. 89, no. 16, pp. 161109–1–3, 2006.

[126] B. Fischer and E. Wintner, "Optical transducer without membrane," in *18th International Congress on Sound & Vibration*, (Rio de Janeiro), 2011.

[127] Y. Suzuki and K. Kido, "Theoretical investigation on a microphone using optical reflection on curved surface," *Acoustical Science and Technology*, vol. 25, no. 1, pp. 45–49, 2004.

[128] Y. Suzuki and K. Kido, "Theoretical investigation on the sensitivity of a microphone using the change in the total reflection of light by sound," *Acoustical Science and Technology*, vol. 29, no. 4, pp. 283–290, 2008.

[129] "IEC international standard 61094-2, Measurement microphones - Part 2: Primary methods for pressure calibration of laboratory standard microphones by the reciprocity technique," 2009.

[130] "IEC international standard 61094-3, Measurement microphones - Part 3: Primary method for free-field calibration of laboratory standard microphones by reciprocity technique," 2009.

[131] L. Zipser and H. H. Franke, "Refracto-vibrometry for visualizing ultrasound in gases, fluids and condensed matter," in *IEEE Ultrasonic Symposium Proceedings*, vol. 1–6, pp. 395–398, 2007.

[132] L. Zipser and H. H. Franke, "Refracto-vibrometry - a novel method for visualizing sound waves in transparent media," in *Acoustics'08 Paris*, (Paris), 2008.

[133] C. Vuye, *Measurement and modeling of sound and vibration fields using a scanning laser Doppler vibrometer*. PhD thesis, Vakgroep Toegepaste Mechanica, Faculteit Ingenieurswetenschappen, Vrije Universiteit Brussel, October 2011.

[134] S. H. Jack, D. B. Hann, and C. A. Greated, "Influence of the acousto-optic effect on laser Doppler anemometry signals," *Review of Scientific Instruments*, vol. 69, no. 12, pp. 4074–4081, 1998.

[135] R. I. Crickmore, S. H. Jack, D. B. Hann, and C. A. Greated, "Laser Doppler anemometry and the acousto-optic effect," *Optics & Laser Technology*, vol. 31, no. 1, pp. 85–94, 1999.

[136] S. H. Jack, D. B. Hann, and C. A. Greated, "The influence of a standing wave on laser Doppler signals," *Measurement Science and Technology*, vol. 10, no. 12, pp. 1279–1285, 1999.

[137] D. R. Bacon, R. C. Chivers, and J. N. Som, "The acousto-optic interaction in the interferometric measurement of ultrasonic transducer surface motion," *Ultrasonics*, vol. 31, no. 5, pp. 321–325, 1993.

[138] D. Certon, G. Ferin, O. B. Matar, J. Guyonvarch, J. Remenieras, and F. Patat, "Influence of acousto-optic interactions on the determination of the diffracted field by an array obtained from displacement measurements," *Ultrasonics*, vol. 42, no. 1-9, pp. 465–471, 2004.

[139] O. A. Sapozhnikov, A. V. Morozov, and D. Cathignol, "Piezoelectric transducer surface vibration characterization using acoustic holography and laser vibrometry," in *IEEE Ultrasonics Symposium*, vol. 1, pp. 161–164, 2004.

[140] A. V. Morozov, *Étude de la vibration des transducteurs piézoélectriques par vibrométrie laser et holographie acoustique*. PhD thesis, Universite Claude Bernard - Lyon 1, January 2006.

[141] M. P. Cooling, *Characterisation of underwater ultrasonics sources and fields by means of laser Doppler vibrometry*. PhD thesis, Institute of Sound and Vibration research, Faculty of Engineering, Science and Mathematics, University of Southampton, November 2010.

[142] M. P. Cooling, V. Humphrey, P. Theobald, and S. Robinson, "Underwater ultrasonic field characterization using laser Doppler vibrometry of transducer motion," in *20th International Congress on Acoustics*, 2010.

[143] V. F. Humphrey, M. Cooling, P. Theobald, and S. Robinson, "The influence of the acousto-optic effect on LDV measurements of underwater transducer vibration and resultant field predictions," in *Proceedings of the Institute of Acoustics*, vol. 35, 2013.

[144] Polytec, "OFV-505/503 Vibrometer sensor head." On-line, 2012. Data Sheet.

[145] J. Radon, "On the determination of functions from their integral values along certain manifolds," *IEEE Transactions on Medical Imaging*, vol. 5, no. 4, pp. 170–176, 1986. Translated by P. C. Parks from the original German text.

[146] A. C. Kak and M. Slaney, *Principles of Computerized Tomographic Imaging*. New York: IEEE, 1988.

[147] R. Clackdoyle and M. Defrise, "Tomographic reconstruction in the 21st century," *IEEE Signal Processing Magazine*, vol. 27, no. 4, pp. 60–80, 2010.

[148] R. Bracewell, *The Fourier Transform and Its Applications*. McGraw-Hill, 1999. pp. 262–266.

[149] E. W. Hansen and P.-L. Law, "Recursive methods for computing the Abel transform and its inverse," *Journal of the Optical Society of America A*, vol. 2, no. 4, pp. 510–520, 1985.

[150] P. A. Vicharelli and W. P. Lapatovich, "Iterative method for computing the inverse Abel transform," *Applied Physics Letters*, vol. 50, no. 10, pp. 557–559, 1987.

[151] T. J. Asaki, P. R. Campbell, R. Chartrand, C. E. Powell, K. R. Vixie, and B. E. Wohlberg, "Abel inversion using total variation regularization: applications," *Inverse Problems in Science and Engineering*, vol. 14, no. 8, pp. 873–885, 2006.

[152] L. Bahr and R. Lerch, "Beam profile measurements using light refractive tomography," *IEEE Transactions on Ultrasonics, Ferroelectrics and Frequency Control*, vol. 55, no. 2, pp. 405–414, 2008.

[153] L. Bahr and R. Lerch, "Sound pressure measurement utilizing light refractive tomography," in *IEEE International Ultrasonics Symposium*, pp. 840–843, 2008.

[154] Y. Wang and S. Wang, "The application of light refractive tomography in measuring acoustic field close to surface of transducer," in *European Conference on Underwater Acoustics*, (Istanbul), 2010.

[155] L. Chen, S. J. Rupitsch, and R. Lerch, "A reliability study of light refractive tomography utilized for noninvasive measurement of ultrasound pressure fields," *IEEE Transactions on Ultrasonics, Ferroelectrics and Frequency Control*, vol. 59, no. 5, pp. 915–927, 2012.

[156] A. Holm and H. W. Persson, "Optical diffraction tomography applied to airborne ultrasound," *Ultrasonics*, vol. 31, no. 4, pp. 259–265, 1993.

[157] R. Reibold and P. Kwiek, "Ultrasound field mapping by light-diffraction tomography. A review," in *Proceedings of the SPIE - The International Society for Optical Engineering*, vol. 2643, pp. 66–79, 1995.

[158] R. Reibold and P. Kwiek, "Uncertainty considerations of ultrasonic field mapping by light-diffraction tomography," *Ultrasonics*, vol. 35, no. 3, pp. 187–193, 1997.

[159] M. Almqvist, A. Holm, H. W. Persson, and K. Lindström, "Characterization of air-coupled ultrasound transducers in the frequency range 40 kHz–2 MHz using light diffraction tomography," *Ultrasonics*, vol. 37, no. 8, pp. 565–575, 2000.

[160] C. A. Greated, "Measurement of acoustic velocity fields," *Strain*, vol. 22, no. 1, pp. 21–24, 1986.

[161] J. P. Sharpe and C. A. Greated, "A stochastic model for photon correlation measurements in sound fields," *Journal of Physics D: Applied Physics*, vol. 22, no. 10, pp. 1429–1433, 1989.

[162] D. Hann and C. A. Greated, "Acoustic measurements in flows using photon correlation spectroscopy," *Measurement Science and Technology*, vol. 4, pp. 157–164, 1993.

[163] S. D. Conte and C. D. Boor, *Elementary numerical analysis: an algorithmic approach*. New York: McGraw-Hil, 3rd ed., 1980.

[164] F. Jacobsen and P. M. Juhl, *Fundamentals of Linear Acoustics*. Chichester: Wiley, 1st ed., 2013.

[165] T. Koukoulas, P. Theobald, B. Piper, S. Rajagopal, R. Barham, and S. Robinson, "Particle velocity measurements using photon correlation spectroscopy for the direct realisation of the soud pressure unit in airborne acoustics," in *19th International Congress on Sound and Vibration*, (Vilnius), 2012.

[166] T. Koukoulas, B. Piper, and P. Theobald, "Gated photon correlation spectroscopy for acoustical particle velocity measurements in free-field conditions," *Journal of the Acoustical Society of America*, vol. 133, no. 3, pp. 156–161, 2013.

[167] I. Grant and C. A. Greated, "Periodic sampling in laser anemometry," *Journal of Physics E: Scientific Instruments*, vol. 13, no. 5, pp. 571–574, 1980.

[168] F. Jacobsen, S. B. Figueroa, and K. Rasmussen, "A note on the concept of acoustic center," *J. Acoust. Soc. Am.*, vol. 115, no. 4, pp. 1468–1473, 2004.

[169] L. Zipser and H. H. Franke, "Visualisation and measurement of acoustic and fluidic phenomena using a laser-scanning vibrometer," in *5th International Conference on Vibration Measurements by Laser Techniques: Advances and Applications*, vol. 4827, pp. 192–198, 2002.

[170] O. B. Matar, L. Pizarro, D. Certon, J. P. Remenieras, and F. Patat, "Characterization of airborne transducers by optical tomography," *Ultrasonics*, vol. 38, no. 1–8, pp. 787–793, 2000.

[171] J.-P. Remenieras, O. B. Matar, S. Calle, and F. Patat, "Acoustic pressure measurement by acousto-optic tomography," in *IEEE Ultrasonic Symposium*, vol. 1, pp. 505–508, 2001.

[172] P. Theobald, S. Robinson, G. Hayman, and T. Koukoulas, "Acousto-optic tomography for mapping of high-frequency sonar fields," in *Acoustics'08 Paris*, (Paris), 2008.

[173] Y. Oikawa, M. Goto, Y. Ikeda, T. Takizawa, and Y. Yamasaki, "Sound field measurements based on reconstruction from laser projections," in *IEEE International Conference on Acoustics, Speech, and Signal Processing*, (Philadephia), 2005.

[174] T. Sakoda and Y. Sonoda, "Visualization of sound field with uniform phase distribution using laser beam microphone coupled with computerized tomography method," *Acoustical Science and Technology*, vol. 29, no. 4, pp. 295–299, 2008.

[175] Y. Oikawa, T. Hasegawa, Y. Ouchi, Y. Yamasaki, and Y. Ikeda, "Visualization of sound field and sound source vibration using laser measurement method," in *20th International Congress on Acoustics*, (Sydney), 2010.

[176] Y. Sonoda and Y. Nakazono, "Development of optophone with no diaphragm and application to sound measurement in jet flow," *Advances in Acoustics and Vibration, Hindawi Publishing Corporation*, vol. 2012, 2012. Article ID 909437, 17 pages.

Papers A-I

List of errata

The following errata have been found in the appended papers after publication:

Paper C The third line of the first paragraph on page 4 should state $i \rightarrow n$ instead of $i \rightarrow m$.

Paper D Equation (13) on page 5 should define the wavenumber spectrum of the pressure and the velocity as $P(k_x, k_y, z_s, \omega)$ and $V(k_x, k_y, z_s, \omega)$ instead of $P(k_x, k_x, z_s, \omega)$ and $V(k_x, k_x, z_s, \omega)$

Paper E A last minute change of notation caused the following errors,*

- The function $\cos(\theta - \phi)$ should not be written in equations (12), (13), (14) and (18).
- The Jacobian of the transformation in equations (12), (13), (14) is missing an absolute value, that is, the integral equations should end with $|k_{x'}|\, dk_{x'} d\phi$ instead of $k_{x'} dk_{x'} d\phi$.
- The elementary wave function φ on page 5 is missing the filter $|k_{x'}|$ ($\varphi = |k_{x'}|\, e^{-jk_{x'}x' + k_z z_h}$). The same mistake occurs in equation (18).

*The results presented in this paper remain valid because the source code was implemented with the original (correct) notation.

Paper A

18TH INTERNATIONAL CONGRESS ON SOUND & VIBRATION
ICSV18
RIO DE JANEIRO
BRAZIL
10–14 JULY 2011

AN INVESTIGATION OF SOUND FIELDS BASED ON THE ACOUSTO-OPTIC EFFECT

Antoni Torras-Rosell, Salvador Barrera-Figueroa

Danish Fundamental Metrology, Matematiktorvet 307, DK-2800, Kgs. Lyngby, Denmark, e-mail: atr@dfm.dtu.dk

Finn Jacobsen

Acoustic Technology, Department of Electrical Engineering, Technical University of Denmark, Building 352, DK-2800, Kgs. Lyngby, Denmark

Various types of transducers are nowadays capable of translating different properties of sound waves into mechanical/electrical quantities, which can afterwards be reinterpreted into acoustical ones. However, in certain applications, for example when using microphone arrays, the presence of bulk transducers can bias the acoustic measurement. Although this influence can often be either neglected at low frequencies or compensated for (typically in the form of a frequency response), the present work alternatively explores the interaction between sound and light as a means to characterize an acoustic field. This non-invasive technique is based on the so-called acousto-optic effect, i.e., the variations of the refractive index of a medium caused by density fluctuations, which follow sound pressure fluctuations. In the current study, this phenomenon is investigated in air, within the audible frequency range, and in two different measurement scenarios where the sound field is well-known: in a rectangular duct and in an anechoic room. Models for predicting the acousto-optic effect in such scenarios are derived and measurements are carried out with a laser Doppler vibrometer. The results show a fairly good agreement between the experimental and simulated data.

1. Introduction

The propagation of sound inherently involves pressure changes in the medium where the sound is propagating. Thus, sound is often characterized by capturing the pressure fluctuations that follow the acoustic field. There are several factors that can influence the quality of such measurement. Eluding all possible technical aspects related to hardware, software, signal processing, etc., the simple fact of inserting a bulk instrument into a sound field can bias the measurement. In practice, there are several means to circumvent this problem. At low frequencies, transducers can usually be considered transparent. Otherwise, when the wavelength of the sound waves becomes comparable to or smaller than the dimensions of the measuring device, reflection and scattering phenomena occur around the transducer, therefore, changing the pressure fluctuations that would occur in the absence of the transducer. In such case, some transducers are specifically designed to counterbalance this effect or when this is not the case, a transducer-based correction in form of a frequency response can typically be applied at a post-processing stage. Either solution introduces additional, though quantifiable, uncertainties to the measurement process.

The present work presents a completely different measurement principle based on the so-called acousto-optic effect. In this case, the sensing element is not a bulk transducer, but a beam of light that travels through an acoustic space. In the audible frequency range, the sound simply changes the density of the medium along the direction of propagation of the light. This yields small changes in the speed of light that are measurable with interferometric techniques. In the following, it is intended to investigate the acousto-optic effect in two very well-defined measurement scenarios: inside a rectangular duct and in free field conditions.

2. The acousto-optic effect

The acousto-optic effect can be described by combining the mechanical and optical properties of a medium. Under adiabatic conditions, the relationship between pressure (p) and density (ρ) is well-established [1]:

$$p = K\rho^{\gamma}, \tag{1}$$

where γ is the specific-heat ratio and K is a constant. The latter can be easily expressed as a function of the pressure and the density of the gas under static conditions (denoted as p_0 and ρ_0, respectively),

$$p_0 = K\ {\rho_0}^{\gamma} \quad \Rightarrow \quad K = \frac{p_0}{{\rho_0}^{\gamma}}. \tag{2}$$

On the other hand, the Gladstone-Dale equation [2] establishes the correspondence between the density and the index of refraction of a medium (n):

$$n - 1 = G\rho, \tag{3}$$

where G is the so-called Gladstone-Dale constant. The relation between pressure and refractive index can be determined by combining equations (1), (2) and (3),

$$p = p_0 \left(\frac{\rho}{\rho_0}\right)^{\gamma} = p_0 \left(\frac{n-1}{n_0-1}\right)^{\gamma}, \tag{4}$$

where n_0 represents the refractive index under static conditions. Alternatively, taking into account that the pressure of the medium is the superposition of static pressure and sound pressure ($p = p_0 + p_a$), the specific variation of the refractive index caused by a sound field can be found by reversing equation (4),

$$n = (n_0 - 1)\left(\frac{p}{p_0}\right)^{1/\gamma} + 1 = (n_0 - 1)\left(1 + \frac{p_a}{p_0}\right)^{1/\gamma} + 1. \tag{5}$$

It is worth noting that the ratio p_a/p_0 often becomes very small when analyzing sound fields within the audible frequency range. At least, this is the case for sound pressure levels below the hearing threshold of pain. In such case, the latter equation can be approximated by the following first order Taylor expansion:

$$n(x, y, z, t) \cong n_0 + \frac{n_0 - 1}{\gamma p_0} p_a(x, y, z, t). \tag{6}$$

This approximation shows that the variations of the refractive index induced by an acoustic field follow a linear relationship with the sound pressure fluctuations.

3. Measurement principle

The wave equation of an electromagnetic field $\mathbf{E}$,

$$\nabla^2\mathbf{E} - \left(\frac{n}{c_0}\right)^2 \frac{\partial^2\mathbf{E}}{\partial t^2} = 0, \tag{7}$$

has well-known solutions for an homogeneous quiescent medium, i.e., a medium whose properties are independent of position and time. Although the presence of an acoustic field infringes these assumptions, the presented wave equation is still valid when the variations of the refractive index fulfill the following condition [3]:

$$\left| \frac{1}{n} \frac{\partial n}{\partial t} T \right| \ll 1, \tag{8}$$

where T represents the oscillation period of the electric field. This constraint is clearly satisfied in the present case: the sound field gives raise to very small variations of the refractive index, and although the derivative of the refractive index increases with the oscillation frequency of the acoustic field, it is not significant for measurements within the audible frequency range. Under such conditions, the solution to the electromagnetic wave equation when a beam of light is traveling through an acoustic field is:

$$\mathbf{E} = \mathbf{E}_0 \mathrm{e}^{\mathrm{j}(\omega t + \phi)}, \tag{9}$$

where ω is the angular frequency of the electric field, $\mathbf{E}_0$ is a complex number that accounts for the amplitude and the polarization of the electromagnetic wave, and ϕ is the phase contribution that depends on the properties of the medium. Assuming that the beam of light is traveling along the y-direction, the phase contribution ϕ can be written as follows,

$$\phi = k_0 \int_0^l n(x, y, z, t) \mathrm{d}y = k_0 n_0 l + k_0 \frac{n_0 - 1}{\gamma p_0} \int_0^l p(x, y, z, t) \mathrm{d}y, \tag{10}$$

where k_0 is the wavenumber of the electric field in vacuum. Note that in the absence of sound, ϕ reduces to $k_0 n_0 l$, which turns equation (9) to the classical expression of a plane wave. Otherwise, the information about the acoustic field is captured in the phase of the light that travels through the medium and it can be retrieved using a laser Doppler vibrometer (LDV). Although an LDV is often used for measuring mechanical vibrations, the velocity of an LDV can also contain information about the acousto-optic effect:

$$v(t) = \frac{1}{k_0 n_0} \frac{\mathrm{d}\phi}{\mathrm{d}t} = \frac{\mathrm{d}l}{\mathrm{d}t} + \frac{n_0 - 1}{\gamma p_0 n_0} \frac{\mathrm{d}}{\mathrm{d}t} \left(\int_0^l p(x, y, z, t) \mathrm{d}y \right) = v_{\text{mec}}(t) + v_{\text{opt}}(t). \tag{11}$$

As can be seen, when the acousto-optic effect is not significant, the velocity of the LDV corresponds to the time derivative of the physical distance between the LDV and the surface where the light gets reflected from, i.e., the mechanical velocity of the surface. However, when the surface where the light is reflected is regarded to be free of mechanical vibrations, the output of the LDV can be used to characterize the acoustic field perturbing the medium where the light is propagating through.

3.1 Free-field propagation

The sound pressure generated by a monopole in free space can be described with spherical waves,

$$p_a(r, t) = \frac{Q \rho_0 \omega_a}{4\pi r} \cos(\omega_a t - k_a r + \varphi), \tag{12}$$

where Q represents the absolute value of the volume velocity of the monopole, ω_a and k_a are the angular frequency and wavenumber of the acoustic wave, and φ is an arbitrary phase. In the absence of any possible mechanical vibration, the velocity output of the LDV can only be caused by the acousto-optic effect. In particular, the velocity contribution caused by the acousto-optic effect when an LDV is integrating the spherical sound field as indicated in figure 1 is

$$v_{\text{opt}}(t) = \frac{n_0 - 1}{\gamma p_0 n_0} \frac{Q \rho_0 \omega_a}{4\pi} \frac{\mathrm{d}}{\mathrm{d}t} \left(\int_0^l \frac{\cos(\omega_a t - k_a r + \varphi)}{r} \mathrm{d}x \right). \tag{13}$$

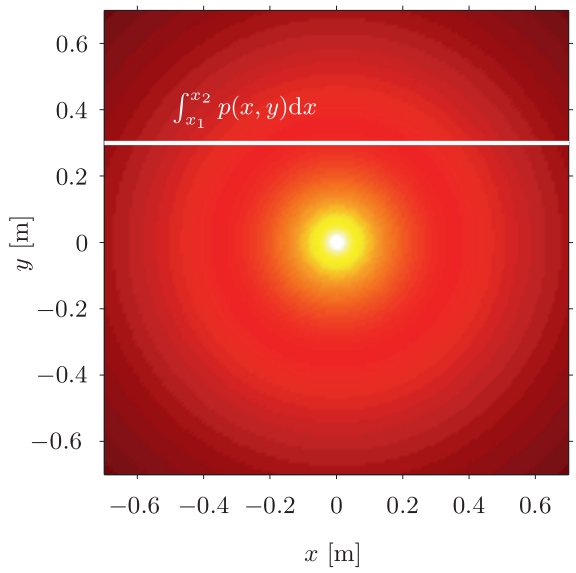

Figure 1: Transversal integration of a spherical sound field.

Since the light emitted by the LDV provides an almost ideal, instantaneous integration of the sound field, time and space can be regarded as independent during the integration process. Therefore,

$$v_{\text{opt}}(t) = \frac{n_0 - 1}{\gamma p_0 n_0} \frac{Q\rho_0\omega_a}{4\pi} \frac{\mathrm{d}}{\mathrm{d}t} \left(\cos(\omega_a t + \varphi) \overbrace{\int_{x_1}^{x_2} \frac{\cos(k_a r)}{r} \mathrm{d}x}^{C(k_a r)} + \sin(\omega_a t + \varphi) \overbrace{\int_{x_1}^{x_2} \frac{\sin(k_a r)}{r} \mathrm{d}x}^{S(k_a r)} \right)$$
$$= \omega_a A_{\text{eq}} \frac{n_0 - 1}{\gamma p_0 n_0} \frac{Q\rho_0\omega_a}{4\pi} \cos(\omega_a t + \varphi + \alpha), \tag{14}$$

where A_{eq} and α are,

$$A_{\text{eq}} = \sqrt{(S(k_a r))^2 + (C(k_a r))^2} \qquad \text{and} \qquad \alpha = \arctan\left(\frac{C(k_a r)}{S(k_a r)}\right). \tag{15}$$

From equation (14), the root mean square (rms) value of $v_{\text{opt}}(t)$ can be related to the rms value of the sound pressure at a distance r from the monopole in the following way,

$$v_{\text{opt,rms}} = \omega_a A_{\text{eq}} \frac{n_0 - 1}{\gamma p_0 n_0} \frac{Q\rho_0\omega_a}{4\pi} \frac{1}{\sqrt{2}} = r\omega_a A_{\text{eq}} \frac{n_0 - 1}{\gamma p_0 n_0} \frac{Q\rho_0\omega_a}{4\pi r} \frac{1}{\sqrt{2}} = r\omega_a A_{\text{eq}} \frac{n_0 - 1}{\gamma p_0 n_0} p_{\text{rms}}, \tag{16}$$

which expressed in dB leads to

$$L_v(\text{dB}) = 20\log\left(\frac{v_{\text{opt,rms}}}{v_{\text{ref}}}\right) = 20\log\left(\frac{p_{\text{rms}}}{p_{\text{ref}}}\right) + 20\log\left(r\omega_a A_{\text{eq}} \frac{n_0 - 1}{\gamma p_0 n_0} \frac{p_{\text{ref}}}{v_{\text{ref}}}\right). \tag{17}$$

This equation presents a means to characterize the sound pressure level of a point source based on the acousto-optic effect measured with an LDV.

3.2 Sound propagation in a rectangular duct

The acousto-optic effect is also investigated in a rectangular duct such as the one depicted in figure 2. In this case, it is rather difficult to avoid any mechanical vibration from the wall of the duct where the light of the LDV is reflected back. Thus, the output of the LDV is in principle a combination of the mechanical velocity of the wall and the apparent velocity caused by the acousto-optic effect.

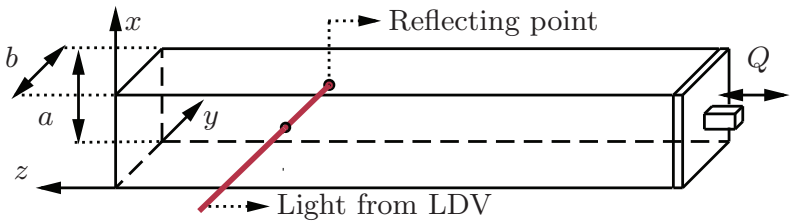

Figure 2: Sketch of the rectangular duct under study.

However, the latter is only comparable to the mechanical velocity when high pressure levels occur inside the duct. This is often the case at low frequencies, when the sound field is dominated by plane waves propagating along the longitudinal direction of the duct. In particular, assuming that all walls of the tube are rigid (from an acoustical point of view), the sound pressure equals

$$p_a(z,t) = \frac{Q\rho_0 c}{S}\frac{\cos(k_a z)}{\sin(k_a L)}\sin(\omega_a t + \varphi), \tag{18}$$

where Q and S are the volume velocity and the surface of the source, which is considered to be a piston with the same cross-sectional area as the duct, L is the total length of the duct and c represents the speed of sound. Then, the velocity contribution caused by the acousto-optic effect can be estimated from equation (11),

$$v_{\text{opt}}(t) = \frac{n_0 - 1}{\gamma p_0 n_0}\frac{\mathrm{d}}{\mathrm{d}t}\left(\int_0^{b(t)} \frac{Q\rho_0 c}{S}\frac{\cos(k_a z)}{\sin(k_a L)}\sin(\omega_a t + \varphi)\mathrm{d}y\right) = \frac{n_0 - 1}{\gamma p_0 n_0}\frac{\mathrm{d}}{\mathrm{d}t}\left(p_a(z,t)b(t)\right). \tag{19}$$

Note that the upper integration limit of the integral is denoted as $b(t)$ instead of b in order to include the vibrations of the wall. These variations of the integration path can be described as a harmonic oscillation that vibrates with the same frequency as the acoustic field,

$$b(t) = b + \delta b(t) = b + \delta b\cos(\omega_a t + \varphi_b) \Longleftrightarrow v_{\text{mec}}(t) = \frac{\mathrm{d}b(t)}{\mathrm{d}t}. \tag{20}$$

Therefore, the total output velocity of the LDV corresponds to,

$$v(t) = v_{\text{mec}}(t) + v_{\text{opt}}(t) = \frac{\mathrm{d}b(t)}{\mathrm{d}t} + \frac{n_0 - 1}{\gamma p_0 n_0}\frac{\mathrm{d}}{\mathrm{d}t}\left(p_a(z,t)b(t)\right) \approx v_{\text{mec}}(t) + b\frac{n_0 - 1}{\gamma p_0 n_0}\frac{\mathrm{d}p_a(z,t)}{\mathrm{d}t}, \tag{21}$$

where the approximation is based on the assumptions that the width of the duct is much larger than the amplitude of the mechanical vibrations, $b \gg \delta b$, and that the acoustic pressure is much less than the atmospheric pressure, $p_a \ll p_0$.

4. Measurement results

4.1 Free-field propagation

The model of the acousto-optic effect for sound waves propagating in free space has been tested in an anechoic room. Figure 3 shows a picture of the measurement setup, which was designed to reduce the influence of mechanical vibrations. Besides, an accelerometer was mounted at the reflecting point in order to monitor the vibration. In practice, the setup turned out to be very effective above 2 kHz. This is shown in figure 4a, where the velocity levels measured with the LDV are significantly higher than the ones measured with the accelerometer. Note that the presented velocity levels are rel-

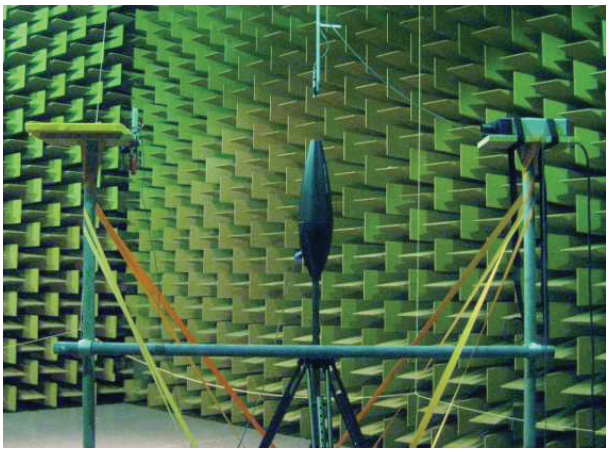

Figure 3: Measurement setup in the anechoic room.

ative to 1 nm/s, i.e., the acousto-optic effect leads to an apparent velocity with a very small amplitude, but yet at least one or two orders of magnitude larger than the mechanical vibrations detected with the accelerometer. Below 2 kHz, the measurement data was compromised by the mechanical vibrations of the structure and the internal noise of the LDV. On the other hand, the upper frequency limit was imposed by the loudspeaker, which could not radiate sound above 10 kHz efficiently.

Disregarding the influence of any mechanical vibration, equation (17) can be used to estimate the sound pressure level produced by the loudspeaker. The result is compared to the sound pressure level measured with a Brüel & Kjær pressure microphone type 4192 in figure 4b. Even though the peaks and dips of the curves occur at the same frequencies, the level difference between them increases with increasing frequency. This is a consequence of using a pressure microphone instead of a free-field microphone. The latter is designed to compensate for the pressure increase that occurs in front of its diaphragm when the wavelength of the sound waves are comparable or smaller than the dimensions of the diaphragm. In spite of the use of the wrong microphone, this demonstrates the great advantage of using the light as a sensor "element" instead of a bulk instrument. Figure 4c shows the pressure predicted with LDV versus the pressure of the microphone compensated for the pressure increase by means of a transfer function correction provided by the manufacturer. In this case, there is a fairly good agreement between the two curves. Nevertheless, the LDV seems to slightly underestimate the pressure towards the high frequencies. At this point, it is important to recall that the presented model of the acousto-optic effect does not account for the directivity of the loudspeaker, i.e., the amplitude A_{eq} accounts for spherical waves emitted by an omnidirectional source. The directivity of the loudspeaker $D(\theta)$ can be included in the model by redefining A_{eq} (denoted with prime from now on),

$$A_{\text{eq}}^{'} = \sqrt{(S'(k_a r))^2 + (C'(k_a r))^2}, \tag{22}$$

where the functions $C^{'}(k_a r)$ and $S^{'}(k_a r)$ correspond to,

$$C^{'}(k_a r) = \int_{x_1}^{x_2} D(\theta)\frac{\cos(k_a r)}{r}\mathrm{d}x \qquad \text{and} \qquad S^{'}(k_a r) = \int_{x_1}^{x_2} D(\theta)\frac{\sin(k_a r)}{r}\mathrm{d}x. \tag{23}$$

As can be seen in figure 4d, this correction of the model gives even better agreement between the two measurement methods.

4.2 Sound propagation in a rectangular duct

The model of the acousto-optic effect described in section 3.2 does not account for higher order modes inside the tube. Thus, the frequency range of interest is limited by the dimension of the tube.

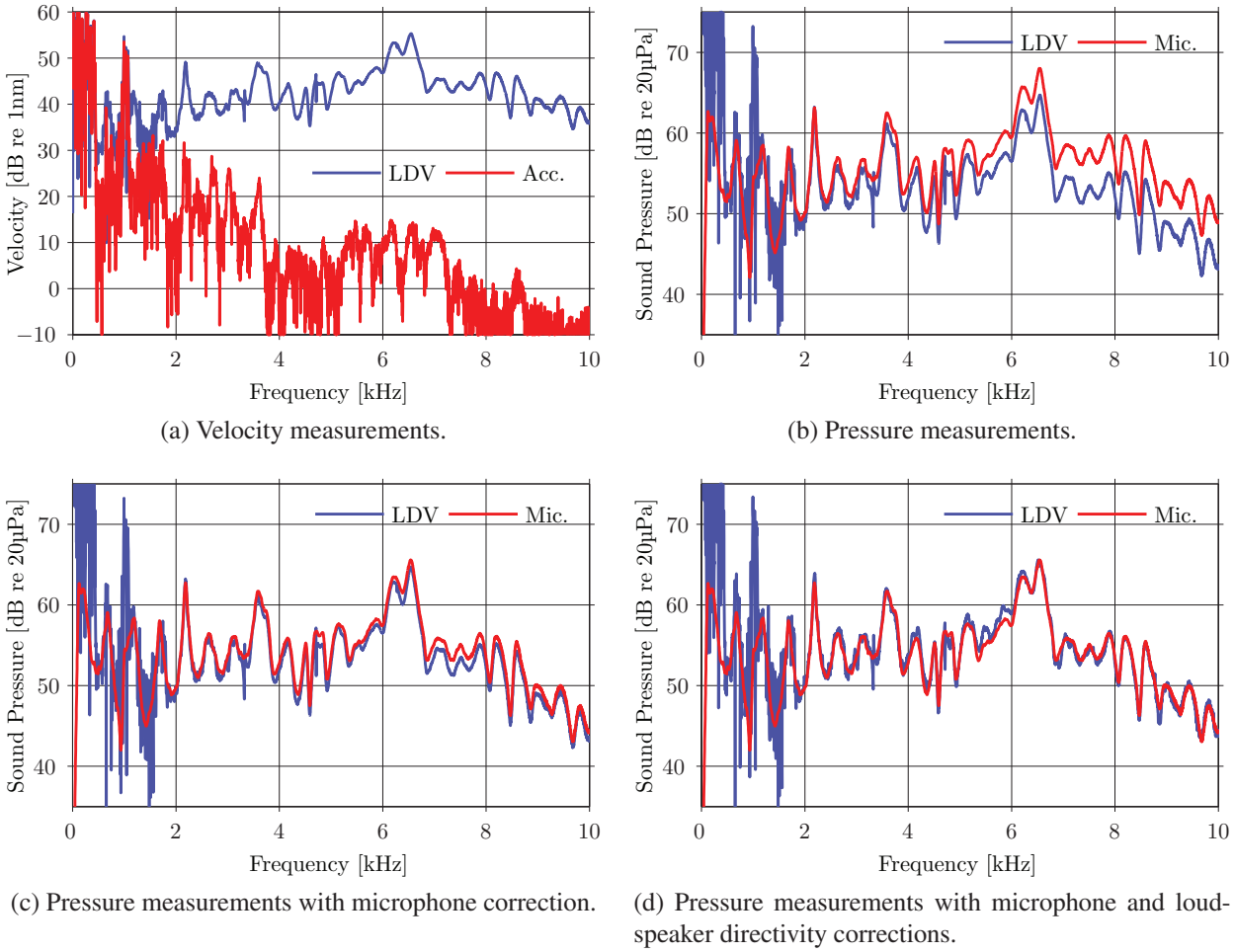

(a) Velocity measurements.

(b) Pressure measurements.

(c) Pressure measurements with microphone correction.

(d) Pressure measurements with microphone and loudspeaker directivity corrections.

Figure 4: Velocity measurement and the corresponding sound pressure levels derived from the model.

In particular, the duct used in these measurements has a cross-sectional area of 4.5×4.5 cm^2, which means that the sound field can be assumed to consist of plane waves below 3.8 kHz, approximately. Furthermore, unlike the measurements carried out in free space, the velocity output of the LDV is not free of mechanical vibrations. As can be seen in figure 5a, the accelerometer placed at the wall of the duct where the light is reflected back measures velocity levels that are not negligible when compared to the levels measured with the LDV. However, the magnitude of the LDV is greater (up to 6 dB) than the one of the accelerometer in most of the frequency range under study. This discrepancy can be explained by the interaction between sound and light, i.e., the LDV does not only measure the mechanical vibration of the duct ($v_{\text{mec}}(t)$), but it also measures an apparent velocity that is caused by the acousto-optic effect ($v_{\text{opt}}(t)$). Figure 5b shows the sound pressure level measured inside the tube. This can be used to estimate $v_{\text{opt}}(t)$ by means of the last term stated in equation (21). The result is presented in figure 5c. As expected, the higher the sound pressure, the larger the amplitude of $v_{\text{opt}}(t)$. Besides, although the pressure at the upper frequency range is not that high, the derivative of the pressure as a function of time (see equation (21)) boosts the acousto-optic effect with increasing frequency, cf. the dynamic range between the lower and higher frequencies in figures 5b and 5c. The model predicts that the velocity of the LDV should correspond to the summation of the mechanical vibration of the duct, which is in practice measured with the accelerometer, and the apparent velocity presented in figure 5c. Although there are several aspects that make the coupling of these two velocities complicated (e.g. the phase mismatch between accelerometer and microphone), the results depicted in figure 5d show a quite good agreement between the measured and simulated data.

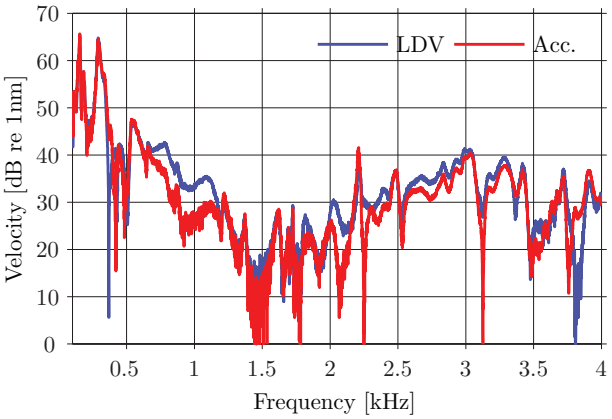

(a) Velocities measured with the LDV and the accelerometer.

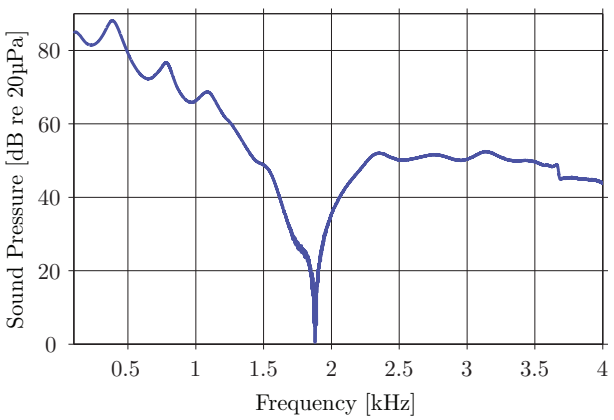

(b) Sound pressure inside the tube.

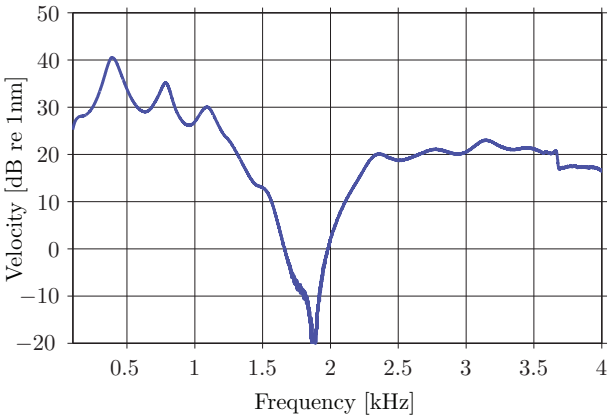

(c) Estimate of the apparent velocity caused by the acousto-optic effect.

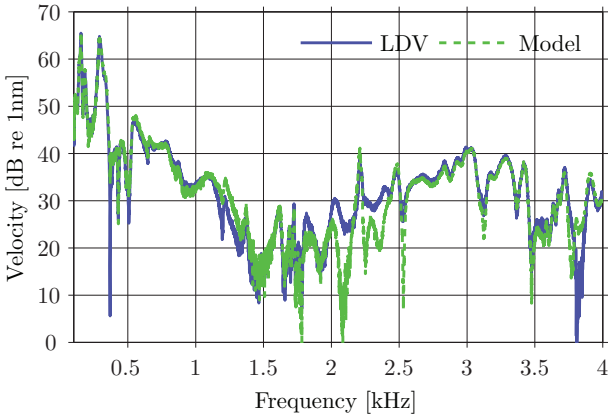

(d) Velocity measured with the LDV vs. velocity predicted with the model.

Figure 5: Measurements results in the rectangular duct.

5. Conclusions

The acousto-optic effect has been measured satisfactorily with an LDV in two different acoustical scenarios: in an anechoic room and in a rectangular duct. Although the LDV is an instrument designed to measure mechanical vibrations, the results obtained in the anechoic room demonstrate that it can also be used to measure sound pressure. Furthermore, unlike most of the conventional measurement techniques, the acousto-optic effect is non-invasive, i.e., the use of light as a "sensor" element (instead of a bulk transducer) leads to the actual value of the sound pressure.

The model of the acousto-optic effect inside a rectangular duct explains reasonably well the velocity level difference observed between the LDV and the accelerometer, which in some frequencies reaches 6 dB. Therefore, care must be taken when assessing velocity measurements from an LDV whose laser beam travels through an intense sound field.

REFERENCES

[1] A. D. Pierce, *Acoustics: an introduction to its physical principles and applications*, Acoustical Society of America, American Institute of Physics (1989).

[2] W. Merzkirch and K. Gersten, Techniques of flow visualization, Tech. rep., *North Atlantic Treaty Organization*, Advisory Group for Aerospace Research and Development (1987).

[3] P. M. Morse and K. U. Ingard, *Theoretical acoustics*, Princeton University Press (1986).

Paper B

Sound field reconstruction using acousto-optic tomography[a)]

Antoni Torras-Rosell[b)] and Salvador Barrera-Figueroa
Danish Fundamental Metrology A/S, Matematiktorvet 307, 2800 Kongens Lyngby, Denmark

Finn Jacobsen
Acoustic Technology, Department of Electrical Engineering, Technical University of Denmark, Ørsteds Plads 352, 2800 Kongens Lyngby, Denmark

(Received 28 September 2011; revised 15 February 2012; accepted 19 February 2012)

When sound propagates through a medium, it results in pressure fluctuations that change the instantaneous density of the medium. Under such circumstances, the refractive index that characterizes the propagation of light is not constant, but influenced by the acoustic field. This kind of interaction is known as the acousto-optic effect. The formulation of this physical phenomenon into a mathematical problem can be described in terms of the Radon transform, which makes it possible to reconstruct an arbitrary sound field using tomography. The present work derives the fundamental equations governing the acousto-optic effect in air, and demonstrates that it can be measured with a laser Doppler vibrometer in the audible frequency range. The tomographic reconstruction is tested by means of computer simulations and measurements. The main features observed in the simulations are also recognized in the experimental results. The effectiveness of the tomographic reconstruction is further confirmed with representations of the very same sound field measured with a traditional microphone array. © *2012 Acoustical Society of America*. [http://dx.doi.org/10.1121/1.3695394]

PACS number(s): 43.35.Sx [JDM] Pages: 3786–3793

I. INTRODUCTION

The acousto-optic effect has been extensively used to characterize ultrasonic waves in underwater acoustics.[1–7] In such measurements, the acoustic properties of sound are determined by measuring the small changes of the refractive index that are induced by the pressure fluctuations of the acoustic field. These variations of the refractive index will cause diffraction and changes of the speed of light that influence the propagation of light in amplitude and phase. In practice, in the low ultrasonic frequency range, diffraction effects can be neglected when the acoustic field has small amplitudes.[2,6,7]

Ultrasonic measurements in air are not commonly based on the acousto-optic effect (although some examples can be found in Refs. 8 and 9). This is perhaps because ultrasound is highly attenuated in air and because there normally is a significant impedance mismatch between the air and the ultrasonic transducer.[8] These constraints are less severe when using conventional loudspeakers and microphones in the audible frequency range. However, only a few investigations have been reported for audible sound,[10–12] and they have been concerned with visualization purposes rather than quantification.

The aim of this work is to demonstrate that light can be used as a means to characterize airborne sound in the audible frequency range. First, the physical principles governing the acousto-optic effect are presented. This will show that sound pressure fluctuations are captured in the phase of a light beam that travels through the medium. Next, we describe the measurement procedure used to retrieve the phase of the light as an apparent velocity measured with a laser Doppler vibrometer (LDV). This apparent velocity is interpreted as a projection of the sound field. Several projections in different directions can be used to reconstruct the acoustic field using tomography. The quality of the tomographic reconstruction is finally assessed by means of simulations and experimental results.

II. ACOUSTO-OPTIC TOMOGRAPHY

A. Acousto-optic effect

The phenomenon of sound inherently involves pressure fluctuations that change the density of the medium. Assuming adiabatic conditions, the total pressure p_t and the density ρ of the medium are related by means of the following expression:[13]

$$\frac{p_t}{p_0} = \left(\frac{\rho}{\rho_0}\right)^{\gamma}, \tag{1}$$

where p_0 and ρ_0 are the pressure and the density under static conditions, and γ is the ratio of specific heats. Note that, when sound propagates, p_t corresponds to the superposition of the static and the acoustic pressures, that is, $p_t = p_0 + p$. The influence of the density variations on the propagation of light can be determined by combining the mechanical and optical properties of the medium. In 1863, Gladstone and Dale established an empirical relation between the refractive index n and the density ρ of various liquids[14]

$$n - 1 = G\rho, \tag{2}$$

[a)]Portions of this work were presented in "Sound field reconstruction based on the acousto-optic effect," Proceedings of Inter-Noise 2011, Osaka, Japan, September 2011.

[b)]Author to whom correspondence should be addressed. Electronic mail: atr@dfm.dtu.dk

 0001-4966/2012/131(5)/3786/8/$30.00

where the Gladstone–Dale constant G is an intrinsic feature of the liquid. This relation also holds for air.[15] The most important property of the latter expression is not the exact value of G, but the fact that density and refractive index exhibit a linear relationship. The relation between the refractive index and the acoustic field can be established by combining Eqs. (1) and (2)

$$n = (n_0 - 1)\left(\frac{p_t}{p_0}\right)^{1/\gamma} + 1 = (n_0 - 1)\left(1 + \frac{p}{p_0}\right)^{1/\gamma} + 1, \tag{3}$$

where n_0 is the index of refraction under standard atmospheric conditions. As shown in Appendix A, this expression can be approximated by a first order Taylor expansion when the acoustic pressure is much smaller than the static pressure, $p \ll p_0$,

$$n \cong n_0 + \frac{n_0 - 1}{\gamma p_0} p. \tag{4}$$

Thus, under weak acousto-optic interaction, the variations of the refractive index are proportional to the sound pressure. For ease of reference, a sound pressure of 1 Pa yields an increase of the refractive index of air of about 2×10^{-9} of its value under static conditions.

B. Measurement principle

The understanding of the physical phenomenon governing the acousto-optic effect opens up the possibility of characterizing sound by measuring light that travels through an acoustic field. In this context, light can be regarded as an electromagnetic wave $\mathbf{E}$ that satisfies the electromagnetic wave equation

$$\nabla^2 \mathbf{E} - \left(\frac{n}{c_0}\right)^2 \frac{\partial^2 \mathbf{E}}{\partial t^2} = 0, \tag{5}$$

where c_0 corresponds to the speed of light in vacuum. Although this fundamental equation is normally derived for waves propagating through a homogeneous quiescent medium (which is not completely true in the presence of sound), correct solutions can still be obtained when the following condition is fulfilled:[16]

$$\left|\frac{1}{n}\frac{\partial n}{\partial t} T\right| \ll 1, \tag{6}$$

where T corresponds to the oscillation period of the electric field. This is indeed the case for weak acousto-optic interaction (see Appendix B for further details). Under such conditions, the acousto-optic effect modifies the phase of light rather than its amplitude. One can think of it as an electromagnetic wave that travels faster or slower depending on the pressure fluctuations caused by the acoustic field. The light travels slower when the medium is denser (pressure increase) and faster otherwise. These ideas bring up the possibility of using the following expression as a solution to the electromagnetic wave equation in the presence of sound

$$\mathbf{E} = \mathbf{E}_0 e^{j(\omega_o t + \phi(x,y,z,t))}, \tag{7}$$

where ω_o is the angular frequency of the light, $\mathbf{E}_0$ is a complex number that accounts for the amplitude and the polarization of the light, and ϕ is the phase term that depends on the acousto-optic effect. As demonstrated in Appendix B, the general solution of ϕ resulting from inserting Eq. (7) into the wave equation is

$$\phi = k_0 \int_{\mathbf{L}} n \mathrm{d}l = k_0 n_0 L_0 + k_0 \frac{n_0 - 1}{\gamma p_0} \int_{\mathbf{L}} p(x, y, z, t) \mathrm{d}l, \tag{8}$$

where k_0 is the wave number of light in vacuum, $\mathbf{L}$ represents the path followed by the light, and L_0 is the corresponding distance. It is worth noting that in the absence of sound, $\phi = k_0 n_0 L_0$, that is, the classical phase shift of a plane wave propagating in a homogeneous quiescent medium. Equation (8) establishes that the phase of a beam of light that travels through an acoustic field is proportional to the line integral of the sound pressure. This can be exploited as a measurement principle for acoustic measurements, but it requires measuring the phase of the light accurately. An LDV can effectively provide this information. In conventional use, the vibrational velocity of a surface measured by the LDV is proportional to the time derivative of the phase of the light

$$v(t) = \frac{1}{k_0 n_0} \frac{\mathrm{d}\phi}{\mathrm{d}t}. \tag{9}$$

In the absence of sound ($\phi = k_0 n_0 L_0$), the velocity retrieved by an LDV is equal to the rate of change of the distance from the head of the LDV to the reflecting point where the laser is pointed, that is, $v(t) = \mathrm{d}L_0/\mathrm{d}t$. However, an LDV can also measure the acousto-optic effect when the vibrations of the surface that reflects the light back to the LDV are negligible.[17] In such a case, $\mathrm{d}L_0/\mathrm{d}t \approx 0$ and the acousto-optic effect [the second term on the right hand side of Eq. (8)] dominates in the time derivative of ϕ

$$v(t) = \frac{n_0 - 1}{\gamma p_0 n_0} \frac{\mathrm{d}}{\mathrm{d}t}\left(\int_{\mathbf{L}} p(x, y, z, t) \mathrm{d}l\right). \tag{10}$$

C. Sound pressure reconstruction

The line integral of the acoustic pressure can be seen as a projection of the sound field in the direction of propagation of the light. These projections can be described mathematically by means of the Radon transform[18]

$$R_p(x', \theta, t) = \int_{-\infty}^{+\infty} p(x, y, t) \mathrm{d}y', \tag{11}$$

where the coordinates x' and y' are related to the coordinates x and y by means of the following rotation matrix:

$$\begin{bmatrix} x' \\ y' \end{bmatrix} = \begin{bmatrix} \cos\theta & \sin\theta \\ -\sin\theta & \cos\theta \end{bmatrix} \begin{bmatrix} x \\ y \end{bmatrix}. \tag{12}$$

This coordinate system transformation is illustrated in Fig. 1. It is easy to see from Eq. (10) that the Radon transform of the sound field under investigation can be obtained from the apparent velocity of the LDV as follows

$$R_p(x',\,\theta,\,t) = \frac{\gamma p_0 n_0}{n_0 - 1}\int v(x',\,\theta,\,t)\mathrm{d}t. \tag{13}$$

Unless assumptions about the symmetry of the sound field are made, the information obtained from a single line scan is, in general, not sufficient to reconstruct the acoustic field.[17] The reconstruction of an arbitrary sound field requires the use of tomography. The sound field is first scanned over a plane, e.g., along a set of parallel lines as indicated in Fig. 1, and this procedure must then be repeated (synchronously) for a series of angles of θ from 0° to 180°. It is not necessary to rotate up to 360° when using a parallel beam scan configuration because the projections obtained for angles $\theta \geq 180°$ are replicas of the scans measured at $\theta - 180°$. With this procedure, the acoustic field is projected into different directions, and thus, the resulting data set constitutes a well-defined inverse problem that can be solved by means of the inverse Radon transform. The latter can in practice be implemented efficiently by means of the filtered backprojection algorithm,[18] which in a parallel beam scan configuration can be defined as

$$\tilde{p}(x,\,y,\,t) = \int_0^{\pi} Q(x',\,\theta,\,t)\mathrm{d}\theta, \tag{14}$$

where $\tilde{p}(x,\,y,\,t)$ denotes the reconstructed sound pressure, and $Q(x',\,\theta,\,t)$ is the so-called "filtered projection"

$$Q(x',\,\theta,\,t) = R_p(x',\,\theta,\,t) * h(x'), \tag{15}$$

that is, the convolution of the measured $R_p(x',\,\theta,\,t)$ with a filter $h(x')$ that accounts for both the filtering required to implement the algorithm with a two-dimensional (2D) spatial

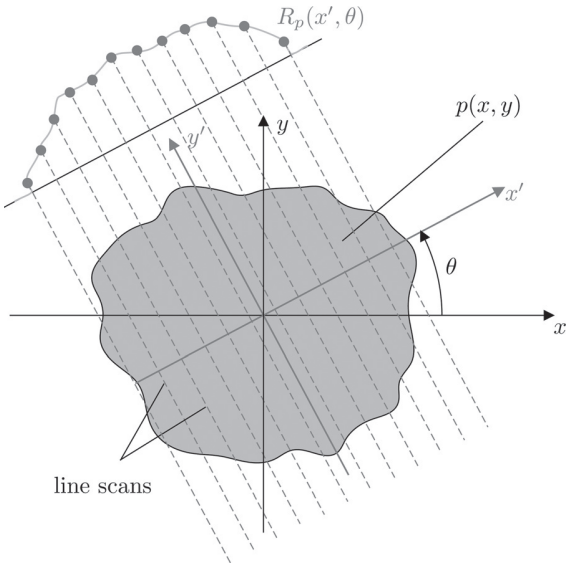

FIG. 1. Sketch of the parallel beam scan setup for obtaining the Radon transform of an acoustic field.

Fourier transform (Ram-Lak filter) and the windowing imposed in the frequency domain in order to reduce the influence of noise outside of the frequency range of interest (e.g., a Hann or a Cosine window). Note that the phase of the light performs a continuous integration of the sound field, not a discrete summation. However, the data set used in the reconstruction algorithm consists of a finite number of samples. This means that one must either estimate the continuous integrals of the inverse Radon transform with numerical approximations or use the inverse discrete Radon transform. The latter option does not account for the spatial resolution used in the measurements. This biases the amplitude of the reconstructed pressure, but it can easily be corrected by dividing the reconstructed pressure by the spatial resolution. In either case, the quality of the reconstruction depends on the spatial and angular resolutions used to sample the Radon transform of the acoustic field.

III. SIMULATION AND EXPERIMENTAL RESULTS

A. Simulations

The interpretation of the acousto-optic effect as the Radon transform of an acoustic field is analyzed by means of a computer simulation. For clarity's sake, the case of study is a monopole that radiates sound at a frequency of 2 kHz. Figure 2(a) shows the instantaneous spherical sound field emitted by the monopole in a plane at a distance of 12 cm from the point source. Figure 2(b) shows the corresponding Radon transform as a function of x' and θ. As can be seen, the Radon transform does not change with the angle of rotation θ. This is a consequence of the spherical symmetry of the sound field under study, i.e., the integral of the acoustic field leads to the same result independently of θ. As mentioned previously, it is only possible in practice to measure a discrete number of points of the Radon transform, and thus, the quality of the reconstruction relies on the separation between the line scans (spatial resolution) and the angular resolution used to rotate the measurement setup in order to scan the sound field in different directions. Figure 3(a) shows the reconstructed sound field when the spatial and angular resolutions are 1 cm and 1°, and Fig. 3(b) corresponds to the spatial and angular resolutions of 4 cm and 10°. As expected, the reconstruction deteriorates when the spatial/angular resolution is coarser, that is, when the number of samples of the Radon transform that are used to compute the inverse transform is reduced.

B. Measurements

For ease of comparison with the simulations presented in Sec. III A, measurements were carried out in an anechoic room of about 1000 m^3 and the sound field was generated by a loudspeaker driven with a pure tone of 2 kHz. The signal emitted by the loudspeaker was synchronized with the data acquisition system, allowing for the reconstruction of the instantaneous sound field. The measuring plane was located 12 cm above the loudspeaker. A picture of the measurement setup with an LDV Type OFV-505 manufactured by Polytec (Waldbronn, Germany) can be seen in Fig. 4(a). Instead of rotating the LDV

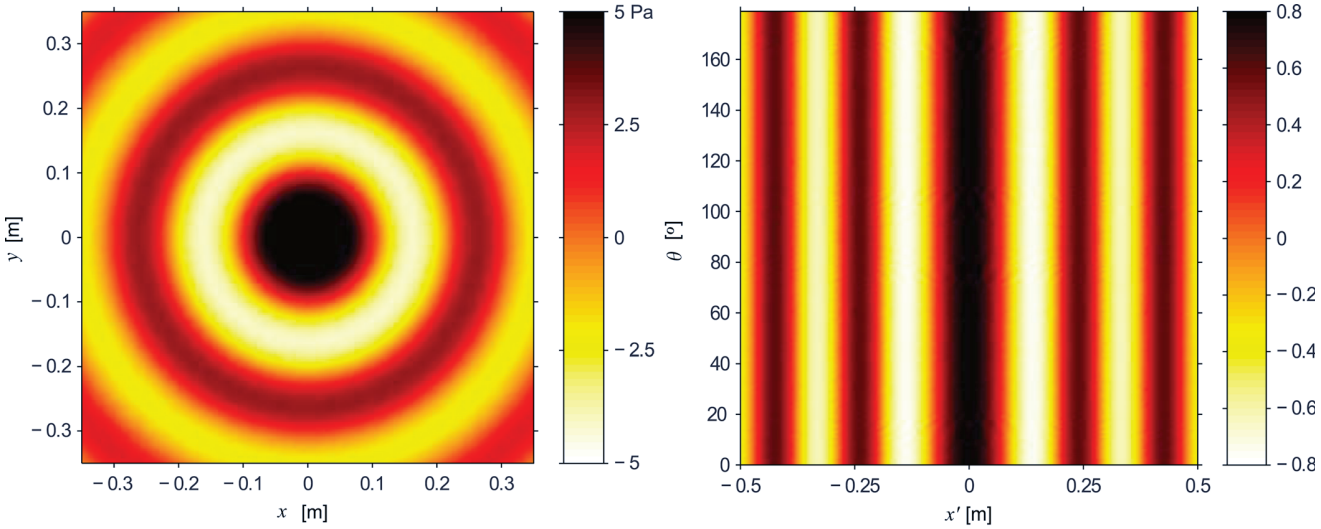

(a) Instantaneous sound field. **(b)** Instantaneous Radon transform.

FIG. 2. (Color online) Monopole located 12 cm away from the simulated plane.

together with the reflecting point, the loudspeaker was placed on a turntable allowing the scanning of the sound field in several directions. In this way, the structure where the LDV and the reflecting point were mounted was more stable. The turntable was moved manually in the perpendicular direction of the light beam allowing scanning in parallel lines. Besides, an accelerometer manufactured by Brüel & Kjær (B&K, Nærum, Denmark) Type 4344 was installed on top of the reflecting point in order to monitor that its acceleration was negligible, and thus, ensuring that the velocity output of the LDV was essentially caused by the acousto-optic effect. The outputs of the LDV and the accelerometer were captured with an external sound card Type HDSPe ExpressCard manufactured by RME (Haimhausen, Germany) that was controlled with a laptop by means of a homemade Matlab program. The measured data was afterwards also analyzed with Matlab.

The Radon transform of the acoustic field generated by the loudspeaker was computed from the velocity measured with the LDV according to Eq. (13). The result obtained when using a spatial resolution of 2 cm and an angular resolution of 10° is depicted in Fig. 4(b). Similar to the simulation presented in Sec. III A, the pattern of vertical lines exhibited by the Radon transform indicates that the measured Radon transform is fairly independent of θ, which means that the reconstructed sound field should be rather rotationally symmetric. The pressure reconstructed after applying the inverse transform is presented in Fig. 5(a). As expected, the resulting sound field is spherically symmetric

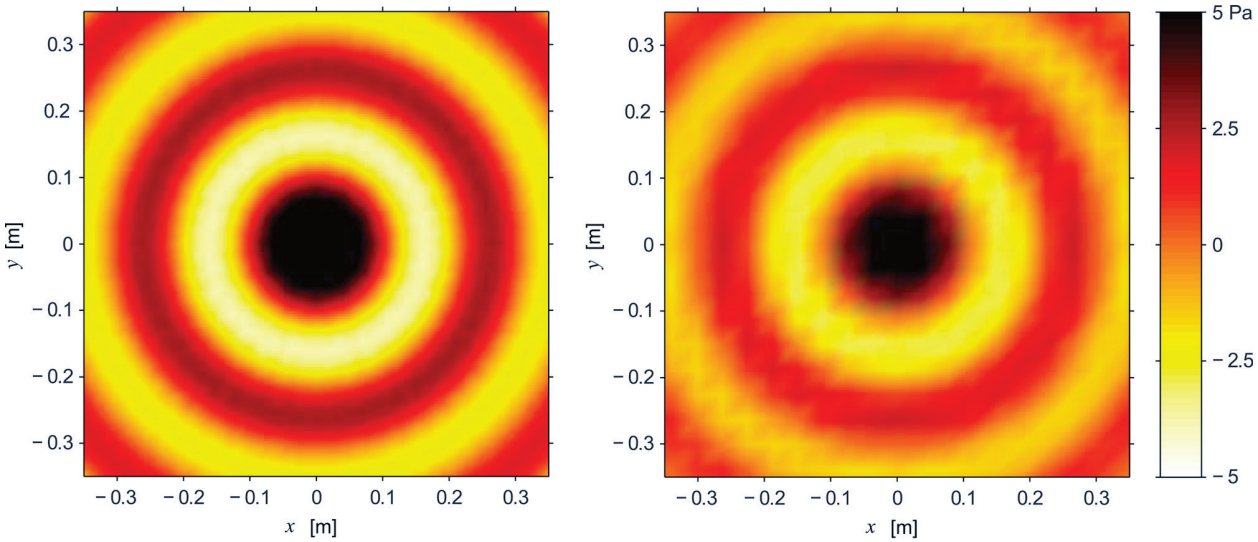

(a) Spatial resolution 1 cm, angular resolution 1°. **(b)** Spatial resolution 4 cm, angular resolution 10°.

FIG. 3. (Color online) Simulation of the tomographic reconstruction of the instantaneous sound field generated by the monopole. The filtered backprojection algorithm included a Lam-Rak filter and a Cosine window.

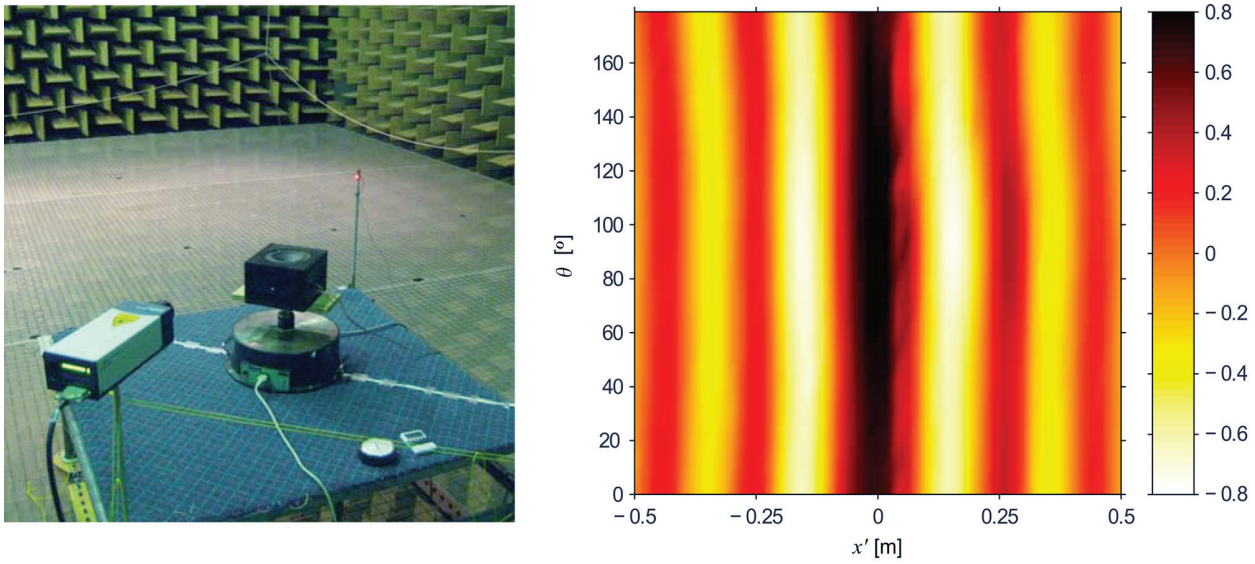

(a) LDV setup. **(b)** Instantaneous Radon transform of the measured acoustic field.

FIG. 4. (Color online) Measurement of the Radon transform of the sound field with an LDV.

and exhibits the periodicities of a 2 kHz pure tone (cf. the simulation results presented in Fig. 3). Figure 5(b) shows the reconstructed field when the spatial and angular resolutions are 4 cm and 10°, that is, with half of the line scans of the previous reconstruction. As observed in the simulations, the result becomes more blurred when decreasing the number of samples of the Radon transform used to reconstruct the sound field.

Finally, complementary measurements were carried out with a microphone array in order to compare the tomographic technique with a more traditional and well-established method. Figure 6(a) shows the planar rectangular microphone array used in this measurement. The array consisted of sixty 1/4 in. microphones (B&K Type 4957) with a spacing of 7.5 cm between the microphones. The measured sound field can be seen in Fig. 6(b). Despite the use of 60 microphones, the spatial resolution of the sampled sound field (7.5 cm) and the covered area (67.5×37.5 cm^2) are not directly comparable to the ones obtained with the tomographic technique. However, the overall amplitudes and pressure distribution are in fairly good agreement with the reconstructed fields shown in Fig. 5.

IV. DISCUSSION

The figures presented in Sec. III represent a single instant of time of the simulated/measured Radon transforms and the corresponding instantaneous pressure reconstructions. They do not represent an average quantity. In fact, the complete output of the tomographic algorithm is a time series of the sound pressure measured over the area scanned

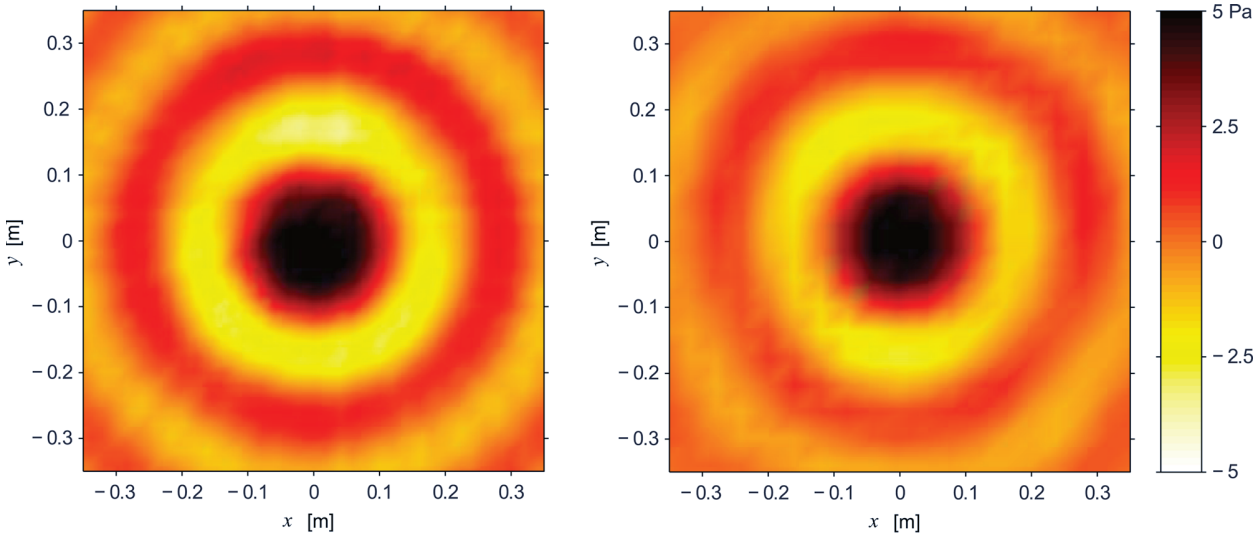

(a) Spatial resolution 2 cm, angular resolution 10°. **(b)** Spatial resolution 4 cm, angular resolution 10°.

FIG. 5. (Color online) Tomographic reconstruction of the instantaneous sound field radiated by the loudspeaker. The filtered backprojection algorithm included a Lam-Rak filter and a Cosine window.

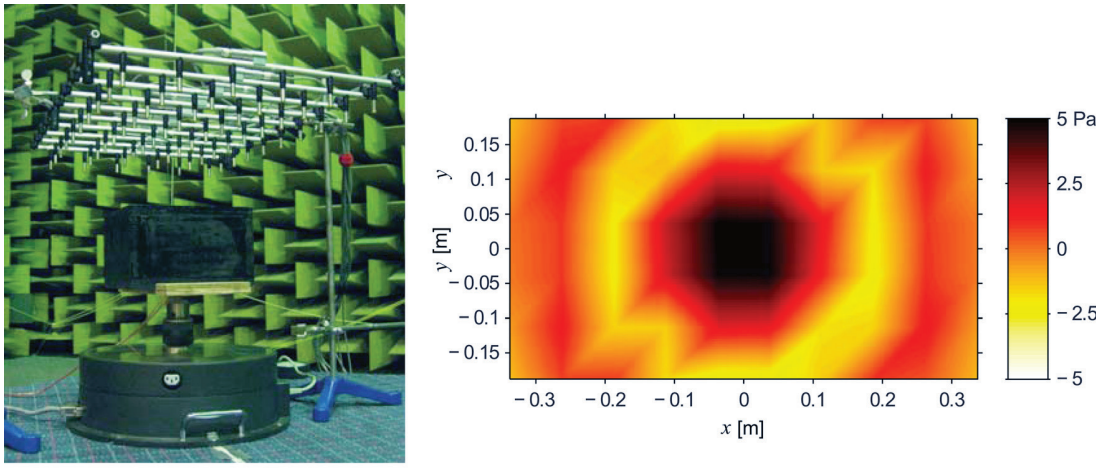

(a) Microphone array setup.

(b) Measured instantaneous pressure.

FIG. 6. (Color online) Sound field measurement with a planar rectangular microphone array.

with the LDV. This can serve the purposes of many sound visualization applications that are implemented nowadays with microphone arrays. Besides, sound visualization based on acousto-optic tomography has the great advantage of being a non-invasive technique. The presence of a large number of transducers often limits the frequency range that can be covered with conventional measurement systems. Increasing the number of transducers in order to enhance the spatial resolution of the array tends to aggravate the influence of the array on the quantities measured at high frequencies. A transducer-based correction in form of a frequency response can be applied at a post-processing stage to counterbalance this effect. There are also some transducers that are specifically designed to compensate for it. Nevertheless, the applied correction will only be valid for a certain direction of incident sound, typically axial incidence. Alternatively, one can, for instance, improve the grid resolution of a microphone array (without increasing the number of transducers) by performing synchronous measurements where the array is simply shifted, say, half of the spacing between transducers. In any case, it is necessary to immerse the array into the acoustic field. This is not the case when using the light as a "sensing" element.

The spatial resolution is also an important issue when using acousto-optic tomography. In spite of the continuous Radon transform measured with the LDV, only a finite number of line scans are captured for each direction of projection θ. Therefore, as in any other discretization problem, aliasing effects may arise if the Nyquist theorem is not fulfilled— the spatial resolution should always be smaller than half the smallest wavelength of interest. Furthermore, it is also recommendable to have roughly as many directions of projection as parallel scans per projection.[18]

The available technology for measuring the acousto-optic effect has not been constructed for this purpose. The LDV is a device specially designed to measure mechanical vibrations, and besides, a feasible measurement setup currently requires one to measure the sound field in a synchronous fashion. Nevertheless, the results achieved with such an off-the-shelf technology are quite satisfactory. Further investigations in this field could eventually lead to a new type of optical device capable of measuring sound from the interaction with light in real time. Thus, acousto-optic tomography may have a great potential in acoustical holography and beamforming.

The present work examines the interaction between sound and light as a means to visualize acoustic fields. However, the refractive index, and thus, the propagation of light can also be perturbed by other phenomena, e.g., the presence of flow or temperature gradients. This could limit the number of applications for acousto-optic tomography. Nevertheless, further research needs to be done in this direction and perhaps new acousto-optic techniques will be developed to compensate for these effects.

V. CONCLUSIONS

The interaction between sound and light has been investigated as a means to characterize airborne sound fields in the audible frequency range. Both simulations and measurements show that the acousto-optic effect can be used to reconstruct an acoustic field using tomography. Despite the technological limitations of the measurement setup, the experimental results demonstrate that instantaneous pressure fluctuations of an acoustic field can be captured with an LDV. The apparent velocity caused by the acousto-optic effect can be interpreted as projections of the acoustic field, which can be described mathematically by means of the Radon transform. Scanning the sound field in parallel lines and projecting it in different directions constitute an inverse problem that can be solved by means of the inverse Radon transform. The results show that the quality of the reconstructed sound field depends on the spatial and angular resolutions used during the measurement. Nevertheless, satisfactory results can be obtained without very fine resolution, especially when considering the number of microphones that would be required to map the sound field with a similar spatial resolution. Furthermore, the use of light as a sensing element (instead of a bulk instrument) makes the acousto-optic effect a non-invasive technique. This together with the fact that the tomographic reconstruction does not

assume anything about the properties of the acoustic field turns the acousto-optic effect into a very attractive measurement principle for the visualization of sound fields.

APPENDIX A: TAYLOR SERIES OF THE REFRACTIVE INDEX

The refractive index changes slightly with the pressure fluctuations caused by an acoustic field. The small magnitude of these variations makes it possible to approximate Eq. (3) with a Taylor expansion. If Eq. (3) is rewritten as

$$n(x) = (n_0 - 1)(1 + x)^{1/\gamma} + 1, \tag{A1}$$

where x corresponds to p/p_0, then the corresponding Taylor series can be calculated from the following expression:

$$n(x) = \sum_{i=0}^{\infty} \frac{n^{(i)}(0)}{i!} x^i, \tag{A2}$$

where $n^{(i)}(0)$ is the ith derivative of the refractive index evaluated at zero. Note that the Taylor series is centered at zero because x fluctuates around this value. Furthermore, the infinite summation stated in Eq. (A2) can in practice be truncated when $|x| \ll 1$. This is indeed the case since the amplitude of the acoustic pressure is much smaller than the value of the static pressure ($|p| \ll p_0$). Therefore,

$$\begin{aligned} n(x) \simeq n(0) + \frac{n'(0)}{1!} x^1 &= n(0) + n'(0)x \\ &= n_0 + \frac{n_0 - 1}{\gamma} x \quad \text{for} \quad |x| \ll 1, \end{aligned} \tag{A3}$$

where $n(0)$ and $n'(0)$ have been determined from Eq. (A1). Finally, substituting x by the ratio of the acoustic pressure to the atmospheric pressure yields the approximation of the index of refraction given by Eq. (4).

APPENDIX B: SOLUTION OF THE ELECTROMAGNETIC WAVE EQUATION

Equation (6) states the condition required in order to guarantee the validity of the solutions obtained from the electromagnetic wave equation in the presence of disturbing sound. Under weak acousto-optic interaction, the magnitude of the variations of the refractive index is very small, and in particular, the overall magnitude of the refractive index can be regarded as very close to unity when the light propagates in air. Moreover, the time derivative of the refractive index is proportional to the angular frequency of oscillation of the acoustic field. Thus, Eq. (6) can be reformulated as

$$\left.\begin{aligned} n &\approx 1 \\ \frac{\partial n}{\partial t} &\propto \omega_a \\ T &= \frac{2\pi}{\omega_o} \end{aligned}\right\} \Rightarrow \left|\frac{1}{n}\frac{\partial n}{\partial t} T\right| \approx \left|2\pi \frac{\omega_a}{\omega_o}\right| \ll 1. \tag{B1}$$

The highest audible frequency is around 20 kHz, whereas the light oscillates at frequencies of the order of terahertz. Therefore, this condition is clearly fulfilled when analyzing the acousto-optic effect in the audible frequency range.

The exact solution to the electromagnetic wave equation in the presence of sound can be derived by inserting Eq. (7) into the wave equation

$$\begin{aligned} &\mathbf{E}\left(j\frac{\partial^2 \phi}{\partial z^2} - \left(\frac{\partial \phi}{\partial z}\right)^2\right) \\ &\quad - \left(\frac{n}{c_0}\right)^2 \mathbf{E}\left(j\frac{\partial^2 \phi}{\partial t^2} - \left(\omega_o + \frac{\partial \phi}{\partial t}\right)^2\right) = 0. \end{aligned} \tag{B2}$$

Without losing generality, it is assumed that the light travels along the z-direction. According to Eq. (B1), the temporal variation of ϕ can be regarded to be much slower than the angular frequency of the electromagnetic field

$$\left|\frac{\partial \phi}{\partial t}\right| \ll \omega_o \quad \text{and} \quad \left|\frac{\partial^2 \phi}{\partial t^2}\right| \ll \omega_o^2. \tag{B3}$$

Equation (B2) now reduces to

$$j\frac{\partial^2 \phi}{\partial z^2} - \left(\frac{\partial \phi}{\partial z}\right)^2 + \left(\frac{n\omega_0}{c_0}\right)^2 = 0. \tag{B4}$$

If the second partial derivative of $\phi(z, t)$ as a function of z is much smaller in absolute value than the square of the first derivative

$$\left|\frac{\partial^2 \phi}{\partial z^2}\right| \ll \left(\frac{\partial \phi}{\partial z}\right)^2, \tag{B5}$$

Eq. (B2) can be further simplified

$$\left(\frac{\partial \phi}{\partial z}\right)^2 = \left(\frac{n\omega_o}{c_0}\right)^2 \Leftrightarrow \frac{\partial \phi}{\partial z} = \pm \frac{n\omega_o}{c_0}, \tag{B6}$$

and therefore ϕ can be found by integrating the refractive index along the propagation path

$$\phi = \phi_0 + \pm \frac{\omega_o}{c_0} \int_{z_1}^{z_2} n \mathrm{d}z = \phi_0 \pm k_0 \int_{z_1}^{z_2} n \mathrm{d}z. \tag{B7}$$

Here z_1 and z_2 are the initial and final positions of the integration, ϕ_0 is simply an integration constant that depends on the used reference system, and the sign must be chosen according to the direction of propagation, that is, "$-$" for waves propagating in the positive direction of z and "$+$" otherwise.

[1]D. Royer and O. Casula, "Quantitative imaging of transient acoustic fields by optical heterodyne interferometry," in *Proceedings of the 1994 IEEE Ultrasonics Symposium* (1994), Vol. 2, pp. 1153–1162.

[2]T. A. Pitts and J. F. Greenleaf, "Three-dimensional optical measurement of instantaneous pressure," J. Acoust. Soc. Am. **108**, 2873–2883 (2000).

[3]J. P. Remenieras, O. B. Matar, S. Calle, and F. Patat, "Acoustic pressure measurement by acousto-optic tomography," in *Proceedings of the 2001 IEEE Ultrasonics Symposium* (2001), Vol. 1, pp. 505–508.
[4]A. R. Harland, J. N. Petzing, and J. R. Tyrer, "Nonperturbing measurements of spatially distributed underwater acoustic fields using a scanning laser Doppler vibrometer," J. Acoust. Soc. Am. **115**, 187–195 (2004).
[5]J. M. Buick, J. A. Cosgrove, P.-A. Douissard, C. A. Greated, and B. Gilabert,, "Application of the acousto-optic effect to pressure measurements in ultrasound fields in water using a laser vibrometer," Rev. Sci. Instrum. **75**, 3203–3207 (2004).
[6]P. D. Theobald, S. P. Robinson, G. Hayman, and T. Koukoulas, "Acousto-optic tomography for mapping of high-frequency sonar fields," in *Proceedings of Acoustics 08* (2008), pp. 2833–2838.
[7]L. Bahr and R. Lerch, "Beam profile measurements using light refractive tomography," IEEE Trans. Ultrason. Ferroelectr. Freq. Control **55**, 405–414 (2008).
[8]X. Jia, G. Quentin, and M. Lassoued,, "Optical heterodyne detection of pulsed ultrasonic pressures," IEEE Trans. Ultrason. Ferroelectr. Freq. Control **40**, 67–69 (1993).
[9]K. Nakamura, M. Hirayama, and S. Ueha, "Measurements of air-borne ultrasound by detecting the modulation in optical refractive index of air," in *Proceedings of the 2002 IEEE Ultrasonics Symposium* (2002), pp. 609–612.
[10]Y. Oikawa, M. Goto, Y. Ikeda, T. Takizawa, and Y. Yamasaki, "Sound field measurements based on reconstruction from laser projections," in *IEEE International Conference on Acoustics, Speech and Signal Processing* (2005), pp. 661–664.
[11]T. Sakoda and Y. Sonoda, "Visualization of sound field with uniform phase distribution using laser beam microphone coupled with computerized tomography method," Acoust. Sci. & Tech. **29**, 295–299 (2008).
[12]Y. Oikawa, T. Hasegawa, Y. Ouchi, Y. Yamasaki, and Y. Ikeda, "Visualization of sound field and sound source vibration using laser measurement method," in *Proceedings of the 20th International Congress on Acoustics* (2010).
[13]A. D. Pierce, *Acoustics: An Introduction to its Physical Principles and Applications* (Acoustical Society of America, Melville, New York, 1989), Chap. 1.
[14]J. H. Gladstone and T. P. Dale, "Researches on the refraction, dispersion, and sensitiveness of liquids," Philos. Trans. R. Soc. London **153**, 317–343 (1863).
[15]W. Merzkirch, *Techniques of Flow Visualization* (Advisory Group for Aerospace Research & Development, Loughton, Essex, 1987).
[16]P. M. Morse and K. U. Ingard, *Theoretical Acoustics* (Princeton University Press, Princeton, New Jersey, 1986), Chap. 13.
[17]A. Torras-Rosell, S. Barrera-Figueroa, and F. Jacobsen, "An investigation of sound fields based on the acousto-optic effect," in *Proceedings of 18th International Congress on Sound & Vibration* (2011).
[18]A. C. Kak and M. Slaney, *Principles of Computerized Tomographic Imaging* (IEEE, New York, 1988), Chaps. 3 and 5.

Paper C

Reconstruction methods for sound visualization based on acousto-optic tomography

Antoni Torras-Rosell [1], Oliver Lylloff [2], Salvador Barrera-Figueroa [3], and Finn Jacobsen [4]

[1, 3] DFM, Danish National Metrology Institute

Matematiktorvet 307, 2800 Kongens Lyngby, Denmark

[2, 4] Acoustic Technology, Department of Electrical Engineering, Technical University of Denmark

Ørsteds Plads 352, 2800 Kongens Lyngby, Denmark

ABSTRACT

The visualization of acoustic fields using acousto-optic tomography has recently proved to yield satisfactory results in the audible frequency range. The current implementation of this visualization technique uses a laser Doppler vibrometer (LDV) to measure the acousto-optic effect, that is, the interaction between sound and light, over an aperture where the acoustic field is to be investigated. By identifying the relationship between the apparent velocity of the LDV and the Radon transform of the acoustic field, it is possible to reconstruct the sound pressure distribution of the scanned area using tomographic techniques. The filtered back projection (FBP) method is the most popular reconstruction algorithm used for tomography in many fields of science. The present study takes the performance of the FBP method in sound visualization as a reference and investigates the use of alternative methods commonly used in inverse problems, e.g., the singular value decomposition and the conjugate gradient methods. A generic formulation for describing the acousto-optic measurement as an inverse problem is thus derived, and the performance of the numerical methods is assessed by means of simulations and experimental results.
Keywords: Acousto-optic, Tomography, Visualization

1. INTRODUCTION

The ability to measure airborne sound by means of the acousto-optic effect, that is, the interaction between sound and light, has recently rendered surprisingly good results for various acoustic applications, namely visualization, localization and identification of acoustic sources.[1–3] The use of light as a sensing element poses a fundamental advantage over conventional measurement techniques: the light does not change the properties of sound when traveling through the acoustic field, which means that the acousto-optic effect is

[1] atr@dfm.dk
[2] s082312@student.dtu.dk
[3] sbf@dfm.dk
[4] fja@elektro.dtu.dk

a non-invasive measurement principle. This is particularly beneficial and crucial at high frequencies, where scattering effects normally corrupt measurements carried out with transducer-based techniques. The present work investigates the possibility of enhancing the visualization of sound fields based on acousto-optic tomography by means of numerical methods. Acousto-optic tomography is usually implemented with the so-called filtered back projection (FBP) method, which is in fact the most renowned tomographic reconstruction algorithm in many fields of science. The numerical methods are seen in this study as a promising alternative to the FBP method because these methods stem from a completely different mathematical principle, and they have been applied successfully to many other areas of research such as medical imaging, seismology and astronomy.

In the following, a brief review about acousto-optic tomography and its formulation as an inverse problem are given. The numerical methods under investigation are then presented. The performance of these methods is examined by means of simulations. The comparison between the numerical methods is possible by analyzing two different performance indicators, namely the mean square error (MSE) and the structural similarity (SSIM) index. Some preliminary experimental results also illustrate the potential of the examined numerical methods. Most of the source code used in this study is based on the open MATLAB toolboxes `Regularization Tools`[4] and `AIRtools`[5].

2. ACOUSTO-OPTIC TOMOGRAPHY

2.1. Measurement principle

The speed of light depends on the density of the medium where the light is traveling. For instance, light travels fastest in vacuum, it slows slightly down in air and it propagates even slower in water. This is just to illustrate that sound waves, as pressure fluctuations, change indeed the density of the medium, and thus, influence the propagation of light as well. The acousto-optic effect is a tiny phenomenon that within the audible frequency range and for sound pressure levels below the threshold of pain can simply be modeled as a modulation effect on the phase of light: light travels slightly faster/slower when the acoustic pressure reduces/increases. Such a small effect can be measured using interferometry, and in particular, with an LDV. This optical instrument is originally intended for measuring mechanical vibrations of a surface where the laser beam is reflected off. However, it can be shown that by keeping the vibrations of the reflecting point negligible and when the laser beam travels across a sufficiently intense sound field, the output of an LDV corresponds to an apparent velocity that fulfills the following expression in the frequency domain,[2]

$$V_{\mathrm{LDV}}(\omega) = j\omega \frac{n_0 - 1}{\gamma p_0 n_0} \int_{\mathbf{L}} P(\vec{r}, \omega) \mathrm{d}l, \tag{1}$$

where $P(\vec{r}, \omega)$ is the temporal Fourier transform of the acoustic pressure, $\mathbf{L}$ represents the path traveled by the laser beam, n_0 and p_0 are the refractive index and pressure of the medium (in this case, air) under static conditions, and γ is the ratio of specific heats. This equation shows that the measurement of the acousto-optic effect does not provide a direct measure of the sound pressure, but rather its line integral along the laser beam. A single line integral is not enough to reconstruct an arbitrary sound field, at least without taking for granted basic assumptions about the nature of the sound field. Instead, a complete reconstruction without incorporating any previous knowledge about the sound field can be achieved using tomography and the Radon transform. The latter is an integral transform named after the Austrian mathematician Johann Radon, who laid down the principles of tomography with his posterior derivation of the inverse Radon transform. The Radon transform of an acoustic field can be expressed as a function of the apparent velocity of the LDV stated in equation (1) as follows,[2]

$$R_p(\theta, x', \omega) = \int_{-L/2}^{L/2} P(x', y', \omega) \mathrm{d}y' = \frac{\gamma p_0 n_0}{n_0 - 1} \frac{V_{\mathrm{LDV}}(\omega)}{j\omega}, \tag{2}$$

where θ is the angle of projection of the acoustic field, x' and y' are the Cartesian coordinates according to the projection angle θ, and L is the total length of the line integral. A sketch of the measurement principle can be seen in Figure 1. The measurement of the acousto-optic effect over a sufficient number of angles of projection and parallel lines constitutes a well-defined problem that relates the unknown data (sound pressure) with the observed data (Radon transform). The trivial solution to this forward problem is to apply the inverse Radon transform. However, such a naive solution will often lead to terrible results due to the presence of noise. In practice, tomographic algorithms incorporate regularization techniques to stabilize results. The FBP method is probably the most well-known tomographic reconstruction algorithm. For parallel line scanning

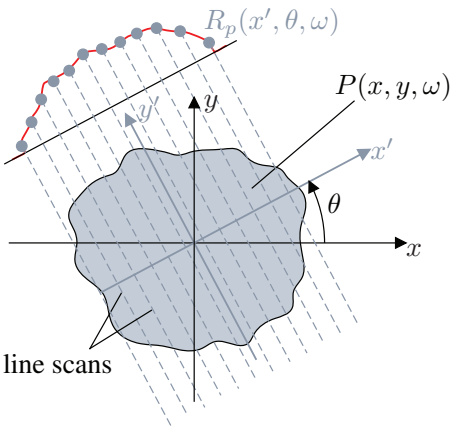

Fig. 1 – Sketch of the acousto-optic measuring principle.

configuration, the sound pressure is reconstructed as follows,[1]

$$P(\vec{r}, \omega) = \int_0^{\pi} Q(\theta, x', \omega) \mathrm{d}\theta, \tag{3}$$

where $Q(\theta, x', \omega)$ is the so-called "filtered projection", which corresponds to the convolution of the measured Radon transform with a filter $h(x')$ that accounts for both the implementation of the reconstruction algorithm using the two-dimensional Fourier transform (Ram-Lak filter) and the regularization (filtering) imposed in the wavenumber domain (e.g. Shepp-Logan filter) to reduce the influence of noise.

2.2. Tomography as an inverse problem

The reconstruction of sound pressure from the Radon transform of an acoustic field can also be described as an inverse problem using a matrix equation of the following form,

$$\mathbf{A}x = b, \tag{4}$$

where x is a column vector with n elements representing the unknown, complex sound pressures ($x \in \mathbb{C}^n$), b is a column vector with m elements corresponding to the measured, complex Radon transform ($b \in \mathbb{C}^m$), and $\mathbf{A}$ is a real matrix with dimensions $m \times n$ that holds the underlying tomographic model ($\mathbf{A} \in \mathbb{R}^{m \times n}$). Unlike the FBP method, one of the great advantages of using numerical methods is the possibility of modeling any tomographic scheme beyond the classical parallel and fan-shaped scanning configurations. The matrix $\mathbf{A}$ is currently implemented with the MATLAB function `radon`, where the columns are the Radon transform of a black image with a single white pixel that is looped over all the positions of the reconstruction aperture.[6] The inversion of equation (4) constitutes a discrete ill-posed problem that arises from the discretization of the forward problem (the Radon transform) and the noise in the measurement vector b. The rest of this section presents five regularization techniques to circumvent the ill-posedness of the problem.

2.2.1. Singular value decomposition

The singular value decomposition (SVD) is an essential theoretical and computational tool for understanding both the ill-posedness and the effects of regularization on linear inverse problems such the one stated in equation (4). The SVD of $\mathbf{A}$ can be defined as,[7]

$$\mathbf{A} = \mathbf{U}\Sigma\mathbf{V}^T = \sum_{i=1}^{n} u_i \sigma_i v_i^T, \tag{5}$$

where σ_i is the i'th singular value, Σ is the corresponding nonnegative diagonal matrix consisting of the singular values appearing in descending order, u_i and v_i are the i'th left and right singular vectors of $\mathbf{A}$, and $\mathbf{U}$ and $\mathbf{V}$ are the corresponding matrices where the singular vectors are arranged in columns, yielding matrices with orthonormal columns. When $\mathbf{A}$ is inverted and applied to equation (4), the following naive solution is obtained:

$$x = \mathbf{A}^{-1} b = \sum_{i=1}^{n} \frac{u_i^T b}{\sigma_i} v_i. \tag{6}$$

The fact that the singular values tend to zero and that each term of the summation is inversely proportional to its singular value result in increasing amplification of the potentially noise-dominated vector product $u_i^T b$ as $i \to m$. To overcome this problem, the following two regularization techniques are considered:

Truncated singular value decomposition (TSVD) is simply, as the name indicates, a truncated version of SVD that stems from the idea that the last terms of the summation stated in equation (6) correspond to very small singular values, and these singular values can potentially amplify the measurement noise yielding meaningless reconstructions. The approach for regularizing the solution is thus to truncate the number of singular values contributing to the final solution,[7]

$$x_k = \sum_{i=1}^{k} \frac{u_i^T b}{\sigma_i} v_i, \quad \text{where} \quad k \leq n. \tag{7}$$

Standard Tikhonov regularization computes the regularized solution by solving the following minimization problem in a least squares sense:

$$\min \left\{ \|\mathbf{A}x - b\|_2^2 + \lambda \|x\|_2^2 \right\}, \tag{8}$$

where λ is the relaxation parameter that controls the weight of the regularization term in the overall minimization problem. Note that, in standard form, the regularization term is simply the energy of the solution vector x. If we include the SVD of $\mathbf{A}$ into the minimization problem, it can be shown that the Tikhonov solution x_λ can be written as follows,[7]

$$x_\lambda = \sum_{i=1}^{m} \varphi_i^{[\lambda]} \frac{u_i^T b}{\sigma_i} v_i, \quad \text{where} \quad \varphi_i^{[\lambda]} = \frac{\sigma_i^2}{\sigma_i^2 + \lambda^2}. \tag{9}$$

In this case, each term of the SVD is weighted with a filter coefficient $\varphi_i^{[\lambda]}$, that basically reduces the undesired amplification of noise caused by the smallest singular values, but with a smoother transition compared to that of the TSVD method ($\varphi_i^{[\lambda]} \approx 1$ when $\sigma_i > \lambda$, and $\varphi_i^{[\lambda]} \approx 0$ when $\sigma_i < \lambda$).

2.2.2. Iterative methods

Iterative regularization relies on matrix multiplications or row action methods, which makes these methods often suitable for large scale problems where an explicit factorization of $\mathbf{A}$ is too cumbersome. Each iteration of an iterative method yields a regularized solution, initially approaching the sought exact solution, but as the number of iterations increases, the algorithm converges to undesired solutions. This behavior is often referred to as semi-convergence. Hence, the number of iterations plays in these methods the role of regularization parameter. In the following, three different iterative regularization methods are considered:

Conjugate gradient least squares (CGLS) is referred to as the most stable implementation of the conjugate gradient method solved in a least squares sense. The core of the algorithm can be summarized in the following five statements:[7]

$$\begin{aligned}
\alpha_k &= \|\mathbf{A}^T r^{(k-1)}\|_2^2 \,/\, \|\mathbf{A} d^{(k-1)}\|_2^2, \\
x^{(k)} &= x^{(k-1)} + \alpha_k d^{(k-1)}, \\
r^{(k)} &= r^{(k-1)} - \alpha_k \mathbf{A} d^{(k-1)}, \\
\beta_k &= \|\mathbf{A}^T r^{(k)}\|_2^2 \,/\, \|\mathbf{A}^T r^{(k-1)}\|_2^2, \\
d^{(k)} &= \mathbf{A}^T r^{(k)} + \beta_k d^{(k-1)}.
\end{aligned} \tag{10}$$

The algorithm is initialized with $x^{(0)}$, $r^{(0)} = b - \mathbf{A}x^{(0)}$ and $d^{(0)} = \mathbf{A}^T r^{(0)}$. With this iteration method, the large singular values seem to converge faster than the rest, meaning that CGLS can effectively regularize the solution when stopping the algorithm long before it converges to the least squares solution.

Landweber iteration is one of the classical iterative methods, originally described in 1951[8]. In its simplest form, the algorithm leads to the following regularized solution,[7]

$$x^{(k)} = x^{(k-1)} + \lambda_k \mathbf{A}^T r^{(k-1)}, \tag{11}$$

where λ_k is a relaxation parameter that can be updated at each iteration k, and $r^{(k-1)}$ is the residual vector of the last iteration. In this study, λ_k is updated in each iteration following a line search strategy[5].

Kaczmarz method is one of the most popular row action methods. These are methods that use only one row of **A** at a time to update the iterative solution, in particular for the Kaczmarz method,[7]

$$x \leftarrow x + \lambda \frac{b_i - a_i^T x}{\|a_i\|_2^2} a_i, \tag{12}$$

where λ is the relaxation parameter, a_i^T is the i'th row of **A**, and for each iteration of the method, all the rows of **A** are swept from top to bottom, that is, $i = 1, \ldots, m$. Note that in this case, the relaxation parameter is kept constant. Although λ was set to 1 in the original paper of Kaczmarz[9], other values between 0 and 2 can also be used ($\lambda \in (0, 2)$). In the present investigation, λ was set to 0.2 due to convergence rate concerns.

3. PERFORMANCE INDICATORS

The presented numerical methods are assessed by means of the following two performance indicators:

Mean square error (MSE) is probably the most common way of quantifying the difference between an estimate and its corresponding true function. In vector notation, the normalized MSE can be calculated as follows,

$$\hat{\delta}_x = \|x_{\text{exact}} - x\|_2^2 \,/\, \|x_{\text{exact}}\|_2^2. \tag{13}$$

Structural similarity (SSIM) index is a method developed for assessing the similarity between two images, and thus, it provides a measure of quality in image reconstruction problems.[10] This index can take values between 0 and 1. The closer the value is to 1, the higher the similarity. In the current study, the images correspond to sound pressure reconstructions obtained with the numerical methods under investigation. The nature of the SSIM index is far from the physical meaning underlying the MSE. It alternatively tries to take advantage of known features of the human visual system, which makes it an interesting approach when assessing a sound visualization technique such as acousto-optic tomography.

4. SIMULATION STUDY

Two different and well-defined sound fields are investigated in the following simulation study, namely the sound fields generated when two monopoles are radiating in phase and in antiphase (dipole case), respectively. Hence, one sound field is dominated by the constructive interference of the two monopoles and the other one features a clear destructive interference between the two point sources. This is illustrated on the

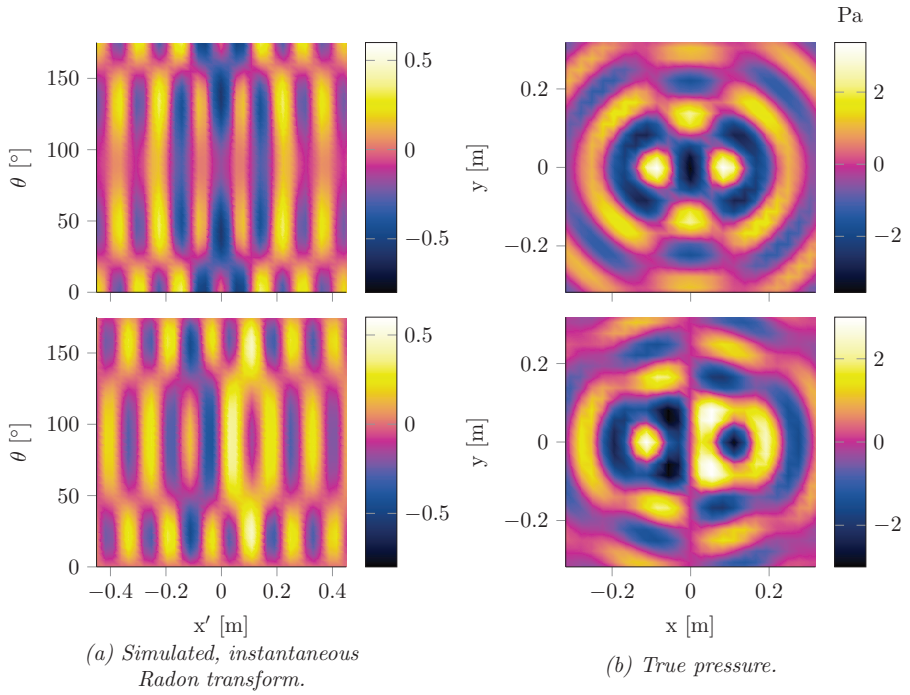

(a) Simulated, instantaneous Radon transform.

(b) True pressure.

Fig. 2 – Instantaneous, theoretical sound fields and their corresponding Radon transforms.

right hand side of figure 2, where the top panels show a instantaneous representation of the acoustic field synthesized by the two monopoles driven in phase and the bottom panels correspond to the dipole case. The different nature of these two acoustic fields makes it possible to draw conclusions about the performance of the numerical methods with a certain independence of the actual sound fields used in the calculations.

The simulation study starts computing the Radon transform of the two acoustic fields under investigation, see left hand side in figure 2. These data are then properly arranged in a column vector that constitutes the right-hand side vector b defined in the matrix equation (4). Once the matrix $\mathbf{A}$ is also set up, the inverse problem is solved with the regularization methods presented in section 2. The evolution of the regularized solutions as a function of the regularization parameters is shown in figure 3. As can be seen, the overall

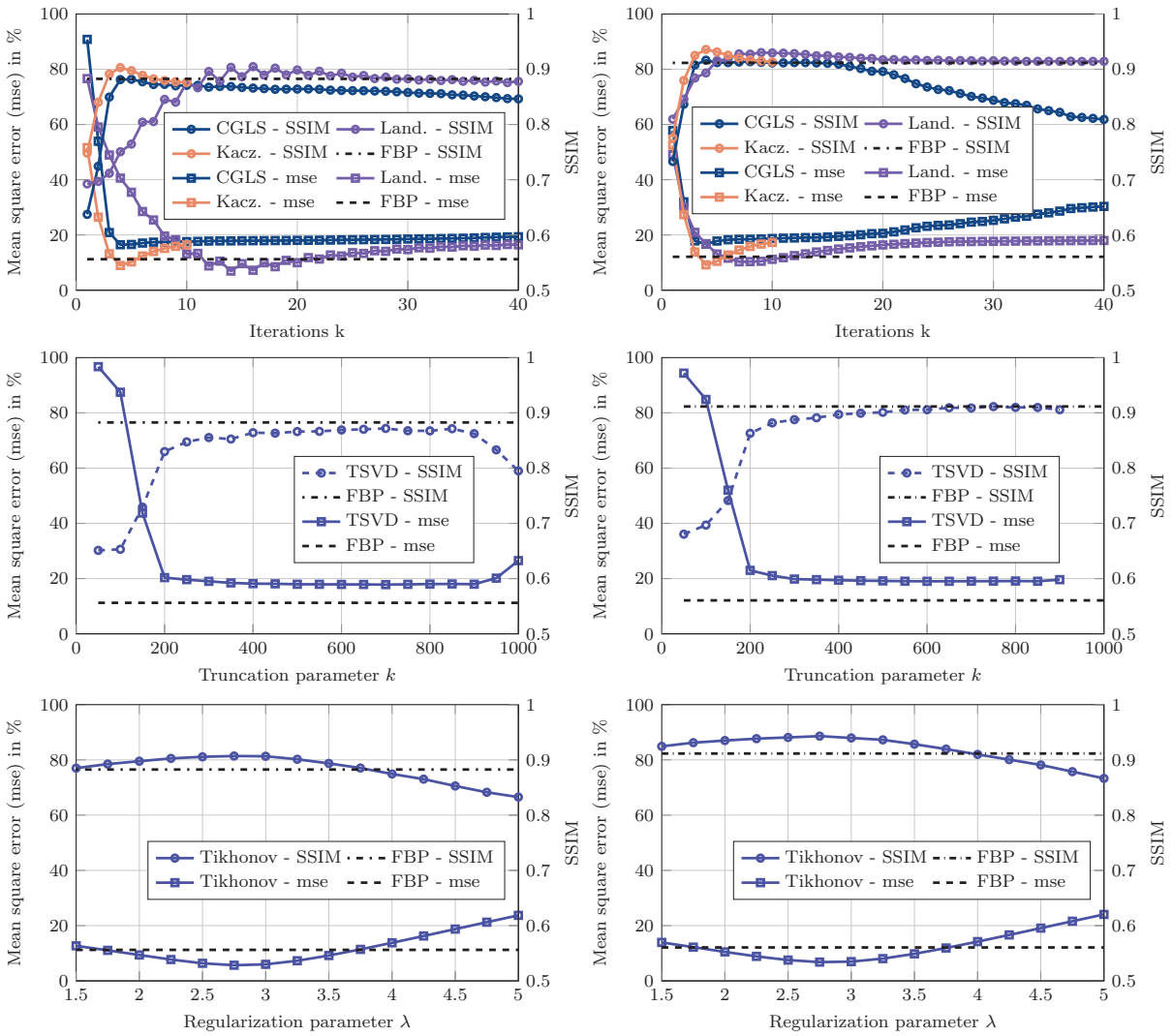

(a) Two monopoles in phase. *(b) Dipole.*

Fig. 3 – Performance of the numerical methods as a function of their regularization parameters.

results obtained for the two sound fields under investigation are approximately the same. This suggests that the results are fairly independent of the actual sound fields used to examine the performance of the numerical methods. The optimal value of the regularization parameter of each method can be identified by looking at the minimum/maximum of the MSE/SSIM curves, respectively. In some cases, this optimal value is not the same for both the MSE and the SSIM index. The two top panels show the results corresponding to the iterative methods (CGLS, Landweber iteration and Kaczmarz method). The CGLS and Kaczmarz methods converge faster than the Landweber iteration. However, when the two monopoles radiate in phase (see the top-left plot), the Landweber iteration presents the best results in terms of MSE and SSIM index. Instead, the Kaczmarz method provides the best results for the dipole case. Although the CGLS method leads to results equally good as the classical FBP in terms of SSIM index, it clearly yields higher values of MSE, and thus, less accurate solutions. Note that both Landweber and Kaczmarz methods perform better than the

FBP method in terms of both MSE and SSIM index. The second row of plots in figure 3 shows the TSVD results. The best regularized solution provided by this method yields approximately the same MSE and SSIM index as the CGLS method, and thus, the overall performance is worse than that of the FBP method. The two bottom plots in figure 3 present the results obtained with Tikhonov regularization. In this case, the smoother regularization of the singular values in comparison to the sudden truncation of the TSVD method yields the best results out of the five numerical methods under investigation.

The performance of each method has also been investigated as a function of the signal-to-noise ratio (SNR), see figure 4. As expected, the MSE increases while the SSIM index decreases as the SNR is worsened.

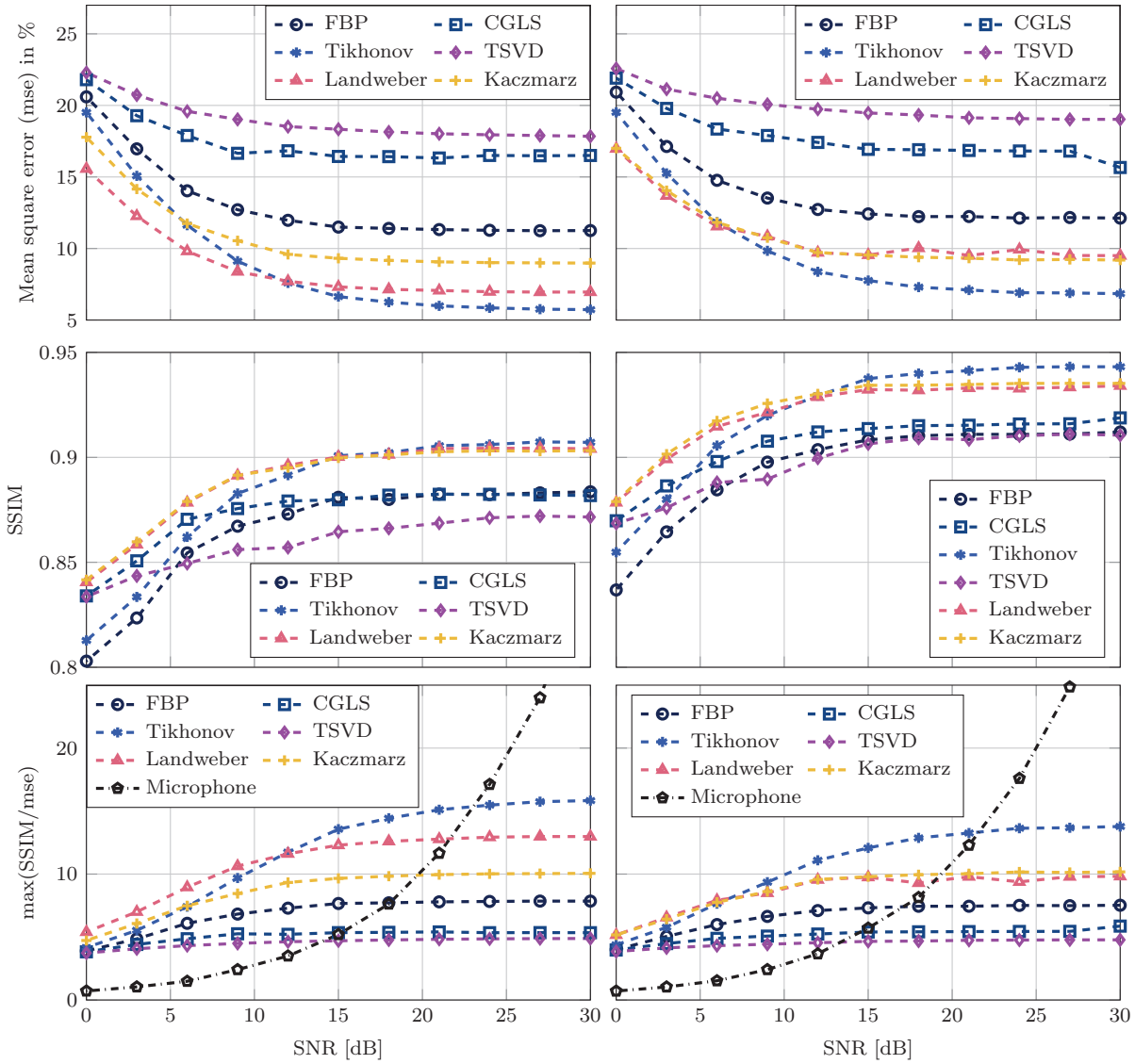

(a) Two monopoles in phase. *(b) Dipole.*

Fig. 4 – Quality of the reconstructions as a function of the SNR. For each SNR, the optimal regularization parameter is first identified in terms of MSE.

In general, the results are similar for both the two monopoles radiating in phase and the dipole. Interestingly, the overall values of MSE are slightly higher for the dipole case, while the performance of the reconstruction methods in terms of SSIM index is slightly worse for the two-monopoles case. This indicates the convenience of considering more than one performance indicator when assessing the quality of the reconstructions. The ratio SSIM/MSE is thus presented in the two bottom plots of figure 4 in order to have an idea of the overall performance of the methods. In short, the larger the ratio, the better the performance. Ideally, when SSIM $\rightarrow$ 1 and MSE $\rightarrow$ 0, then the ratio SSIM/MSE $\rightarrow \infty$. As can be seen, Tikhonov regularization yields the best results for SNRs higher than 12 dB in the two-monopoles case, and 6 dB in the dipole case. In this range of SNRs, the good performance of the Tikhonov regularization is followed by the Landweber and Kaczmarz

methods. The classical FBP method lies in between this group and the other group characterized by poorer performance consisting of the CGLS method and the TSVD. In fact, these two methods yield almost the same results. At lower SNRs, the Landweber and Kaczmarz algorithms yield better results than the Tikhonov regularization. The last two plots in figure 4 also show the ratio SSIM/MSE for a microphone array that would sample the acoustic field at the same positions where the numerical methods reconstruct the pressure. The microphone results are simply biased by the random noise introduced in the simulations. It is interesting to see that the Tikhonov results are better than the ones obtained with the microphone array for SNRs below 23 dB in the two-monopoles case, and 21 dB in the dipole case. The other reconstruction methods progressively outperform the microphone results as the SNR worsens. It is in fact remarkable that all the reconstruction methods investigated for acousto-optic tomography yield better results than the microphone array for SNRs below 14 dB.

Figure 5 shows the sound pressure maps obtained with the microphone array, the FBP method, and the Tikhonov regularization. The simulation is adjusted to a SNR of 18 dB. The first and second rows of plots correspond to the two-monopoles and dipole cases, respectively. As can be seen, the main features of the two sound fields under investigation are clearly identified in all the reconstructions. The microphone results are though visibly more affected by noise, whereas the other pressure maps are smoother. However, a one-dimensional plot of the diagonal of the pressure maps (see figure 6) reveals that the FBP does not reconstruct the peak values accurately. Instead, the Tikhonov results show the best agreement with the theoretical values of the pressure, which is also in agreement with the results presented in figure 4.

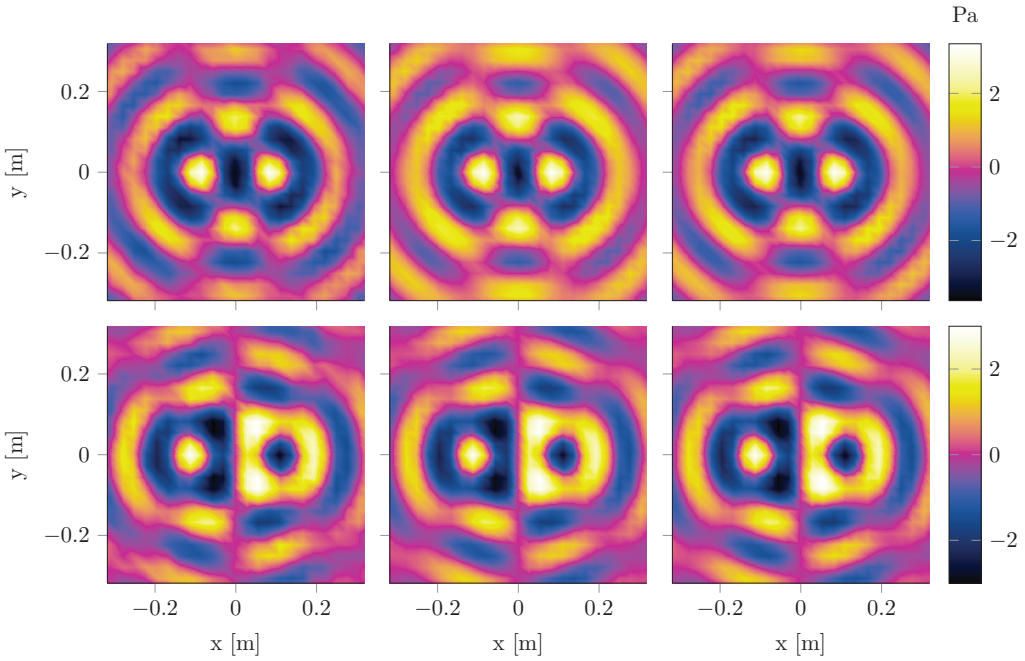

(a) Microphone. *(b) FBP.* *(b) Tikhonov.*

Fig. 5 – Examples of sound field reconstructions for a SNR of 18 dB. The top row corresponds to the two-monopoles case, and the second row shows the results of the dipole.

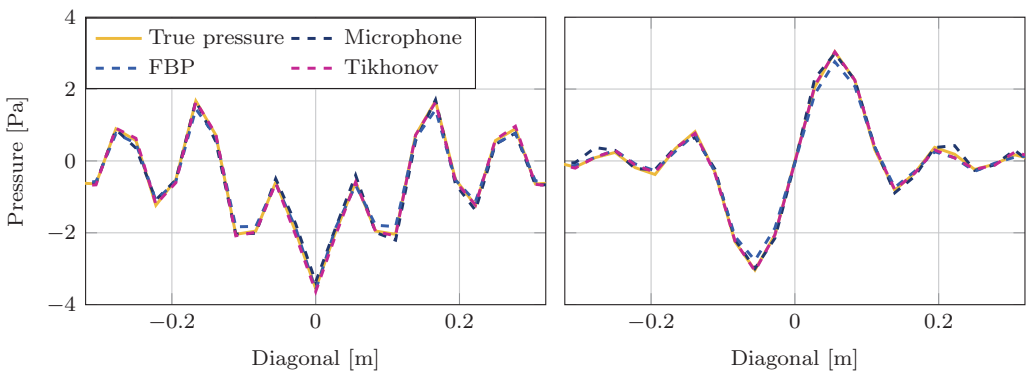

(a) Two monopoles. *(b) Dipole.*

Fig. 6 – Diagonal of the pressure maps shown in Fig. 5.

5. EXPERIMENTAL RESULTS

A set of preliminary measurements were carried out in an anechoic room of 1000 m^3. A picture of the experimental setup can be seen in figure 7. In order to make the measurements somehow comparable to the simulation results, two loudspeakers, whose centers were separated by 20 cm, were driven in phase and in antiphase with a 2.4 kHz pure tone. The measured Radon transforms are shown on the left hand side of

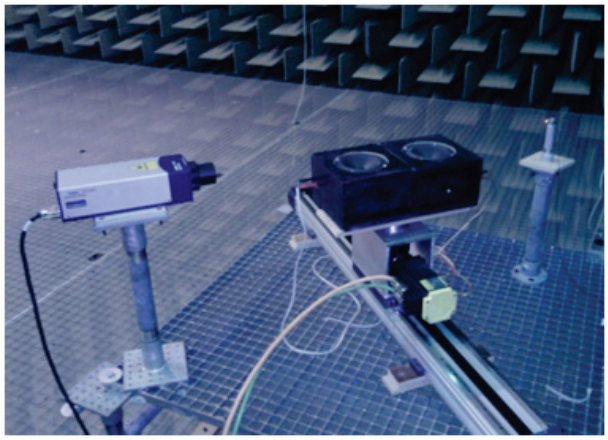

Fig. 7 – Experimental setup used for sound field reconstruction based on acousto-optic tomography.

figure 8, and they are in good agreement with the instantaneous representation examined in the simulation study (cf. figure 2). The corresponding reconstructions based on the FBP method and Tikhonov regularization are presented on the right hand side of figure 8. The first and second rows correspond to the two-monopoles and dipole cases, respectively. As observed in the simulations, both FBP and Tikhonov yield smooth pressure maps, although it must be noted in this case that the SNR during the measurements was around 30 dB approximately. A closer look, in particular among the dipole reconstructions, shows that the FBP method leads to lower pressures at the peaks of the reconstruction maps. This is in agreement with the simulations results shown in figure 6. The rest of the numerical methods were also examined and led to similar pressure maps as the ones presented in figure 8.

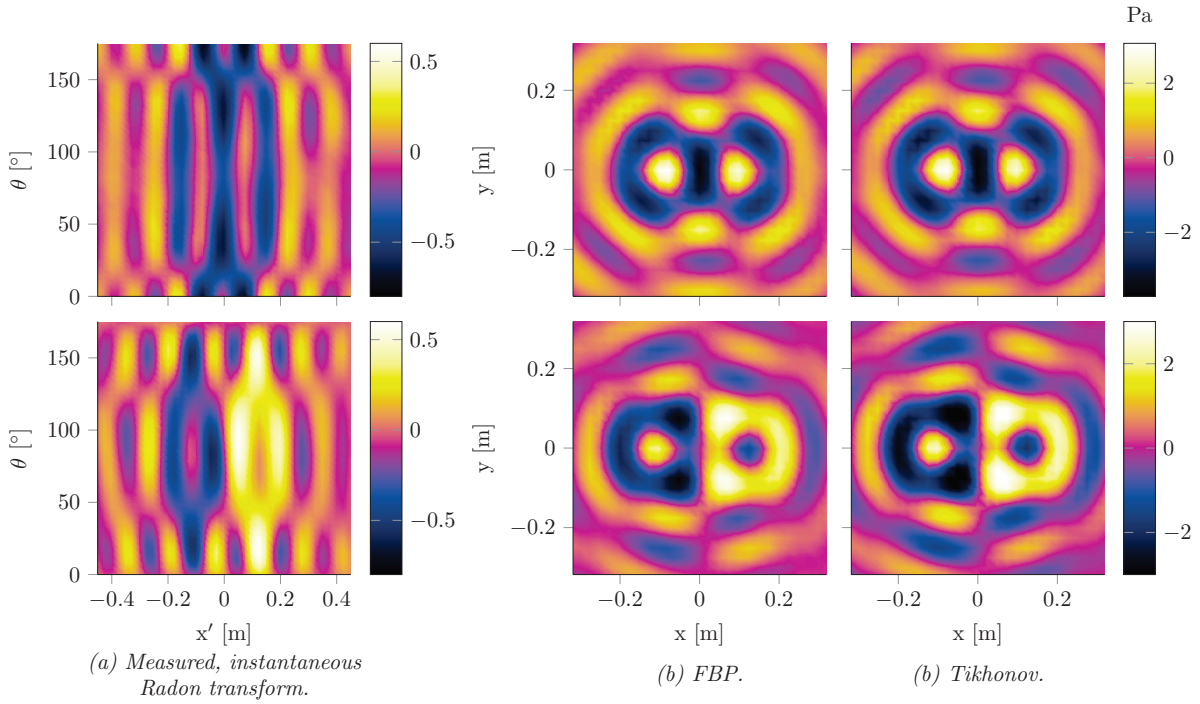

(a) Measured, instantaneous Radon transform. *(b) FBP.* *(b) Tikhonov.*

Fig. 8 – Experimental results obtained in the anechoic room with a SNR of about 30 dB. The top row shows the results of the two-monopoles case, and the second row shows the results of the dipole case.

6. SUMMARY AND CONCLUSIONS

The reconstruction of acoustic fields based on acousto-optic tomography has been implemented with numerical methods. This is possible by describing the tomographic reconstruction as a discrete inverse problem. Five different regularization techniques have been examined to tackle the ill-posedness of the tomographic problem. The investigated techniques have been assessed by means of two performance indicators, namely the MSE and the SSIM index. The latter is a quality parameter originally designed for image processing, and thus, it assesses the quality of the tomographic reconstructions from a visual point of view. This is a very suitable alternative to the classical MSE parameter, especially if we bear in mind that acousto-optic tomography is basically a sound visualization technique. Both the MSE and the SSIM index identify the optimal regularization parameter of each method in the same range of values, though they do not provide exactly the same value. Hence, this points out that to rely the quality of the reconstruction on a visual inspection procedure of the resulting acoustic image is not a guarantee that the optimum solution is achieved, though it will typically be fairly close to it. The overall results show that the numerical methods can lead to successful sound field reconstructions. In particular, three out of the five methods (Tikhonov regularization being the best, Landweber iteration and Kaczmarz method) have consistently proved superior to the classical FBP method. The numerical methods also seem fairly robust to low SNRs. In fact, when comparing the results to that of a microphone array, Tikhonov regularization yields better reconstructions for SNRs lower than 21 dB approximately, and all the tomographic methods present better SSIM/MSE ratios for SNRs lower than 14 dB.

The main challenge of using numerical methods for reconstructing acoustic fields is the choice of the optimal regularization parameter. Typically, the optimal value differs from problem to problem. Therefore, it is necessary to investigate in the future the use of parameter choice methods that could make this choice automatically without compromising the final reconstruction significantly. On the other hand, it should also be noted that numerical methods can in principle be implemented for any tomographic scheme, while the classical FBP method is normally restricted to parallel and fan-shaped scanning configurations. This makes acousto-optic tomography more versatile, and it can ease the complexity of the measurement setup currently required.

REFERENCES

[1] A. Torras-Rosell, S. Barrera-Figueroa, and F. Jacobsen, "Sound field reconstruction using acousto-optic tomography", J. Acoust. Soc. Am. **131**, 3786–3793 (2012).

[2] A. Torras-Rosell, S. Barrera-Figueroa, and F. Jacobsen, "An acousto-optic beamformer", J. Acoust. Soc. Am. **132**, 144–149 (2012).

[3] A. Torras-Rosell, S. Barrera-Figueroa, and F. Jacobsen, "The versatility of the acousto-optic measuring principle in characterizing sound fields", in *Proceedings of the Institute of Acoustics*, volume 35, 242–250 (Nottingham, UK) (2013).

[4] P. C. Hansen, "Regularization tools version 4.0 for matlab 7.3", Numerical Algorithms **46**, 189–194 (2007).

[5] P. C. Hansen and M. Saxild-Hansen, "Air tools - A MATLAB package of algebraic iterative reconstruction methods", Journal of Computational and Applied Mathematics **236**, 2167–2178 (2012).

[6] M. Bertero and P. Boccacci, *Introduction to Inverse Problems in Imaging* (Institute of Physics Publishing, Bristol, UK) (1998).

[7] P. C. Hansen, *Rank-Deficient and Discrete Ill-Posed Problems: Numerical Aspects of Linear Inversion* (Society for Industrial and Applied Mathematics (SIAM), Philadelphia, USA) (1998).

[8] L. Landweber, "An iteration formula for fredholm integral equations of the first kind", American Journal of Mathematics **73**, 615–624 (1951).

[9] S. Kaczmarz, "Angenherte auflsung von systemen linearer gleichungen", Bulletin International de l'Acadmie Polonaise des Sciences et des Lettres **35**, 355–357 (1937).

[10] Z. Wang, A. C. Bovik, H. R. Sheikh, and E. P. Simoncelli, "Image quality assessment: From error visibility to structural similarity", IEEE Transactions on Image Processing **13**, 600–612 (2004).

Paper D

Investigating the use of the acousto-optic effect for acoustic holography

Antoni Torras-Rosell[a,1)]
Efren Fernandez-Grande[b,2)]
Finn Jacobsen[c,2)]
Salvador Barrera-Figueroa[d,1)]

[1]Danish Fundamental Metrology A/S, Matematiktorvet 307, 2800 Kgs. Lyngby, Denmark

[2]Acoustic Technology, Department of Electrical Engineering, Technical University of Denmark Ørsteds Plads 352, 2800 Kgs. Lyngby, Denmark.

Recent studies have demonstrated that the acousto-optic effect, that is, the interaction between sound and light, can be used as a means to visualize acoustic fields in the audible frequency range. The changes of density caused by sound waves propagating in air induce phase shifts to a laser beam that travels through the acoustic field. This phenomenon can in practice be captured with a laser Doppler vibrometer (LDV), and the pressure distribution of the acoustic field can be reconstructed using tomography. The present work investigates the potential of the acousto-optic effect in acoustic holography. Two different holographic methods are examined for this purpose. One method first reconstructs the hologram plane using acousto-optic tomography and then propagates it using conventional near-field acoustic holography (NAH). The other method exploits the so-called Fourier Slice Theorem and bases all the calculations of the holographic algorithm on the Radon transform of the acoustic field. The validity of the proposed methods is examined in a simple study case by means of simulations and preliminary measurements.

a) email: atr@dfm.dtu.dk
b) email: efg@elektro.dtu.dk
c) email: fja@elektro.dtu.dk
d) email: sbf@dfm.dtu.dk

1 INTRODUCTION

Near-field acoustic holography (NAH) is a sound source identification technique that makes it possible to reconstruct the entire acoustic field, that is, sound pressure, particle velocity and sound intensity, over a three-dimensional (3D) space, based on a two-dimensional (2D) measurement of the sound field with an array of acoustic transducers.[1-5] NAH has been widely investigated since the 1980s,[1-3] and there exist several methods to implement it (e.g., Fourier based NAH,[1-3] SONAH,[4] the equivalent source method,[6] Inverse Boundary element method[7,8]). Here is yet another attempt to contribute in this field from a completely different point of view. Recent studies have shown that the characterization of audible sound by means of the interaction between sound and light is possible.[9,10] This opens up for the possibility of using an original measurement principle in many acoustical applications, and perhaps, new properties will appear for improving the performance of the existing methods. The basis of this investigation is to explore the potential use of the acousto-optic effect in NAH. In what follows, it is described how to use the acousto-optic effect to measure the sound pressure distribution in a plane. This will lead to some spectral properties between the spatial Fourier transform and the Radon transform of an acoustic field that can be interesting for NAH. The theory is then examined by means of computer simulations and some preliminary measurements.

2 THEORY

2.1 The Acousto-Optic Effect

The measurement principle exploited when using the acousto-optic effect in air and within the audible frequency range is based on the idea that electromagnetic waves such as light are not diffracted by the presence of acoustic waves but simply phase-modulated. The light travels fastest in vacuum and generally slower with increasing density of the medium. The phenomenon of sound inherently involves pressure fluctuations that cause density variations of the medium. Thus, roughly speaking, sound waves make the light to propagate faster/slower depending on whether they cause a pressure decrease/increase in the medium of propagation. However, this is a small effect that requires measuring the phase of light very accurately. Such degree of precision can be achieved using an interferometric device such as a laser Doppler vibrometer (LDV). Although an LDV is typically used to map the mechanical velocity of a vibrating surface, it can be shown that when the LDV is pointing to a nonvibrating surface and the laser beam is traveling through an intense sound field, the output of the LDV corresponds to an apparent velocity caused by the acousto-optic effect,[10]

$$v(t) = \frac{n_0 - 1}{\gamma p_0 n_0} \frac{d}{dt} \left(\int_L p(x,y,z,t) dl \right), \tag{1}$$

where n_0 and p_0 correspond to the refractive index and the static pressure of the medium under static conditions, γ is the ratio of specific heats, and $p(x,y,z,t)$ is the sound pressure integrated by the laser beam along the path represented by L. Figure 1 depicts an sketch of this measurement method. As described in the next section, the reformulation of the apparent velocity measured with the LDV as a function of the Radon transform of the acoustic field makes it possible to reconstruct the sound pressure using tomography.

2.2 The Radon and the Spatial Fourier Transforms

The Radon transform is a mathematical transform widely used in tomography that consists on the line integral of a function over a set of given paths, e.g. parallel lines.[11] For the present study case, the Radon transform of the sound pressure can be defined as follows

$$R_p(x',\theta,z,\omega) = \int_{-\infty}^{+\infty} P(x,y,z,\omega)dy' , \tag{2}$$

where $P(x,y,z,\omega)$ is the temporal Fourier transform of the sound pressure $p(x,y,z,t)$, and the coordinates x' and y' are related to the coordinates x and y by means of the following rotation matrix:

$$\begin{bmatrix} x' \\ y' \end{bmatrix} = \begin{bmatrix} \cos\theta & \sin\theta \\ -\sin\theta & \cos\theta \end{bmatrix} \begin{bmatrix} x \\ y \end{bmatrix} . \tag{3}$$

As can be seen in Fig. 2, $R_p(x',\theta,z,\omega)$ can be interpreted as the projection of the sound field towards the direction of the y'-axis. By Fourier transforming Eqn. (1),

$$V(\omega) = j\omega \frac{n_0 - 1}{\gamma p_0 n_0} \left(\int_L P(x,y,z,\omega)dl \right), \tag{4}$$

it is easy to see that $R_p(x',\theta,z,\omega)$ can be directly retrieved from the apparent velocity measured with the LDV,

$$\widetilde{R}_p(x',\theta,z,\omega) = \int_L P(x,y,z,\omega)dl = \frac{\gamma p_0 n_0}{n_0 - 1} \frac{V(\omega)}{j\omega} , \tag{5}$$

where the symbol ~ denotes that the sound field is in practice integrated over a finite path L. By projecting the sound field into a sufficient number of angles θ, it is possible to reconstruct the original sound field by means of the inverse Radon transform. This is an inverse problem that can in practice be implemented using tomographic algorithms. [10]

Since the definition of the Radon transform given in Eqn. (2) is based on $P(x,y,z,\omega)$, the 2D spatial Fourier transform (wavenumber spectrum) of an acoustic field can accordingly be defined as (following $e^{-j\omega t}$ convention):

$$P(k_x,k_y,z,\omega) = \int_{-\infty-\infty}^{+\infty+\infty} P(x,y,z,\omega) e^{-j(k_x x + k_y y)} dxdy . \tag{6}$$

Note that for k_y=0, the latter equation can be rewritten as:

$$P(k_x,0,z,\omega) = \int_{-\infty-\infty}^{+\infty+\infty} P(x,y,z,\omega) e^{-jk_x x} dxdy = \int_{-\infty}^{+\infty} \left(\int_{-\infty}^{+\infty} P(x,y,z,\omega)dy \right) e^{-jk_x x} dx . \tag{7}$$

This equation demonstrates that $P(k_x,0,z,\omega)$ can be calculated as the 1D spatial Fourier transform of the projection of the sound field towards the y-axis, or in other words, the 1D spatial Fourier transform of the Radon transform of the acoustic field for θ=0:

$$P(k_x,0,z,\omega)=\int_{-\infty}^{+\infty}R_p(x',0,z,\omega)e^{-jk_xx}dx. \tag{8}$$

Let us now consider a more general case by expressing the 2D spatial Fourier transform defined in Eqn. (6) as a function of the (x',y') coordinate system:

$$\begin{aligned}P(k_x,k_y,z,\omega)&=\int_{-\infty-\infty}^{+\infty+\infty}P(x',y',z,\omega)e^{-j(k_x(x'\cos(\theta)-y'\sin(\theta))+k_y(x'\sin(\theta)+y'\cos(\theta)))}dx'dy'\\&=\int_{-\infty-\infty}^{+\infty+\infty}P(x',y',z,\omega)e^{-j((k_x\cos(\theta)+k_y\sin(\theta))x'+(-k_x\sin(\theta))+k_y\cos(\theta))y')}dx'dy'\\&=\int_{-\infty-\infty}^{+\infty+\infty}P(x',y',z,\omega)e^{-j(k'_xx'+k'_yy')}dx'dy'=P(k'_x,k'_y,z,\omega),\end{aligned} \tag{9}$$

where k'_x and k'_y are related to k_x and k_y by means of the same rotation matrix presented in Eqn. (3):

$$\begin{bmatrix}k'_x\\k'_y\end{bmatrix}=\begin{bmatrix}\cos\theta & \sin\theta\\-\sin\theta & \cos\theta\end{bmatrix}\begin{bmatrix}k_x\\k_y\end{bmatrix}. \tag{10}$$

It is now possible to establish a more general relationship between the 2D spatial Fourier transform and the Radon transform of an arbitrary sound field for k'_y=0:

$$P(k'_x,0,z,\omega)=\int_{-\infty}^{+\infty}\left(\int_{-\infty}^{+\infty}P(x',y',z,\omega)dy'\right)e^{-jk'_xx'}dx'=\int_{-\infty}^{+\infty}R_p(x',\theta,z,\omega)e^{-jk'_xx'}dx'. \tag{11}$$

This result implies that the wavenumber spectrum on the k'_x-axis can be calculated from projections of the sound field taken when the (x',y') coordinates are rotated by θ with respect to the (x,y) coordinates, see Fig. 3. This relationship is known as the Fourier Slice Theorem[11].

2.3 Application to acoustical holography

Conventional NAH techniques usually transform the measured hologram into the k-space where it is easy to apply the corresponding propagator,

$$\begin{aligned}P(k_x,k_y,z_s,\omega)&=P(k_x,k_y,z_h,\omega)\cdot G_p=P(k_x,k_y,z_h,\omega)\cdot e^{jk_z(z_s-z_h)},\\V(k_x,k_y,z_s,\omega)&=P(k_x,k_y,z_h,\omega)\cdot G_v=P(k_x,k_y,z_h,\omega)\cdot\frac{k_z}{\rho_0ck}e^{jk_z(z_s-z_h)},\end{aligned} \tag{12}$$

where G_p and G_v are the pressure and velocity propagators from the measurement plane $z=z_h$ to the reconstruction plane $z=z_s$, and $k_z = \sqrt{k^2 - k_x^2 - k_y^2}$. Beyond all the signal processing efforts that need to be employed in order to ensure that the solution provided by this simple formulation of the NAH is unique and stable, we are now concerned with the fact that the 2D spatial Fourier transform yields an homogeneous grid of data points on the (k_x,k_y) plane. Equation (11) shows that by projecting the sound field into a set of different directions, it is possible to calculate several diagonals of the wavenumber spectrum. This yields a circularly symmetric grid of points in the wavenumber domain. Figure 4 sketches the two mentioned layouts of data points in the *k*-space. As can be seen, the diagonals obtained when using the Radon transform of the acoustic field yield a higher density of points at low spatial frequencies. To exploit this feature of the Radon transform, the Fourier-based NAH technique defined in Eqn. (2) can be rewritten as follows

$$\begin{aligned} P(k_x,k_x,z_s,\omega) &= F_{x'}^{\theta}\left\{R_p(x',\theta,z_h,\omega)\right\}\cdot G_p = F_{x'}^{\theta}\left\{R_p(x',\theta,z_s,\omega)\right\}, \\ V(k_x,k_x,z_s,\omega) &= F_{x'}^{\theta}\left\{R_p(x',\theta,z_h,\omega)\right\}\cdot G_v = F_{x'}^{\theta}\left\{R_v(x',\theta,z_s,\omega)\right\}, \end{aligned} \tag{13}$$

where $F_{x'}^{\theta}\left\{R_p(x',\theta,z_h,\omega)\right\}$ denotes the 1D Fourier transform along the *x'*-axis of the Radon transform measured at the hologram plane ($z=z_h$) and calculated for each of the directions of projection θ (see Fig. 3). The expressions for G_p and G_v are fundamentally the same, although k_z needs to be calculated based on the circular symmetry of the k_x and k_y values (see Eqn. (10) and Fig. 4). Once the hologram plane is propagated, the Radon transform of the pressure and velocity fields can be obtained on the reconstruction plane by 1D inverse Fourier transforming the diagonals of $P(k_x,k_y,z_s,\omega)$ and $V(k_x,k_y,z_s,\omega)$, that is, by inverse Fourier transforming $F_{x'}^{\theta}\left\{R_p(x',\theta,z_s,\omega)\right\}$ and $F_{x'}^{\theta}\left\{R_v(x',\theta,z_h,\omega)\right\}$. Finally, $P(x,y,z_s,\omega)$ and $V(x,y,z_s,\omega)$ can be retrieved from $R_p(x',\theta,z_s,\omega)$ and $R_v(x',\theta,z_s,\omega)$ using the inverse Radon transform.

3 SIMULATIONS

To ease the assessment of the simulation results, a very simple study case is examined: a monopole radiating into free space. The hologram plane is located 5 cm away from the source (z_h = 5 cm) whereas the reconstruction plane is placed at z_s = 3 cm. In order to make the simulations a bit more realistic, the calculations were contaminated with random noise that was adjusted to produce a signal-to-noise ratio (SNR) of 30 dB. The number of data points used in the calculations was limited to 81 for conventional NAH method (e.g. this could correspond to an array of 9x9 microphones) and to 90 for the proposed NAH technique based on the Radon transform (denoted as Nearfield Acousto-Optic Holography, NAOH). In both cases, the propagated hologram needs to be regularized in the wavenumber domain in order to secure stable results. This is done by applying an exponential tapered window.[3] The values of the rate of decay of the window (α) and the cut-off frequency (k_c) are stated in Table 1. All holograms were zero-padded to produce a matrix of 1024x1024 samples in the wavenumber domain.

Figure 5 shows the sound pressure distributions at the reconstructed plane at 2 kHz. The left panel represents the true pressure map (understanding in this case 'true' pressure as the one resulting from the analytical expressions of a point source). The central and right panels correspond to the results obtained with conventional NAH and NAOH respectively. Similar plots for the transversal velocity field are presented in Fig. 6. As a supplement, the corresponding

wavenumber spectra of the presented pressure and velocity fields are depicted in Figs. 7 and 8 respectively. Overall, the results achieved at this frequency with the NAOH method seem to be slightly better than the ones obtained with conventional NAH. However, several simulations at different frequencies and also with various filtering/regularization settings showed that this is not always the case. Figure 9 illustrates it for three different frequencies of analysis.

Additionally, the acousto-optic effect was also used to reconstruct the instantaneous pressure integrated by the laser beam at the hologram plane (this was done using acousto-optic tomography[10]). The reconstructed hologram was then propagated using conventional NAH technique. The results obtained with this alternative method are also depicted in Fig. 9 with a green dashed line and denoted as AOT-NAH. As can be seen, the results obtained with AOT-NAH are quite often lying in between the results of NAH and NAOH, which is somehow what one would expect since the acoustic field is measured using the Radon transform, but the hologram is propagated with conventional NAH algorithm.

4 MEASUREMENTS

Some preliminary experimental results have been obtained from a previous set of measurements that were originally intended for reconstructing an acoustic field using acousto-optic tomography. The measurements were performed in an anechoic room with a loudspeaker emitting a 2 kHz pure tone. The Radon transform of the acoustic field was measured 12 cm away from the loudspeaker. The reconstruction plane was located 3 cm in front of the loudspeaker. The pressure and the velocity fields reconstructed using NAOH and the corresponding wavenumber spectra are shown in Figs. 10 and 11 respectively. Unfortunately, these results cannot be confronted with any set of conventional NAH measurements at this stage of the study. This together with the fact that the hologram plane was located at a relatively far away position from the source in terms of NAH (z_h = 12 cm) makes any attempt to assess the experimental realization of the proposed method difficult. Nevertheless, a comparison between the NAOH and the AOT-NAH results is still possible. As can be seen in Fig. 12, the agreement between the NAOH and the AOT-NAH methods seems to be consistent with the simulations, that is, they provide approximately the same results.

5 DISCUSSION, CONCLUSIONS AND FUTURE WORK

The simulation results accomplished with the proposed NAOH technique are comparable to the ones obtained with conventional NAH. This confirms the underlying relationship between the Radon transform and the wavenumber spectrum. However, the variability of the results when changing the filtering/regularization parameters makes it difficult to assess whether NAOH can perform any better than conventional NAH consistently. The realization of this variability and the quest for possible solutions are part of the ongoing work. One of the aspects that need to be addressed is that the current implementation of the inverse Radon transform is based on the so-called filtered back projection algorithm. This is a Fourier-based method, and thus, additional filtering processes take place when performing the inverse Radon transform. This can potentially influence the effectiveness of the regularization imposed in the holographic algorithm. This could perhaps be avoided if the inverse Radon transform was computed with an iterative algorithm. Once the causes of the variability on the simulation results are resolved, it is intended to carry out new measurements with conditions similar to the ones assumed in the simulations.

Additional investigations will be carried out in order to examine whether the unique spectral properties of NAOH can be further improved to take advantages of the non-uniform distribution of data points in the wavenumber domain.

6 REFERENCES

1. E. G. Williams, J. D. Maynard, and E. Skudrzyk, "Sound source reconstructions using a microphone array", *J. Acoust. Soc. of Am.*, **68**(1), (1980)

2. J. D. Maynard, E. G. Williams, and Y. Lee,, "Nearfield acoustic holography I: Theory of generalized holography and the development of NAH", *J. Acoust. Soc. of Am.*, **78**(4), (1985)

3. E. G. Williams, "Fourier Acoustics. Sound radiation and Nearfield Acoustical Holography", Academic Press, San Diego, (1999)

4. J. Hald, "Basic theory and properties of statistically optimized near-field acoustical holography", *J. Acoust. Soc. of Am.*, **125**(4), (2009)

5. F. Jacobsen and Y. Liu, "Near field acoustic holography with particle velocity transducers", *J. Acoust. Soc. of Am.*, **118**(5), (2005)

6. A. Sarkissian, "Method of superposition applied to patch near-field acoustic holography", *J. Acoust. Soc. of Am.*, **118**(2), (2005)

7. R. Bai, "Application of BEM (boundary element method)-based acoustic holography to radiation analysis of sound sources with arbitrarily shaped geometries", *J. Acoust. Soc. of Am.*, **92**(1), (1992)

8. W. A. Veronesi and J. D. Maynard, "Digital holographic reconstruction of sources with arbitrarily shaped geometries", *J. Acoust. Soc. of Am.*, **85**(2), 1989.

9. Y. Oikawa, T. Hasegawa, Y. Ouchi, Y. Yamasaki and Y. Ikeda, "Visualization of sound field and sound source vibration using laser measurement method", *Proc. 20th International Congress on Acoustics*, (2010)

10. A. Torras-Rosell, S. Barrera-Figueroa and F. Jacobsen, "Sound field reconstructions using acousto-optic tomography", *J. Acoust. Soc. of Am.*, **131**(5), (2012)

11. A. C. Kak and M. Slaney, "Principles of Computerized Tomographic Imaging", IEEE, New York (1988)

Table 1 – Parameters of the filter used in the holographic algorithm.

Parameter	500 Hz	1 kHz	2 kHz
α	0.1	0.1	0.1
k_c	35.4	42.5	55.0

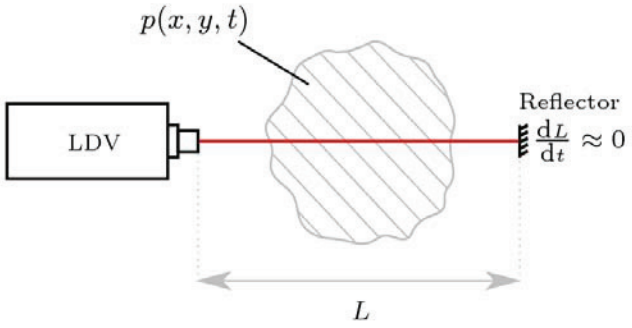

Fig. 1 – Sketch of the measurement setup used to measure the acousto-optic effect with an LDV.

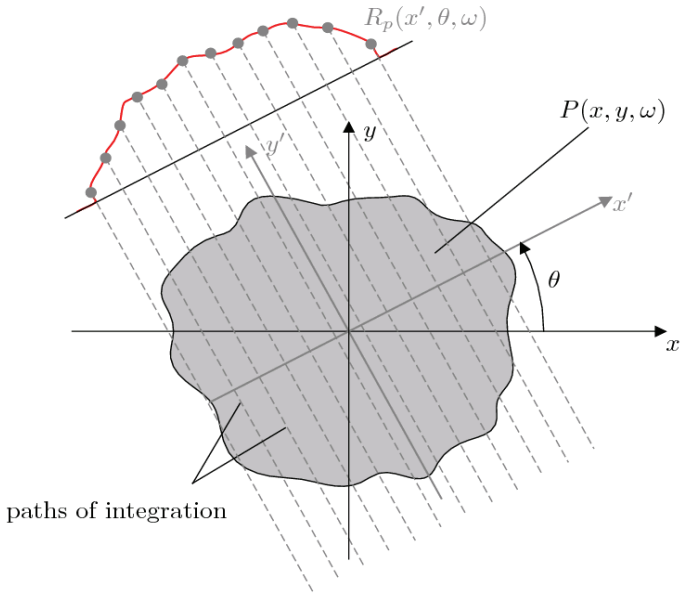

Fig. 2 – Interpretation of the Radon transform as a projection of the sound field .

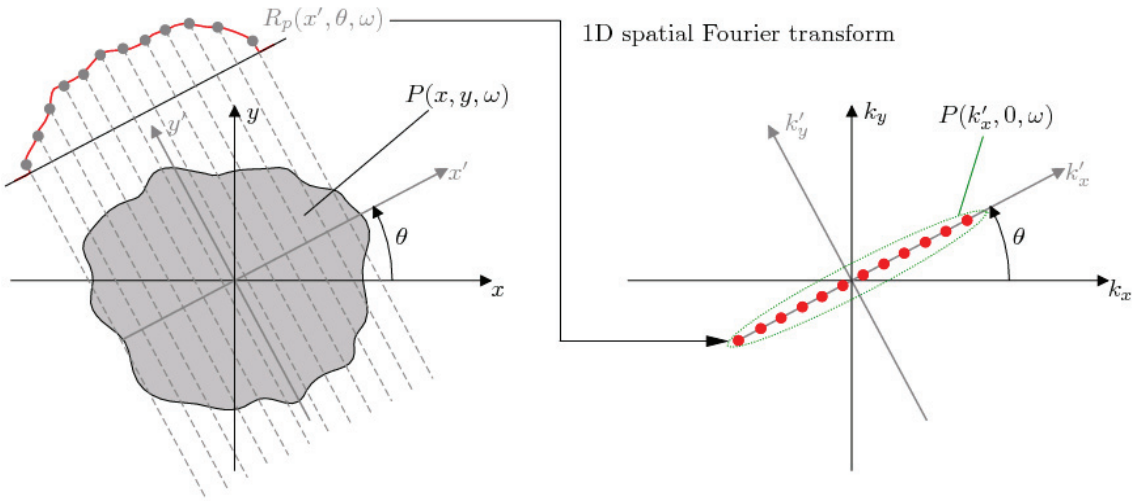

Fig. 3 – The projections of the sound field towards the direction of the y'-axis can be used to compute a diagonal of the wavenumber spectrum.

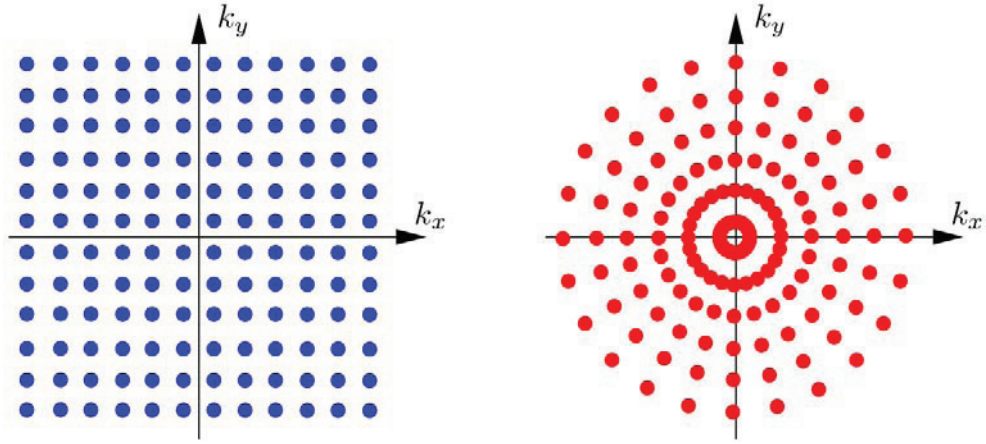

Fig. 4 – Examples of homogeneous and circularly symmetric grids in the k-space.

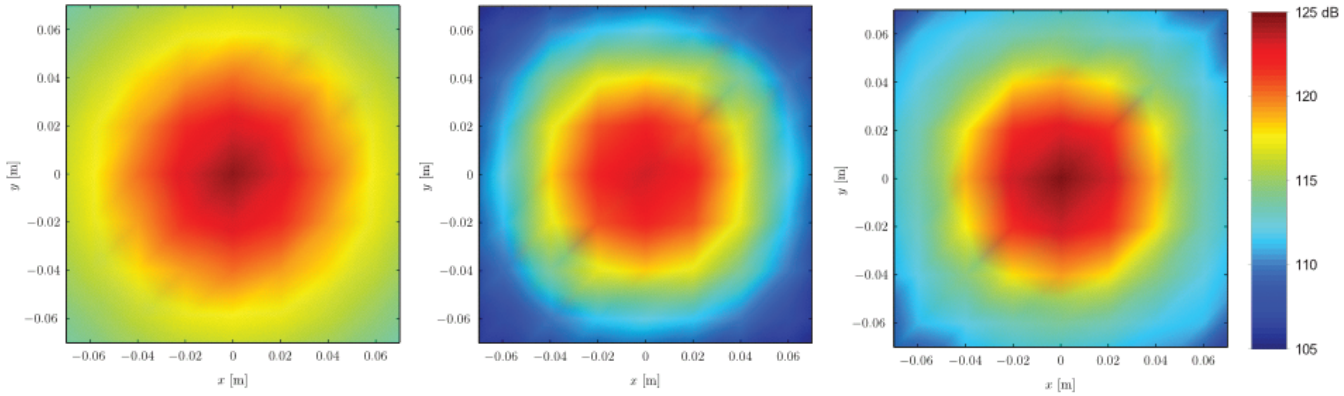

(a) *True* (b) *NAH* (c) *NAOH*

Fig. 5 – Sound pressure distribution at the reconstruction plane at 2 kHz (z_s = 3 cm and z_h = 5 cm).

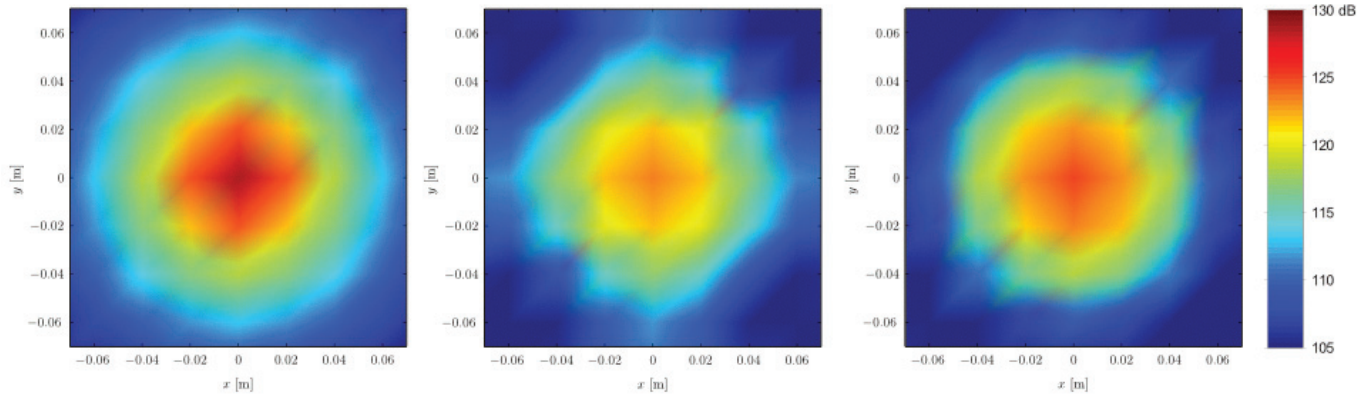

(a) *True* (b) *NAH* (c) *NAOH*

Fig. 6 – Transversal velocity component at the reconstruction plane at 2 kHz (z_s = 3 cm and z_h = 5 cm).

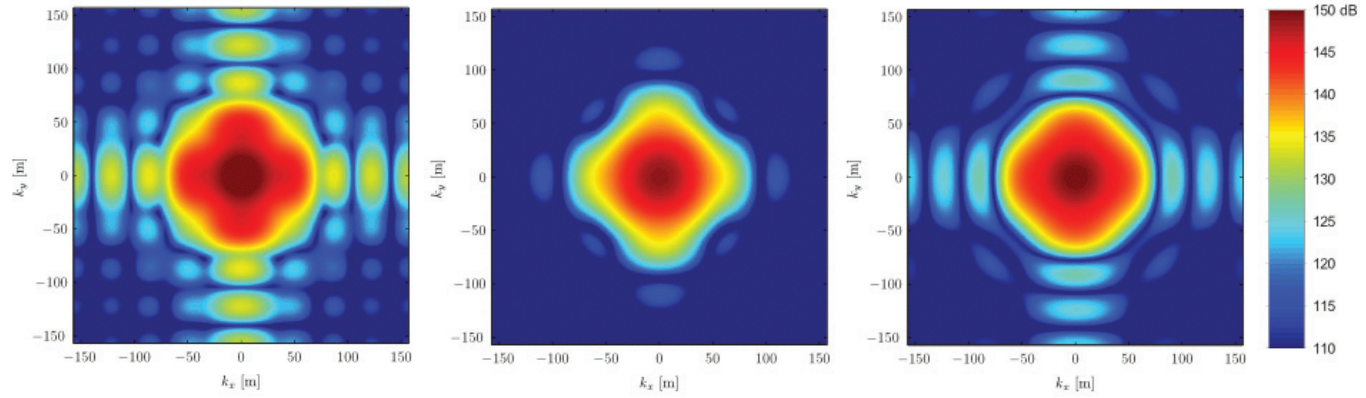

(a) *True* (b) *NAH* (c) *NAOH*

Fig. 7 – Wavenumber spectrum of the reconstructed sound pressure field at 2 kHz (z_s = 3 cm and z_h = 5 cm).

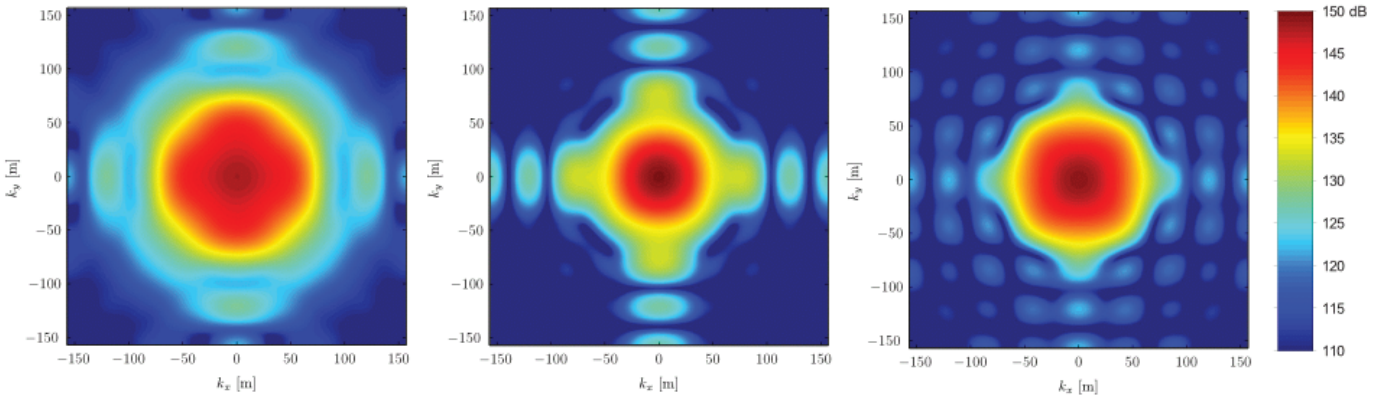

(a) *True* (b) *NAH* (c) *NAOH*

Fig. 8 – Wavenumber spectrum of the reconstructed transversal velocity field at 2 kHz (z_s = 3 cm and z_h = 5 cm).

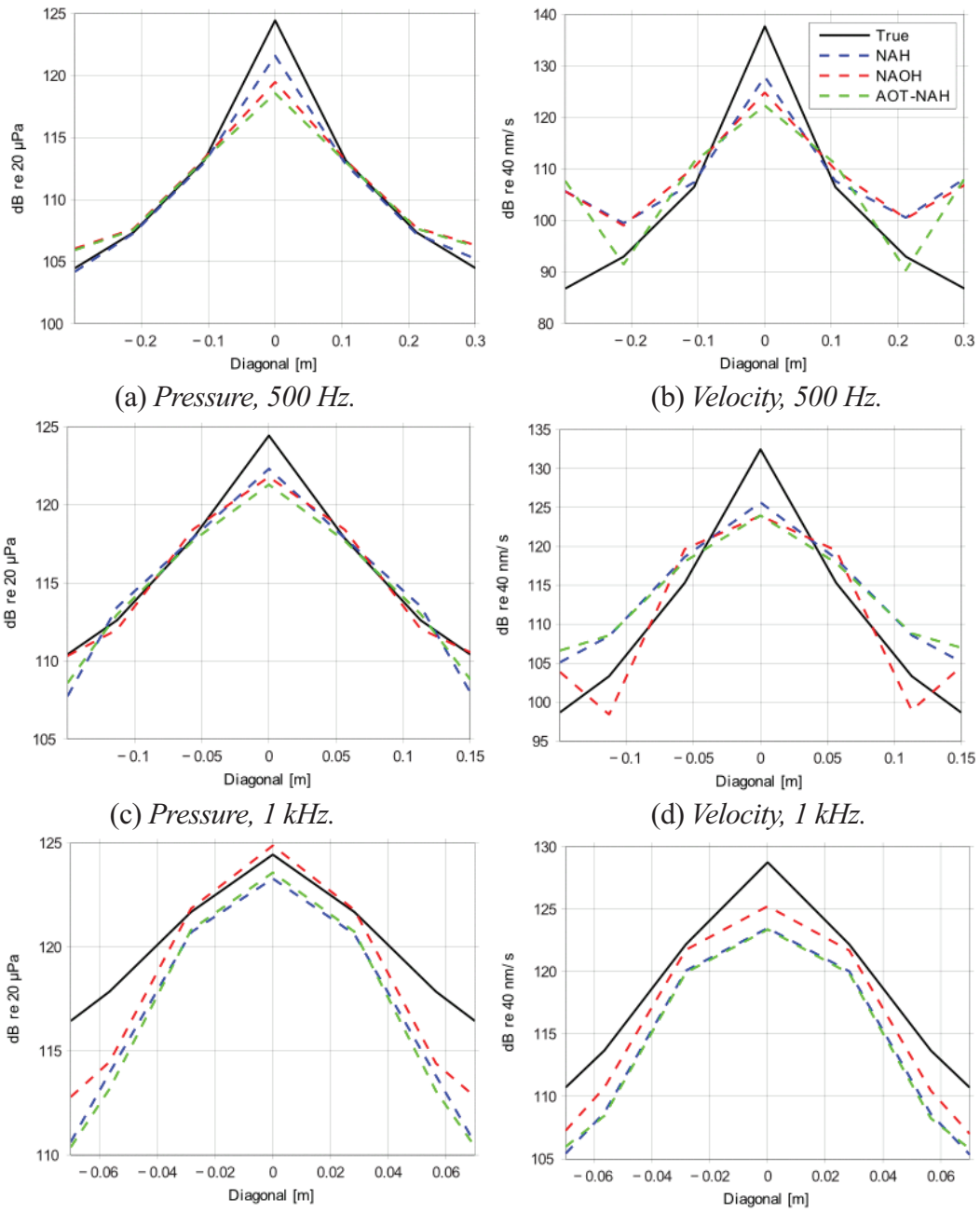

(a) *Pressure, 500 Hz.* (b) *Velocity, 500 Hz.*

(c) *Pressure, 1 kHz.* (d) *Velocity, 1 kHz.*

(e) *Pressure, 2 kHz.* (f) *Velocity, 2 kHz.*

Fig. 9 – Results at the diagonal of the reconstructed plane (z_s = 3 cm and z_h = 5 cm). The spatial resolution is 7.5 cm at 500 Hz, 4 cm at 1 kHz, and 2 cm at 2 kHz. The angular resolution in the NAOH technique is 18 degrees in all cases.

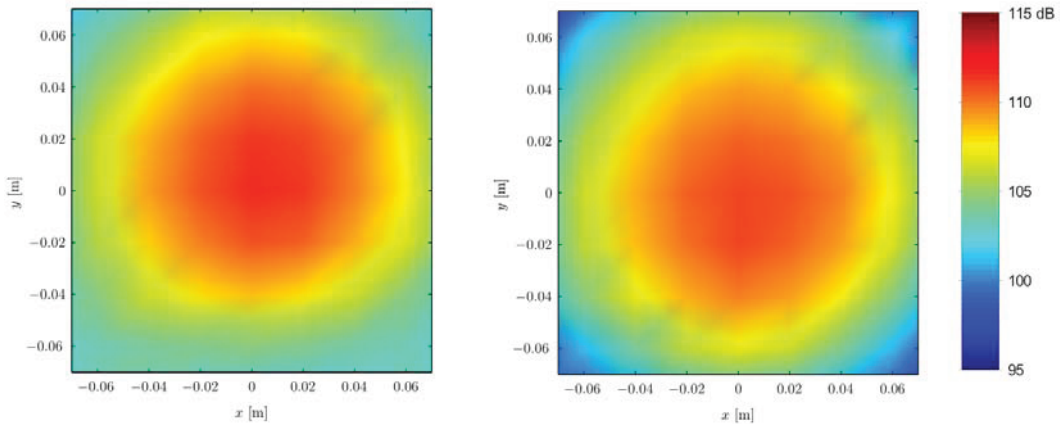

(a) *Pressure* (b) *Transversal velocity*

Fig. 10 – Experimental results of the pressure and the velocity fields reconstructed at z_s = 3 cm.

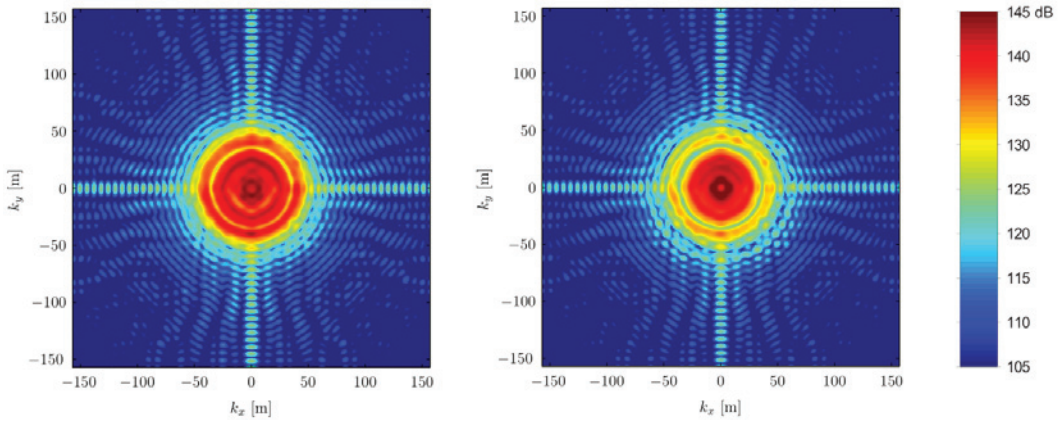

(a) *Pressure* (b) *Transversal velocity*

Fig. 11 – Wavenumber spectra of the measurements results at z_s = 3 cm.

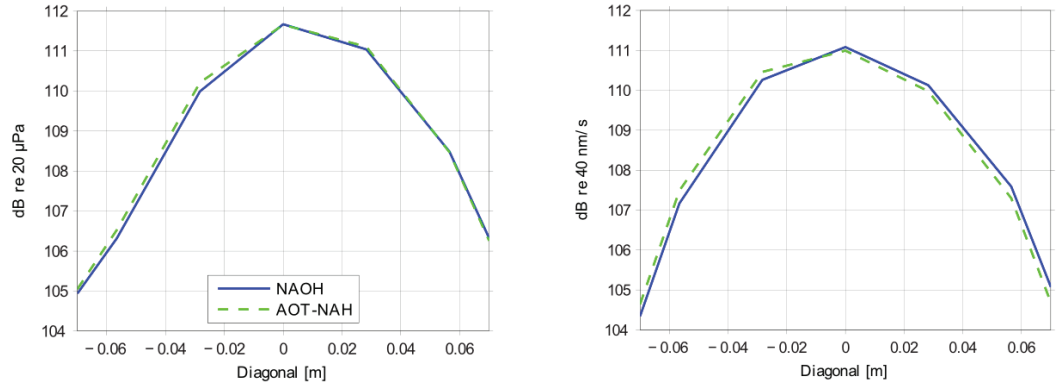

(a) *Pressure* (b) *Transversal velocity*

Fig. 12 – Measurement results at the diagonal of the reconstructed plane (z_s = 3 cm and z_h = 12 cm). In this case, the spatial resolution is 2 cm and the angular resolution is 10 degrees.

Paper E

Holographic reconstruction of sound fields based on the acousto-optic effect

Efren Fernandez-Grande [1], Antoni Torras-Rosell [2], and Finn Jacobsen [3]

[1 3] Acoustic Technology, Department of Electrical Engineering,

DTU - Technical University of Denmark, Ørsteds Plads 352, 2800 Kgs. Lyngby, Denmark

[2] DFM, Danish National Metrology Institute, Matematiktorvet 307,

2800 Kgs. Lyngby, Denmark

ABSTRACT

Recent studies have shown that it is possible to measure a sound field using acousto-optic tomography. The acousto-optic effect, i.e., the interaction between sound and light, can be used to measure an arbitrary sound field by scanning it with a laser Doppler vibrometer (LDV) over an aperture; This can be described mathematically by means of the Radon transform of the acoustic field. An interesting feature of this measurement technique is that the spatial characteristics of the sound field are captured in the measurement. Therefore, the technique has an inherent holographic potential, implicitly yielding a full characterization of the sound field. In this study, a direct projection of the Radon transform from one plane to another and into the space domain, based on an elementary wave expansion is proposed. The relationship between the Radon and the wavenumber domains is examined, and the reconstruction potential of the method analyzed. The study includes both numerical and experimental results.

Keywords: Near-field acoustic holography (NAH); Sound visualization; Acousto-optic effect

1. INTRODUCTION

Sound source identification and sound visualization methods are a very useful tool for studying the sound radiated by acoustic sources. They make it possible to localize and quantify the sound radiated by a source, or parts of a source, and study the mechanisms that produce the acoustic radiation based on measurements in-situ. Consequently, they are a useful tool in the design of acoustic sources, or for reducing their noise output. Some of the most popular methods are based on measurement with arrays of transducers, such as beamforming [1] and near-field acoustic holography (NAH). [2–4]

Recent studies [5–7] have shown hat it is possible to measure the sound pressure over an aperture via tomographic measurements based on the acousto-optic effect, i.e., the interaction between sound and light.

[1] efr@elektro.dtu.dk
[2] atr@dfm.dk

Using a laser Doppler vibrometer (LDV), it is possible to scan the sound field over an area and obtain the Radon transform of the sound pressure. From these data, the actual pressure in space domain can be retrieved via the corresponding inverse transform.

This measurement principle has an inherent holographic potential, which is examined in this paper. The potential stems from he fact that the amplitude and phase of the sound waves is measured over an area, thus it is possible to predict the sound field in a different plane via a holographic reconstruction. This is closely related to acoustic holography and NAH, except that the starting point is not the sound pressure sampled with an array of microphones, but the Radon transform obtained from the measurement of the sound pressure via the acousto-optic effect with a laser Doppler vibrometer. The holographic reconstruction from the Radon transform can be based on an explicit spatial Fourier transformation of the measured field (with FFT), as in the original NAH processing.[3] This possibility was recently examined,[8] and is in a way is analogous to the filtered back-projection method,[9] except that the wavenumber spectrum is propagated from one plane to another prior to the inverse transformation yielding the pressure in a different plane.

In this paper a reconstruction technique is proposed which directly projects the Radon transform from one plane to another and into space domain by means of an elementary plane wave expansion.[10] This is in a way similar to the Fourier based reconstruction, only that in this case the solution of the system does not rely on explicit Fourier transformations, and thus some of the limitations related to the DFT are avoided or minimized, most notably wraparound error and truncation errors related to the finite aperture.

The present study examines the relationship between the Radon domain and the wavenumber domain, the reconstruction based on the plane wave expansion, and the potential of the technique. Numerical results are shown, and a simple experimental measurement is included.

2. THEORY

A. The acousto-optic effect and tomography

The acousto-optic effect describes the interaction between sound and light, when the refractive index of the medium is changed by the presence of sound waves, which inherently involve pressure fluctuations, and consequently density changes. In the audible frequency range, this phenomenon can simply be understood as a phase modulation of the light that propagates through the acoustic field, or in other words, the light travels slightly faster/slower when the sound pressure decreases/increases. This small effect can be measured with a laser Doppler vibrometer (LDV) by letting the beam of light travel through the medium where acoustic waves are present, and focusing the beam on a steady surface. An important requisite for measuring the acousto-optic effect is that the reflecting surface remains still, otherwise the LDV will also sense mechanical vibrations that will compromise the measurement. It can be shown that the apparent velocity measured with the LDV due to the acousto-optic effect is,[7]

$$v_{\mathrm{LDV}}(t) = \frac{n_0 - 1}{\gamma p_0 n_0} \frac{d}{dt} \left(\int_L p(x, y, z, t) dl \right), \tag{1}$$

where n_0 and p_0 are the static refractive index and pressure of the medium under static conditions, γ the ratio of specific heats, and the integral of $p(x, y, z, t)$ corresponds to the projection of the sound pressure along the path L followed by the laser beam. This is further explained in the next subsection.

It is important to note that the line integral in Eq. (1) can be used to estimate the Radon transform of the sound pressure. If the sound field is scanned as shown in Fig. 1, the Radon transform can be retrieved from the apparent velocity of the LDV as

$$R(x', \phi, z_h, \omega) = \frac{\gamma p_0 n_0}{n_0 - 1} \frac{V_{\mathrm{LDV}}(\omega)}{j\omega}, \tag{2}$$

where R is the Radon transform of the sound pressure in the frequency domain, V_{LDV} is the apparent velocity of the LDV also expressed in the frequency domain, ϕ is the rotation angle of each scan, which is taken for a set of parallel lines along the x' axis, and z_h is the measurement plane. Note that we consider now the stationary harmonic case, with the convention $e^{j\omega t}$.

B. Relation between the Radon and the wavenumber domain

In acoustics, it is common to use the wavenumber transform to analyze the spatial characteristics of a sound field,[1,4] which has proven to be a powerful experimental tool used in combination with array measurements. The Radon transform is another integral transform, commonly used in tomography, that results from

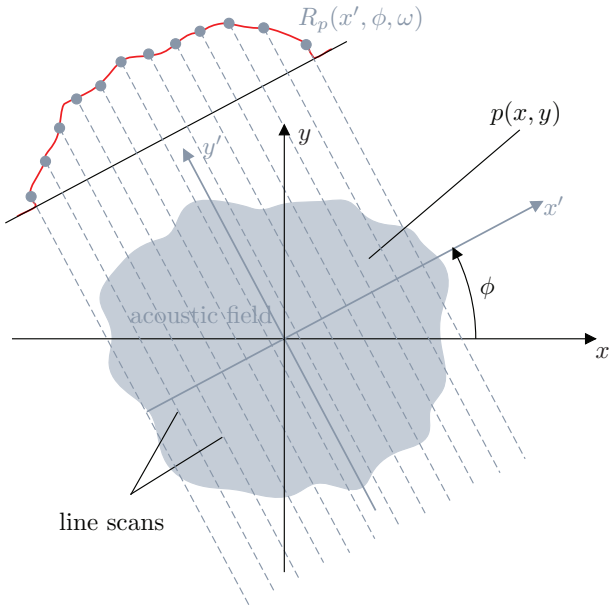

Fig. 1 – Diagram of the Radon transform of an acoustic field

integrating a function over straight lines. Nonetheless, the Radon transform also yields a spatial characterization of the sound field, in a way similar to the wavenumber domain.

Given a certain sound field in a plane $p(x, y)$, the tomographic measurement entails scanning the field in a series of projections. We consider here the scanning based on parallel projections over a series of angles ϕ from 0 to π, as shown in Fig. 1. This operation is expressed mathematically as the Radon transform of the sound field[9] (disregarding the time dependency),

$$R(x', \phi) = \int_{-\infty}^{\infty} p(x, y) dy', \tag{3}$$

which expresses the fact that the sound field $p(x, y)$ is integrated along a line y' (see Fig. 1). This (x', y') coordinate system used for the Radon transform is simply a rotated version of the original (x, y), as expressed by the rotation matrix

$$\begin{bmatrix} x' \\ y' \end{bmatrix} = \begin{bmatrix} \cos(\phi) & \sin(\phi) \\ -\sin(\phi) & \cos(\phi) \end{bmatrix} \cdot \begin{bmatrix} x \\ y \end{bmatrix}, \tag{4}$$

so that $R(x', \phi)$ corresponds to the values of the projections of the sound field along y' for each projection angle ϕ across the x' coordinate.

The well-known 'Fourier slice theorem' or 'projection-slice theorem' reveals the relation between the Radon and the wavenumber spectrum $P(k_x, k_y)$, where the Fourier transform of each of the projections corresponds to a diagonal in the wavenumber,

$$P(k_{x'}, \phi) = \int_{-\infty}^{\infty} R(x', \phi) e^{jk'_x x'} dx' = \int_{-\infty}^{\infty} \left(\int_{-\infty}^{\infty} p(x', y') dy' \right) e^{jk'_x x'} dx', \tag{5}$$

where use of Eq. (3) has been made. The resulting $P(k_{x'}, \phi)$ corresponds to a diagonal of the wavenumber spectrum, as illustrated in Fig. 2. This important relationship is well documented in the literature.[9]

In the present study we approach this relation from a somewhat different perspective. The spatial domain can be expressed in polar coordinates, $p(r, \theta) \equiv p(x, y)$, where $x = r\cos(\theta)$, $y = r\sin(\theta)$, so that the rotation coordinates become $x' = r\cos(\theta - \phi)$, $y' = r\sin(\theta - \phi)$. The Jacobian of the transformation yields $dxdy = dx'dy' = rdrd\theta$. Equation (5) can thus be expressed as

$$P(k_{x'}, \phi) = \int_0^{2\pi} \int_0^{\infty} p(r, \theta) e^{jk'_x r cos(\theta - \phi)} r dr d\theta. \tag{6}$$

Additionally, if the wavenumber domain is expressed in polar coordinates ($P(k_r, \phi_k) \equiv P(k_x, k_y)$), with

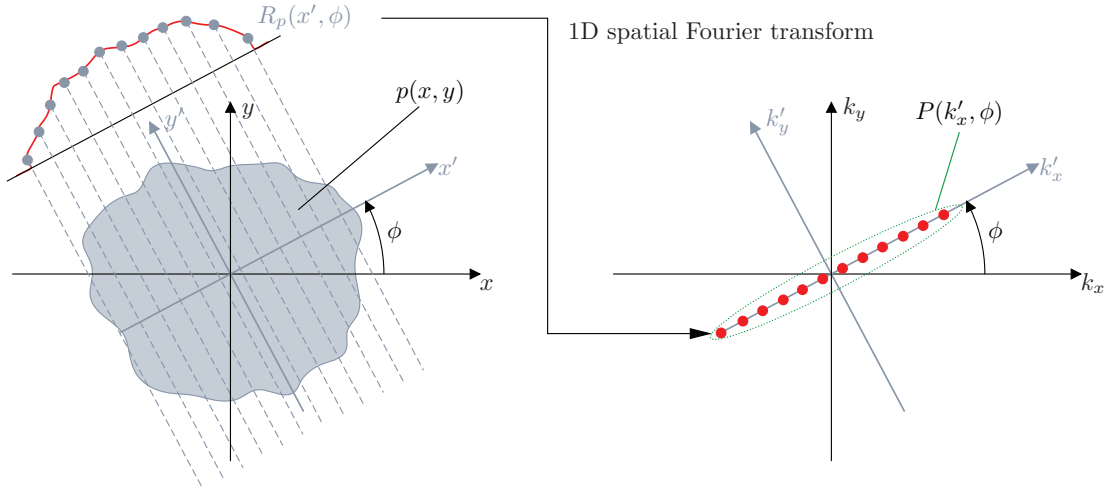

Fig. 2 – Sketch of the Fourier or projection-slice theorem

$k_x = k_r \cos(\phi_k)$ and $k_y = k_r \sin(\phi_k)$, the expression for the wavenumber transform becomes naturally

$$P(k_r, \phi_k) = \int\int_{-\infty}^{\infty} p(x, y) e^{j(k_x x + k_y y)} dx dy = \int_0^{2\pi} \int_0^{\infty} p(r, \theta) e^{j k_r r cos(\theta - \phi_k)} r dr d\theta. \tag{7}$$

This shows the relationship between the Radon and wavenumber domains. It is obvious from these last two equations (6-7) that the rotation angle in the Radon transform ϕ corresponds to the polar angle of the wavenumber domain ϕ_k. However, the projection angle ϕ will span from 0 to π, but when expressing it as ϕ_k (the Radon transform in polar coordinates) it spans from 0 to 2π ($\phi_k = \phi + (\pi/2)(\text{sgn}(k_{x'}) - 1)$). Similarly, $k_{x'}$ and k_r are related by $k_r = |k_{x'}|$, with $-\infty < k_{x'} < \infty$ and $0 \leq k_r < \infty$.

C. Holography from the Radon transform

The fundamental principle behind holographic methods is that the entire sound field can be reconstructed in three dimensions by accounting for the propagation of the sound waves from the measurement position to another. This can be done by operating in the wavenumber domain, which can be obtained by Fourier transforming the field explicitly via FFT's.[3,8] An alternative way of operating, is using an elementary wave expansion, which avoids explicit Fourier transforms, thus several of the shortcomings and errors related to the DFT or FFT are easily overcome.[11]

Given the sound field measured in a plane z_h, the wavenumber spectrum can be expressed as

$$P(k_{x'}, \phi, z_h) = \int_{-\infty}^{\infty} R(x', \phi, z_h) e^{j k_{x'} x'} dx', \tag{8}$$

where z_h denotes the measurement plane, and $P(k_{x'}, \phi, z_h) \equiv P(k_{x'}, \phi) e^{-j k_z z_h}$. The corresponding inverse transform is

$$R(x', \phi, z_h) = \frac{1}{2\pi} \int_{-\infty}^{\infty} P(k_{x'}, \phi, z_h) e^{-j k_{x'} x'} dk_{x'}, \tag{9}$$

which expresses the fact that the Radon domain in the plane z_h can be described by a plane wave expansion for each of the projection angles (although in this case we are considering infinitely many waves).

As anticipated in the previous section, the wavenumber spectrum obtained from the Radon transform via the projection slice theorem is equivalent to the wavenumber spectrum in polar coordinates $P(k_{x'}, \phi, z_h) \equiv P(k_r, \phi_k, z_h)$, with the difference that $P(k_{x'}, \phi, z_h)$ is not strictly in polar coordinates since $-\infty < k_{x'} < \infty$ and $0 \leq \phi \leq \pi$, whereas for $P(k_r, \phi_k, z_h)$ the coordinates satisfy $0 \leq k_r < \infty$ and $0 \leq \phi_k \leq 2\pi$. In the following we will express the wavenumber spectrum in these pseudo-polar coordinates as $P(k_{x'}, \phi, z_h)$.

In acoustic holography it is possible to extrapolate the acoustic field from one plane to another by propagating the waves present in the hologram plane z_h to the reconstruction plane z_s,[3,4]

$$P(k_{x'}, \phi_k, z_s) = P(k_{x'}, \phi_k, z_h) \cdot e^{-j k_z (z_s - z_h)}, \tag{10}$$

where

$$k_z = \begin{cases} \sqrt{k^2 - k_{x'}^2} & \text{if } k \geq |k_{x'}| \\ j\sqrt{k^2 - k_{x'}^2} & \text{if } k < |k_{x'}|, \end{cases} \tag{11}$$

indicates the propagating or evanescent waves in the z direction. It follows that after calculating the wavenumber spectrum from the Radon transform, it is possible to reconstruct or predict the sound field in a different plane than measured, $z = z_s$ as

$$p(r, \theta, z_s) = \frac{1}{(2\pi)^2} \int_0^{\pi} \int_{-\infty}^{\infty} P(k_{x'}, \phi, z_h) e^{-jk_{x'}x' cos(\theta-\phi)+jk_z(z_h-z_s)} k_{x'} dk_{x'} d\phi. \tag{12}$$

Making use of Euler's equation of motion (conservation of momentum), the particle velocity vector can be calculated, e.g. z-component, as

$$u_z(r, \theta, z_s) = \frac{-1}{j\omega\rho} \frac{\partial p}{\partial z} = \frac{1}{(2\pi)^2} \int_0^{\pi} \int_{-\infty}^{\infty} \frac{k_z}{\rho c k} P(k_{x'}, \phi, z_h) e^{-jk_{x'}x' cos(\theta-\phi)+jk_z(z_h-z_s)} k_{x'} dk_{x'} d\phi, \tag{13}$$

where ρ is the density of the medium and k is the wavenumber in air. It follows that it is possible to calculate the sound intensity vector too from Eqs. (12) and (13).

Finally, making use of Eqs. (8) and (12), the reconstructed sound pressure can be expressed by

$$p(r, \theta, z_s) = \frac{1}{(2\pi)^2} \int_0^{\pi} \int_{-\infty}^{\infty} \left(\int_{-\infty}^{\infty} R(x', \phi, z_h) e^{-jk_{x'}x'} dx' \right) e^{-jk_{x'}x' cos(\theta-\phi)+jk_z(z_h-z_s)} k_{x'} dk_{x'} d\phi. \tag{14}$$

D. Discrete implementation

So far, we have considered an ideal continuous case. In practice, we implement Eq. (9) based on a discrete number of N plane waves,

$$R(r, \phi_m) = \sum_{n=1}^{N} B_{nm} \varphi_n = \sum_{n=1}^{N} B_{nm} e^{-j(k_{x'n}x' + k_{zn}z_h)}, \tag{15}$$

which shows the useful property that the transformation of each projection angle ϕ_m depends on the n waves traveling in that direction only, as follows from the projection-slice theorem. This equation can be expressed in matrix form as

$$\mathbf{r} = \mathbf{A}\mathbf{b}, \tag{16}$$

where $\mathbf{r}$ is a vector containing the measured Radon transform, $\mathbf{b}$ a vector with the corresponding coefficients (i.e., the coefficients of the wavenumber spectrum), and $\mathbf{A}$ is a matrix containing the elementary wave functions φ in the measurement plane z_h, which are $\varphi = e^{-j(k_{x'}x' + k_z z_h)}$. The pressure in the reconstruction plane can be expressed as

$$\mathbf{p}_s = \mathbf{A}_s \mathbf{b}, \tag{17}$$

where the matrix $\mathbf{A}_s$ contains the elementary waves in the reconstruction plane z_s. In this case, the reconstruction matrix projects the field from the wavenumber domain into space domain, so the elementary functions depend both on r and θ,

$$\varphi_s = e^{-j(k_{x'}x' \cos(\theta-\phi) + k_z z_s)}, \tag{18}$$

Equation (16) can be inverted to solve for the coefficients of the expansion in a least squares sense. It should be noted that the pseudo-inversion must be regularized,[12] since the back-propagation towards a sound source is an inverse ill-posed problem (due to the presence of decaying evanescent waves),

$$\mathbf{b} = (\mathbf{A}^H \mathbf{A} + \lambda \mathbf{I})^{-1} \mathbf{A}^H \mathbf{r}, \tag{19}$$

where λ is the regularization parameter (in this expression using Tikhonov regularization) and the superscript H denotes the Hermitian transpose. Making use of this equation and Eq. (17), the reconstructed pressure in the prediction plane can finally be expressed as

$$\mathbf{p}_s = \mathbf{A}_s (\mathbf{A}^H \mathbf{A} + \lambda \mathbf{I})^{-1} \mathbf{A}^H \mathbf{r}, \tag{20}$$

where it becomes apparent that the measured Radon transform can be used to project directly the sound pressure into a different plane than measured. Equation (20) can be understood as a transfer function between the measured Radon transform and the predicted reconstructed pressure, where the transfer matrix $\mathbf{H} = \mathbf{A}_s(\mathbf{A}^H\mathbf{A} + \lambda\mathbf{I})^{-1}\mathbf{A}^H$ accounts for the propagation of the sound waves from the measured to the reconstruction plane and from Radon to space domain.

Similarly, as in Eq. (13), the particle velocity can be calculated by using a reconstruction matrix $\mathbf{D}_s$ with the derivative of the elementary wave functions with respect to the corresponding component,

$$\mathbf{u}_{zs} = \mathbf{D}_{zs}(\mathbf{A}^H\mathbf{A} + \lambda\mathbf{I})^{-1}\mathbf{A}^H\mathbf{r}. \tag{21}$$

The elementary wave functions in the reconstruction matrix $\mathbf{D}_{zs}$ are

$$\frac{-1}{j\omega\rho}\frac{\partial\varphi_s}{\partial z} = \frac{k_z}{\rho ck}e^{-j(k_{x'}x'cos(\theta-\phi)+k_z z_h)}. \tag{22}$$

The matrices in Eqs. (20) and (21) can be based on a continuous wavenumber spectrum, by using infinitely many waves expressed as an integral in the wavenumber domain. In this way the wraparound error is solved completely, since there are no replicated apertures in space domain. This is analogous to the approach suggested by Hald for statistically optimized near-field acoustic holography (SONAH).[10]

Additionally, it is possible to pose the problem in a least norm sense, which is computationally more efficient since the characteristic dimensions of the matrices in the inversion will be smaller (there will typically be more elementary waves in the expansion than measurement positions).[10] However, due to the projection-slice theorem, it is worth noting that the inversion of the elementary wave matrix can be done separately for each of the projection angles, as it follows from Eq. (15). This makes it computationally efficient, and many waves can be used in the expansion without any drastic influence in the computational cost.

3. NUMERICAL RESULTS

A numerical study was carried out to examine the elementary wave method proposed in this paper. A simple monopole source was used to simulate the measurements from which the Radon transform is obtained (as described in section 2.A). The sound pressure radiated by the monopole was scanned over an aperture of 95 cm, over 37 positions with an inter-spacing of approximately 2.5 cm between parallel lines. The number of projection angles was also 37, thus with a resolution of about 5^o. The measurement plane was $z_h = 5$ cm and the reconstruction one $z_s = 3$ cm. Tikhonov regularization was used for the reconstruction and the regularization parameter was chosen with the generalized cross-validation method.[13] Measurement noise of 35 dB signal-to-noise ratio (SNR) was added to the simulated measurements.

Figure 3 shows the simulated measurement of the Radon transform of the sound pressure radiated by the monopole. It is apparent that the transform is identical for every projection angle, since the sound field is rotationally symmetrical, thus the monopole is always at $x' = 0$.

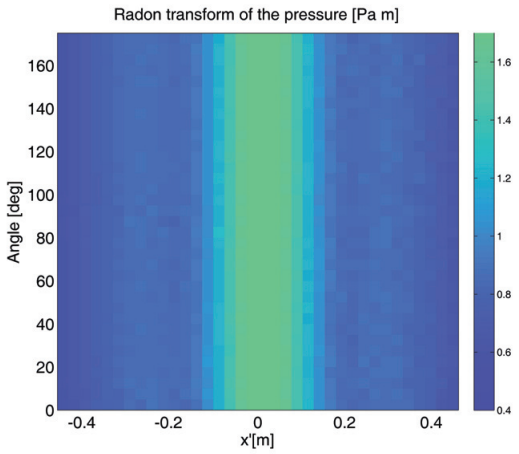

Fig. 3 – Radon transform of the sound field radiated by a monopole; Measurement plane $z_h = 5$ cm, 2000 Hz.

The reconstructed sound pressure field is shown in Fig. 4. It should be noted that the values outside a radius of 47.5 cm are just padded values, because they are out of the reconstruction area. Figure 4 (right)

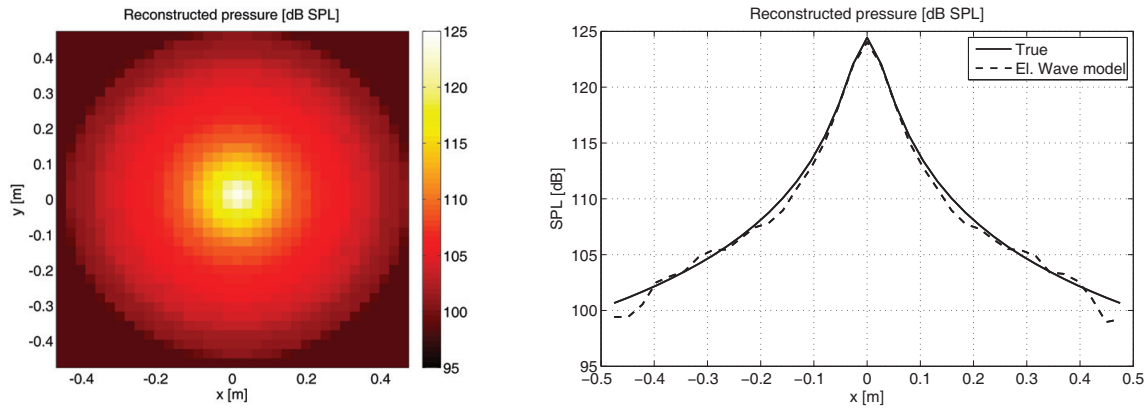

Fig. 4 – Reconstruction of the sound pressure radiated by a monopole based on the proposed elementary wave model (numerical). Measurement plane $z_h = 5$ cm, reconstruction plane $z_s = 3$ cm, 2000 Hz; Surface plot of the magnitude (left); Comparison with the true theoretical pressure (right).

shows the reconstructed pressure compared to the theoretical true pressure radiated by the monopole along a straight line in the x axis. The method recovers the sound pressure satisfactorily, with an overall error below 10% (spatially averaged over the aperture). It is of particular interest to verify that the reconstruction towards the end of the aperture is accurate, tending to follow the value of the true pressure, without a drastic influence of the finite aperture. Figure 5 compares the reconstruction of the sound pressure from the elementary wave

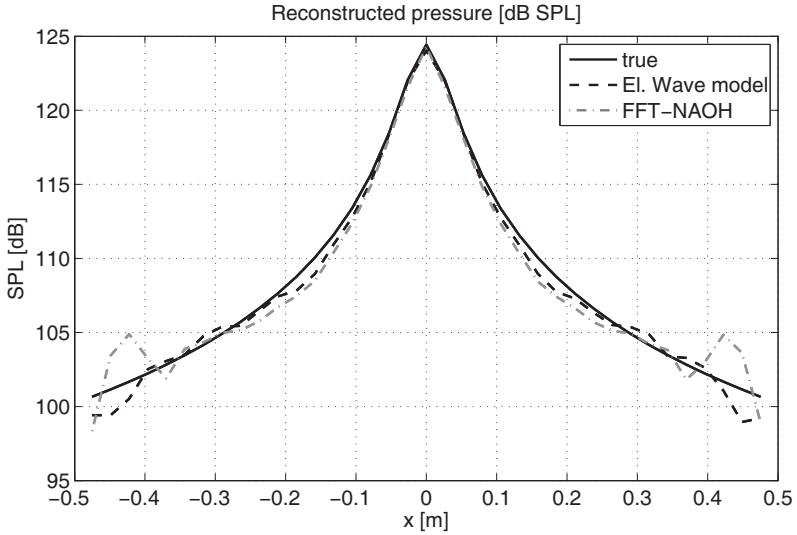

Fig. 5 – Comparison of the reconstructions of the pressure by a monopole obtained with the proposed elementary wave expansion and the FFT based reconstruction.[8] Measurement plane $z_h = 5$ cm, reconstruction plane $z_s = 3$ cm, 2000 Hz.

model proposed in this paper with the method based on FFT processing proposed in Ref. 8. As expected, the reconstruction based on the elementary wave model is more accurate, in particular towards the edges of the aperture where the FFT processing is notably affected by the errors related to the finite aperture. The spatially averaged error is of 28 % for the FFT method, whereas of just 10 % for the method proposed in this paper.

4. EXPERIMENTAL RESULTS

A simple experimental study was conducted to test the proposed method. The measurements were carried out in the anechoic chamber at the Technical University of Denmark, DTU. The sound pressure radiated by a closed box loudspeaker was scanned using a Polytec laser Doppler vibrometer and an automatic scanning robot. The loudspeaker was displaced 10 cm from the center of the aperture, at $(x, y, z) = (0, 0.1, 0)$ m, and was measured over an aperture of 90 cm with 37 parallel lines, over 37 projection angles. The

measurement plane was $z_h = 3$ cm and the reconstruction took place at $z_s = 2$ cm. A pure tone of 2400 Hz was used for the measurements, that were synchronized and performed sequentially over each position. See Fig. 6 (only one loudspeaker was excited).

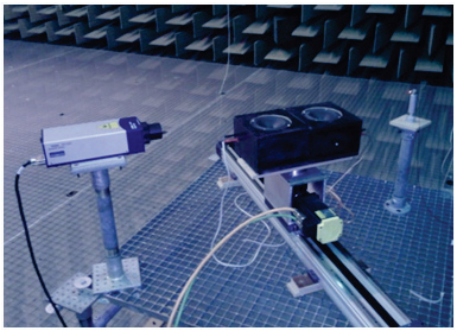

Fig. 6 – Measurement set-up. Only the loudspeaker to the left side of the picture was driven.

The obtained results are shown in Fig. 7. The left of the figure shows the measured Radon transform, where the fact that the loudspeaker is displaced from the center of the aperture can be noticed from the curvature in the magnitude of the plot. This is because depending on the projection angle, the loudspeaker appeared between $x' = 0$ and $x' = 10$ cm.

Figure 7 (right) shows the reconstructed sound pressure, where the position of the loudspeaker can be clearly noticed, coinciding with the maximum pressure lvels. Again, the values beyond a radius of 0.45 cm are outside of the aperture, and have just been padded to a constant value in the figure, although they do not belong to the actual reconstruction. The reconstructed pressure behaves as expected, with maximum pressure about $(0, 0.1, 0)$ m, and decaying away towards the edges of the aperture. There is some effects of scattering due to the set-up and the presence of an adjacent loudspeaker box. All in all, the results prove that the method is successful at recovering the measured sound field, and that the measured Radon transform can be used to directly reconstruct the pressure in the prediction plane satisfactorily.

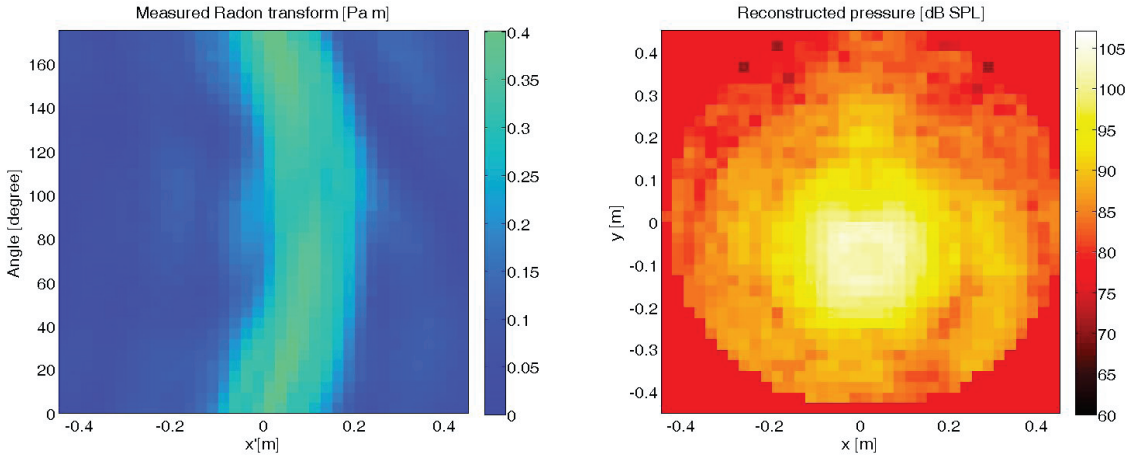

Fig. 7 – Measured Radon transform of the sound field radiated by the loudspeaker at $(x, y, z) = (0, 0.1, 0)$ m (left); Reconstructed sound pressure (right). Measurement plane $z_h = 3$ cm, reconstruction plane $z_s = 2$ cm, 2400 Hz.

5. DISCUSSION AND FUTURE WORK

The results from this study show that the proposed method can accurately reconstruct the measured sound field, even close to the edges of the aperture, where truncation could potentially be a problem. It can be considered as a 'patch method', meaning that an accurate reconstruction can be achieved even if the measurement aperture is smaller than the extent of the source or the sound field radiated by it. Contrarily, conventional DFT or FFT-based methods suffer significantly from the errors associated to the finite measurement aperture, namely the replicated apertures that give rise to wrap-around error, and finite aperture

errors. When using conventional FFT processing, zero-padding and windowing can be used to mitigate these sources of error, but at the expense of discarding useful data. It could be possible to extend artificially the measured field outside from the aperture for a better accuracy, as done in Ref. 14. This is however at the cost of increased computational complexity.

The elementary waves used in the present study are planar, which seems like the natural choice given that the measurement procedure relies on scanning the field over straight lines with a laser beam. Other approaches that make it possible to reconstruct the field over an arbitrary surface will be examined. It should be mentioned however, that due to the measurement over straight beams, conformal measurements could be challenging, and may imply large propagation distances to reconstruct the field on an arbitrary surface. This is currently ongoing work. Additionally, the reconstruction of sound fields from more realistic sources will be examined in the future, since the sound fields examined in this study are significantly simpler than the ones typically found in sound source identification problems.

6. CONCLUSIONS

In this study, a method to attain a holographic reconstruction based on the Radon transform of an acoustic field measured with the acousto-optic effect has been proposed. The method is based on an elementary plane wave expansion that makes it possible to project the Radon transform from one plane to another and directly into space domain. The method solves the problem in a least squares sense (or least norm), and thus some of the limitations related to the Fourier transform are avoided (mostly wraparound and finite aperture errors). The relation between the Radon and the wavenumber domains has been examined, and the ideal continuous case explained. A discrete implementation of the method has been introduced, from which it is possible to directly account for the propagation of the field from one plane to another and from the Radon into space domain. Both the numerical and experimental investigations show promising results that verify the enhanced accuracy of the proposed holographic reconstruction.

ACKNOWLEDGMENTS

This work was partly supported by a post-doctoral grant from the Danish Council for Independent Research (DFF) #12-126364/FTP.

REFERENCES

[1] J. Hald, *Handbook of Signal Processing in Acoustics, Ch. 9* (Springer) (2008).

[2] E. G. Williams and J. D. Maynard, "Holographic Imaging without the Wavelength Resolution Limit", Phys. Rev. Lett. **45**, 554–557 (1980).

[3] J. D. Maynard, E. G. Williams, and Y. Lee, "Nearfield acoustic holography I: Theory of generalized holography and the development of NAH", J. Acoust. Soc. Am **78(4)**, 1395–1413 (1985).

[4] E. G. Williams, *Fourier Acoustics - sound Radiation and Nearfield acoustic Holography* (Academic Press, San Diego) (1999).

[5] T. Sakoda and Y. Sonoda, "Visualization of sound field with uniform phase distribution using laser beam microphone coupled with computerized tomography method", Acoustical Science and Technology **29**, 295–299 (2008).

[6] Y. Oikawa, T. Hasegawa, Y. Ouchi, Y. Yamasaki, and Y. Ikeda, "Visualization of sound field and sound source vibration using laser measurement method", in *Proceedings of 20th International Congress on Acoustics* (2010).

[7] A. Torras-Rosell, S. Barrera-Figueroa, and F. Jacobsen, "Sound field reconstruction using acousto-optic tomography", . Acoust. Soc. of Am. **131(5)**, 3786–3793 (2012).

[8] A. Torras-Rosell, E. Fernandez-Grande, S. Barrera-Figueroa, and F. Jacobsen, "Investigating the use of the acousto-optic effect for acoustic holography", Proc. 41st International Congress and Exposition on Noise Control Engineering, New York (2012).

[9] A. C. Kak and M. Slaney, *Principles of Computerized Tomographic Imaging* (IEEE PRess, New york) (1988).

[10] J. Hald, "Basic theory and properties of statistically optimized near-field acoustical holography", J. Acoust. Soc. Am **125(4)**, 2105–2120 (2009).

[11] R. Steiner and J. Hald, "Near-field Acoustical Holography Without the Errors and Limitations Caused by the Use of Spatial DFT", International Journal of Acoustics and Vibration **6** (2001).

[12] P. C. Hansen, "Analysis of discrete ill-posed problems by means of the L-curve", society for Industrial Applied Mathematics **34**, 561–580 (1992).

[13] P. C. Hansen, *Rank-deficient and discrete ill-posed problems: numerical aspects of linear inversion* (SIAM) (1997).

[14] E. G. Williams, "Continuation of acoustic near-fields", J. Acoust. Soc. Am **113(3)**, 1273–1281 (2003).

Paper F

An acousto-optic beamformer[a)]

Antoni Torras-Rosell[b)] and Salvador Barrera-Figueroa
Danish Fundamental Metrology A/S, Matematiktorvet 307, 2800 Kgs. Lyngby, Denmark

Finn Jacobsen
Acoustic Technology, Department of Electrical Engineering, Technical University of Denmark, Ørsteds Plads 352, 2800 Kgs. Lyngby, Denmark

(Received 15 December 2011; revised 9 May 2012; accepted 15 May 2012)

There is a great variety of beamforming techniques that can be used for localization of sound sources. The differences among them usually lie in the array layout or in the specific signal processing algorithm used to compute the beamforming output. Any beamforming system consists of a finite number of transducers, which makes beamforming methods vulnerable to spatial aliasing above a certain frequency. The present work uses the acousto-optic effect, i.e., the interaction between sound and light, to localize sound sources in a plane. The use of a beam of light as the sensing element is equivalent to a continuous line aperture with an infinite number of microphones. This makes the proposed acousto-optic beamformer immune to spatial aliasing. This unique feature is illustrated by means of simulations and experimental results within the entire audible frequency range. For ease of comparison, the study is supplemented with measurements carried out with a line array of microphones. © *2012 Acoustical Society of America*. [http://dx.doi.org/10.1121/1.4726047]

PACS number(s): 43.35.Sx, 43.60.Fg [HCS] Pages: 144–149

I. INTRODUCTION

The information provided by a single transducer such as a microphone is often enough to characterize the acoustical properties of that point of the medium where the transducer is placed. However, the direction of propagation of sound cannot be determined from measurement with a single microphone. This problem is overcome by using several transducers placed at different positions that measure the sound field simultaneously, that is, using an array of sensors. The correlation between the signals captured by the array can be processed with beamforming techniques in order to determine the position of sound sources. The resolution of the beamformer (width of the main lobe) and the strength of the side lobes (ghost sources) strongly depend on the number of sensors and the geometry of the array.[1,2] The minimization of side lobe levels by optimizing the sensor positions and weightings has been extensively investigated.[3–5] Alternatively, adaptive beamforming techniques render highly selective spatial filtering based on iterative algorithms.[1,2,6,7] The specific distribution of the sensors as well as the beamforming technique used to detect the source can also be designed to take advantage of the decomposition of the sound field into a set of orthogonal functions, and of the scattering effects caused by the object where the microphones are embedded, e.g., a sphere or a cylinder.[8–11]

In any case, there is an inherent difficulty that is always present when using arrays of transducers: spatial aliasing. The operating frequency range of a beamformer is bounded by the finite number of sensors that, in practice, can be used to collect the input data. The present work proposes a measurement method based on the acousto-optic effect that is immune to spatial aliasing. In what follows, the theoretical principles of this measurement principle are described and compared to conventional delay and sum beamforming (DSB). The validity of the theory is assessed by means of computer simulations and experimental results that cover the entire audible frequency range.

II. BEAMFORMING AND SPATIAL FILTERING

The localization of sound sources in the far field is usually based on the assumption that the waves impinging on the sensor array can be regarded as plane waves. This hypothesis makes it possible to localize sound by simply analyzing the phase mismatch between the signals measured with a microphone array. The following definition of classical DSB clearly exploits this feature:

$$b_{\mathrm{DS}}(\theta) = \left| \sum_{m=0}^{M-1} w_m \tilde{p}_m p_m^*(\theta) \right|^2, \tag{1}$$

where w_m is the weighting coefficient of the mth microphone, M is the total number of microphones, $\tilde{p}_m$ is the temporal Fourier transform of the sound pressure measured at the mth microphone, and $p_m^*(\theta)$ represents the theoretical complex conjugated pressure of a plane wave impinging on the mth microphone from a certain direction θ. It is easy to see that the output of the beamformer assumes a maximum when the phases of the measured signals are aligned with the ones of the theoretical plane wave, that is, when the phase of $p_m^*(\theta)$ compensates for the propagation delays caused by the layout of the microphone array.

Figure 1 shows a plane wave $P_0 e^{j(\omega t - \vec{k}\cdot\vec{r})}$ impinging on a line array positioned along the x-direction. According to the

[a)]Portions of this work were presented in "A beamforming system based on the acousto-optic effect," Proceedings of Euronoise 2012, Prague, Czech Republic, June 2012.

[b)]Author to whom correspondence should be addressed. Electronic mail: atr@dfm.dtu.dk

 0001-4966/2012/132(1)/144/6/$30.00

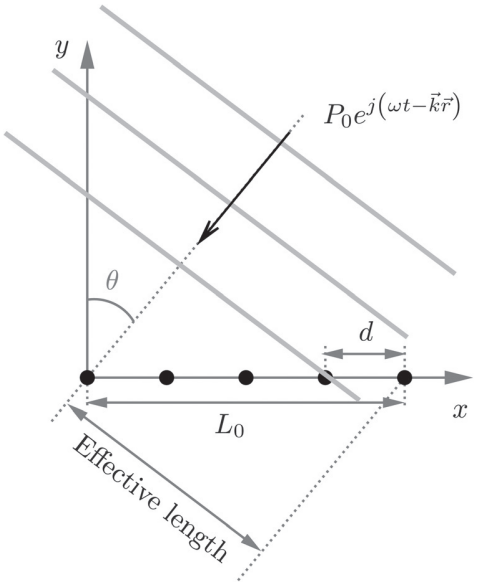

FIG. 1. Sketch of a plane wave impinging on a line array of microphones.

coordinate system depicted in Fig. 1, the output of the beamformer stated in Eq. (1) corresponds to the following expression:[2]

$$b_{\mathrm{DS}}(\theta) = \left| \frac{\tilde{P}_0}{M} \frac{\sin\left(k(\sin\tilde{\theta} - \sin\theta)Md/2\right)}{\sin\left(k(\sin\tilde{\theta} - \sin\theta)d/2\right)} \right|^2, \tag{2}$$

where $\tilde{P}_0$ and $\tilde{\theta}$ correspond to the amplitude and the incident direction, respectively, of the sound measured at the microphone positions, whereas θ represents the incident direction of the theoretical plane wave. In this result, it is assumed that all microphones are equally important ($w_m = 1/M$) and that the amplitude of the theoretical complex conjugated pressure $p_m^*(\theta)$ equals unity. Three examples of beamforming patterns obtained using Eq. (2) are shown in Fig. 2 for a line array of 19 microphones and three different source positions.

As can be seen in Figs. 2(a) and 2(b), there are two main lobes in the directivity pattern because the line array cannot distinguish between the real source and its corresponding image source. These main lobes are overlapped in Fig. 2(c). Besides, it is worth noting that the main lobe becomes wider as the incident sound approaches grazing incidence. This means that sound sources placed in front of the line array are easier to discriminate than lateral sources. This is a consequence of the shortening of the effective length of the line array when steering it electronically toward the sides (see the sketch shown in Fig. 1).

From another point of view, when the frequency range under analysis is high enough to obtain a beamforming pattern that is not omnidirectional, a line array can also be seen as spatial filter rather than a beamformer. For instance, when no electronic delays are applied to the measured pressures ($\theta = 0$), the output of the beamformer stated in Eq. (2) is simply the sum of the microphone signals

$$b_{DS}(0) = \left| \frac{\tilde{P}_0}{M} \frac{\sin\left(k(d/2)M\sin\tilde{\theta}\right)}{\sin\left(k(d/2)\sin\tilde{\theta}\right)} \right|^2. \tag{3}$$

This expression yields a spatial selectivity that equals the beamforming pattern depicted in Fig. 2(a), which indeed attenuates sound waves coming from an oblique direction significantly.

III. SPATIAL ALIASING

Spatial aliasing arises from the fact that beamforming techniques base their calculations on a finite number of input signals that correspond to certain positions in the acoustic field under investigation. Although the Nyquist sampling theorem states that no aliasing effects arise when the spacing between transducers is less than half the wavelength of the sound under study, the trade-off limits the operational frequency range of any given transducer array. Figure 3 illustrates the effects of spatial aliasing for a line array of 19 microphones with a spacing of 3.75 cm. The beamforming

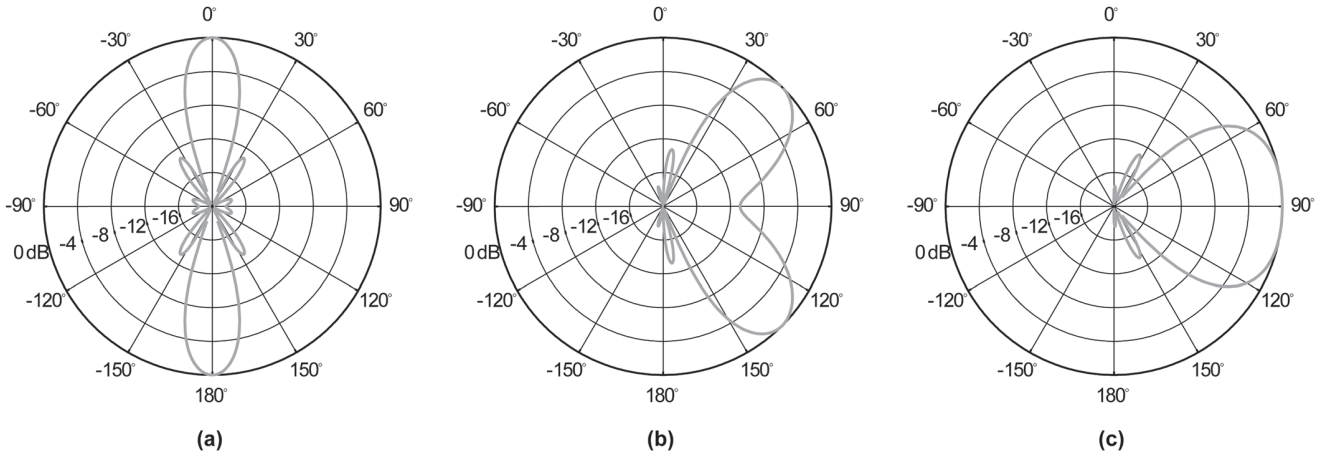

FIG. 2. Beamforming patterns of a line array of 19 microphones at 1.25 kHz. The sound source is located at (a) 0°, (b) 45°, and (c) 90°. The spacing between the microphones is 3.75 cm.

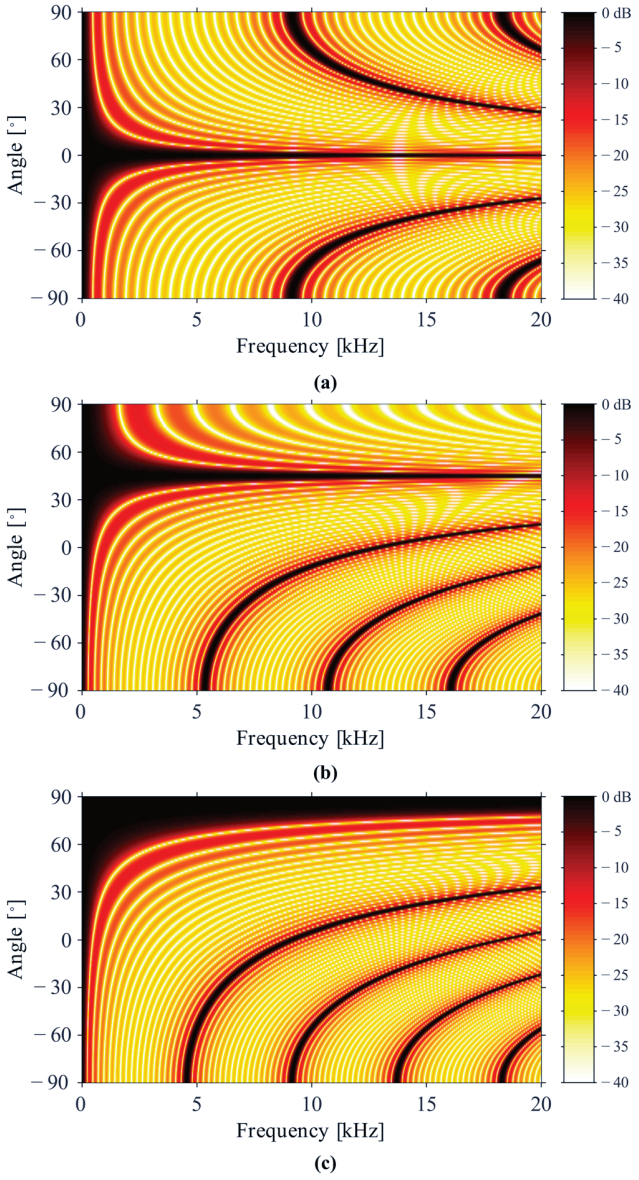

FIG. 3. (Color online) Beamforming patterns of a line array of 19 microphones as a function of frequency. The sound source is located at (a) 0°, (b) 45°, and (c) 90°. The spacing between the microphones is 3.75 cm.

maps are limited to $-90° \leq \theta \leq 90°$ because the line array provides symmetric patterns outside this interval of looking directions. As can be seen, spatial aliasing artifacts appear at lower frequencies when the source is located toward the sides [above 9 kHz in Fig. 3(a), above 5.5 kHz in Fig. 3(b), and above 4.5 kHz in Fig. 3(c)]. However, no aliasing effects can be seen below the Nyquist frequency, which for this line array is approximately 4.5 kHz.

Similar to Fig. 2(a), the beampattern shown in Fig. 3(a) can also be interpreted as the spatial selectivity obtained when no delay is applied to the input signals, that is, when the output of the beamformer is simply the sum of the microphone signals. Mathematically speaking, the aliasing effect is just a consequence of adding up a finite number of sound pressures. In theory, this problem could be prevented if the discrete summation of pressures was substituted by the continuous integral of sound pressures along the line defined by the array

$$\begin{aligned} b_{\mathrm{DS}}(0) &= \left|\frac{1}{L_0}\int_{\mathbf{L}} P(x,y,\omega)\,\mathrm{d}l\right|^2 \\ &= \left|\frac{1}{L_0}\int_0^{L_0} \tilde{P}_0 e^{j(\omega t-\vec{k}\cdot\vec{r})}\,\mathrm{d}x\right|^2 \\ &= \left|\frac{\tilde{P}_0 e^{j\omega t}}{L_0}\int_0^{L_0} e^{jk\sin\tilde{\theta}x}\,\mathrm{d}x\right|^2 \\ &= \left|\tilde{P}_0\,\mathrm{sinc}(k(L_0/2)\sin\tilde{\theta})\right|^2, \end{aligned} \tag{4}$$

where $P(x,y,\omega)$ is the temporal Fourier transform of the sound pressure along the line of integration $\mathbf{L}$, and L_0 is the corresponding total length of the array. The immunity to spatial aliasing of this result can be seen in Fig. 4 [cf. Fig. 3(a)]. This mathematical solution would of course imply an infinite number of transducers, which is not feasible in practice. However, recent studies have proved that this integral can actually be measured with a completely different measurement principle that is based on the interaction between sound and light, namely, the acousto-optic effect.[12]

IV. ACOUSTO-OPTIC BEAMFORMER

Waves travel differently depending on the medium of propagation. For instance, electromagnetic waves travel slower in dense media and faster otherwise (vacuum represents the extreme case). The phenomenon of sound in air inherently involves pressure fluctuations that at the same time cause density changes. These density variations also alter the refractive index of the medium, which in turn influences the propagation of light.[13,14] This physical phenomenon is known as the acousto-optic effect and it has been widely investigated with ultrasonic waves.[15–21] In air and within the audible frequency range, the acousto-optic effect mainly affects the speed of light, whereas diffraction effects can be disregarded. Particularly, it can be shown that the phase of a beam of light that travels through an acoustic field is proportional to the integral of the pressure distribution $p(x,y,t)$ of the acoustic field,[12]

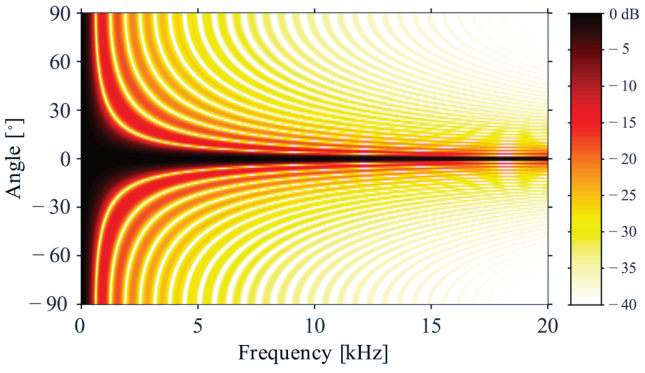

FIG. 4. (Color online) Beamforming pattern free of aliasing effects obtained with a continuous integration of the sound pressure along a 54 cm long straight line.

$$\phi = k_0 n_0 \left(L_0 + \frac{n_0 - 1}{\gamma p_0 n_0} \int_{\mathbf{L}} p(x, y, t) \mathrm{d}l \right), \tag{5}$$

where k_0 is the wave number of light in vacuum, n_0 and p_0 are the refractive index and the atmospheric pressure under static conditions, and γ is the ratio of specific heats. In this equation, L_0 denotes the length of the beam of light.

The time derivative of the phase of a beam of light can be measured accurately using interferometric techniques, and in particular, using a laser Doppler vibrometer (LDV). The velocities retrieved with an LDV conventionally correspond to changes of the phase of light that are caused by mechanical vibrations of a surface ($\mathrm{d}L_0(t)/\mathrm{d}t$). However, when the laser beam travels through an acoustic field and the reflecting point where the laser is pointed is designed so as to minimize any mechanical vibration ($\mathrm{d}L_0(t)/\mathrm{d}t \approx 0$), the output of the LDV corresponds to an apparent velocity that is actually caused by the acousto-optic effect[12]

$$v(t) = \frac{n_0 - 1}{\gamma p_0 n_0} \frac{\mathrm{d}}{\mathrm{d}t} \left(\int_{\mathbf{L}} p(x, y, t) \mathrm{d}l \right). \tag{6}$$

This unconventional use of the LDV is illustrated in Fig. 5 for the present study case, that is, when the sound source is located in the far field.

By combining Eq. (4) and the Fourier transform of Eq. (6),

$$V(\omega) = j\omega \frac{n_0 - 1}{\gamma p_0 n_0} \left(\int_{\mathbf{L}} P(x, y, \omega) \mathrm{d}l \right), \tag{7}$$

it is possible to define the following beamforming output based on the apparent velocity of the LDV that is caused by the acousto-optic effect:

$$b_{\mathrm{AO}} = b_{\mathrm{DS}}(0) = \left| \frac{1}{L_0} \frac{\gamma p_0 n_0}{n_0 - 1} \frac{V(\omega)}{j\omega} \right|^2. \tag{8}$$

Note that b_{AO} is independent of θ; that is, the presented acousto-optic beamformer cannot change the looking direction electronically. Instead, one has to steer the laser beam physically toward the angular positions that are to be investigated.

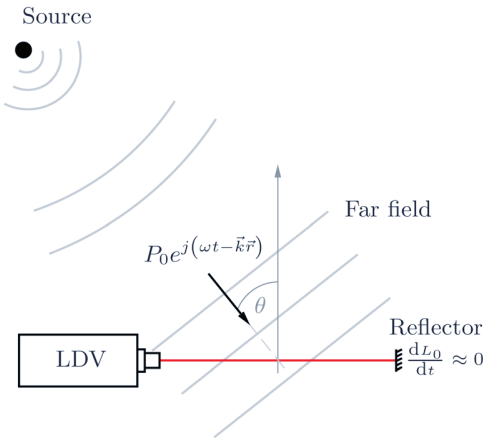

FIG. 5. (Color online) Sketch of the measurement scenario that makes it possible to measure the acousto-optic effect with an LDV.

V. EXPERIMENTAL SETUP AND MEASUREMENT RESULTS

A. Acousto-optic beamforming

The presented theory is based on the assumption that the sound waves used to localize the acoustic source are planar. In order to comply with this requirement, the measurements were carried out in a fully anechoic room of about 1000 m^3, with a loudspeaker Type BM6 (Dynaudio, Skanderborg, Denmark) located 5 m away from the beamforming system. A picture of the experimental setup is shown in Fig. 6.

The acousto-optic beamformer consisted of a beam of light generated by an LDV Type OFV-505 (Polytec, Waldbronn, Germany). The light propagated a distance of 54 cm and then it was reflected back to the LDV. An accelerometer Type 4344 (Brüel & Kjær, Nærum, Denmark) was mounted on the reflecting point to ensure that mechanical vibrations from the structure were not influencing the velocity measured with the LDV. An example of this monitoring procedure is illustrated in Fig. 7. The output of the accelerometer showed that the measurement setup was fairly immune to mechanical vibrations generated by sound waves impinging on the beamformer above approximately 2 kHz. A pocket signal generator NTI Type Minirator MR1 (NTI, Schaan, Liechtenstein) was used to synthesize white noise with energy from 0 Hz up to 20 kHz. The equipment shown in Fig. 6 was covered with as much absorbing material as possible in order to reduce the scattering effects at high frequencies. The entire structure sustaining the beamforming system was installed on a turntable allowing the acousto-optic beamformer to rotate in steps of 1°. All signals were captured with a B&K Pulse analyzer. No efforts were made to compensate for the coloration of the excitation signal induced by the loudspeaker's transfer function. Instead, the beamforming pattern was normalized to its maximum at each frequency component. The beamforming pattern

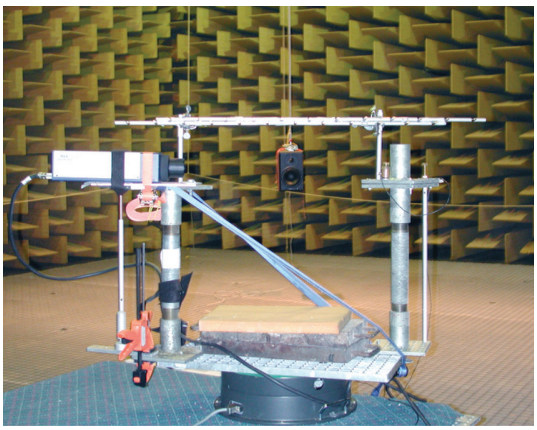

FIG. 6. (Color online) Experimental setup. The LDV is located on the left hand side of the structure. The accelerometer is mounted on the right hand side aligned with the laser beam emitted by the LDV. The loudspeaker is at the center of the picture, but at a distance of 5 m from the beamforming system. The line array located on top of the acousto-optic beamformer was installed afterward to perform measurements with conventional DSB.

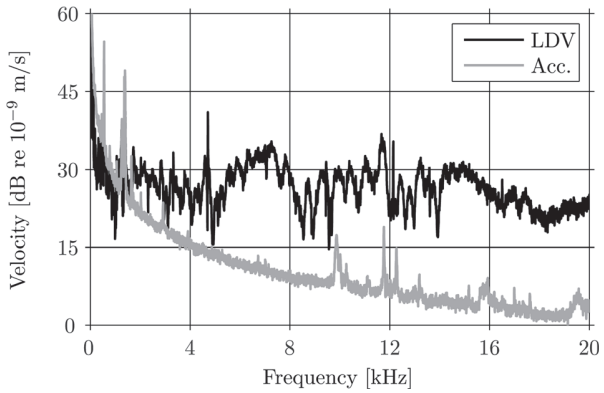

FIG. 7. An example of the velocity measured with the LDV vs the velocity of the accelerometer. The mechanical vibrations measured with the accelerometer are significantly weaker than the velocity output of the LDV above approximately 2 kHz.

resulting from using Eq. (8) together with the mentioned normalization criterion is depicted in Fig. 8. As can be seen, the main lobe can be clearly identified at 0°, and as predicted, there is no trace of spatial aliasing in the entire audible frequency range. As expected, the beampattern becomes broader at low frequencies. However, the artifacts observed below 2 kHz are caused by the background noise of the LDV and the mechanical vibrations of the structure (see also Fig. 7). The side lobes of the beamforming pattern can be recognized to some extent, although they do not appear as clear as in the theoretical results presented in Fig. 4. A reason for this is that the simulation results depicted in Fig. 4 do not take account of the influence of noise or other possible sources of error such as mechanical vibrations and scattering of the experimental setup.

B. Conventional microphone beamforming

Two line arrays of nine and ten microphones (1/4 in. B&K Type 4957) with a spacing of 7.5 cm were superimposed to form a global line array of 19 microphones with a spacing of 3.75 cm; see Fig. 6. The signals captured by the microphones were processed as described in Eq. (1). Figure 9 shows the beamforming patterns corresponding to three different positions of the loudspeaker (0°, 45°, and 90°). The beamforming patterns measured with the microphone array

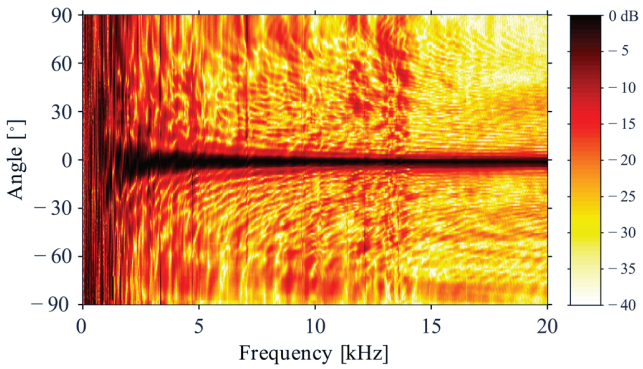

FIG. 8. (Color online) Beamforming pattern measured with the LDV. No spatial aliasing effects can be seen along the entire audible frequency range.

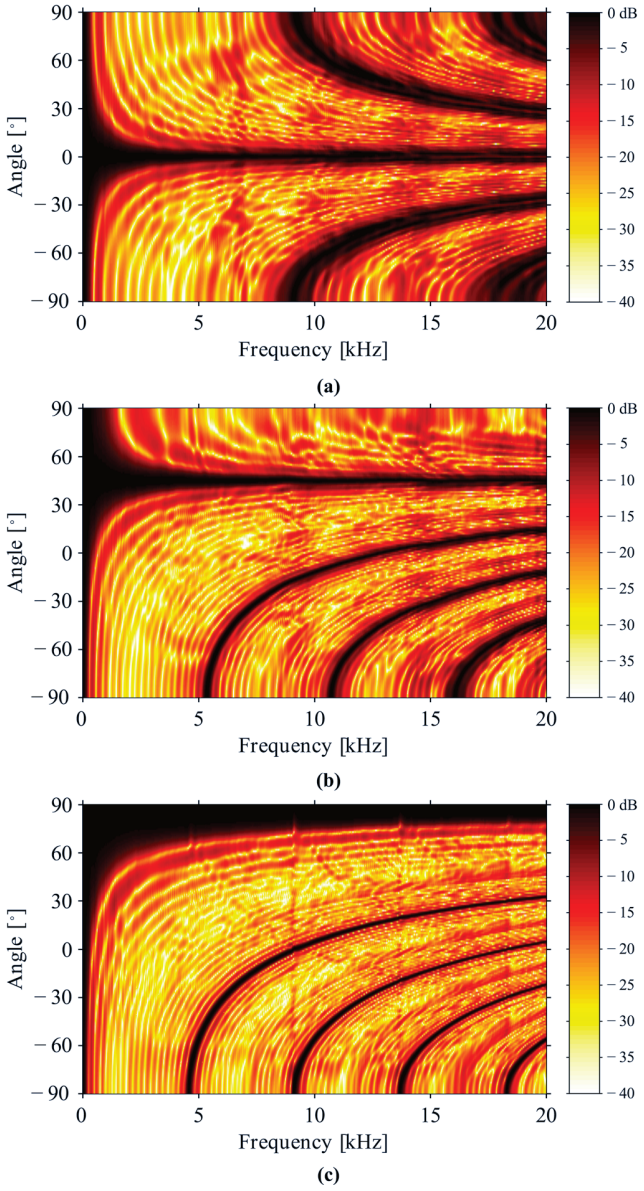

FIG. 9. (Color online) Beamforming patterns measured with a line array of 19 microphones and a spacing of 3.75 cm. The loudspeaker was located at (a) 0°, (b) 45°, and (c) 90°.

are in good agreement with the theoretical beampatterns presented in Fig. 3. As expected, the beampatterns become more directive with increasing frequency but the main lobe becomes broader when the source is located at an oblique position [this is particularly clear in Fig. 9(c)]. Furthermore, the ghost sources induced by spatial aliasing contaminate approximately the same regions of the beamforming maps predicted in Fig. 3. The deviations between the theoretical and the experimental results can be explained by the presence of background noise, misalignment/mislocation of some of the transducers of the home-made array, and scattering caused by the equipment. Besides, the manufacturer of the 1/4 in. microphones used states that these transducers should be used from 50 Hz up to 10 kHz. Hence, erratic behavior, e.g., phase mismatch between the microphones, may have occurred above 10 kHz. In any case, unlike the

acousto-optic beamformer, it is clear from the results that the bandwidth of the delay and sum beamformer is bounded to the frequency range free of spatial aliasing, which corresponds to approximately 4.5 kHz for this particular array.

VI. CONCLUSIONS

A measurement principle based on the acousto-optic effect for localization of sound sources has been demonstrated by means of theoretical analysis and experimental results. Despite the difficulties encountered when assembling the experimental setup, the presented acousto-optic beamformer proves to be immune to spatial aliasing. This is a feature that can never be achieved with a transducer array. The presented method not only extends the frequency range of analysis, but it is also a non-invasive technique. Transducer-based methods always require the immersion of a device into the sound field under investigation. This is especially critical at high frequencies, where a large number of transducers are required to avoid spatial aliasing, but at the same time it turns the array into a bulk instrument that can yield scattering effects. The use of light as a sensing element does not influence the sound.

There is yet another major difference between the presented acousto-optic beamformer and conventional beamforming techniques. The acousto-optic beamformer is a spatial filter that amplifies sound that propagates perpendicularly to the beam of light, and attenuates otherwise. This means that, unlike conventional beamforming, one has to steer the acousto-optic beamformer physically into a set of different angular directions in order to obtain a complete map of the acoustical space under investigation. Similarly to radar antennas used for air traffic control, the acousto-optic beamformer could in practice rotate at a constant rate, sweeping the different positions of interest. This would not even be required in some particular cases, e.g., surveillance purposes, where it was only necessary to listen to a single direction. Nevertheless, this trade-off does not outshine the advantages of the acousto-optic beamformer.

[1]B. D. V. Veen and K. M. Buckley, "Beamforming: A versatile approach to spatial filtering," IEEE ASSP Mag. **5**, 4–24 (1988).

[2]D. H. Johnson and D. E. Dudgeon, *Array Signal Processing: Concepts and Techniques* (Prentice-Hall, Englewood Cliffs, NJ, 1993), Chaps. 4 and 7.

[3]V. Murino, A. Trucco, and C. S. Regazzoni, "Synthesis of unequally spaced arrays by simulated annealing," IEEE Trans. Signal Process. **44**, 119–123 (1996).

[4]A. Trucco and V. Murino, "Stochastic optimization of linear sparse arrays," IEEE J. Ocean. Eng. **24**, 291–299 (1999).

[5]S. Kay and S. Saha, "Design of sparse linear arrays by Monte Carlo importance sampling," IEEE J. Ocean. Eng. **27**, 790–799 (2002).

[6]O. Hoshuyama and A. Sugiyama, *Microphone Arrays: Signal Processing Techniques and Applications* (Springer, Berlin, 2001), Chap. 5.

[7]M. V. Greening and J. E. Perkins, "Adaptive beamforming for nonstationary arrays," J. Acoust. Soc. Am. **112**, 2872–2881 (2002).

[8]E. Tiana-Roig, F. Jacobsen, and E. Fernandez-Grande, "Beamforming with a circular microphone array for localization of environmental noise sources," J. Acoust. Soc. Am. **128**, 3535–3542 (2010).

[9]E. Tiana-Roig, F. Jacobsen, and E. Fernandez-Grande, "Beamforming with a circular array of microphones mounted on a rigid sphere (L)," J. Acoust. Soc. Am. **130**, 1095–1098 (2011).

[10]B. Rafaely, "Plane-wave decomposition of the sound field on a sphere by spherical convolution," J. Acoust. Soc. Am. **116**, 2149–2157 (2004).

[11]G. A. Daigle, M. R. Stinson, and J. G. Ryan, "Beamforming with air-coupled surface waves around a sphere and circular cylinder (L)," J. Acoust. Soc. Am. **117**, 3373–3376 (2005).

[12]A. Torras-Rosell, S. Barrera-Figueroa, and F. Jacobsen, "Sound field reconstruction using acousto-optic tomography," J. Acoust. Soc. Am. **131**, 3786–3793 (2012).

[13]J. H. Gladstone and T. P. Dale, "Researches on the refraction, dispersion, and sensitiveness of liquids," Philos. Trans. R. Soc. London **153**, 317–343 (1863).

[14]W. Merzkirch, *Techniques of Flow Visualization* (Advisory Group for Aerospace Research & Development, Loughton, Essex, 1987).

[15]P. Debye and F. W. Sears, "On the scattering of light by supersonic waves," Proc. Natl. Acad. Sci. U.S.A. **18**, 409–414 (1932).

[16]C. V. Raman and N. S. Nagendra Nath, "The diffraction of light by high frequency sound waves: Part I," Proc. Indian Acad. Sci., Sect. A **2**, 406–412 (1935).

[17]C. V. Raman and N. S. Nagendra Nath, "The diffraction of light by high frequency sound waves: Part II," Proc. Indian Acad. Sci., Sect. A **2**, 413–420 (1935).

[18]C. V. Raman and N. S. Nagendra Nath, "The diffraction of light by high frequency sound waves: Part III," Proc. Indian Acad. Sci., Sect. A **3**, 75–84 (1936).

[19]C. V. Raman and N. S. Nagendra Nath, "The diffraction of light by high frequency sound waves: Part IV," in Proc. Indian Acad. Sci., Sect. A **3**, 119–125 (1936).

[20]C. V. Raman and N. S. Nagendra Nath, "The diffraction of light by high frequency sound waves: Part V," in Proc. Indian Acad. Sci., Sect. A **3**, 459–465 (1936).

[21]C. F. Quate, C. D. W. Wilkinson, and D. K. Winslow, "Interaction of light and microwave sound," Proc. IEEE **53**, 1604–1623 (1965).

Paper G

EURONOISE Prague 2012

A beamforming system based on the acousto-optic effect

Antoni Torras-Rosell atr@dfm.dtu.dk
Danish Fundamental Metrology A/S, Matematiktorvet 307, 2800 Kgs. Lyngby, Denmark.

Finn Jacobsen fja@elektro.dtu.dk
Acoustic Technology, Department of Electrical Engineering, Technical University of Denmark, Ørsteds Plads 352, 2800 Kgs. Lyngby, Denmark.

Salvador Barrera-Figueroa sbf@dfm.dtu.dk
Danish Fundamental Metrology A/S, Matematiktorvet 307, 2800 Kgs. Lyngby, Denmark.

Summary
Beamforming techniques are usually based on microphone arrays. The present work uses a beam of light as a sensor element, and describes a beamforming system that locates sound sources based on the acousto-optic effect, this is, the interaction between sound and light. The use of light as a sensing element makes this method immune to spatial aliasing. This feature is illustrated by means of simulation and experimental results. For ease of comparison, the study is supplemented with results obtained with a line array of microphones.

PACS no. 43.35.Sx, 43.60.Fg

1. Introduction

Beamforming techniques localize sound sources using a finite number of input signals that are captured with an ensemble of transducers. The lower frequency range of analysis is typically related to the dimensions of the array, that is, below a certain frequency the information captured with the transducers of the array is almost identical, and thus, the beamforming output becomes omnidirectional. The upper frequency is usually limited by the dimensions of the transducers (to avoid scattering effects) and/or the spatial sampling performed by the layout of the array (to prevent aliasing effects). The scattering can partly be compensated for applying a frequency response correction that will only counteract the possible effects for a certain direction of incident sound, typically axial incidence. The spatial aliasing problem is in practice more difficult to circumvent because the straightforward solution of increasing the density of transducers in the array layout also compromises the transparency of the array versus the incident sound field. In any case, spatial aliasing above a certain frequency is unavoidable when using a finite number of transducers.

ISSN 2226-5147
ISBN 978-80-01-05013-2

The present work proposes a beamforming system that uses the acousto-optic effect to localize sound sources in the far field. The use of a beam of light as a sensing element makes this beamforming system immune to spatial aliasing. The article is organized in the following manner: First, for ease of comparison, a brief section describing the effects of spatial aliasing in conventional Delay-and-Sum beamforming (DSB) is given. Then follows a section about the physical principles governing the acousto-optic beamformer. The performance of the acousto-optic beamformer is assessed by means of experimental results and compared with results obtained with DSB. Before the conclusions, a few comments on the possibility of using this method in nearfield beamforming are discussed.

2. Conventional beamforming and spatial aliasing

In the far field, the localization of acoustic sources can usually be reduced to a simpler task: the identification of direction of propagation of plane waves. Thus, when using microphone arrays, no relevant information is contained in the sound pressure levels of the sensors, these are approximately the same at all positions, but the key feature that indeed unravels the location of the source is the phase difference between the signals captured by the transducers. Classical DSB clearly benefits from this, that is, the beamforming output is

maximum when the phase shifts applied to the sensor signals compensate for the propagation delays caused by the layout of the microphone array. For the particular case of a line array of microphones, the beamforming output can be written analytically as follows[1],

$$b_{DS}(\theta) = \left| \frac{1}{M} \sum_{m=0}^{M-1} \tilde{p}_m e^{-jkmd\sin\theta} \right|^2 = \left| \frac{\tilde{P}_0}{M} \frac{\sin\left(k(\sin\tilde{\theta} - \sin\theta)Md/2\right)}{\sin\left(k(\sin\tilde{\theta} - \sin\theta)d/2\right)} \right|^2, \quad (1)$$

where all microphones are assumed to be equally important, $\tilde{p}_m$ represents the Fourier transform of the sound pressure of the m'th microphone, d and M are the microphone spacing and the total number of microphones, k is the wavenumber, $e^{-jkmd\sin\theta}$ is the phase shift introduced to the m'th microphone in order to compensate for the delay experienced by incident waves coming from the direction θ, and $\tilde{P}_0$ and $\tilde{\theta}$ correspond to the amplitude and the incident direction of the actual sound measured at the microphone positions. Figure 1 shows the beamforming output of a line array of 19 microphones when the acoustic source is located at three different positions. The reference angle $\theta = 0°$ corresponds to the perpendicular direction of the line array. As can be seen in panels (a) and (b), the output consists of two mainlobes because the symmetry of the line array makes it impossible to distinguish between the real source and its corresponding image source. Note that these two mainlobes are overlapped in panel (c) and that they become wider as the incident sound approaches grazing incidence.

The prominent C-shaped curves observed at high frequencies are the result of spatial aliasing. The number of transducers per unit length is not sufficient to map the location of the source correctly at high frequencies, yet misleading to the presence of ghost sources. The Nyquist theorem states that the spacing between the transducers must always be smaller than half the wavelength (or equivalently $f < c/(2d)$), otherwise spatial aliasing can corrupt the measurement. The Nyquist frequency of the line array simulated in Figure 1 is approximately 4.5 kHz. This corresponds to the worst case scenario, which occurs when the source is aligned with the line array, see panel (c).

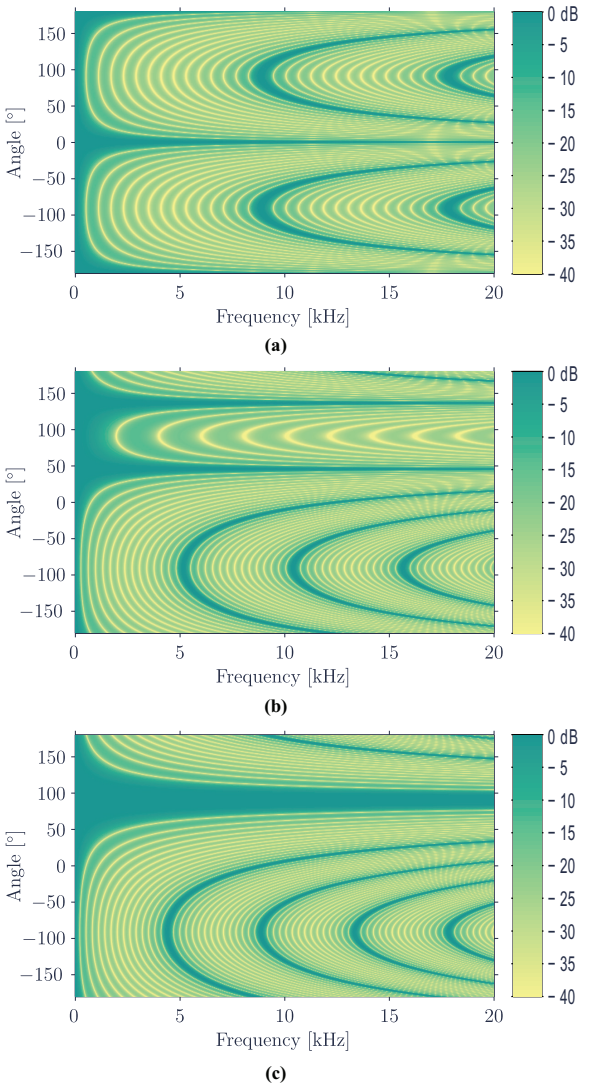

Figure 1: Beamforming ouput of a line array of 19 microphones as a function of frequency. Three source positions are simulated: (a) 0°, (b) 45° and (c) 90°. The spacing between the microphones is 3.75 cm.

3. Acousto-optic beamformer

Waves travel differently depending on the medium of propagation. For instance, electromagnetic waves generally travel slower in dense media and faster otherwise (vacuum corresponds to the extreme case). The phenomenon of sound in air inherently involves pressure changes that at the same time cause density fluctuations. Hence, sound waves can in principle influence the propagation of electromagnetic waves such as light. This is the so-called acousto-optic effect, a physical phenomenon that has been widely investigated with ultrasonic waves [2, 3, 4]. Recent studies show that the acousto-optic effect can also be measured within the audible frequency range using a laser Doppler vibrometer (LDV)[5, 6]. In this frequency range and with sound pressure levels below the threshold of pain, sound waves cannot diffract light, but only make it travel a bit faster (pressure decrease) or slower (pressure increase). All the information about the acousto-optic effect is thus contained in the phase of light, not its amplitude. In particular, it can be shown that the phase of a beam of light traveling through an acoustical space is [6]

$$\phi = k_0 n_0 L_0 + k_0 \frac{n_0 - 1}{\gamma p_0} \int_{\mathbf{L}} p(x, y, t) \mathrm{d}l, \quad (2)$$

where k_0 is the wavenumber of light in vacuum, n_0 and p_0 are the refractive index and the atmospheric pressure under static conditions, γ is the ratio of specific heats, $p(x, y, t)$ corresponds to the sound pressure along the line integral, $\mathbf{L}$ represents the propagation path, and L_0 is the total length.

With a proper measurement setup, carefully designed to minimize the mechanical vibrations of the structure where the LDV and the reflecting point are mounted, the apparent velocity captured by the LDV due to the interaction between sound and light is [6]

$$v(t) = \frac{n_0 - 1}{\gamma p_0 n_0} \frac{\mathrm{d}}{\mathrm{d}t} \left(\int_{\mathbf{L}} p(x, y, t) \mathrm{d}l \right). \tag{3}$$

Figure 2 sketches the measurement setup that makes it possible to measure this phenomenon. The most interesting feature of Equation (2) is that it contains the value of the continuous integral of the sound pressure along the path traveled by the light. Beamforming techniques base their calculations on a finite number of input signals, and this is indeed what causes aliasing. In particular, when no delays are applied to the sensor signals, for $\theta = 0°$ in Equation (1), the beamforming output is simply the summation of the measured signals. Theoretically, if an infinite number of sensors were placed along a finite line of length L_0, the following result could be achieved,

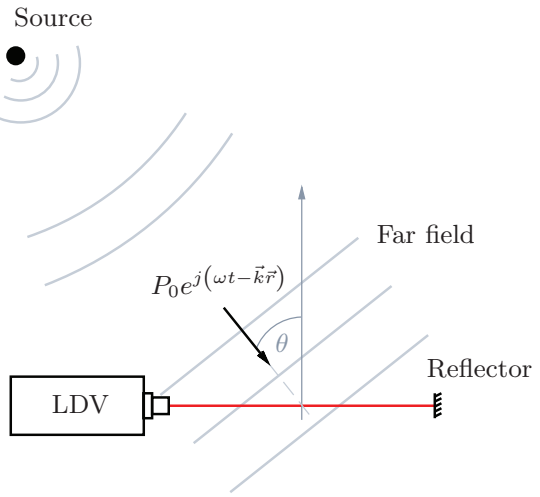

Figure 2: Sketch of the acousto-optic beamforming system.

$$\lim_{M \to \infty} \sum_{m=0}^{M-1} \tilde{p}_m d = \int_0^{L_0} P(x, y, \omega) \mathrm{d}l, \tag{4}$$

where $P(x, y, \omega)$ is the temporal Fourier transform of $p(x, y, t)$. Such an ideal situation would yield an infinite spatial resolution ($d \to 0$) that would make any aliasing effects disappear. Even though the use of an infinite number of transducers is in practice not feasible, the continuous integral of the sound pressure can alternatively be calculated using the acousto-optic effect. Fourier transforming Equation (3) yields,

$$V(\omega) = j\omega \frac{n_0 - 1}{\gamma p_0 n_0} \left(\int_{\mathbf{L}} P(x, y, \omega) \mathrm{d}l \right), \tag{5}$$

and thus,

$$\int_{\mathbf{L}} P(x, y, \omega) \mathrm{d}l = \frac{\gamma p_0 n_0}{n_0 - 1} \frac{V(\omega)}{j\omega}. \tag{6}$$

This expression can be used to define a beamforming output that is immune to spatial aliasing:

$$\begin{aligned} b_{AO} &= \left| \frac{1}{L_0} \int_0^L P(x, y, \omega) \mathrm{d}l \right|^2 \\ &= \left| \frac{1}{L_0} \frac{\gamma p_0 n_0}{n_0 - 1} \frac{V(\omega)}{j\omega} \right|^2. \end{aligned} \tag{7}$$

Analytically, the continuous integral of plane waves traveling through a beam of light of length L_0 yields the following beamforming output:

$$\begin{aligned} b_{AO} &= \left| \frac{1}{L_0} \int_0^{L_0} \tilde{P}_0 e^{j(\omega t - \vec{k} \cdot \vec{r})} \mathrm{d}x \right|^2 \\ &= \left| \frac{\tilde{P}_0 e^{j\omega t}}{L_0} \int_0^{L_0} e^{jk \sin\tilde{\theta} x} \mathrm{d}x \right|^2 \\ &= \left| \tilde{P}_0 \mathrm{sinc}\left(k \sin\tilde{\theta} L_0 / 2 \right) \right|^2. \end{aligned} \tag{8}$$

Taking into account that $L_0 = (M - 1)d$, the similarity between Equations (1) and (8) when $\theta = 0$ is worth noting. The immunity to spatial aliasing of the defined acousto-optic beamformer is illustrated in the beamforming pattern depicted in Figure 3. Note that the acousto-optic beamformer b_{AO} is independent of θ, that is, it cannot steer the looking direction of the beamformer electronically as in conventional beamforming systems. Instead, one has to steer the laser beam manually towards those angular directions of interest.

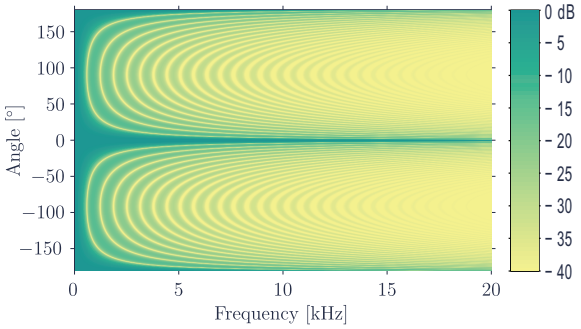

Figure 3: Beamforming output of the acousto-optic beamformer as a function of frequency ($L_0 = 54$ cm).

4. Results and discussion

The measurements were carried out in an anechoic room of about 1000 m^3. A loudspeaker radiating white noise was placed at a distance of 5 m from the beamforming system in order to fulfill the far field conditions described in the theory. A picture of the measurement setup is shown in Figure 4. Quite some efforts were spent on minimizing the mechanical vibrations of the structure holding the beamforming system. Moreover, an accelerometer (B&K Type 4344) was mounted on the reflecting point to monitor the residual mechanical vibrations that could bias the velocity measured with the LDV (a Polytec OFV-505). The output of the accelerometer showed that the measurement setup was fairly immune to sound generated by mechanical vibrations above 2 kHz. The setup was covered with absorbing material in order to reduce the possible effects of scattering from the equipment. The beamforming system was installed on a turntable allowing to steer the laser beam of the LDV towards different directions. Given the symmetry of the beamforming pattern, the acousto-optic beamformer was only rotated 180° instead of 360°. The results are presented in Figure 5. Despite the mechanical vibrations of the structure below 2 kHz, the measured acousto-optic beamforming pattern resembles very much the one presented in Figure 3. Although the background noise, some resonances of the structure and the scattering from the equipment do not allow to see the sidelobes as clearly as in the ideal simulation, the experimental results confirm that the beamforming output is definitely free of aliasing artifacts.

For comparison's sake, supplementary measurements were carried out with a line array of 19 microphones (B&K Type 4957) using conventional DSB.

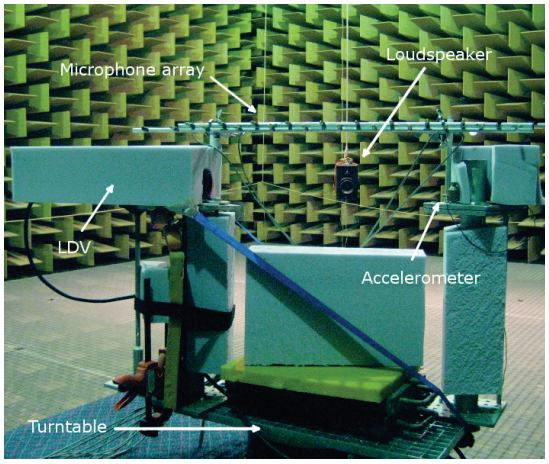

Figure 4: Measurement setup. The loudspeaker was placed 5 m far away from the beamforming systems ($L_0 = 54$ cm, $d = 3.75$ cm).

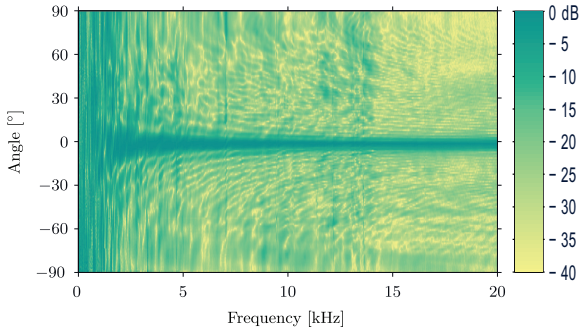

Figure 5: Beamforming pattern measured with the acousto-optic beamformer as a function of frequency ($L_0 = 54$ cm).

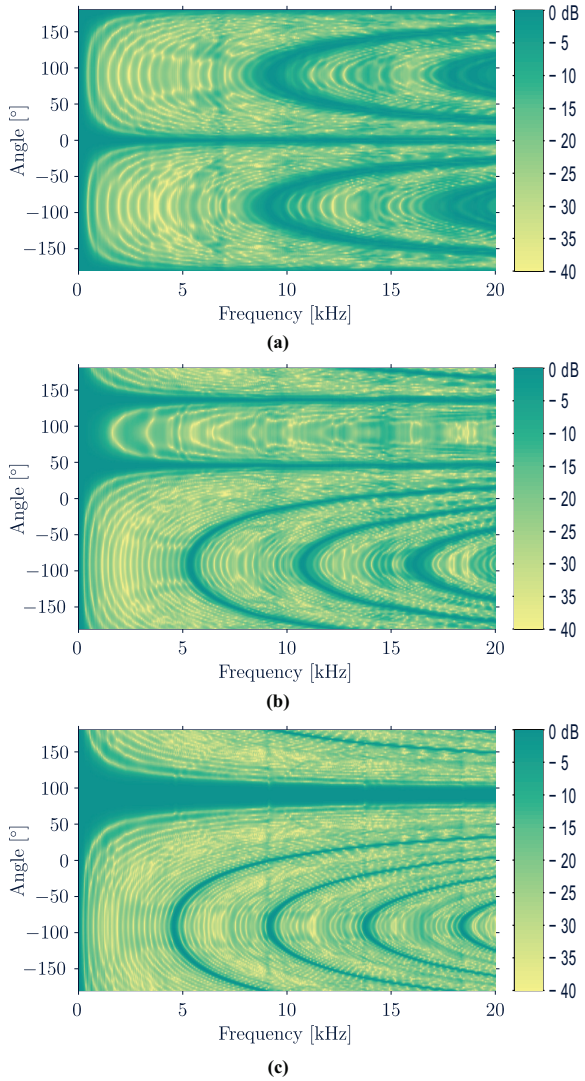

Figure 6: Beamforming patterns measured with a line array of 19 microphones as a function of frequency. Three source positions were measured: (a) 0°, (b) 45° and (c) 90°. The spacing between the microphones was 3.75 cm.

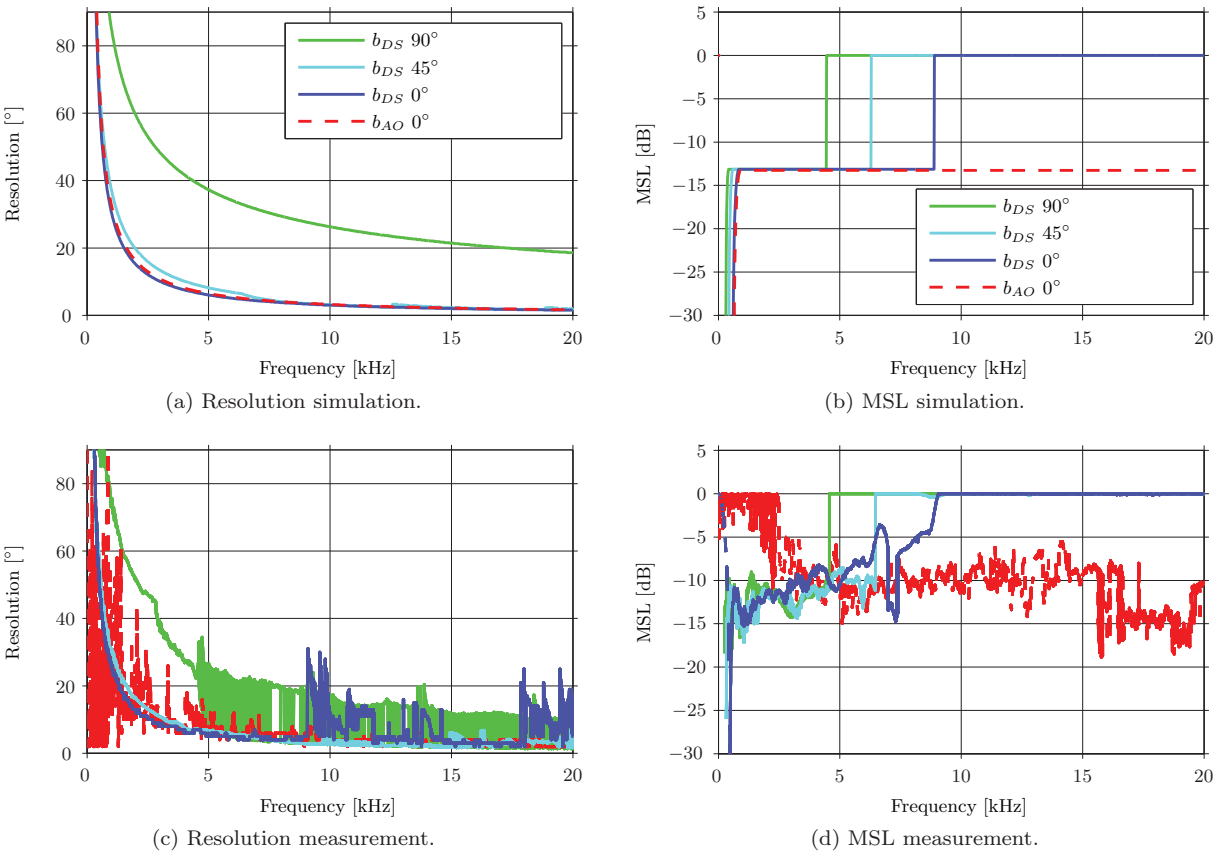

(a) Resolution simulation.

(b) MSL simulation.

(c) Resolution measurement.

(d) MSL measurement.

Figure 7: Resolution and MSL of the microphone array and the acousto-optic beamformer. Three different source positions were tested with the microphone array (0°, 45°, 90°) and only one with the acousto-optic beamformer (0°).

The results can be seen in Figure 6. Again, the beamforming outputs are subject to noise, vibrations of the structure and scattering effects, but in addition to these, there could be some misalignment between the microphones caused by the homemade array layout. Nevertheless, aliasing artifacts arise at approximately the same frequencies predicted in the simulations.

A good way to assess the performance of a beamforming system is to use the so-called resolution (normally defined at −3 dB of the mainlobe) and the maximum sidelobe level (MSL), that is, the level difference between the mainlobe and the most prominent secondary lobe. The former characterizes the minimum angle necessary to resolve two sources, whereas the latter indicates the possible influence of ghost sources. Figure 7 shows the resolution and the MSL of the line array and the acousto-optic beamformer analyzed in the simulations and the measurements. As can be seen, both resolution and MSL are quite noisy in the measurements. None of the possible sources of error (noise, vibrations, etc.) are included in the simulations. However, the main features observed in the simulations can also be identified in the measurements, that is, the acousto-optic beamformer has almost the same resolution as the line array when the source is located at $\tilde{\theta} = 0°$ and its MSL does not equal 0 dB at high frequencies due to its immunity to spatial aliasing. Instead, the MSL obtained with the line array clearly illustrates the limitations of using a finite number of microphones above the Nyquist frequency.

5. A note on nearfield beamforming

Sound sources can be detected with the proposed acousto-optic beamformer successfully provided that the waves impinging on the beamforming system have a planar wavefront. Roughly speaking, wavefronts parallel to the laser beam produce larger amplitudes of the LDV's signal than those whose symmetry do not fit the straight light of the laser beam, e.g. spherical waves. Hence, the localization of sound sources in the nearfield using the acousto-optic effect seems so far complicated. An example of the beamforming pattern that would be obtained in the nearfield is simulated in figure 8. As can be seen, the energy of the mainlobe seems to smear out around the angular position of the actual source ($\tilde{\theta} = 0°$) and the sidelobes also become more prominent (cf. Figure 3).

Alternatively, sound sources could in principle be localized in the nearfield using acousto-optic tomog-

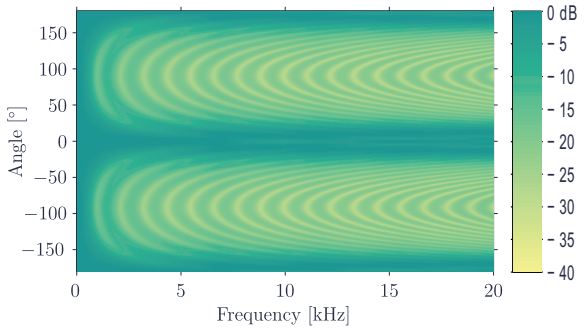

Figure 8: Acousto-optic beamforming output simulated in the nearfield. The source is located 0.4 m from the center of the laser beam ($L_0 = 30$ cm).

raphy [6]. In this measurement technique, the acousto-optic effect is used to reconstruct the acoustic pressure over a surface. The reconstructed sound field could be processed with a conventional nearfield beamforming technique. However, the output of the tomographic reconstruction provides the sound pressure distribution over a finite number of points, and thus, spatial aliasing plays again an important role.

6. Conclusions

The acousto-optic beamformer is a beamforming system immune to spatial aliasing. This makes it possible to extend the frequency range of analysis to all audible frequencies. The price to pay for such an ideal property is that the acousto-optic beamformer cannot steer the looking direction of the system electronically. One has to rotate the laser beam manually into the angular positions of interest. This could be implemented in practice in a similar way as the radar antennas used in air traffic control, that is, the acousto-optic beamformer could rotate at a constant speed, sweeping the acoustical space under investigation. In some cases where only one looking direction is of interest, e.g. in some surveillance applications, this drawback would not even be a problem.

The results also show that when comparing an acousto-optic beamformer to a conventional line array of microphones, both present approximately the same resolution and MSL figures when the source is located in front of the beamforming system (and below the Nyquist frequency). However, although the line array can steer electronically the looking direction towards the sides, both resolution and MSL worsens considerably as the source approaches a grazing angular position.

References

[1] D. H. Johnson and D. E. Dudgeon: Array signal processing: Concepts and techniques. Prentice-Hall, Englewood Cliffs, NJ, 1993.

[2] P. Debye and F. W. Sears: On the scattering of light by supersonic waves. Proc. National Academy of Sciences of the United States of America **18** (6) 409–414 (1932).

[3] C. V. Raman and N. S. Nagendra Nath: The diffraction of light by high frequency sound waves: Parts I–V. Proc. Indian Academy of Sciences, section A (1935 and 1936).

[4] C. F. Quate, C. D. W. Wilkinson and D. K. Winslow: Interaction of light and microwave sound. Proc. IEEE **53** (10) 1604–1623 (1965).

[5] Y. Oikawa, T. Hasegawa, Y. Ouchi, Y. Yamasaki, and Y. Ikeda: Visualization of sound field and sound source vibration using laser measurement method. Proc. 20th International Congress on Acoustics (2010).

[6] A. Torras-Rosell, S. Barrera-Figueroa and F. Jacobsen: Sound field reconstruction using acousto-optic tomography. J. Acoust. Soc. Am. **131** (5) (2012).

Paper H

THE VERSATILITY OF THE ACOUSTO-OPTIC MEASURING PRINCIPLE IN CHARACTERIZING SOUND FIELDS

A Torras-Rosell DFM, Danish National Metrology Institute, Kongens Lyngby, Denmark
S Barrera-Figueroa DFM, Danish National Metrology Institute, Kongens Lyngby, Denmark
F Jacobsen Acoustic Technology, Technical University of Denmark, Kongens Lyngby, Denmark

1 INTRODUCTION

One of the typical problems in determining the quantities describing an acoustic field, e.g. sound pressure and particle velocity, is the influence of the transducer on the actual properties of sound to be measured when the transducer is immersed into the field. Typically, the influence of the transducer is either disregarded by assuming that the dimensions of the transducer are small compared with the wavelength of the sound wave, or subtracted by means of a transducer-based correction, typically in form of a frequency response, previously determined in a realization of an idealized sound field (e.g. free or diffuse field). Either solution introduces additional uncertainties to the measurement process, however quantifiable. Optical methods do not incur this problem because the "sensing" element is not a bulk transducer but a beam of light that does not change the properties of sound, thus giving the actual value of the acoustic quantities. Among the optical techniques used nowadays for characterizing sound fields, the acousto-optic effect, that is, the interaction between sound and light, has recently rendered promising results as a non-invasive measuring principle within the audible frequency range. When a laser beam travels through an acoustic field, it captures the properties of sound along the optical path and encodes this information into its phase as a line integral of the pressure. While this line integral does not provide a direct measure of the pressure distribution along the scanned line, there are ways to exploiting the potential of this measurement. This paper presents three different acoustic applications founded on the acousto-optic effect, namely the visualization of sound based on acousto-optic tomography, the localization of noise sources employing an acousto-optic beamformer, and the identification of acoustic sources using near-field acousto-optic holography. The theoretical aspects of each of these applications are underlined and supplemented with experimental results.

2 THE ACOUSTO-OPTIC EFFECT

The interaction between sound and light is in this paper only studied within the audible frequency range and under sound pressure levels below the threshold of pain. The former condition implies that diffraction effects can be disregarded from the physical description of the acousto-optic effect. This is not always the case at higher frequencies, in the ultrasonic domain. The latter condition makes it possible to relate the changes of refractive index of the medium, in this case air, to linear variations of the acoustic pressure. This simplifies the model used to couple the optical and acoustical properties of the medium significantly. Under the mentioned conditions, the refractive index can be written as follows,[1]

$$n \cong n_0 + \frac{n_0 - 1}{\gamma p_0} p \,, \tag{1}$$

where n_0 and p_0 are the refractive index and the atmospheric pressure under static conditions respectively, γ is the ratio of specific heats, and p is the acoustic pressure. Note that the second term on the right hand side of the previous equation, which represents the acousto-optic effect, is extremely small compared to n_0. For example, in air and under standard atmospheric conditions (p_0 = 101.3 kPa), a sound pressure of 1 Pa induces a variation of the refractive index that is nine orders of magnitude smaller than n_0. The characterization of acoustic fields by means of the acousto-optic

effect requires measuring such small changes of refractive index. By recalling that the speed of light is inversely proportional to the refractive index, the acousto-optic effect can be understood in this context as a modulation effect on the phase of light: the light travels slightly slower/faster when the acoustic pressure increases/decreases. This can in practice be detected using interferometry, and in particular, the experimental results presented in the following sections were carried out employing a laser Doppler vibrometer (LDV). Although this optical device is designed to measure mechanical vibrations, it can be shown that the output of a vibrometer whose laser beam is traveling through a sufficiently intense sound field and reflected off a surface with negligible vibrations corresponds to an apparent velocity such as,[1]

$$v_{LDV}(t) = \frac{n_0 - 1}{\gamma p_0 n_0} \frac{d}{dt} \left(\int_{\boldsymbol{L}} p(\vec{r}, t)\, dl \right), \tag{2}$$

where $\boldsymbol{L}$ represents the path travelled by the light. This expression shows that the acoustic information captured by the LDV does not correspond to a direct measure of the pressure at a certain position, but to a line integral of the pressure along the path followed by the laser beam. The following sections illustrate three possible ways of exploiting this measurement principle for three different purposes.

3 ACOUSTIC IMAGING

Since the acousto-optic measuring principle does not provide a direct measure of the pressure but rather a measure of its line integral, the reconstruction of the actual pressure can be achieved using tomography and the Radon transform. The Radon transform of an acoustic field can simply be defined as the projection of the acoustic pressure into a set of parallel straight lines:

$$R_p(\theta, x', t) = \int_{-L/2}^{L/2} p(\vec{r}, t)\, dy'. \tag{3}$$

The sketch presented on the left hand side in Figure 1 illustrates the measurement principle as well as the system of coordinates used in this definition of the Radon transform. At this point, the apparent velocity presented in Eq. 2 can accordingly be reformulated as a function of the Radon transform of the acoustic field:

$$v_{LDV}(t) = \frac{n_0 - 1}{\gamma p_0 n_0} \frac{dR_p(\theta, x', t)}{dt}. \tag{4}$$

Thus, the Radon transform along a certain line can be determined by integrating the measured velocity in time:

$$\tilde{R}_p(\theta, x', t) = \frac{\gamma p_0 n_0}{n_0 - 1} \int v_{LDV}(t) dt. \tag{5}$$

The Radon transform is here denoted with a tilde to emphasize that it is a measured quantity, and thus, it is vulnerable to measurement noise. There is no need here to consider any integration constant, because such a constant (DC component in time) has no acoustic information. By measuring the acousto-optic effect over a sufficient number of angles of projection θ and a sufficient number of parallel line scans along the coordinate x', the original sound pressure distribution can be reconstructed using the inverse Radon transform.[2] This is in practice done with tomographic algorithms, which try to circumvent the problems arisen by the presence of extraneous noise during the measurement. The present work uses the so-called filtered back projection method, which is the most popular reconstruction algorithm in tomography for many fields of science. For a parallel line scanning configuration, this method estimates the pressure as follows,[2]

$$\tilde{p}(\vec{r}, t) = \int_0^{\pi} Q(\theta, x', t) d\theta, \tag{6}$$

where $Q(\theta, x', t)$ is the so-called "filtered projection":

$$Q(\theta, x', t) = \tilde{R}_p(\theta, x', t) * h(x'). \quad (7)$$

This "filtered projection" is simply the measured Radon transform convolved with a filter $h(x')$ that accounts for both the implementation of the reconstruction algorithm using the two-dimensional spatial Fourier transform (Ram-Lak filter) and the filtering imposed in the frequency domain in order to reduce the influence of noise outside of the frequency range of interest (e.g. a Cosine window). Generally speaking, the quality of the reconstruction is enhanced with increasing the total number of scans (the number of parallel lines times the number of angles of projection). It is recommendable to have as many angles of projection as parallel line scans approximately.[2]

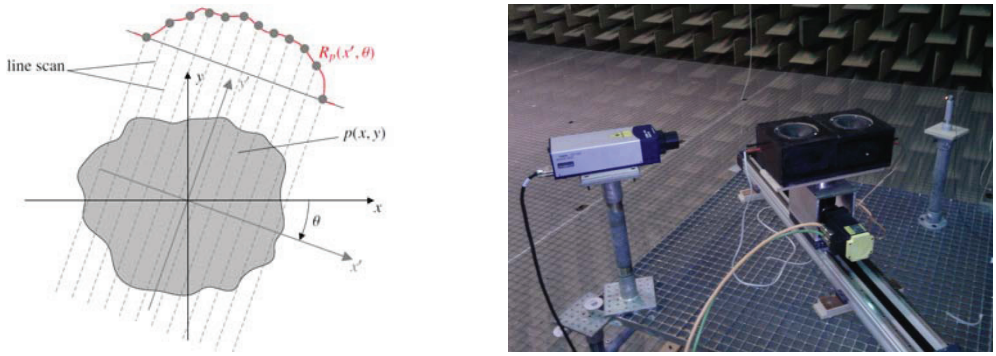

Figure 1: Sketch and measurement setup of the tomographic system.

The presented sound visualization technique is examined in the following for a measurement setup consisting of two loudspeakers whose centres were separated by 20 cm. The experiments were conducted in an anechoic room of about 1000 m^3. A picture of the experimental setup can be seen on the right hand side in Figure 1. The loudspeakers were mounted on two motors that made it possible to translate the speakers along the x' axis (from -0.45 to 0.45 m with a spatial resolution of 2.5 cm) and rotate them at different angles of projection (from 0 to 180 degrees with an angular resolution of 4.9 degrees approximately). A total of 1369 scans were performed. The measurement plane was located 5 cm above the loudspeakers. Note that the reflecting point where the laser was reflected off was continuously monitored with an accelerometer in order to ensure that mechanical vibrations were negligible.

The plot shown on the left hand side in Figure 2 presents the measured Radon transform when the loudspeakers were driven in phase with a 2.4 kHz pure tone. The plot shown on the right hand side in Figure 2 corresponds to the case where the loudspeakers were driven in antiphase.

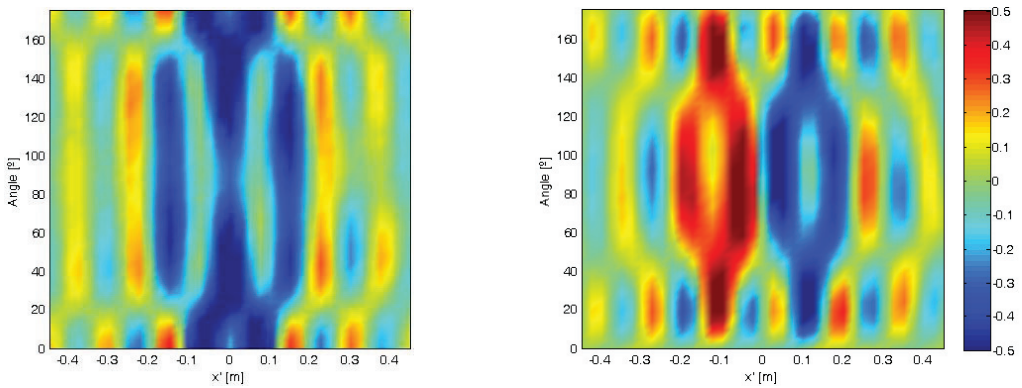

Figure 2: Instantaneous Radon transform measured with the LDV when the two loudspeakers were radiating in phase (on the left hand side) and in antiphase (on the right hand side). The measurement plane was located 5 cm above the speakers.

The respective even and odd symmetries of the measured Radon transforms are in good agreement with the nature of the sound fields under investigation, that is, two sound sources radiating in phase and in antiphase. The corresponding sound pressure maps reconstructed with the filtered back projection method are presented in Figure 3. As expected, the centres of the loudspeakers appear 20 cm apart from each other approximately, and the overall pressure distributions clearly illustrate whether the loudspeakers are driven in phase or in antiphase.

To further validate the quality of the reconstructions, measurements with a free field microphone were conducted at the same plane where the sound field was scanned with the LDV. For ease of comparison, a total of 1369 microphone positions were measured synchronously, yielding a virtual array of concentric circles. The results are shown in Figure 4. As can be seen, the pressure maps measured with the microphone compare well with the results obtained with the acousto-optic effect (cf. Figures 3 and 4). This demonstrates the potential of the presented acousto-optic tomography method, not only to visualize acoustic fields, but also to quantify them.

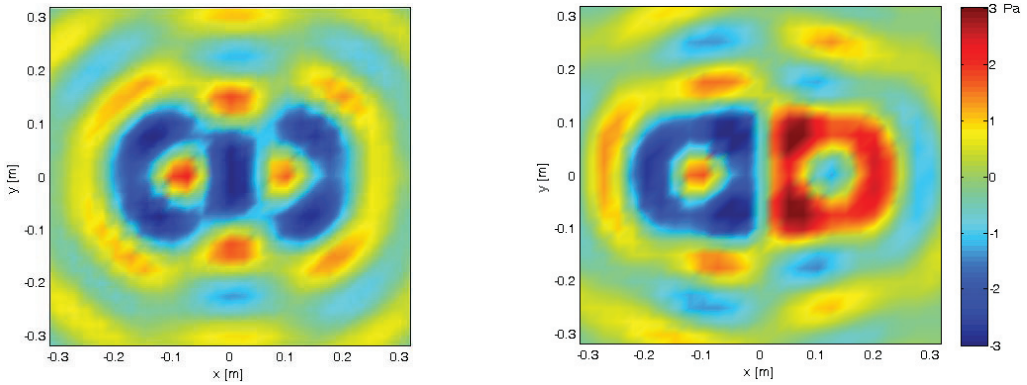

Figure 3: Instantaneous sound pressure reconstructed with the filtered back projection method when the two loudspeakers were radiating in phase (on the left hand side) and in antiphase (on the right hand side).

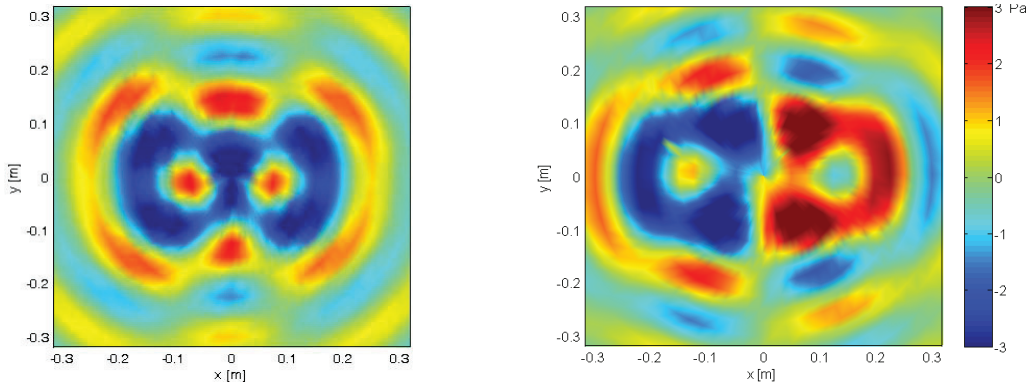

Figure 4: Sound pressure maps obtained with a free field microphone when the two loudspeakers were radiating in phase (on the left hand side) and in antiphase (on the right hand side).

4 SOURCE LOCALIZATION

Beamforming techniques are widely used in acoustics for the localization of sound sources in the far-field. This is a technique often based on microphone arrays that uses the phase mismatch among the sensors to identify the position of the acoustic sources. The performance of a beamforming technique can be assessed by means of the so-called resolution and maximum side lobe level. The optimization of these two parameters ensures that the beamforming system can

accurately separate two acoustic sources and that the output of the beamformer is not contaminated with ghost sources. There exists a great variety of approaches for enhancing the output of a beamforming system, e.g. by designing the layout of the array as well as the weighting functions of the sensors,[3,4] by mounting the sensors on a well-defined geometry such as a sphere that makes it possible to take advantage of the decomposition of the sound field into a set of orthogonal functions,[5,6] or by using deconvolution techniques at a post-processing stage to clean the measured beamforming map.[7] However, a common problem that cannot be overcome by any conventional beamforming technique is spatial aliasing. As a consequence, beamforming systems can only be used up to a certain frequency that is characteristic of each beamformer, though easily predictable by means of the Nyquist theorem when the spacing between transducers is constant. Just as in digital signal processing, where the signals sampled in time can yield temporal aliasing, spatial aliasing arises from the fact that the array used to measure the acoustic field consists of a finite number of microphones, thus sampling the acoustic field with a finite spatial resolution. This can for instance be illustrated with the beamforming output of a line array of microphones based on classical delay and sum beamforming,[3]

$$b_{DSB}(\theta) = \sum_{m=1}^{M} \tilde{p}_m \, e^{-jkmd\sin\theta} \tag{8}$$

where $\tilde{p}_m$is the complex pressure of the m'th microphone, M is the total number of microphones, k is the wavenumber, d is the spacing between transducers and $e^{-jkmd\sin\theta}$ is the phase shift introduced to the m'th microphone in order to compensate for the delay experienced by the incident waves coming from the direction θ.Note that when θ equals zero, the beamforming output simply consists on the summation of pressures of the line array, and mathematically speaking, spatial aliasing comes from this finite summation of pressures. In theory, there would not be spatial aliasing if the line array consisted of an infinity number of microphones placed infinitely close to each other,

$$\lim_{\substack{M\to\infty \\ d\to 0}} \sum_{m=1}^{M} \tilde{p}_m \, d \; = \int_{\boldsymbol{L}} P(\vec{r},\omega)dl, \tag{9}$$

where $\boldsymbol{L}$ represents here the straight line where the line array is located. This is of course not possible in reality, but the continuous line integral of the sound pressure can in fact be measured with an LDV whose laser beam travels along $\boldsymbol{L}$. By taking the temporal Fourier transform of the apparent velocity of the LDV presented in Equation (2),

$$V_{LDV}(\omega) = j\omega \frac{n_0 - 1}{\gamma p_0 n_0}\left(\int_{\boldsymbol{L}} P(\vec{r},\omega)dl\right), \tag{10}$$

the following beamforming output can be defined based on the information captured with acousto-optic effect:[8]

$$b_{AO} = \left|\frac{1}{L}\int_{\boldsymbol{L}} P(\vec{r},\omega)dl\right|^2 = \left|\frac{1}{L}\,\frac{\gamma p_0 n_0}{n_0 - 1}\,\frac{V_{LDV}(\omega)}{j\omega}\right|^2. \tag{11}$$

Figure 5 shows a sketch of the measuring principle as well as a picture of the experimental setup used to validate the presented acousto-optic beamformer. The measurements were carried out in the same anechoic room mentioned in the previous section. A loudspeaker was located 5 m away from the beamforming system to ensure the far-field condition. The loudspeaker was excited with a broad band signal that covered the entire audible frequency range. The acousto-optic beamformer was mounted on a turntable that made it possible to steer the system into different looking directions. All the equipment was covered with absorbing material to reduce the scattering effects at high frequencies. The assumption that the LDV was mainly measuring the acousto-optic effect instead of mechanical vibrations was regularly monitored with an accelerometer that was attached on the surface where the laser was reflected off.

The beamforming map obtained with the acousto-optic measuring principle can be seen on the left hand side in Figure 6. For ease of comparison, the same measurements were repeated with a line array of 19 microphones using the delay and sum beamforming technique. The corresponding results can be seen on the right hand side of Figure 6. As can be seen both beamforming patterns are fairly similar below 9 kHz approximately. As usual, the lower frequencies are more difficult to resolve due to the tendency of the beamforming algorithm to become more omnidirectional towards the low frequencies. Above 9 kHz, the results obtained with the delay and sum beamforming technique are contaminated with ghost sources that are caused by spatial aliasing. This is not a problem for the proposed acousto-optic beamformer, which indeed can cover the entire audible frequency range without traces of spatial aliasing. Note that the noise observed on the acousto-optic beamforming map below 2 kHz was mainly induced by the mechanical vibrations of the structure where the beamforming system was mounted. However, the overall performance of the acousto-optic beamformer proved the applicability of the proposed measurement principle to sound source localization.

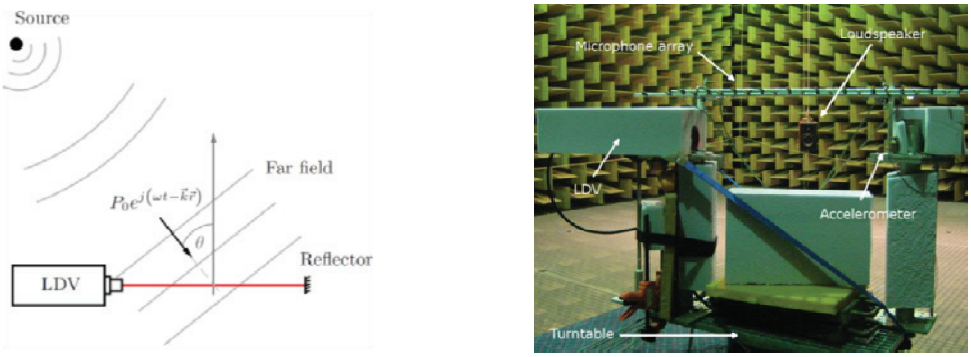

Figure 5: Sketch and experimental setup of the acousto-optic beamformer.

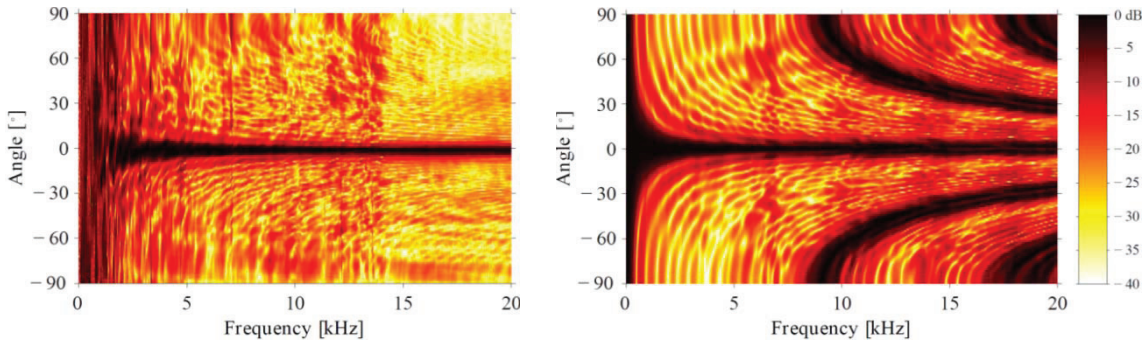

Figure 6: Beamforming results. On the left hand side, the map obtained with the acousto-optic beamformer. On the right hand side, the results achieved with a line arrays of 19 microphones.

5 ACOUSTIC HOLOGRAPHY

This section describes how to use the acousto-optic effect not to reconstruct the sound pressure on a measurement plane as presented in section 3, but to predict any acoustic property of a sound source on a parallel plane, different from the one where the acousto-optic effect is in fact measured. Such a measurement technique has been already developed for transducer arrays since the early 80's, under the name of near-field acoustic holography (NAH).[9-11] The power of this sound source identification technique lies on the fact that it is capable of reconstructing an entire acoustic field, that is, sound pressure, particle velocity and sound intensity, over a three-dimensional space, based on a two-dimensional measurement. Nowadays, there are several methods to implement NAH, e.g. Fourier-based NAH,[9-11] statistically optimized NAH (SONAH),[12] and the equivalent source method.[13] In the following, the conventional Fourier-based NAH method is adapted by means of the Fourier

slice theorem to make it possible to exploit the acousto-optic effect for holography purposes. Fourier-based NAH bases all its calculations on the wavenumber spectrum, that is, the two-dimensional spatial Fourier transform of the acoustic quantities captured on the measurement plane, typically referred to as hologram. The Fourier slice theorem states that the diagonals of the wavenumber spectrum are connected to the Radon transform of the measured acoustic field by means of a one-dimension spatial Fourier transform. Each of these diagonals is directly related to an angle of projection of the Radon transform, see Figure 7.

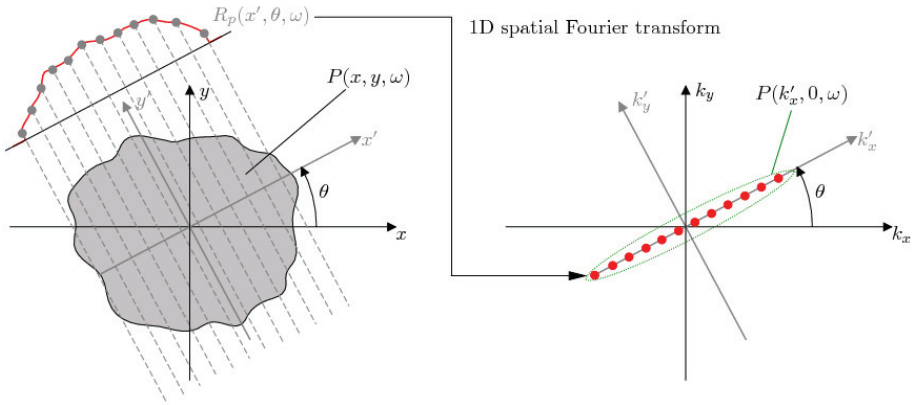

Figure 7: The Fourier slice theorem established the relationship between the Radon transform and diagonals of the wavenumber spectrum.

The proposed holographic method, denoted as near-field acousto-optic holography (NAOH) from now on, uses the apparent velocity of the LDV captured on the hologram plane to compute the diagonals of the wavenumber spectrum. This yields a sampling pattern on the wavenumber domain consisting on data points arranged in concentric circles as illustrated in Figure 8. Unlike the sampling pattern obtained with conventional NAH, where all the data points are uniformly distributed, NAOH presents a higher concentration of points towards the centre of the wavenumber domain (cf. the two examples shown in Figure 8). This is seen as a very interesting and beneficial feature, because Fourier-based NAH usually requires to filter out (regularise) the high spatial frequency components of the spectrum, in order to prevent the noise from dominating the reconstruction process when back-projecting the hologram to the prediction plane. NAOH has either no data points or a lower concentration of them than conventional techniques at these critical spatial frequencies. In short, the proposed NAOH method estimates the wavenumber spectra of the sound pressure and the particle velocity at the prediction plane ($z = z_s$) as follows,[14]

$$\begin{aligned} P_s(k_x, k_y, \omega) &= P_h(k_x, k_y, \omega) \cdot G_p = F^{\theta}_{x'}\{\tilde{R}_p(\theta, x', \omega)\} \cdot e^{jk_z(z_s - z_h)}, \\ V_s(k_x, k_y, \omega) &= P_h(k_x, k_y, \omega) \cdot G_v = F^{\theta}_{x'}\{\tilde{R}_p(\theta, x', \omega)\} \cdot \frac{k_z}{\rho_0 ck} e^{jk_z(z_s - z_h)}, \end{aligned} \tag{12}$$

where $F^{\theta}_{x'}\{\tilde{R}_p(\theta, x', \omega)\}$ denotes the one dimensional Fourier transform along the x'-axis of the Radon transform measured at the hologram plane ($z = z_h$), G_p and G_v represent the so-called pressure and velocity propagators, ρ_0 is the static density of the medium, c is the speed of sound, and k_z equals $\sqrt{k^2 - k_x^2 - k_y^2}$. Note that the propagators are defined in the same way as in Fourier-based NAH. The only difference is the exact values of k_z, which basically depend on the sampling points k_x and k_y in the wavenumber domain.

In order to validate the proposed method, the Radon transforms measured in Figure 2 (see section 3) were propagated to a new plane located 3 cm above the loudspeakers (the hologram was thus back-propagated 2 cm). The resulting sound pressures can be seen in Figure 9. As expected, the overall pressure distributions are fairly similar to the ones presented at the hologram (see Figure 3), but the overall energy of the reconstructed aperture is larger due to the fact that the prediction plan is closer to the sound sources. The validity of the proposed method was further confirmed by

comparing these results to reconstructions based on acousto-optic tomography of the very same sound field directly measured at the prediction plane. The results are presented in Figure 10. As can be seen, the agreement between the pressures predicted with the NAOH method and the acousto-optic tomography method is very good. It is worth mentioning that the NAOH method has not required the use of any regularization technique in order to stabilise the results. Although the signal-to-noise ratio was good during the measurements, the unique spectral features of the NAOH method further reduce the influence of extraneous noise at high spatial frequencies. Besides, with the presented NAOH method, it is also possible to estimate the particle velocity and the acoustic

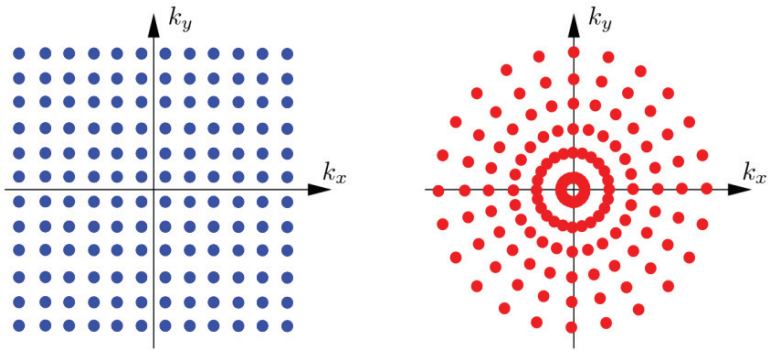

Figure 8: Data points sampled in the wavenumber domain when using conventional NAH (on the left hand side) and when using NAOH (on the right hand side).

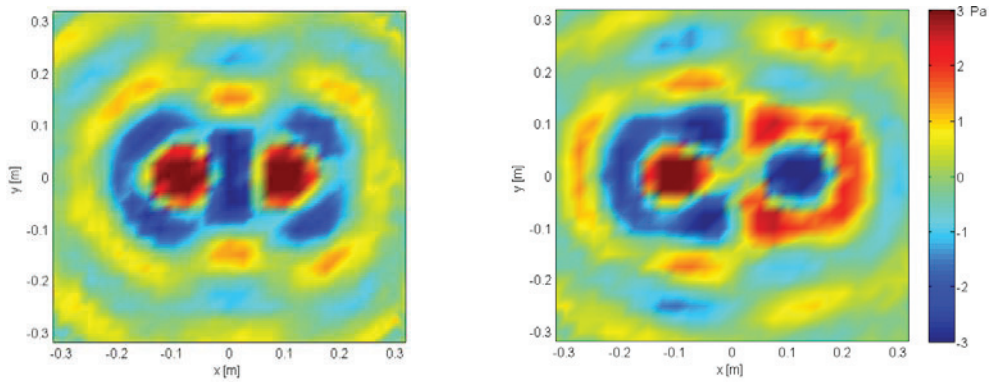

Figure 9: Instantaneous sound pressure estimated with NAOH on the prediction plane when the two loudspeakers are driven in phase (on the left hand side) and in antiphase (on the right hand side). The hologram and prediction planes were located 5 and 3 cm respectively above the loudspeakers.

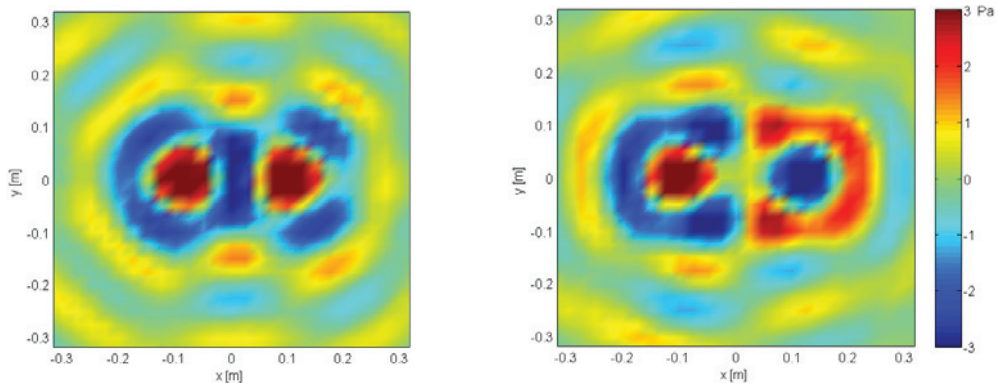

Figure 10: Instantaneous sound pressure distribution reconstructed with acousto-optic tomography from measurements taken directly on the prediction plan (3 cm above the loudspeakers). The loudspeakers were driven in phase (on the left hand side) and in antiphase (on the right hand side).

intensity of a sound field, thus giving a complete insight of the sound properties radiated by an acoustic source using the acousto-optic effect.

6 CONCLUSIONS

The present paper describes the versatility of the acousto-optic measuring principle for three different acoustic applications: visualization, localization and identification of acoustic sources. Each of these applications benefits from different measurement techniques (tomography, beamforming and holography) that are especially adapted to exploit different properties of the acousto-optic effect. The results achieved with the acousto-optic measuring principle are in good agreement with results obtained with conventional techniques based on microphone measurements. This proves that the acousto-optic effect is not only a measuring principle that can provide a qualitative description of an acoustic field, but it can also characterize an acoustic field quantitatively to a surprisingly good extent if we take into account that the instrumentation used to measure this phenomenon is not design for this purpose. In addition to that, the acousto-optic measuring principle renders unique properties that cannot be achieved with conventional techniques: it is a non-invasive technique, it is immune to spatial aliasing in beamforming applications and it provides unique spectral properties that soften the need for regularization techniques in holographic applications. All in all, it seems plausible that the acousto-optic effect may have an important role on the future of acoustic measurements within the audible frequency range.

7 REFERENCES

1. A. Torras-Rosell, S. Barrera-Figueroa and F. Jacobsen, ´Sound field reconstruction using acousto-optic tomography', J. Acoust. Soc. of Am. 131(5) 3786-3793 (2012).
2. A. C. Kak and M. Slaney. Principles of Computerized Tomographic Imaging, IEEE, New York (1988).
3. D. H. Johnson and D. E. Dudgeon. Array Signal Processing: Concepts and Techniques. Prentice-Hall, Englewood Cliffs, NJ (1993).
4. B. D. V. Veen and K. M. Buckley, ´Beamforming: A versatile approach to spatial filtering', IEEE ASSP Magazine 5(2) 4–24 (1988).
5. B. Rafaely, ´Plane-wave decomposition of the sound field on a sphere by spherical convolution', J. Acoust. Soc. of Am. 116(4) 2149–2157 (2004).
6. E. Tiana-Roig, F. Jacobsen, and E. Fernandez-Grande, ´Beamforming with a circular microphone array for localization of environmental noise sources', J. Acoust. Soc. of Am. 128(6) 3535–3542 (2010).
7. E. Tiana-Roig and F. Jacobsen, Acoustical source mapping based on deconvolution approaches for circular microphone arrays, Proc. 40th International Congress and Exposition on Noise Control Engineering, Osaka (2012).
8. A. Torras-Rosell, S. Barrera-Figueroa and F. Jacobsen, ´An acousto-optic beamformer', J. Acoust. Soc. of Am. 132(1) 144-149 (2012).
9. E. G. Williams, J. D. Maynard, and E. Skudrzyk, ´Sound source reconstructions using a microphone array', J. Acoust. Soc. of Am. 68(1) 340-344 (1980).
10. J. D. Maynard, E. G. Williams, and Y. Lee,, ´Nearfield acoustic holography I: Theory of generalized holography and the development of NAH', J. Acoust. Soc. of Am. 78(4) 1395-1413 (1985).
11. E. G. Williams. Fourier Acoustics: Sound radiation and Nearfield Acoustical Holography, Academic Press, San Diego (1999).
12. J. Hald, ´Basic theory and properties of statistically optimized near-field acoustical holography', J. Acoust. Soc. of Am. 125(4) 2105-2120 (2009).
13. A. Sarkissian, ´Method of superposition applied to patch near-field acoustic holography', J. Acoust. Soc. of Am. 118(2) 671-678 (2005).
14. A. Torras-Rosell, E. Fernandez-Grande, S. Barrera-Figueroa and F. Jacobsen, Investigating the use of the acousto-optic effect for acoustic holography, Proc. 41st International Congress and Exposition on Noise Control Engineering, New York (2012).

Paper I

ADVANCES IN THE FREE-FIELD MEASUREMENT OF ACOUSTIC PARTICLE VELOCITY USING GATED PHOTON CORRELATION SPECTROSCOPY

B Piper Acoustics Group, National Physical Laboratory, Teddington, Middlesex, UK
T Koukoulas Acoustics Group, National Physical Laboratory, Teddington, Middlesex, UK
A Torras-Rosell DFM, Danish National Metrology Institute, 2800 Kongens Lyngby, Denmark
P Theobald Acoustics Group, National Physical Laboratory, Teddington, Middlesex, UK

1 INTRODUCTION

Gated photon correlation spectroscopy (PCS) offers a viable alternative to the current free field primary standard for microphone calibration which is based on the reciprocity method[1]. For a calibration in a pressure field, reciprocity can be performed to a high level of certainty. However, the uncertainty in free field reciprocity calibrations is strongly dominated by the free field correction applied and suffers from low signal to noise ratios above 10 kHz. Reciprocity based calibrations are also limited to a small number of microphone types that feature a standard geometry.

Gated PCS is an optical method that measures particle velocity directly, and therefore is an absolute measure of acoustic pressure, at a single point. In this case, two coherent laser beams intersect and produce an interference fringe pattern; as particles cross through fringes, photons are scattered with a periodicity directly related to the particle velocity. Analysis of the first minima in the auto-correlation function (ACF) of the measured time series of these scattered photons allows for the calculation of the acoustic particle velocity using Equation 1[2], where f is the acoustic frequency λ is the optical wavelength, θ is the half angle between the intersecting laser beams and t_{min} is the time to the first minima in the ACF:

$$u_m = \frac{3.832\, f\, \lambda}{4sin(\theta)\, \sin(\pi f t_{min})} \quad (1)$$

The free-field acoustic pressure is directly proportional to the measured particle velocity through knowledge of the speed of sound and density of air. This measurement can be used as a direct reference to calibrate a microphone of any type and shape including MEMS microphones.

Previous research has mainly focused on applying PCS[3-5] and other optical techniques, such as Laser Doppler Anemometry (LDA)[6-8], Laser Doppler Velocimetry (LDV)[9,10] and Particle Image Velocimetry (PIV)[11,12], in standing wave tubes. The most recent research has explored how gated PCS can be applied in a free field chamber[13,14], placing the optical system outside and passing the beams through the chamber walls. Results have been shown that give a good agreement with a laboratory standard microphone for frequencies in the range 1 - 4 kHz at sound pressure levels (SPLs) between 106 dB and 116 dB.

One of the main challenges in using gated PCS for measuring particle velocities in a free-field chamber, is the existence of non-acoustic air flow, which has a mean velocity with turbulent fluctuations for a given measurement period. These velocities will be averaged with the acoustic velocity and therefore a signal processing approach is required which will allow for the mean flow to be decoupled. One approach to overcome this is to make separate measurements at the positive and negative peaks of the acoustic particle velocity and find the average therefore cancelling out the contribution of the air flow on each.

This paper describes the latest development of this work with details of hardware improvements that allow for measurements to be made over a wider range of frequencies and a comparison of two approaches to gating the velocity peaks.

2 OVERVIEW OF THE GATED PCS SYSTEM AND IMPOROVMENTS TO THE MEASUREMENT SYSTEM

Figure 1 shows the set-up of the measurement system. The optical delivery and collection systems are placed outside the chamber and the beams are based through holes in the chamber wall. Inside the chamber single frequency sine waves are produced by a horn coupled compression driver.

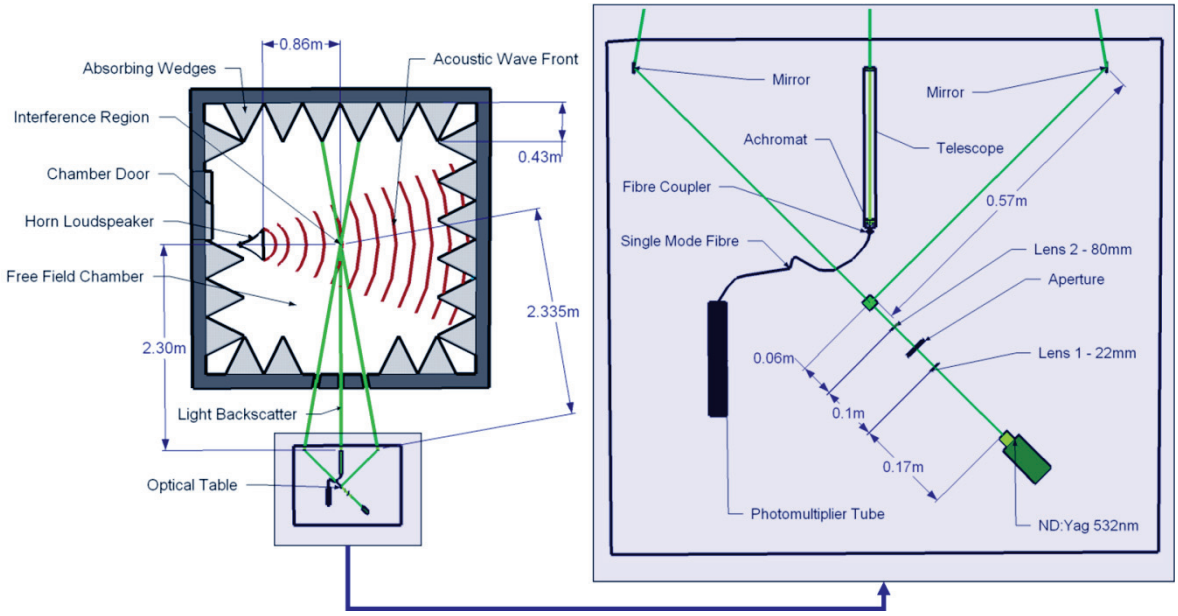

Figure 1 – Set-up of gated PCS system for measuring acoustic particle velocities inside a free field chamber.

2.1 Optical Delivery System

The aim of the optical delivery system is to create a stable interference region at the centre of the chamber where the beams intersect at their focal waists. This is achieved by expanding the laser beam and then focussing it in the far field. The main optical source is a frequency-doubled Nd:YAG laser, with a wavelength of 532 nm and 300 mW optical power. The primary beam is split into two beams of equal intensity by a cubic beam splitter. A pair of mirrors is then used to direct the two beams into the chamber. Previous measurements[14] using this system have featured an ellipsoid region with dimensions of 2 mm * 11 mm * 2 mm and with a fringe spacing of 1.6 μm.

A pair of plano-convex lenses, with focal lengths 22 mm and 80 mm, is placed 100mm apart in the laser path. This allows the focusing of the crossing laser beams in the chamber, producing an ellipsoid with approximate dimensions of 1 mm * 5.5 mm * 1 mm and a fringe spacing of 1.48 μm. In the previous measurements[14] the measurement plane was also subject to a small degree of tilt such that one laser beam was rising slightly as it passed into the chamber and the other was falling, but nevertheless crossing accurately via suitably adjusting the mirrors. This was due to instability in the mounting of the laser source and slight misalignment of the beam splitter. To overcome these issues the laser source has been mounted on a specially engineered heavy duty fixed platform and the beam splitter has been mounted on an adjustable tilting platform, allowing for any misalignment to be corrected. These improvements have also improved the stability of the set-up reducing the need for time consuming realignments.

2.2 Optical Collection System

The optical collection system consists of a custom made refracting telescope, an achromatic lens, a single mode fibre which is matched to the wavelength of the laser source, and a photomultiplier tube. The telescope effectively magnifies the image of the interference region inside the chamber through a small opening in the chamber wall. An achromatic lens is placed directly after the telescope to focus the image collected by the telescope into the opening of the single mode fibre. The single mode fibre is then coupled to the photomultiplier tube via a collimator arrangement. The telescope used for the measurements in this paper was mounted on a tilting platform aligned along the measurement axis such that the vertical angle could be matched to the return angle of the backscatter, maximising the number of photons captured from the interference region.

2.3 Improvements to the Acoustic Delivery System

The acoustic delivery system consists of a power amplifier and a compression driver coupled to a horn to maximise the efficiency of the driver. Such a system allows for the production of an undistorted high amplitude signal. Previously a Canford Audio TOA SC-630 horn speaker was used driven by a Sony TA-F 500 ES. This was capable of producing the required signal between 900 Hz and 4 kHz although featuring some distortion at the SPLs required for measurements at 4 kHz. This set-up was replaced with a Samson 200 servo amplifier and a Faital Pro HF144 coupled to a Faital Pro LTH142 horn. Figure 2 shows the measured frequency response of the loudspeaker and horn at 1 m for a 1 W input signal assuming a nominal load of 8 Ω. The loudspeaker has a power handling rating of 80 W and therefore it is capable of delivering SPLs in excess of 120 dB (re: 20 μPa) across the frequency range of interest.

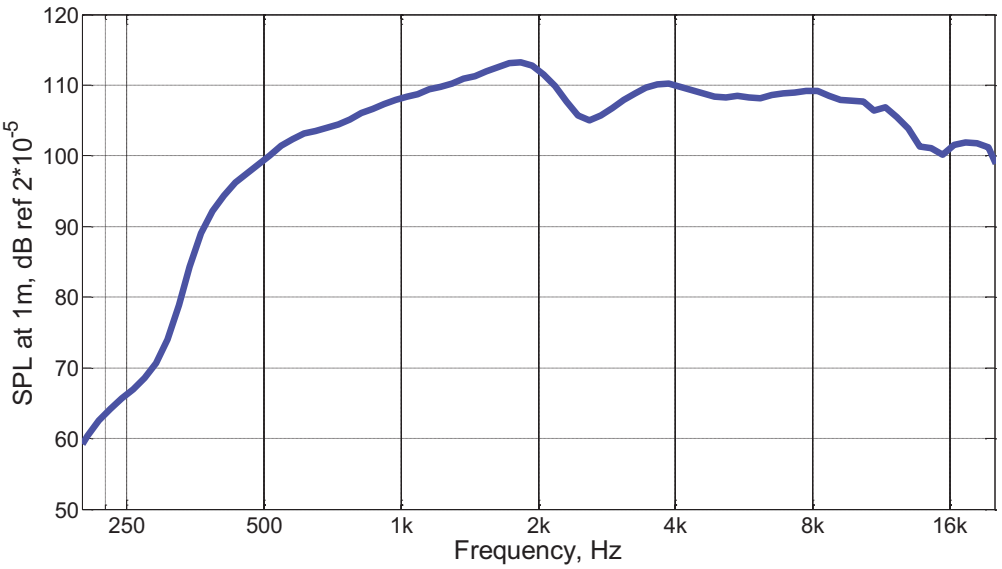

Figure 2 – Measured Frequency Response of Faital Pro HF144 coupled to Faital Pro LTH142 Horn at 1 m for a 1 W input signal assuming nominal load of 8 Ω

2.4 Methods of Gating the ACFs

Gating is used to allow the auto-correlation measurement to take place for the peak acoustic particle velocity of the sine wave being measured, whilst rejecting the lower velocity components that occur between the positive and negative peaks. Measuring both the positive and negative peaks allows the velocity component generated by the mean air flow in the chamber to be isolated

and removed. This is a valid approach if the mean flow velocity in the axis of the acoustic wave is less than half the peak acoustic particle velocity. The gating is applied to the auto correlation measurements by using a pulse as a trigger. The frequency of the pulse is set to twice the frequency of the acoustic wave to be measured with a 50% duty cycle. This gives a gate length of ¼ of the acoustic wavelength. A delay is used to control which part of the acoustic wave is being gated allowing for the total phase response of the system to be accounted for.

Two gating approaches are used in this paper. **Method A** consists of measuring two separate ACFs, one for the positive velocity peak and one for the negative velocity peak. The results are then analysed and the average of the two is found. This assumes that the mean air flow is steady over a measurement period of a few minutes. Analysis of the difference between the two ACFs gives an estimate of the mean flow present during the measurement which can be useful for ensuring the quality of the measurements. **Method B** consists of measuring alternate positive and negative velocity peaks in the same measurement. This is achieved by setting the number of cycles in the pulse trigger to 2 meaning that both peaks are measured in every second cycle of the acoustic wave. This approach has the advantage of averaging out the mean flow on individual cycles of the acoustic signal but the result is a single measurement so analysis of the first minima alone does not give an indication of the magnitude of the mean flow velocity.

3 OPTICAL MEASUREMENT RESULTS AND COMPARISON TO MICROPHONE MEASUREMENTS

The measurements shown in this section use the set-up and methods described in the previous section. In order to collect enough photons to measure a meaningful ACF a small amount of seeding particles must be introduced into the chamber of dimensions similar to the fringe spacing of the interference region. For these measurements a commercial fog generator was used. A burst from a fog generator was put into the chamber and then the chamber doors were closed. The fog was left for at least an hour to settle so that the larger particles gradually fall due to gravity, thus allowing only the smaller particles to remain airborne and the air flow and temperature gradients introduced to the room by the seeding are reduced to a minimum. This resulted in measurement counts of 20-40 thousand photon counts per second (kpcs) for the duration of the measurements. It is possible to measure ACFs using counts as low as 10 kpcs using the same set-up but the ACFs feature higher levels of noise and therefore the quality of the measurements degrade and the velocity estimations are more variable.

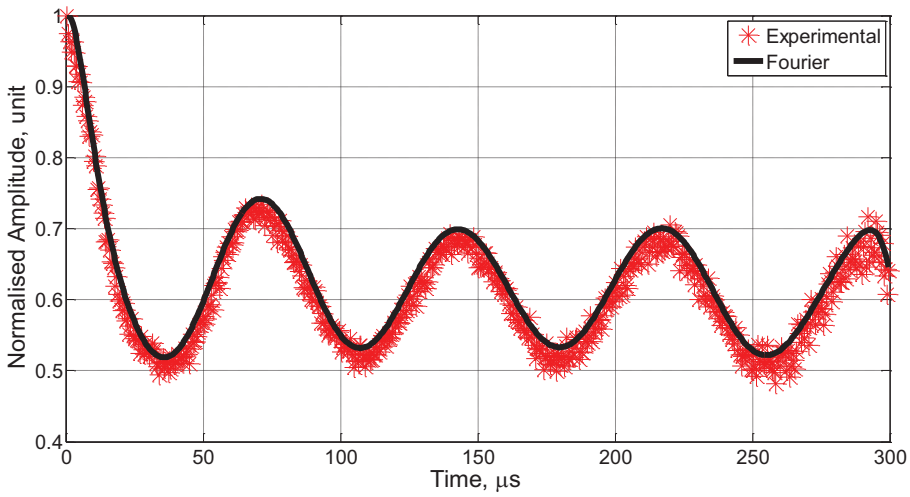

Figure 3 - Experimental gated ACF from positive peak of a 750 Hz pure tone

Figure 3 shows an ACF measured for a 750 Hz sine wave gated on the positive peak. An 8th order Fourier fit is applied to the data to give a computational estimate of the time of the first minima. This is considered an acceptable approach since a single velocity component will result in the ACF being a Bessel function. As the gate length is several times larger than the time to the first minima the ACF shows several peaks and troughs. At higher frequencies the gate length is shorter since it is set as ¼ of a wavelength and therefore the number of peaks and troughs is reduced. The result of this is that higher SPLs are required to measure meaningful ACFs at higher frequencies with the required SPL at 10 kHz for the first minima to occur clearly within the ACF being approximately 117dB (re: 20 μPa), depending on the exact details of the measurement set-up.

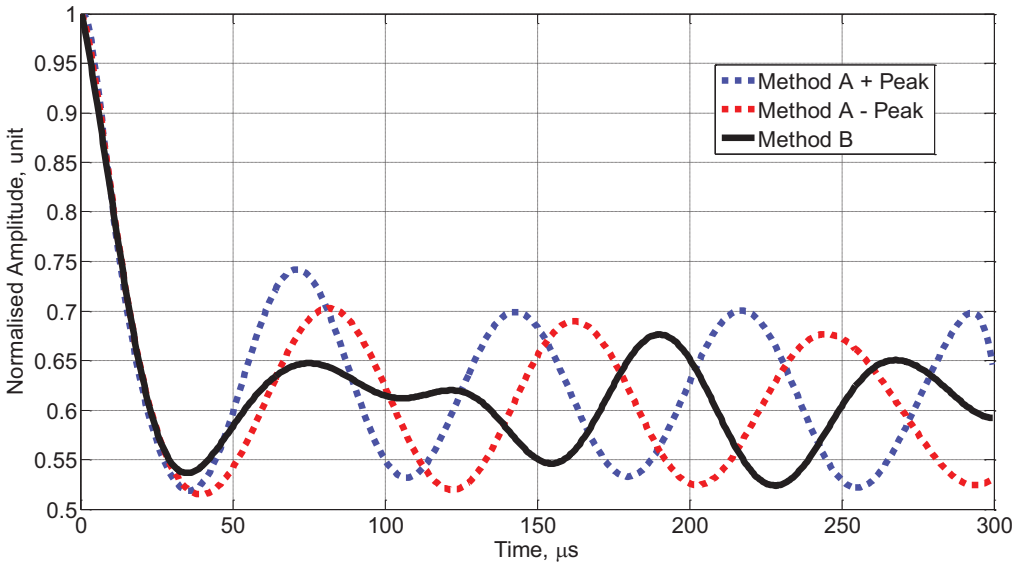

Figure 4 – Comparison of ACFs measured using gating method A and B

Figure 4 shows the Fourier functions fitted using gating methods A and B. By examining the two ACFs which make up method A, it is clear that the first minima corresponding to the negative peak occurs at a larger time shift than the first minima corresponding to the positive peak. This is due to the influence of the mean flow. The velocities are found by applying Equation 1 to these time shifts and the average velocity of the two gives the acoustic particle velocity. The ACF measured using method B shows a similar first minima to the positive peak of method A. The structure after the first minima however is different and deviates from the average between the two curves of method A. Understanding of what causes this deviation may offer an alternative approach for assessing the quality of the measurement to that of method A, where the magnitude of the mean flow contribution is considered.

ACFs, using both gating methods, were measured for a number of frequencies between 500 Hz and 8 kHz. For each frequency at least 3 valid ACFs were measured for each method, with the gates positioned approximately at the velocity peaks of the acoustic waves. The bin size of each ACF was set to give at least 250 points in each measurement. Measurements were made in a number of sessions over several days. In between each session a Bruel and Kjaer 4180 ½" microphone, which had been calibrated using the pressure reciprocity method, was positioned at the interference region pointing in the direction of the loudspeaker. The peak to peak output voltage of the microphone was measured using an oscilloscope. These voltages where then converted into SPL using the sensitivity data generated by the reciprocity calibration and the pressure to free field correction given by IEC 61094-7[15].

Table 1 shows a comparison of the SPLs measured using the two gating methods and the microphone. The differences appear to be similar for both methods and mostly lower SPLs than

those measured by the microphone. The differences are higher at the frequency extremes. It is likely that the free field chamber is not truly anechoic at 500 Hz and therefore the large differences shown here may be due to reflections of the acoustic wave. At high frequencies the SPLs required are high and the ACFs have a shorter length meaning fewer photons are captured so the influence of measurement noise is higher. The uncertainty in the microphone measurement is also higher at high frequency since the free field correction is larger and inaccuracies in the microphone placement will be more significant. It is unclear at this stage whether method A or B is better since any systematic difference is lost within the measurement uncertainties.

Frequency kHz	Bin size µs	Optical SPL Method A dB	Optical SPL Method B dB	Microphone SPL dB	Difference Method A dB	Difference Method B dB
0.5	0.5	105.18	105.05	105.48	-0.30	-0.42
0.75	0.5	110.76	110.94	110.68	0.08	0.26
1	0.5	111.72	111.78	112.04	-0.31	-0.26
1.5	0.5	112.60	112.95	112.84	-0.24	0.11
2	0.25	111.34	111.22	111.57	-0.22	-0.35
2.5	0.25	112.91	112.89	112.93	-0.01	-0.04
3	0.25	115.75	115.98	115.60	0.15	0.39
3.5	0.25	118.67	119.00	119.06	-0.39	-0.06
4	0.25	119.12	119.05	118.94	0.19	0.11
5	0.1	119.45	119.78	119.93	-0.49	-0.15
6	0.1	119.37	119.69	119.46	-0.09	0.23
7	0.1	119.76	120.08	120.21	-0.44	-0.12
8	0.1	119.85	119.97	120.15	-0.30	-0.18

Table 1- Measured SPLs using the optical method for separately gated peaks (Method A) and simultaneously gated peaks (Method B) and comparison with microphone.

These results demonstrate that the improvements made to the measurement system have allowed the frequency range to be extended down to 500 Hz and up to 8 kHz. This is a significant improvement on the 1 – 4 kHz range that was previously possible.

One further issue which effects the measurements is the need to centre the measurement gate exactly on the acoustic velocity peak. The horn, compression driver and amplifier all introduce a phase shift and there is a delay due to time of flight and any latency in the signal processing. To find the total lag at an individual frequency, measurements need to be made at a number of gate positions within the acoustic cycle. Figure 5 shows examples of this for 2 kHz and 5 kHz where a significant difference in peak position is shown between the two frequencies.

The next stages of this research include analysing the sources of uncertainty, measuring the true phase response of the system, examining alternative signal processing methods which allow for measurements to be made at lower SPLs, characterising and quantifying the effect of the seeding particles and implementing the system in a larger free-field chamber allowing for measurements at lower frequencies.

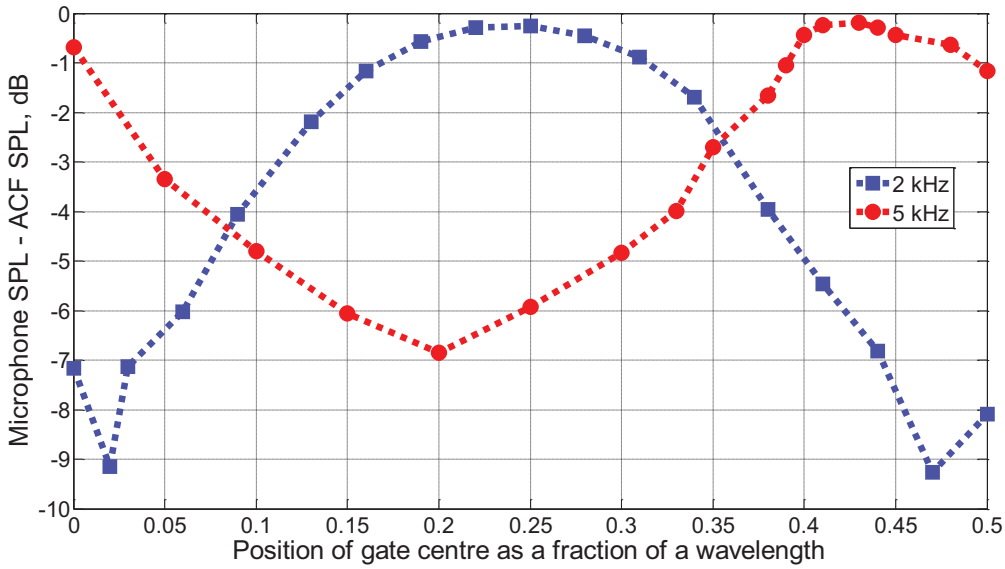

Figure 5 – Difference between SPL measured with a Microphone and SPL measured using gated PCS for gates centre at a number of positions within the acoustic cycle at 2 kHz (blue) and 5 kHz (red).

4 CONCLUSIONS

This paper has described a system for measuring free field acoustic particle velocity using a gated photon correlation spectroscopy method. This work is motivated by the need to directly measure the unit of acoustic pressure and may lead to the realisation of a new primary standard for free field microphone calibration.

Details of the measurement system are given with the latest improvements highlighted including improvements to the optical delivery system producing a smaller interference region, the collection telescope allowing for more efficient collection of the backscatter and an upgrade of the acoustic delivery system.

Measured data is shown for two gating methods and compared to measurements made with laboratory standard microphone. The measurements show good agreement of less than 0.6 dB for all measurements. Experimental identification of the acoustical particle velocity is shown for 2 frequencies demonstrating that knowledge of the phase response of the system is crucial to improving the accuracy of the measurements.

Further work to improve the accuracy and repeatability of the system has been identified which should allow the system to be developed into a new standard for the free-field calibration of microphones.

This work was funded by the National Measurement Office of the UK Department of Business Innovation and Skills.

5 REFERENCES

1. IEC 61094-3: 1995, “Measurement microphones – Part 3: Primary method for the free-field calibration of laboratory standard microphones by the reciprocity technique”.
2. J. P. Sharpe, and C. A. Greated, “A stochastic model for photon correlation measurements in sound fields,” J. Phys. D 22, 1429–1433. (1989).
3. D. Hann, and C. A. Greated, “Acoustic Measurements in Flows Using Photon Correlation Spectroscopy”, Meas. Sci. Technol., Vol. 4, 157-164. (1993).
4. T. MacGillivray, D. Campbell, C. Greated, and R. Barham, “The Development of a Microphone Calibration Technique Using Photon Correlation Spectroscopy,” Acta Acust, Vol. 89, 39-376. (2003).
5. T. Koukoulas, P. Theobald, T. Schlicke, and R. Barham, “Towards a future primary method for microphone calibration: Optical measurement of acoustic velocity in low seeding conditions,” Opt. Lasers Eng. Vol. 46, 791–796. (2008).
6. J. S. Cullen, C. A. Greated, and D. M. Campbell, “LDA Measurement of Sound: Amplitude Modulation of Laser Doppler Signals”, Meas. Sci. Technol., Vol. 10, 812-823. (1999).
7. T. MacGillivray, D. Campbell, C. Greated, and R. Barham, “The Development of a Microphone Calibration Technique Using Laser Doppler Anemometry,” Acta Acust, Vol. 88, 135-141. (2002).
8. M. W. Thompson, and A. A. Atchley, “Simultaneous Measurement of Acoustic and Streaming Velocities in a Standing Wave Using Laser Doppler Anemometry, J. Acoust. Soc. Am. Vol. 117(4), 1828-1838. (2005).
9. B. Gazengel, S. Poggi, and J. C. Valiere, “Evaluation of the Performance of Two Acquisition and Signal Processing Systems for Measuring Particle Velocities in Air by Means of Laser Doppler Velocimetry, Meas. Sci. Technol., Vol. 14, 2047-2064. (2003).
10. A. Degroot, R. MacDonald, O. Richoux, B. Gazengal, and M. Campbell, “Suitability of Laser Doppler Velocimetry for the Calibration of Pressure Microphones”, Applied Acoustics, Vol. 69, 1308-1317. (2008).
11. J. P. Sharpe, C. A. Greated, C. Gray, and D. M. Campbell, “The Measurement of Acoustic Streaming Using Particle Image Velocimetry”, Acustica, Vol. 68, 168-172. (1989).
12. M. Campbell, J. A. Cosgrove, C. A. Greated, S. Jack and D. Rockliff, “Review of LDA and PIV Applied to the Measurement of Sound and Acoustic Streaming”, Optics & Laser Technology, Vol. 32, 629-639. (2000).
13. T. Koukoulas, P. Theobald, B. Piper, S. Rajagopal, S. Robinson and R. Barham, “Particle Velocity Measurements Using Photon Correlation Spectroscopy For The Direct Realisation of The Sound Pressure Unit in Airborne Acoustics”, Proc. 19th ICSV, Vol. 3, 1769-1776, Vilnius. (2012).
14. T. Koukoulas, B. Piper, and P Theobald, “Gated photon correlation spectroscopy for acoustical particle velocity measurements in free-field conditions”, J. Acoust. Soc. Am. Vol. 133, Issue 3, EL156-EL161. (2013).
15. IEC 61094-7: Measurement microphones - Part 7: Values for the difference between free-field and pressure sensitivity levels of laboratory standard microphones

www.elektro.dtu.dk

Department of Electrical Engineering
Acoustic Technology
Technical University of Denmark
Ørsteds Plads
Building 348
DK-2800 Kgs. Lyngby
Denmark
Tel: (+45) 45 25 38 00
Fax: (+45) 45 93 16 34
Email: info@elektro.dtu.dk

ISBN 978-87-92465-46-7